ถ่านกัมมันต์จากไม้: การเตรียม การปรับปรุงสมบัติพื้นผิว และการศึกษาการดูดซับ

นางสาวยุวรัตน์ เงินเย็น

วิทยานิพนธ์นี้เป็นส่วนหนึ่งของการศึกษาหลักสูตรปริญญาวิศวกรรมศาสตรดุษฎีบัณฑิต
สาขาวิชาวิศวกรรมเคมี
มหาวิทยาลัยเทคโนโลยีสุรนารี
ปีการศึกษา 2550

WOOD-BASED ACTIVATED CARBON: PREPARATION, SURFACE MODIFICATION, AND ADSORPTION STUDY

Yuvarat Ngernyen

A Thesis Submitted in Partial Fulfillment of the Requirements for the

Degree of Doctor of Philosophy in Chemical Engineering

Suranaree University of Technology

Academic Year 2007

WOOD-BASED ACTIVATED CARBON: PREPARATION, SURFACE MODIFICATION, AND ADSORPTION STUDY

Suranaree University of Technology has approved this thesis submitted in partial fulfillment of the requirements for the Degree of Doctor of Philosophy.

Thesis Examining Committee

_____

(Dr. Terasut Sookkumnerd)

Chairperson

_____

(Assoc. Prof. Dr. Chaiyot Tangsathitkulchai)

Member (Thesis Advisor)

_____

(Assoc. Prof. Dr. Malee Tangsathitkulchai)

Member

_____

(Assoc. Prof. Dr. Nurak Grisdanurak)

Member

_____

(Asst. Prof. Dr. Ratanawan Kiattikomol)

Member

_____	_____
(Prof. Dr. Pairote Sattayatham)	(Assoc. Prof. Dr. Vorapot Khompis)
Vice Rector for Academic Affairs	Dean of Institute of Engineering

ยุวรัตน์ เงินเย็น : ถ่านกัมมันต์จากไม้: การเตรียม การปรับปรุงสมบัติพื้นผิว และการศึกษาการดูดซับ (WOOD-BASED ACTIVATED CARBON: PREPARATION, SURFACE MODIFICATION, AND ADSORPTION STUDY) อาจารย์ที่ปรึกษา : รองศาสตราจารย์ ดร.ชัยยศ ตั้งสถิตย์กุลชัย, 298 หน้า.

งานวิจัยนี้มีวัตถุประสงค์เพื่อศึกษาการเตรียม การปรับปรุงสมบัติพื้นผิว และการศึกษากระบวนการดูดซับของถ่านกัมมันต์จากไม้ยูคาลิปตัสและไม้กระถินณรงค์ ขอบเขตเขตของงานวิจัยนี้ครอบคลุมถึงการเตรียมถ่านกัมมันต์โดยวิธีกระตุ้นทางเคมีและทางกายภาพเพื่อศึกษาผลของสภาวะการเตรียมต่อโครงสร้างความพรุนของถ่านกัมมันต์ การปรับปรุงสมบัติพื้นผิวของถ่านกัมมันต์โดยวิธีออกซิเดชันเพื่อเพิ่มสมบัติความเป็นขั้ว และการนำถ่านกัมมันต์ที่ปรับเคมีพื้นผิวแล้วมาศึกษาสมดุลการดูดซับไอน้ำ ไอของเมทานอล และเอธานอล และโลหะหนักที่มีประจุบวกจากสารละลาย เพื่อศึกษาบทบาทของหมู่ฟังก์ชันพื้นผิว

ผลการทดลองพบว่า สำหรับไม้ทั้งสองชนิด การกระตุ้นทางเคมีด้วยกรดฟอสฟอริกให้ถ่านกัมมันต์ที่มีพื้นที่ผิวและปริมาตรรูพรุนรวมสูงกว่าการกระตุ้นทางกายภาพด้วยก๊าซคาร์บอนไดออกไซด์ โดยการกระตุ้นด้วยก๊าซคาร์บอนไดออกไซด์ให้ถ่านกัมมันต์ที่รูพรุนส่วนใหญ่เป็นรูพรุนขนาดเล็ก ในขณะที่การกระตุ้นด้วยกรดฟอสฟอริกให้ถ่านกัมมันต์ที่มีสัดส่วนรูพรุนขนาดกลางและใหญ่เพิ่มมากขึ้น สำหรับการกระตุ้นทั้งสองวิธีภายใต้สภาวะการเตรียมเหมือนกัน ไม้ยูคาลิปตัสจะให้ความพรุนสูงกว่าไม้กระถินณรงค์

การเพิ่มหมู่ฟังก์ชันออกซิเจนชนิดต่าง ๆ บนพื้นผิวของถ่านกัมมันต์ที่เตรียมจากไม้ยูคาลิปตัสทำโดยการออกซิเดชันด้วยไฮโดรเจนเปอร์ออกไซด์ แอมโมเนียมเปอร์ออกซิไดซัลเฟต กรดไนตริก และอากาศ โดยปริมาณและชนิดของหมู่ฟังก์ชันบนพื้นผิวสามารถวิเคราะห์ด้วยวิธีการไทเทรตโดยกรดและเบส, ฟลูเรียทรานสฟอร์ม อินฟราเรด สเปกโทรสโคปี, เอกซเรย์โฟโตอิเล็กตรอน สเปกโทรสโคปี, การวิเคราะห์แบบแยกธาตุ และค่าความเป็นกรดเป็นด่างที่ประจุพื้นผิวเป็นศูนย์ จากผลการทดลองพบว่า ปริมาณของหมู่ฟังก์ชันกรดเพิ่มขึ้นหลังจากออกซิเดชันด้วยสารออกซิไดซ์ชนิดต่าง ๆ โดยหมู่กรดคาร์บอกซิลิกมีร้อยละการเพิ่มขึ้นมากที่สุด รองลงมาคือ หมู่ฟีนอลิกและหมู่แลคโทนิก ตามลำดับ การเพิ่มเวลา อุณหภูมิ และความเข้มข้นของกรดขณะออกซิเดชัน จะช่วยเพิ่มปริมาณของแต่ละหมู่ฟังก์ชันและปริมาณหมู่กรดรวม แต่ไม่พบการเปลี่ยนแปลงสัดส่วนของหมู่ฟังก์ชันต่าง ๆ หลังการออกซิเดชันของทุกสารออกซิไดซ์ สำหรับการออกซิเดชันด้วยอากาศพบว่า ให้ปริมาณหมู่กรดคาร์บอกซิลิกและปริมาณหมู่กรดรวมสูงสุดเมื่อเปรียบเทียบกับการใช้สารออกซิไดซ์ชนิดอื่น ๆ นอกจากนี้ ยังพบว่าโครงสร้างความพรุนของถ่านกัมมันต์เริ่มต้นมีผลต่อการเกิดหมู่ฟังก์ชันเมื่อใช้กรดไนตริกเป็นสารออกซิไดซ์ โดยจะมีความ

เข้มข้นกรดต่ำสุดที่สามารถให้ปริมาณหมู่กรดได้มากที่สุด โดยความเข้มข้นนี้มีค่าเพิ่มขึ้นตามพื้นที่ผิวของถ่านกัมมันต์เริ่มต้นที่มากขึ้น นอกจากนี้ กระบวนการเตรียมถ่านกัมมันต์ยังมีผลต่อปริมาณการเกิดหมู่ฟังก์ชัน กล่าวคือ เมื่อออกซิเดชันที่สภาวะเดียวกัน ถ่านกัมมันต์ที่เตรียมโดยวิธีกระตุ้นทางเคมีจะให้ปริมาณหมู่กรดรวมสูงกว่าถ่านกัมมันต์ที่เตรียมโดยวิธีทางกายภาพ สำหรับถ่านกัมมันต์ที่ถูกออกซิไดซ์แล้วและนำไปผ่านกระบวนการให้ความร้อนที่อุณหภูมิสูง เพื่อศึกษาการเปลี่ยนแปลงหมู่ฟังก์ชันออกซิเจน พบว่ากระบวนการให้ความร้อนทำให้ปริมาณหมู่ฟังก์ชันกรดรวมลดลง โดยหมู่กรดคาร์บอกซิลิกจะมีความเสถียรทางความร้อนน้อยที่สุด ตามด้วยหมู่แลคโทนิก และหมู่ฟีนอลิก ตามลำดับ

การดูดซับไอน้ำซึ่งเป็นสารที่มีขั้วสูงและมีขนาดโมเลกุลเล็ก พบว่า ปริมาณการดูดซับขึ้นกับโครงสร้างความพรุนและหมู่ฟังก์ชันพื้นผิวบนถ่านกัมมันต์ ในขณะที่การดูดซับไอเมทานอลและไอเอธานอลซึ่งเป็นสารที่มีขั้วต่ำกว่าและมีขนาดโมเลกุลใหญ่กว่า พบว่า ขึ้นกับโครงสร้างความพรุนของถ่านกัมมันต์เท่านั้น ปริมาณการดูดซับไอน้ำจะเพิ่มขึ้นเมื่อพื้นที่ผิวปริมาตรรูพรุน และหมู่กรดคาร์บอกซิลิกของถ่านกัมมันต์เพิ่มมากขึ้น และกระบวนการทางความร้อนซึ่งทำให้หมู่กรดคาร์บอกซิลิกลดลงจะส่งผลให้ปริมาณการดูดซับไอน้ำลดลงด้วย ดังนั้น หมู่กรดคาร์บอกซิลิกเป็นหมู่ฟังก์ชันพื้นผิวที่มีบทบาทสำคัญในการดูดซับไอน้ำ

การดูดซับไอออนตะกั่ว สังกะสี ทองแดง และแคลเซียมจากสารละลาย มีค่าเพิ่มขึ้นเมื่อถ่านกัมมันต์ถูกออกซิไดซ์ โดยสามารถดูดซับตะกั่วได้สูงสุด รองลงมาคือ สังกะสี ทองแดง และแคลเซียม ตามลำดับ และการดูดซับในระบบสารคู่ของโลหะเหล่านี้ พบว่า มีแนวโน้มลดลงเมื่อเทียบกับการดูดซับในระบบสารเดี่ยว โดยการมีแคลเซียมอยู่ในระบบสารคู่จะไม่ส่งผลกระทบต่อการดูดซับของสารอีกตัวหนึ่ง

สาขาวิชา วิศวกรรมเคมี ลายมือชื่อนักศึกษา_____

ปีการศึกษา 2550 ลายมือชื่ออาจารย์ที่ปรึกษา_____

ลายมือชื่ออาจารย์ที่ปรึกษาร่วม_____

YUVARAT NGERNYEN : WOOD-BASED ACTIVATED CARBON: PREPARATION, SURFACE MODIFICATION, AND ADSORPTION STUDY. THESIS ADVISOR : ASSOC. PROF. CHAIYOT TANGSATHITKULCHAI, Ph.D. 298 PP.

ACTIVATED CARBON/SURFACE MODIFICATION/ADSORPTION/ WOOD PRECURSORS

The overall objective of this thesis research was to perform an extensive study on the preparation, surface modification, and adsorption of activated carbon from eucalyptus and wattle woods. The scope of the research covered the preparation of activated carbon by chemical and physical activation under different conditions, surface modification of activated carbon by oxidation methods to enhance the hydrophilic characteristic, and the studies of equilibrium adsorption of water vapor, methanol vapor, ethanol vapor, and heavy metal cations from solution on surface-modified activated carbon to investigate the role of surface functional groups.

On the preparation results, for both woods, chemical activation with H_3PO_4 was found to give activated carbon with higher surface area and total pore volume than that obtained by physical activation with CO_2. Activated carbons derived from CO_2 activation produced mainly micropore whereas H_3PO_4 activation produced activated carbons with higher proportions of mesopore and macropore volume. For both activation methods, eucalyptus wood gave better pore development than wattle wood under the same preparation conditions studied.

Various types of oxygen functional groups were introduced onto the surface of eucalyptus wood-based activated carbon through oxidation using H_2O_2, $(NH_4)_2S_2O_8$, HNO_3, and air. Acid/base titration, Fourier Transform Infrared spectroscopy (FTIR), X-ray Photoelectron spectroscopy (XPS), elemental analysis, and pH at the point of zero charge (pH_{pzc}) were used to characterize the amount and types of surface functional groups. The results showed that the content of acidic oxygen functional groups increased after oxidation with all oxidizing agents used. The percent increase in functional group concentration followed the order, carboxylic acid > phenolic > lactonic for all oxidation methods. The increasing of oxidation time, oxidation temperature, and acid concentration increased the total acid group and the amount of each acidic functional group, whereas the distribution of each functional group remained unaffected after all oxidation treatments. Air oxidation gave the highest total acidic groups and highest amount of carboxylic acid in the carbon as compared with the oxidation in liquid phase. Porous structure of the original activated carbon had an effect on the introduction of oxygen functional groups when using HNO_3 as oxidizing agent. There existed a minimum acid concentration corresponding to the available surface area that could introduce maximum amount of acidic surface groups. The preparation method of activated carbon also had a direct effect on the amount and distribution of functional groups with the original activated carbon prepared by chemical method giving higher total acidic groups compared to the original activated carbon prepared by physical method at the same oxidation conditions. The oxidized activated carbon was also heat treated at high temperatures to study the change in oxygen functional groups related to their thermal stabilities. It was found that heat treatment process decreased the amount of total acidic functional

groups with carboxylic acid group having the least thermal stability followed by lactonic and phenolic groups.

The adsorption of polar molecules with higher polarizability and smaller molecular size (water vapor) was found to depend on both porous structure and surface functional groups of the carbon, while the adsorptions of lower polarizability and larger molecular size (methanol and ethanol vapors) depended only on the porous structure of carbons. The amount of water adsorbed was found to increase with carbon having higher surface area and pore volume as well as higher carboxylic acid group. Heat treatment process which lowered the amount of the carboxylic acid group decreased the amount of water adsorbed. Therefore, carboxylic acid group played an important role in the process of water adsorption.

The adsorption of Pb^{2+}, Zn^{2+}, Cu^{2+}, and Ca^{2+} ions was enhanced by the surface oxidation of activated carbon with the order of $Pb^{2+} > Zn^{2+} > Cu^{2+} > Ca^{2+}$. The competitive adsorptions in binary systems of these ions decreased the uptake of individual metal ions in solutions, with the presence of Ca^{2+} in the binary system giving no effect on the adsorption of the other ion.

School of Chemical Engineering Student's Signature _____

Academic Year 2007 Advisor's Signature _____

Co-advisor's Signature _____

ACKNOWLEDGEMENTS

Firstly, I would like to express my sincere gratitude to my thesis advisor, Assoc. Prof. Dr. Chaiyot Tangsathitkulchai, for giving me the opportunity to study in this PhD program. He has taught me substantially that will be important for the development of my future career.

My sincere thanks also extended to Assoc. Prof. Dr. Malee Tangsathitkulchai. Her kind advice during this study was invaluable to me. I am grateful to all the teachers in the School of Chemical Engineering, Suranaree University of Technology (SUT).

During my time in Northern Carbon Research Laboratories (NCRL), University of Newcastle upon Tyne, I would like to thank Prof. K. Mark Thomas and Dr. Ashleigh J. Fletcher for advice, expertise and assistance. I also would like to thank all postgraduate students at NCRL.

I wish to thank various members of past and present postgraduate students at SUT. Many thanks go to Dr. Supunnee Junpirom for all assistances. Financial support from The Royal Golden Jubilee (RGJ) Ph.D. Program under The Thailand Research Fund is greatly appreciated (Grant 1.C.TS/45/A.1 PHD/0132/ 2545).

Finally, I am indebted to all the members of my family for their kind support and understanding through out my study.

Yuvarat Ngernyen

TABLE OF CONTENTS

Page

ABSTRACT (THAI)…….……. I

ABSTRACT (ENGLISH) ……...……III

ACKNOWLEDGEMENTS…….……VI

TABLE OF CONTENTS…….…….. VII

LIST OF TABLES…….……...XIV

LIST OF FIGURES…….. XXI

SYMBOLS AND ABBREVIATIONS…..…….. XXXIII

CHAPTER

I INTRODUCTION……..... 1

1.1 Rationale of the Study……1

1.2 Research Objectives……...3

1.3 Scope of the Study……. 4

1.3.1 Preparation of activated carbon……. 4

1.3.2 Surface modification of activated carbon…….. 4

1.3.3 Adsorption study of surface-modified activated carbon..... 5

1.4 Research Development……...…... 5

1.5 Outcomes of the Research……..... 6

1.6 References……..……... 7

TABLE OF CONTENTS (Continued)

Page

II THEORY AND LITERATURE REVIEW…….8

2.1 Biomass……..……...8

2.2 Wood…….……...……10

2.3 Activated carbon……..12

2.3.1 Manufacture of activated carbon…….……14

2.3.1.1 Physical activation…… 14

2.3.1.2 Chemical activation……...15

2.3.2 Pore size and classification of activated carbon……...16

2.3.3 Application of activated carbon……...16

2.3.3.1 Liquid phase application……...16

2.3.3.2 Gas phase application……...….18

2.3.4 The surface chemistry of activated carbon……... 18

2.3.4.1 Surface functional groups……....…. 18

2.3.4.2 Method of analysis of surface functional groups……...……...21

2.4 Adsorption……...……27

2.4.1 Type of adsorption……...27

2.4.1.1 Physical adsorption……...27

2.4.1.2 Chemical adsorption……. 28

2.4.2 Adsorption isotherms……...29

TABLE OF CONTENTS (Continued)

Page

2.5 Review of literatures……...…… 31

2.5.1 Preparation of wood-based activated carbon……... 31

2.5.1.1 Physical activation…… 31

2.5.1.2 Chemical activation……...34

2.5.2 Surface modification of wood-based activated carbon..... 37

2.5.3 Adsorption on wood-based activated carbon……...40

2.5.3.1 Liquid phase adsorption.……...40

2.5.3.2 Gas phase adsorption.……... 42

2.6 References……...…… 45

III PREPARATION OF ACTIVATED CARBON……... 54

ABSTRACT.…….54

3.1 Introduction..……55

3.2 Apparatus and Methods..…… 57

3.2.1 Apparatus and chemicals..……... 57

3.2.2 Methods……58

3.2.2.1 Chemical activation……...……58

3.2.2.2 Physical activation…….……... 60

3.2.2.3 Characterization of precursors and activated carbon…… 61

TABLE OF CONTENTS (Continued)

Page

3.3 Results and Discussion.……66

3.3.1 Properties of raw materials...……... 66

3.3.2 Chemical activation..……70

3.3.2.1 Effect of carbonization temperature……..70

3.3.2.2 Effect of chemical weight ratio…….80

3.3.2.3 Effect of carbonization time……..87

3.3.2.4 Effect of impregnation time……..91

3.3.3 Physical activation……... 97

3.3.3.1 Effect of carbonization temperature and time.....97

3.3.3.2 Effect of activation temperature and time….....106

3.3.3.3 Effect of CO_2 concentration…….……...125

3.3.4 General discussion……. 132

3.4 Conclusions……137

3.5 References.…….138

IV SURFACE MODIFICATION OF ACTIVATED CARBON… 143

ABSTRACT……143

4.1 Introduction……144

4.2 Apparatus and Methods……. 148

TABLE OF CONTENTS (Continued)

Page

4.2.1 Apparatus……... 148

4.2.2 Chemicals……...148

4.2.3 Methods……..149

4.2.3.1 Liquid phase oxidation.....150

4.2.3.2 Gas phase oxidation ……... 153

4.2.3.3 Characterization of modified activated carbons…….153

4.3 Results and Discussion……...156

4.3.1 Original activated carbons……. 156

4.3.2 Effect of oxidizing agent on surface modification of activated carbon…….……...160

4.3.2.1 N_2 adsorption results…….....160

4.3.2.2 Boehm's results…….....162

4.3.2.3 FTIR results…….....177

4.3.2.4 XPS and elemental results.....179

4.3.2.5 pH_{pzc} results.....183

4.3.3 Effect of porous structure on the incorporation of surface functional groups.....186

4.3.4 Effect of heat treatment on surface functional groups.....192

TABLE OF CONTENTS (Continued)

Page

4.5 References……..199

V ADSORPTION STUDY OF SURFACE-MODIFIED ACTIVATED CARBON…….. 205

ABSTRACT……205

5.1 Introduction……206

5.2 Apparatus and Methods……. 208

5.2.1 Apparatus and chemicals……... 208

5.2.2 Methods……..208

5.2.2.1 Vapor adsorption…….208

5.2.2.2 Heavy metal ions adsorption……...210

5.3 Results and Discussion……...211

5.3.1 Equilibria of vapor adsorption …….. 211

5.3.1.1 Vapor adsorption on unmodified activated carbon…….. 211

5.3.1.2 Vapor adsorption on modified activated carbon…….. 238

5.3.2 Equilibria of heavy metal ions adsorption on modified activated carbon…….256

5.3.2.1 Single ion adsorption…….. 258

5.3.2.2 Binary mixture adsorption…….. 273

TABLE OF CONTENTS (Continued)

Page

5.4 Conclusions……281

5.5 References……..283

VI CONCLUSTIONS AND RECOMMENDATIONS……288

6.1 Conclusions……288

6.2 Recommendations……..293

APPENDIX LIST OF PUBLICATIONS…… 295

BIOGRAPHY……...298

LIST OF TABLES

Table **Page**

2.1 Chemical composition of wood..……. 12

2.2 Typical properties of commercial activated carbons produced from wood..……..14

2.3 Applications of activated carbon in liquid and gas phase…..……. 17

2.4 IR assignments of functional groups on activated carbon surfaces...…….. 23

2.5 Position and assignments of the XPS peaks.…….…..…….25

2.6 Comparison of parameters of type of adsorption process…….…..…….28

3.1 Preparation conditions used for prepare activated carbon by chemical activation with H_3PO_4……..…….59

3.2 Preparation conditions used for prepare activated carbon by physical activation with CO_2……..……..61

3.3 Analysis of raw materials……..……...67

3.4 Effect of carbonization temperature on the porous properties of prepared activated carbons by chemical activation……..……71

3.5 Proximate analysis of prepared activated carbons by chemical activation at different carbonization temperature…… 79

3.6 Effect of chemical weight ratio on the porous properties of prepared activated carbons by chemical activation……..……81

LIST OF TABLES (Continued)

Table **Page**

3.7 Effect of carbonization time on the porous properties of prepared activated carbons by chemical activation……..88

3.8 Effect of impregnation time on the porous properties of prepared activated carbons by chemical activation……..93

3.9 Effect of carbonization temperature on the porous properties of prepared activated carbons by physical activation……. 98

3.10 Effect of carbonization time on the porous properties of prepared activated carbons by physical activation…….102

3.11 Properties of char prepared at carbonization temperature of 400^{o}C for 1 hour using heating rate 25^{o}C/min……...105

3.12 Effect of activation temperature and time on the porous properties of activated carbons prepared from eucalyptus wood by physical activation……...110

3.13 Effect of activation temperature and time on the porous properties of activated carbons prepared from wattle wood by physical activation....……...111

3.14 Parameters of empirical equations for estimating porous properties of activated carbon from % burn-off…….116

LIST OF TABLES (Continued)

Table **Page**

3.15 Proximate analysis of prepared activated carbons by physical activation at different activation temperature for 1 hour……124

3.16 Effect of CO_2 concentration on the porous properties of prepared activated carbons by physical activation…….126

3.17 Parameters of empirical equations for estimating porous properties of activated carbon from % burn-off cover all preparation conditions studied……... 131

4.1 Preparation conditions and porous characteristics of original activated carbons …….....150

4.2 The experimental conditions for studying the surface modification by liquid and gas phase oxidation…….152

4.3 Porous properties and Boehm titration results of original activated carbons prepared from chemical and physical activations…….. 157

4.4 Porous characteristics obtained from N_2 adsorption isotherm of the original and oxidized activated carbons..…….161

4.5 Boehm titration results of original and H_2O_2 oxidized activated carbons ……...163

LIST OF TABLES (Continued)

Table **Page**

4.6 Boehm titration results of original and $(NH_4)_2S_2O_8$ oxidized activated carbons……166

4.7 Boehm titration results of original and HNO_3 oxidized activated carbons……...168

4.8 Boehm titration results of original and air oxidized activated carbons ……...171

4.9 Comparison of Boehm titration results of original activated carbon and oxidized activated carbons with highest surface acidic functional groups obtained from each oxidizing agent……... 175

4.10 Surface atomic concentration obtained from the C_{1s} and O_{1s} XPS regions of original and oxidized activated carbons …….. 181

4.11 Elemental analysis results of original and oxidized activated carbons …….. 182

4.12 The results of pH_{pzc} of the original and oxidized activated carbons…..…….. 185

4.13 Porous properties and Boehm titration results of original and oxidized activated carbons with different porous structure…….…... 188

4.14 Comparison of acidic functional groups of original and oxidized activated carbons prepared by chemical and physical activations…….…. ……... 191

LIST OF TABLES (Continued)

Table **Page**

4.15 Boehm titration results of original, oxidized, and heat treated activated carbons ……..……..194

4.16 Porous characteristics results of original, oxidized, and heat treated activated carbons……197

5.1 Preparation conditions and porous characteristics of unmodified activated carbons used to study the adsorption of water, methanol, and ethanol vapors …… 212

5.2 Surface functional groups of unmodified activated carbons obtained from Boehm titration..…….213

5.3 Parameters obtained from Dubinin-Serpinsky (DS) equation of unmodified activated carbons and amount of total acidic oxygen functional groups from Boehm titration..……...221

5.4 Parameters obtained from Do and Do model of unmodified activated carbons and amount of total acidic oxygen functional groups from Boehm titration..……224

5.5 Estimated relative pressure range from volumetric amount of water adsorbed corresponding to volume of various pore sizes for sample AC1 at 20^{o}C ……... 225

LIST OF TABLES (Continued)

Table **Page**

5.6 Parameters obtained from the modified Do and Do model for sample AC1 and amount of total acidic oxygen functional groups from Boehm titration..……228

5.7 Porous properties and surface functional groups of original and oxidized activated carbons prepared by CO_2 activation..……239

5.8 Porous properties and surface functional groups of original, oxidized, and heat treated activated carbons…….....241

5.9 Porous properties and surface functional groups of original and oxidized activated carbons prepared by H_3PO_4 activation……..242

5.10 Parameters obtained from Dubinin-Serpinsky (DS) and Do and Do models of original and oxidized activated carbons prepared by H_3PO_4 activation and amount of total acidic oxygen functional groups from Boehm titration..……..251

5.11 Parameters obtained from Dubinin-Serpinsky (DS), Do and Do, and modified Do and Do models of original, oxidized, and heat treated activated carbons and amount of total acidic oxygen functional groups from Boehm titration.……253

LIST OF TABLES (Continued)

Table **Page**

5.12 Porous properties and surface functional groups of original and oxidized activated carbons for study the effect of surface functional groups on the heavy metal ions adsorption……...257

5.13 Langmuir parameters obtained from metal ion adsorption isotherms…… 272

5.14 Parameters obtained from linear relationship between maximum amount of metal ions adsorbed and content of acidic functional groups…… 264

5.15 Langmuir parameters obtained from proton displacement isotherms of sample HNO_3 re 1M 24h ……..267

5.16 Relationship between proton displaced and metal ion adsorbed of sample HNO_3 re 1M 24h ……...270

5.17 Parameters for metal ions in the binary systems of Pb^{2+}/Cu^{2+}, Pb^{2+}/Zn^{2+}, and Zn^{2+}/Cu^{2+}on sample HNO_3 re 1M 24h ……..277

LIST OF FIGURES

Figure **Page**

2.1 Molecular structures of (a) cellulose, (b) hemicellulose, and (c) lignin.……9

2.2 Structure in cross section of (a) hardwood and (b) softwood…..…… 11

2.3 A schematic representation of the structure of activated carbon..…..……. 13

2.4 Type of (a) acidic and (b) basic oxygen functional groups.……..……...20

2.5 Type of nitrogen functional groups……..……... 21

2.6 Deconvolution of XPS spectra of (a) C_{1s} and (b) O_{1s} peaks…… 24

2.7 The influence of pH on surface charge: (a) pH < pH_{pzc}, (b) pH = pH_{pzc}, and (c) pH > pH_{pzc}…….…… 26

2.8 Types of adsorption isotherms according to the IUPAC classification..……...29

3.1 Schematic diagram of the experimental apparatus for preparing activated carbons by chemical activation..……...59

3.2 TGA and DTG curves of (a) eucalyptus and (b) wattle woods heated at 25^{o}C/min under nitrogen atmosphere……... 69

3.3 Effect of carbonization temperature on the porous properties of activated carbons prepared from (a) eucalyptus and (b) wattle woods by chemical activation……..72

LIST OF FIGURES (Continued)

Figure **Page**

3.4 Mechanism of phosphate linkages (a) phosphate ester and (b) polyphosphate ester formation by reaction of cellulose with H_3PO_4…..…….74

3.5 The breakdown of phosphate linkage at temperature above 450^oC……..……76

3.6 Adsorption and desorption isotherms of N_2 at −196^oC of activated carbons prepared from (a) eucalyptus and (b) wattle woods by chemical activation at different carbonization temperature…… 78

3.7 Effect of chemical weight ratio on the porous properties of activated carbons prepared from (a) eucalyptus and (b) wattle woods by chemical activation……. 82

3.8 Pore size distribution of activated carbons prepared from eucalyptus wood by chemical activation at different chemical weight ratio.……. 84

3.9 Adsorption and desorption isotherms of N_2 at −196^oC of activated carbons prepared from (a) eucalyptus and (b) wattle woods by chemical activation at different chemical weight ratio..……. 86

3.10 Effect of carbonization time on the porous properties of activated carbons prepared from (a) eucalyptus and (b) wattle woods by chemical activation…….. 89

LIST OF FIGURES (Continued)

Figure **Page**

3.11 Adsorption and desorption isotherms of N_2 at −196^{o}C of activated carbons prepared from (a) eucalyptus and (b) wattle woods by chemical activation at different carbonization time..…….. 91

3.12 Effect of impregnation time on the porous properties of activated carbons prepared from (a) eucalyptus and (b) wattle woods by chemical activation…….. 94

3.13 Adsorption and desorption isotherms of N_2 at −196^{o}C of activated carbons prepared from (a) eucalyptus and (b) wattle woods by chemical activation at different impregnation time……..... 96

3.14 Effect of the carbonization temperature on the porous properties of the activated carbon prepared from (a) eucalyptus and (b) wattle woods by physical activation……...99

3.15 Effect of the carbonization time on the porous properties of the activated carbon prepared from (a) eucalyptus and (b) wattle woods by physical activation…….……103

3.16 Burn-off of the chars at various times and temperatures of activation (a) eucalyptus and (b) wattle woods……..107

3.17 Burn-off of the chars at various temperatures and times of activation (a) eucalyptus and (b) wattle woods……..107

LIST OF FIGURES (Continued)

Figure **Page**

3.18 Contour of % burn-off as a function of activation time and temperature (a) eucalyptus and (b) wattle woods…….. 108

3.19 Effect of the activation temperature and activation time on the porous properties of the activated carbon prepared from eucalyptus wood by physical activation…… 112

3.20 Effect of the activation temperature and activation time on the porous properties of the activated carbon prepared from wattle wood by physical activation……...113

3.21 Effect of char burn-off on the porous properties of the activated carbon prepared by physical activation…….. 116

3.22 Adsorption and desorption isotherms of N_2 at −196^{o}C of activated carbons prepared from (a) eucalyptus and (b) wattle woods by physical activation at activation temperature 600^{o}C and 700^{o}C…… 118

3.23 Adsorption and desorption isotherms of N_2 at −196^{o}C of activated carbons prepared from (a) eucalyptus and (b) wattle woods by physical activation at activation temperature 800^{o}C, 850^{o}C, and 900^{o}C……..119

LIST OF FIGURES (Continued)

Figure **Page**

3.24 Pore size distribution of activated carbons prepared from eucalyptus wood by physical activation at activation temperature of (a) 900^{o}C, (b) 800^{o}C, (c) 700^{o}C, and (d) 600^{o}C for 1 hour……122

3.25 Effect of CO_2 concentration on the porous properties of activated carbons prepared from eucalyptus and wattle woods by physical activation……..……. 127

3.26 Adsorption and desorption isotherms of N_2 at −196^{o}C of activated carbons prepared from (a) eucalyptus and (b) wattle woods by physical activation different CO_2 concentration…..…..... 129

3.27 Effect of burn-off on the porous properties of the activated carbon prepared by physical activation covering all preparation conditions studied…..... 130

3.28 Yields of activated carbons prepared from (a) eucalyptus and (b) wattle woods by chemical activation and physical activation methods at different activation temperature……...133

3.29 Comparison of the porous properties of activated carbons prepared from (a) eucalyptus and (b) wattle woods by chemical activation and physical activation methods at different activation temperature…… 134

LIST OF FIGURES (Continued)

Figure **Page**

3.30 Scanning electron micrographs of activated carbons prepared from eucalyptus wood by (a) chemical activation and (b) physical activation methods by at activation temperature 600^{o}C……..135

3.31 Comparison of the proximate analysis of activated carbons prepared from (a) eucalyptus and (b) wattle woods by chemical activation and physical activation methods at different activation temperature…… 136

4.1 Content of surface functional groups of the original activated carbons prepared from chemical and physical activations…….....158

4.2 Adsorption and desorption isotherms of N_2 at −196^{o}C of original and oxidized activated carbons……..... 162

4.3 Contents of surface functional groups of the original activated carbon and activated carbons oxidized with H_2O_2…….....163

4.4 Contents of surface functional groups of the original activated carbon and activated carbons oxidized with $(NH_4)_2S_2O_8$……..... 166

4.5 Contents of surface functional groups of the original activated carbon and activated carbons oxidized with HNO_3……..... 169

4.6 The formation of ketone involving in the oxidation with nitric acid by reflux method..…….. 170

LIST OF FIGURES (Continued)

Figure **Page**

4.7 Contents of surface functional groups of the original activated carbon and activated carbons oxidized with air..……...172

4.8 Contents of surface functional groups of the original activated carbon and oxidized activated carbons with maximum surface acidic functional groups obtained from each oxidizing agent..……. 176

4.9 FTIR spectra of the original and oxidized activated carbons..……...178

4.10 XPS spectra of (a) O_{1s} and (b) C_{1s} of the original and oxidized activated carbons..……...180

4.11 Relationship between oxygen content and amount of acidic functional groups of the original and oxidized activated carbons……. 183

4.12 pH drift method to obtain the pH_{pzc} of the original and oxidized activated carbons ……..……184

4.13 Relationship between pH_{pzc} and content of acidic functional groups of the original and oxidized activated carbons……..…….186

4.14 Contents of acidic functional groups of original and oxidized activated carbons with different porous structure……..…… 189

4.15 Possible formation of lactonic group from carboxylic acid and phenolic …….. 189

LIST OF FIGURES (Continued)

Figure **Page**

4.16 Comparison of acidic functional groups obtained from HNO_3 oxidation by reflux method for 24 hours of original activated carbons prepared by chemical and physical activations……192

4.17 Contents of surface functional groups of the original, oxidized, and heat treated activated carbons……. 194

5.1 Diagrammatic of Intelligent Gravimetric Analyzer for vapor adsorption experiment……209

5.2 Water vapor adsorption-desorption isotherms at 20 – 30^{o}C of (a) sample AC1 and (b) sample AC ……..214

5.3 Comparison of water vapor adsorption isotherms between sample AC1 and sample AC at (a) 20^{o}C, (b) 25^{o}C, (c) 30^{o}C, and (d) 20 – 30^{o}C……...217

5.4 Fitting of the Dubinin-Serpinsky (DS) model to the water vapor adsorption isotherms of unmodified activated carbons at (a) 20^{o}C, (b) 25^{o}C, and (c) 30^{o}C……..... 220

5.5 Fitting of the Do and Do model to the water vapor adsorption isotherms of unmodified activated carbons at (a) 20^{o}C, (b) 25^{o}C, and (c) 30^{o}C.…….....223

LIST OF FIGURES (Continued)

Figure **Page**

5.6 Fitting of the modified Do and Do model to the water vapor adsorption isotherms for sample AC1 at (a) 20°C, (b) 25°C, and (c) 30°C……..……. 227

5.7 Isosteric heat of water vapor adsorption with relative pressure of sample AC……. 229

5.8 Methanol vapor adsorption-desorption isotherms at 10 – 30°C of (a) sample AC1 and (b) sample AC ……. 231

5.9 Comparison of methanol vapor adsorption isotherms between sample AC1 and sample AC at (a) 10°C, (b) 20°C, and (c) 30°C……232

5.10 Ethanol vapor adsorption-desorption isotherms at 10 – 30°C of (a) sample AC1 and (b) sample AC…….. 234

5.11 Comparison of ethanol vapor adsorption isotherms between sample AC1 and sample AC at (a) 10°C, (b) 20°C, and (c) 30°C……..235

5.12 Isosteric heat of methanol and ethanol vapors adsorption with amount adsorbed of sample AC…….....236

5.13 Comparison of water, methanol, and ethanol vapor adsorption isotherms at 20 and 30°C of (a) sample AC1 and (b) sample AC……. 237

5.14 Chemical structure of (a) methanol and (b) ethanol……..... 238

5.15 Water vapor adsorption isotherms at 30°C of original and oxidized activated carbons prepared by CO_2 activation……..... 243

LIST OF FIGURES (Continued)

Figure **Page**

5.16 Water vapor adsorption isotherms at 30°C of original and oxidized activated carbons prepared by CO_2 activation…… 244

5.17 Water vapor adsorption isotherms at 30°C of original and oxidized activated carbons prepared by H_3PO_4 activation…….245

5.18 Comparison of water vapor adsorption isotherms at 30°C of samples with have comparable surface area of the original samples but have significant difference in surface functional groups ……..……..247

5.19 Water vapor adsorption isotherms at 30°C of original, oxidized, and heat treated activated carbons …….248

5.20 Fitting of (a) Dubinin-Serpinsky (DS) and (b) Do and Do models to the water vapor adsorption isotherms at 30°C of original and oxidized samples prepared by H_3PO_4 activation ……..250

5.21 Fitting of (a) Dubinin-Serpinsky (DS), (b) Do and Do, and (c) modified Do and Do models to the water vapor adsorption isotherms at 30°C of original, oxidized, and heat treated activated carbons ……...252

5.22 Adsorption isotherms of (a) methanol and (b) ethanol vapors at 30°C of original activated carbon (AC) and sample HNO_3 re 1M 24h ……..256

LIST OF FIGURES (Continued)

Figure **Page**

5.23 Adsorption isotherms at 30^{o}C of (a) Pb^{2+}, (b) Zn^{2+}, (c) Cu^{2+}, and (d) Ca^{2+} on original and oxidized activated carbons and (e) maximum uptake of all four metal ions on each carbon sample…….. 259

5.24 Adsorption isotherms at 30^{o}C of heavy metal ions on (a) original sample, (b) at 30^{o}C H_2O_2 24h, and (c) sample HNO_3 re 1M 24h and (d) maximum uptake on all three samples……..260

5.25 Relationship between maximum amount of metal ions adsorbed derived from Langmuir model and content of acidic functional groups of the original and oxidized carbons…….. 264

5.26 Proton displacement of (a) Pb^{2+}, (b) Zn^{2+}, (c) Cu^{2+}, and (d) Ca^{2+} of sample HNO_3 re 1M 24h …….. 266

5.27 Variation of H^{+} displaced with (a) Pb^{2+}, (b) Zn^{2+}, (c) Cu^{2+}, and (d) Ca^{2+} ions adsorbed on sample HNO_3 re 1M 24h …….269

5.28 Comparison of amount of metal adsorbed and proton displacement of (a) Pb^{2+}, (b) Zn^{2+}, (c) Cu^{2+}, and (d) Ca^{2+} of sample HNO_3 re 1M 24h …….. 271

5.29 Postulated complexation reaction between copper (II) and Surface functional groups on activated carbon…….....272

5.30 Binary system of Pb^{2+} and Cu^{2+} adsorption on sample HNO_3 re 1M 24h at 30^{o}C……... 274

LIST OF FIGURES (Continued)

Figure **Page**

5.31 Binary system of Pb^{2+} and Zn^{2+} adsorption on sample HNO_3 re 1M 24h at 30^oC……...274

5.32 Binary system of Zn^{2+} and Cu^{2+} adsorption on sample HNO_3 re 1M 24h at 30^oC……...275

5.33 Binary systems of (a) Pb^{2+} and Ca^{2+} and (b) Cu^{2+} and Ca^{2+} adsorptions on original activated carbon (AC) and sample HNO_3 re 1M 24h at 30^oC…….....279

5.34 Adsorption isotherms of (a) Pb^{2+}, (b) Zn^{2+}, (c) Cu^{2+}, and (d) Ca^{2+} on sample HNO_3 re 1M 24h at 30^oC in both single and binary systems…….281

SYMBOLS AND ABBREVIATIONS

a_m	=	molecular projected area [16.2 $Å^2$/molecule for N_2 at –196^oC]
b	=	Langmuir constant [L/mmol]
b_H	=	Langmuir constant for proton displacemeant
c	=	ratio of the rate constants for Dubinin and Serpinsky (DS) equation
C	=	non-dimensional constant for Brunauer-Emmett-Teller (BET) equation
C	=	integration constant for van't Hoff equation
C_o	=	initial metal ion concentration in solution [mM]
C_e	=	final equilibrium metal ion concentration in solution [mM]
C_μ	=	water adsorbed amount for DS and Do and Do equation
$C_{\mu s}$	=	saturation concentration in the micropore for Do and Do equation
$C_{\mu o}$	=	concentration of the primary sites for DS equation
d	=	density conversion factor [0.0015468 cm^3 liquid/cm^3 STP for N_2 at –196^oC]
E_o	=	characteristic energy [J/mol]
H	=	amount of proton displacement
H_e	=	equilibrium amount of proton displacement
H_m	=	maximum amount of proton displacement
k	=	loss of the secondary sites for DS equation
K_f	=	chemisorption equilibrium constant for Do and Do equation

SYMBOLS AND ABBREVIATIONS (Continued)

K_μ	=	micropore equilibrium constant for Do and Do equation
n	=	amount of gas adsorbed [mol/g]
n_m	=	monolayer amount adsorbed [mol/g]
n_o	=	limiting micropore volume for Dubinin-Radushkevich (DR) equation [cm^3/g]
N_A	=	Avogadro number [6.023×10^{23} molecules/mole]
P	=	pressure
P^o	=	saturation vapor pressure
q_e	=	amount of metal ion adsorbed at equilibrium [mmol/g]
q_m	=	maximum amount of metal ion adsorbed [mmol/g]
Q_{st}	=	isosteric heat of adsorption
R	=	universal gas constant [8.314×10^{-3} J/mol K]
R^2	=	correlation coefficient
SSE	=	sum square of error
S_{BET}	=	specific surface area by BET equation [m^2/g]
S_o	=	concentration of surface active groups for Do and Do equation
T	=	temperature
V	=	volume of metal solution
$V_{meso+mac}$	=	mesopore and macropore volume [cm^3/g]
V_{mic}	=	micropore volume by DR equation [cm^3/g]
V_T	=	total pore volume [cm^3/g]

SYMBOLS AND ABBREVIATIONS (Continued)

$V_{0.99}$	=	amount of volume adsorbed at relative pressure (P/P^o) = 0.99 [cm^3 STP/g]
W	=	weight of activated carbon
W_F	=	weight of ash
W_0	=	weight of wood
W_1	=	weight of char
W_{110}	=	weight of sample at 110^{o}C
W_{850}	=	weight of sample at 850^{o}C
x	=	relative pressure (P/P^o) for DS and Do and Do equation
β	=	non-dimensional affinity coefficient [0.33 for N_2]

CHAPTER I

INTRODUCTION

1.1 Rationale of the Study

Activated carbon is a versatile adsorbent and because of its large surface area and pore volume is capable of adsorbing a wide variety of molecules both in liquid and gas phases. It can be produced from a variety of carbonaceous materials including agricultural by-products (such as corn hull, rice straw, nutshell, coconut shell, oil-palm shell and peach stone), wood, coal, petroleum coke, and tyre, etc.

The high adsorption capacity of activated carbon is associated with their well developed porous structure and large internal surface areas. In addition to the physical structure, activated carbons possess a chemical structure as well. The surface chemistry of activated carbons involves both hydrophobic graphene layers and hydrophilic surface functional groups. Organic compounds are largely adsorbed on the hydrophobic graphene layer, whereas other polar species such as water vapor, alcohol vapor, and heavy metal ions are selectively adsorbed on the hydrophilic functional groups. Predominant types of surface functional group on activated carbon are surface oxygen functionality. Modification of the surface chemistry of activated carbon to increase the amount of surface oxygen functional groups can be carried out by treating the carbon with oxidizing agents either in the gas phase (such as air, O_2, and O_3) or in aqueous solution (such as HNO_3, H_2O_2, $(NH_4)_2S_2O_8$, and H_2SO_4).

Because of their valueless wastes and abundant availability from a local sawmill, eucalyptus and wattle woods in the form of shaving were selected to be the potential precursors for the production of activated carbons in this research. Only a limited number of works have been reported on preparing activated carbon from eucalyptus wood (Tancredi, Cordero, Rodríguez-Mirasol, and Rodríguez, 1996; Arriagada, García, Molina-Sabio, and Rodríguez-Reinoso, 1997) and in particular there have been virtually no studies on the preparation of activated carbon from wattle wood. Therefore, this research is directed primarily toward studying the preparation of activated carbons from both woods to gain knowledge on the effect of preparation conditions on their porous characteristics.

Water vapor is known to have an appreciable effect on the adsorption of contaminants from air or gas streams resulting in a decrease in the breakthrough time for the activated carbon bed and is therefore detrimental to the performance of the activated carbon adsorption bed (Foley, Thomas, Forshaw, Stanton, and Norman, 1997). The adsorption of water molecules on activated carbon surface is strongly influenced by the presence of hydrophilic functional groups which play the role of primary adsorption centers by forming the bonds between the adsorbed molecules and the functional groups, and the uptake of water vapor is thus enhanced by theses functional groups. Therefore, it was decided to study the equilibrium of water adsorption on activated carbons whose surfaces were modified by oxidation methods to investigate the role of surface functional groups on the adsorption behavior. Volatile organic compounds (VOCs) such as alcohol vapors are pollutants emitted from chemical process industries and very harmful for both human health and environment, even at very low concentrations (Lillo-Ródenas, Cazorla-Amorós, and

Linares-Solano, 2005). The adsorption of methanol and ethanol vapors were therefore included in this research.

According to the World Health Organization, the most toxic heavy metals present in wastewater are lead, zinc, copper, aluminium, cadmium, chromium, cobalt, iron, magnesium, mercury, and nickel (Rivera-Utrilla and Sánchez-Polo, 2003). The adsorption process of metal ion species from aqueous solution depends on the surface chemistry of activated carbon, the nature of the chemical interaction between metal ion species and the surface groups, the speciation of the metal ion solution and the adsorption conditions (e.g. pH, temperature, etc). There have been a number of reports on the modification of activated carbons to enhance the adsorption of aqueous metal species, for which the most common procedure is oxidation method. Therefore, this work was set up to study the adsorption of lead, zinc, and copper on activated carbons modified by oxidation methods.

1.2 Research Objectives

1.2.1 To prepare activated carbons from eucalyptus and wattle woods by chemical and physical activation.

1.2.2 To incorporate oxygen functional groups on activated carbon surfaces by oxidation methods.

1.2.3 To investigate the role of surface functional groups of activated carbon on the adsorption process.

1.3 Scope of the Study

1.3.1 Preparation of activated carbon

1.3.1.1 Activated carbons are prepared from eucalyptus and wattle woods by chemical activation using phosphoric acid (H_3PO_4) and by physical activation using carbon dioxide (CO_2). For chemical activation, the effect of preparation conditions, including chemical weight ratio of wood and H_3PO_4, impregnation time, carbonization temperature, and carbonization time is studied. The effect of preparation conditions including carbonization temperature, carbonization time, activation temperature, activation time, and activating agent concentration is studied for physical activation.

1.3.1.2 The porous structures of the prepared activated carbons are characterized by nitrogen gas (N_2) adsorption at -196^oC.

1.3.2 Surface modification of activated carbon

1.3.2.1 Incorporating and modifying activated carbon surfaces to obtain varying types and concentrations of oxygen functional groups by liquid phase oxidation using nitric acid (HNO_3), hydrogen peroxide (H_2O_2), and ammonium peroxydisulfate ($(NH_4)_2S_2O_8$) and gas phase oxidation using air are performed. For liquid phase oxidation, the effect of modification conditions including oxidation time, oxidation temperature, and oxidizing agent concentration is studied. The effect of modification conditions such as oxidation temperature and oxidation time is studied for gas phase oxidation.

1.3.2.2 The surface functional groups of the modified activated carbons by using acid/base titration, Fourier Transform Infrared spectroscopy (FTIR), X-ray

Photoelectron spectroscopy (XPS), elemental analysis, proximate analysis, and pH at the point of zero charge (pH_{pzc}) are undertaken.

1.3.2.3 The porous structures of the modified activated carbons by analyzing the adsorption isotherm data of N_2 at -196^oC are determined.

1.3.2.4 The effects of porous structure and heat treatment process on the distribution of surface functional groups are investigated.

1.3.3 Adsorption study of surface-modified activated carbon

1.3.3.1 The adsorptions of water, methanol, and ethanol vapors on the prepared activated carbon (without surface modification) are studied.

1.3.3.2 The role of surface functional groups of the surface-modified activated carbons on the adsorption of water, methanol, and ethanol vapors is investigated.

1.3.3.3 The role of surface functional groups of the surface-modified activated carbons on the single adsorption of heavy metal ions i.e. Pb^{2+} (aq), Zn^{2+} (aq), Cu^{2+} (aq), and Ca^{2+} (aq) and the binary mixture of Pb^{2+}/Cu^{2+}, Pb^{2+}/Zn^{2+}, Pb^{2+}/Ca^{2+}, Zn^{2+}/Cu^{2+}, and Cu^{2+}/Ca^{2+} is investigated.

1.4 Research Development

This thesis is divided into 6 chapters. **Chapter I** introduces the rationale of this research. The objectives and scope of this research are also presented in this chapter. The basic theories of biomass, wood, activated carbon, and adsorption are provided in **Chapter II**. The literatures of the preparation, surface modification, and adsorption study on wood-based activated carbon are reviewed in this chapter. **Chapter III** presents the preparation of activated carbons from eucalyptus and wattle

woods by chemical activation using H_3PO_4 and physical activation using carbon dioxide CO_2. **Chapter IV** is focused on the surface modification of eucalyptus wood-based activated carbon prepared from H_3PO_4 activation by liquid phase oxidation using HNO_3, H_2O_2, and $(NH_4)_2S_2O_8$ and gas phase oxidation using air. The eucalyptus wood-based activated carbon prepared from CO_2 activation is also used to study the effect of porous structure and heat treatment process on the distribution of surface functional groups. To explore the role of prepared (unmodified) activated carbon and modified activated carbon, the adsorption studies of water, methanol, and ethanol vapors and metal ions are reported in **Chapter V**. Finally, **Chapter VI** concludes the results obtained from Chapter III, Chapter IV, and Chapter V. The recommendations for future study is also presented in this chapter.

1.5 Outcomes of the Research

1.5.1 Knowledge of the optimum preparation conditions for producing activated carbons from eucalyptus and wattle woods will be achieved.

1.5.2 Gaining knowledge on the modification of activated carbon surfaces to achieve varying types and concentrations of surface functional groups.

1.5.3 Understanding the role and effect of surface functional groups on the adsorption process.

1.6 References

Arriagada, R., García, R., Molina-Sabio, M., and Rodríguez-Reinoso, F. (1997). Effect of steam activation on the porosity and chemical nature of activated carbons from *Eucalyptus globulus* and peach stones. **Micropor. Mater.** 8: 123-130.

Foley, N. J., Thomas, K. M., Forshaw, P. L., Stanton, D., and Norman, P. R. (1997). Kinetics of water vapor adsorption on activated carbon. **Langmuir** 13: 2083-2089.

Lillo-Ródenas, M. A., Cazorla-Amorós, D., and Linares-Solano, A. (2005). Behaviour of activated carbons with different pore size distributions and surface oxygen groups for benzene and toluene adsorption at low concentrations. **Carbon** 43: 1758-1767.

Rivera-Utrilla, J. and Sánchez-Polo, M. (2003). Adsorption of Cr(III) on ozonised activated carbon. Importance of Cπ–cation interactions. **Wat. Res.** 37: 3335-3340.

Tancredi, N., Cordero, T., Rodríguez-Mirasol, J., and Rodríguez, J. J. (1996). Activated carbons from Uruguayan eucalyptus wood. **Fuel** 75: 1701-1706.

CHAPTER II

THEORY AND LITERATURE REVIEW

2.1 Biomass

Biomass is a term used for all organic matter such as crop, forestry, and agricultural waste. Biomass is a complex material which is composed of three major components i.e. cellulose, hemicellulose, and lignin.

Cellulose is a linear and long chain polymer made up of repeating units of glucose ($C_6H_{12}O_6$). Cellulose has a crystalline structure and strong strength through hydrogen bonds that develop between OH groups. Hemicellulose is a branched polymer consists of glucose and other sugars units such as galactose, mannose, xylose, rhamnose, and arabinose. In contrast to cellulose which is crystalline and strong, hemicellulose has an amorphous structure with little strength (Kent, 1992). Lignin is a polymer which is composed of phenol units. Lignin is formed by the removal of water from sugars to create aromatic structures (Hon and Shiraishi, 2001). The molecular structures of cellulose, hemicellulose, and lignin are shown in Figure 2.1.

Biomass is widely used as a source of fuel in industries, for example, the use of cassava root to generate electricity in tapioca starch plants, the use of sugar cane bagasse as fuel for boilers in sugar mills, and the use of rice husk as fuel in rice mills.

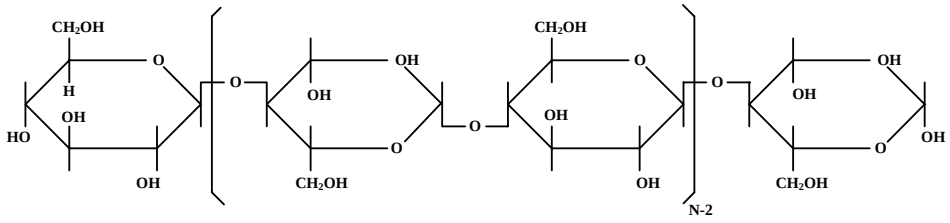

(a) cellulose

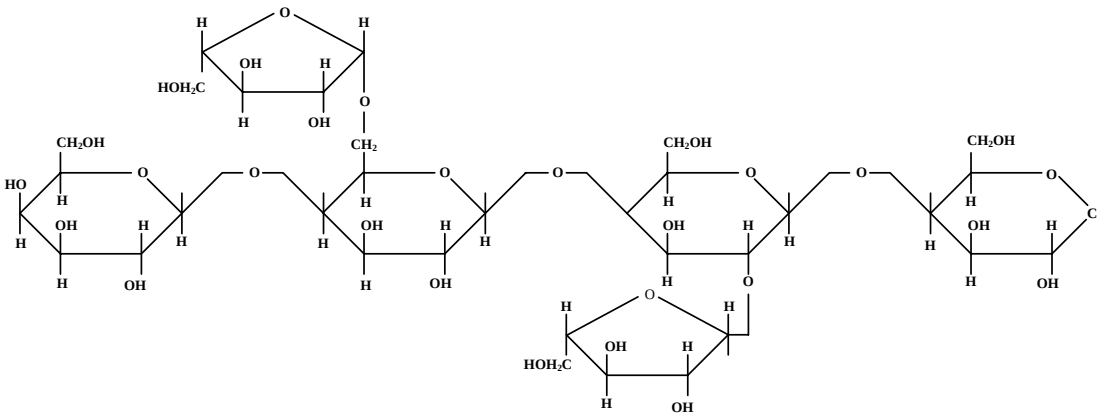

(b) hemicellulose

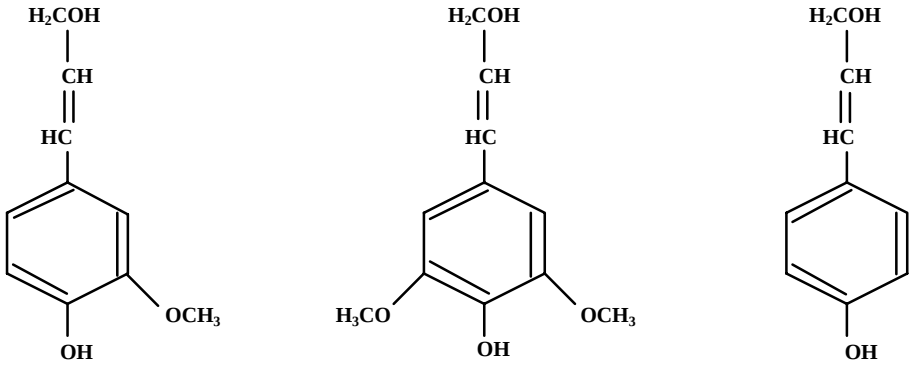

(c) lignin

Figure 2.1 Molecular structures of (a) cellulose, (b) hemicellulose, and (c) lignin (Jagtoyen and Derbyshire, 1998).

2.2 Wood

Wood is a polymer composite and may be divided into two major groups i.e. cell structure and all other substances which are commonly called extractive (Hon and Shiraishi, 2001).

Cell structure consists of cellulose, hemicellulose, and lignin while extractive is not part of the wood structure but it contributes to properties such as color, odor, taste, density, and decay resistance. Extractive includes tannin, starch, oil, resin, gum, latex, fatty acid, fat, and wax. These components are termed extractive because they can be removed from wood by extraction with solvents such as water, alcohol, acetone, benzene, or ether (Rowell, Young, and Rowell, 1997).

All wood species are classified as either hardwood or softwood. Hardwood is the broad-leafed, deciduous tree which drops its leaves at the end of the growing season while softwood is evergreen tree. Hardwood is referred to as porous wood while softwood is referred as nonporous wood (The United States Department of Agriculture, Forest Products Laboratory, 1999). Figure 2.2 shows the difference in the structure and Table 2.1 shows the chemical composition of both woods. From Table 2.1, it is noted that hardwood has a higher proportion of cellulose and hemicellulose than softwood while softwood has a higher proportion of lignin than hardwood. It is anticipated that the difference in cellulosic composition of wood should have an effect on the porous characteristics of the prepared activated carbon.

Eucalyptus and wattle woods are the native plant of Australia. Eucalyptus wood comprises over 700 – 800 species (Soerianegara and Lemmens, 1999) while wattle wood comprises over 650 species (Colman, 2001). As a result, the classification of both woods are complicated and confused. Eucalyptus and wattle

woods can be propagated easily from seed and cuttings. These woods are fast growing woods. The major uses of eucalyptus wood are the production of pulp for paper manufacture and a supplier of firewood which burns very quickly because of the high oil content. The leaves and twigs of many eucalyptus species contain eucalypt oil which is an important product for liniment, cough medication, perfume, soap, detergent, disinfectant, and pesticide. Wattle wood is used for firewood, making furniture, and used as an ornamental and shade tree.

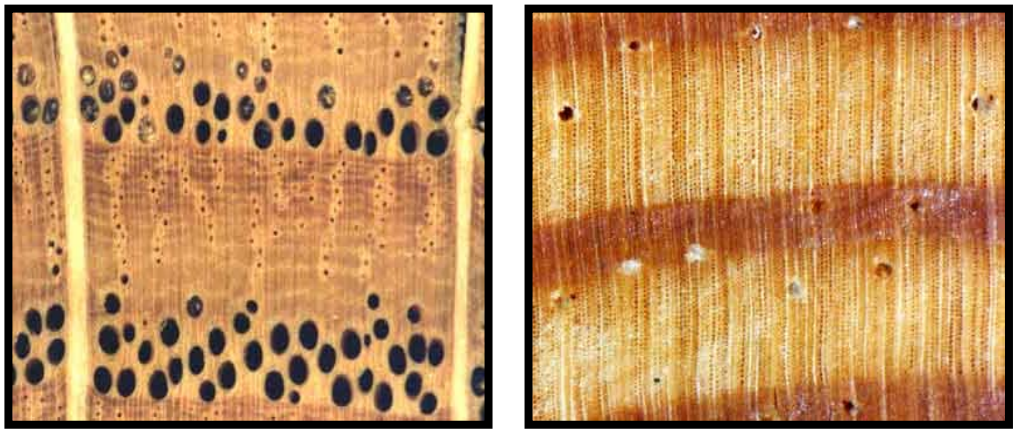

(a) hardwood (b) softwood

Figure 2.2 Structure in cross section of (a) hardwood and (b) softwood (Society of Wood Science and Technology, 2003).

Table 2.1 Chemical composition of wood.

References	Cellulose (wt%)	Hemicellulose (wt%)	Lignin (wt%)
UW Civil Engineering (2002)			
Softwood	42 ± 2	27 ± 2	28 ± 3
Hardwood	45 ± 2	30 ± 5	20 ± 4
UC Forest Products Laboratory (2003)			
Softwood	40 – 44	25 – 29	25 – 31
Hardwood	43 – 47	25 – 35	16 – 24
Gardner (2003)			
Softwood	40 – 45	25 – 30	25 – 35
Hardwood	40 – 50	25 – 35	15 – 25

2.3 Activated Carbon

Activated carbon is an amorphous solid with a large surface area and pore volume. It contains hydrophobic graphene layers and hydrophilic functional groups, therefore it is able to adsorb a wide variety of molecules in both liquid and gas phases. Figure 2.3 represents schematic structure of activated carbon which consists of aromatic sheets and strips, often bent. Activated carbon has been widely used for gas separation, the recovery of solvent, the removal of organic pollutant from drinking water, and as a catalyst support.

Figure 2.3 A schematic representation of the structure of activated carbon (Bansal, Donnet, and Stoeckli, 1988).

Activated carbon can be produced from a variety of carbonaceous materials including wood, agricultural by-products, coal, petroleum coke, and tyre. Approximately half of the raw materials used for activated carbon production are lignocellulosic materials (Bansal, Donnet, and Stoeckli, 1988 quoted in Durán-Valle, Gómez-Corzo, Pastor-Villegas, and Gómez-Serrano, 2005). The choice of raw material depends on its availability, cost, and purity but the manufacturing process and application of the product are also important considerations. Properties of commercial activated carbons produced from wood are shown in Table 2.2.

Table 2.2 Typical properties of commercial activated carbons produced from wood.

Manufacturer	BET surface area (m^2/g)	Total pore volume (cm^3/g)	Ash (wt%)	Moisture (%)	Iodine Number	References
Westvaco						Howe-Grant
WV-A 1100	1750	1.2	–	10	–	(1992)
SA-20	1400 – 1800	2.2 – 2.5	3 – 5	–	> 1000	
Winfield						Winfield
WF-12	1000	–	8	12	950	Industries
WF-22S	1400	–	4	10	–	(2005)
Norit						Jonge, Breure,
CA1	1250	1.55	4	–	900	and Andel (1996)
ELF						Seippel, Ulbig,
L3S	1150	0.659	–	–	–	and Schulz
CPL	1700	1.122	–	–	–	(2000)

2.3.1 Manufacture of activated carbon

There are two manufacturing processes to produce activated carbon i.e. physical and chemical activation.

2.3.1.1 Physical activation

There are two physical activation methods i.e. one-step procedure and two-step procedure. In the two-step procedure, raw material is carbonized in an inert atmosphere at temperature between 400 – 800^{o}C to produce

char with rudimentary porosity and the resulting char is activated at high temperatures (800 – 1100^{o}C) with activating gases (e.g. CO_2, air, steam, or a mixture of these gases) to further develop the surface area and porosity. During carbonization, the moisture and volatile matter are removed off as CO, CO_2, H_2, CH_4, and other hydrocarbons then char with high carbon content is produced. By eliminating the need for a separate carbonization process, the two steps can be combined into a one-step procedure. The one-step activation is achieved by heating at 600 – 900^{o}C in the presence of activating agent. The one-step procedure is preferable than two-step procedure because of lower activation temperature used, thereby reducing production cost in terms of energy.

2.3.1.2 Chemical activation

Chemical activation is a single step method. In this method, the raw material is first impregnated with a chemical activating agent and then carbonized in an inert atmosphere at temperatures in the range from 400 – 800^{o}C. The temperature used in chemical activation is lower than that used in the physical activation. The activated carbon is then washed with water to remove the chemical agent. Then, the activated carbon is dried.

Chemical activating agents used are dehydrating agents that inhibit the formation of tar and other by-products, thus enhancing the yield of carbon (Howe-Grant, 1992). Examples of chemical activating agents are metal substances (such as $ZnCl_2$ and $AlCl_3$), alkali and alkaline earth metal substances (such as KOH, K_2CO_3, NaOH, Na_2CO_3, or $MgCl_2$), and some acids (such as H_3PO_4 and H_2SO_4). Activated carbon with very high surface area has been achieved by chemical activation compared with physical activation due to the effectiveness of chemical

activating agents. The other advantages of chemical activation are lower energy cost and higher product yield due to lower activation temperature than physical activation. A problem associated with chemical activation is the incorporation of impurities in the activated carbon as a result of the impregnation of chemical agent.

2.3.2 Pore size and classification of activated carbon

Pore size of activated carbon is classified by the International Union of Pure and Applied Chemistry (IUPAC) as micropore (pore width < 2 nm), mesopore (pore width 2 – 50 nm), and macropore (pore width > 50 nm) (Howe-Grant, 1992).

Activated carbon is classified on the basis of its particle size and particle shapes into two general forms i.e. granular activated carbon (GAC) and powdered activated carbon (PAC). PAC has an average particle size of 15 – 25 μm while GAC has a larger size. Thus, PAC presents a higher external surface area per unit weight than GAC (Bansal et al., 1988).

2.3.3 Applications of activated carbon

2.3.3.1 Liquid phase applications

Liquid phase application accounts for nearly 80% of the total use of activated carbon (Burchell, 1999). Activated carbon used in liquid phase applications typically has a high fraction of macropore. This is to permit the liquid phase molecule to diffuse more rapidly into the rest of the pore structure. Activated carbon for liquid phase application is produced from low-density material such as sawdust or peat (Bansal et al., 1988). Table 2.3 shows the applications of activated carbon in liquid phase.

Table 2.3 Applications of activated carbon in liquid and gas phase (Howe-Grant, 1992).

	Applications
Liquid phase	• *Potable water treatment*: remove toxic and organic material • *Groundwater remediation*: adsorb contaminant • *Industrial and municipal wastewater treatment*: remove residual toxic and organic compound after the primary filtration and secondary biological treatment • *Sweetener decolorization*: purify of sugar and corn syrup • *Chemical processing*: remove impurity to achieve high quality (for example remove organic contaminant from solution in the production of alum, soda ash and, potassium hydroxide) • *Food, beverage and cooking oil production*: remove taste and odor from vodka and in the production of alcoholic beverages
Gas phase	• *Solvent recovery* • *Gasoline emission control*: capture gasoline vapor that escape from venting in automotive fuel systems • *Adsorption of radio nuclides*: control krypton and xenon radio nuclides from nuclear power plant • *Protection against atmospheric contaminant*: filter breathing air to protect against a variety of toxic or noxious vapor including war gas, industrial chemical, solvent, and odorous compounds • *Process stream separation*: separate aromatic compound vapor from lighter vapor in petroleum refining process stream and to recover gasoline component from natural gas

2.3.3.2 Gas phase applications

This application accounts for about 20% of the total use of activated carbon (Burchell, 1999). Activated carbon used in gas phase application requires smaller pore size while activated carbon for liquid phase application tends to have larger pore size. Activated carbon for gas phase application is hard and dense granular material produced from high-density raw material such as coconut shell, palm kernel shell, coal, or coke (Bansal et al., 1988). Table 2.3 also shows the applications of activated carbon in gas phase.

2.3.4 The surface chemistry of activated carbon

The surface chemistry of activated carbon determines their acid–base, adsorptive, hydrophilic–hydrophobic, and catalytic properties (Jankowska, Świątkowski, and Choma, 1991). It is related to the presence of heteroatoms rather than carbon within the carbon matrix. The most common heteroatoms are oxygen, nitrogen, phosphorus, hydrogen, chlorine, and sulphur. These heteroatoms are built into a carbon matrix in the forms of functional groups. Functional groups can be acidic or basic in character.

2.3.4.1 Surface functional groups

The concentration and type of functional groups incorporated on activated carbon surface are dependent on the modification method and raw material. Oxygen and nitrogen functional groups are common functional groups incorporated on activated carbon surfaces, usually on the edges of graphene layers by various methods, which influence the physical and chemical properties of activated carbon surfaces.

Oxygen functional groups

There are two different modification methods used to incorporate oxygen functional groups on activated carbon surface i.e. liquid phase and gas phase oxidation. Liquid phase oxidation involves the reaction between the activated carbon surface and oxidizing solutions such as HNO_3, H_2O_2, $(NH_4)_2S_2O_8$, H_2SO_4, $HClO_4$, and NaOCl. Gas phase oxidation involves the reaction of activated carbon surface with oxidizing gases such as O_2, O_3, and air.

The presence of oxygen functional groups gives activated carbon an acid–base character (Jankowska, Świątkowski, and Choma, 1991). Examples of acidic oxygen functional groups are carboxyl, phenol, and lactone while carbonyl and chromene are typical of basic character. Acidic and basic oxygen functional groups are shown in Figure 2.4 (a) and (b), respectively. The acidic functional groups on activated carbon surface can increase the adsorption capacities of metal cations and basic dyes, whereas basic functional groups can increase the adsorption capacities of dyes with anionic characteristics (Pereira, Soares, Órfão, and Figueiredo, 2003; Attia, Rashwan, Khedr, 2006).

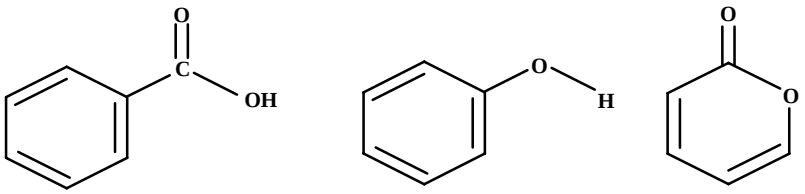

carboxylic acid (pKa 3 – 6) | phenolic (pKa 8 – 11) | lactone (pKa 7 – 9)

(a) acidic oxygen functional groups

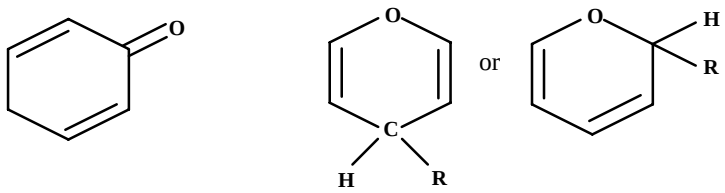

carbonyl | chromene

(b) basic oxygen functional groups

Figure 2.4 Types of (a) acidic and (b) basic oxygen functional groups.

Nitrogen functional groups

Nitrogen functional groups are incorporated on activated carbon surface by ammonia or HCN treatment (Lahaye, 1998). Figure 2.5 shows the types of nitrogen functional groups. The nitrogen functional groups on activated carbon surface can increase the adsorption of phenol and acidic gas such as SO_2 (Shen, Li, and Liu, 2008).

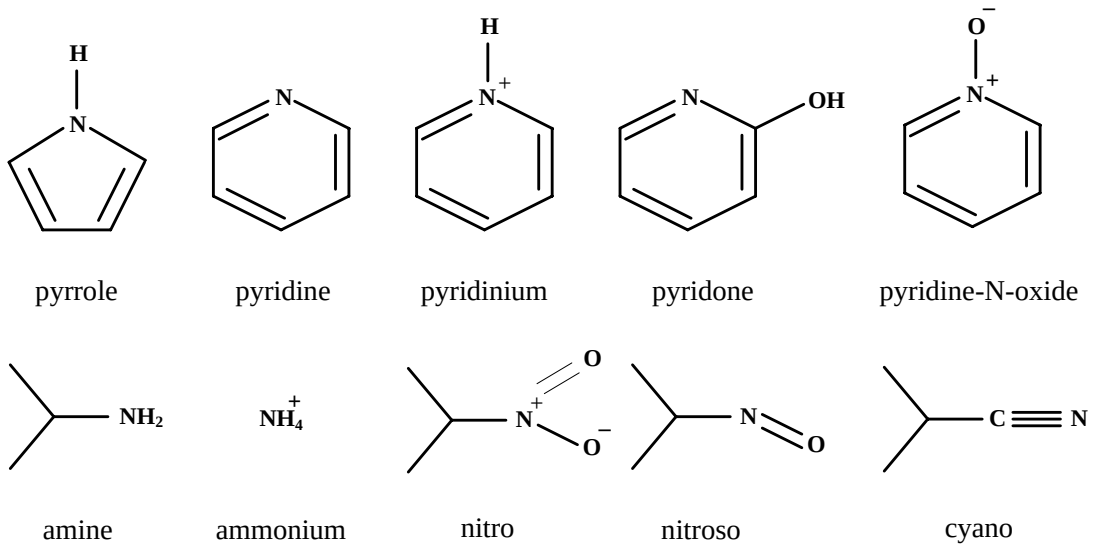

Figure 2.5 Types of nitrogen functional groups.

2.3.4.2 Method of analysis of surface functional groups

Analytical techniques consisting of acid/base titration, Fourier Transform Infrared spectroscopy (FTIR), X-ray Photoelectron spectroscopy (XPS), and pH at the point of zero charge (pH_{pzc}) have been used to characterize surface functional groups on activated carbon surfaces.

Acid/base titration

The classical acid/base titration approach is Boehm's method. This method involves selective neutralization of acidic oxygen groups with bases of various strengths. This method assumes that the following groups become neutralized as follows (Boehm, 1994): carboxylic groups in a solution of sodium bicarbonate ($NaHCO_3$), carboxylic and lactonic groups in a solution of sodium carbonate (Na_2CO_3), carboxylic, lactonic, and phenolic groups in a solution of sodium hydroxide (NaOH), and carboxylic, lactonic, phenolic, and carbonyl groups in a solution of sodium ethoxide ($NaOC_2H_5$). Conversely, the basic oxygen groups on

activated carbon surface are determined based on the neutralization with hydrochloric acid (HCl).

Fourier Transform Infrared spectroscopy (FTIR)

FTIR is an analytical technique used to identify various functional groups presenting on activated carbon surfaces. This technique measures the absorption of various infrared light wavelengths. Table 2.4 summarizes the wavelength regions of the functional groups present on carbon surfaces.

X-ray Photoelectron spectroscopy (XPS)

XPS is a widely used technique to characterize the surface functional groups in the activated carbon. This method is very sensitive to all chemical elements on the sample but not sensitive to hydrogen or helium. The analysis is based on the binding energies and intensities of photoelectron peaks of carbon, oxygen, nitrogen, or other heteroatoms present on the activated carbon surface. The peaks occur at specific energies related to the binding energies of core electrons emitted from the sample (Brundle, Evans, and Wilson, 1992). The identification of oxygen and nitrogen functional groups is based on the analysis of deconvoluted C_{1s}, O_{1s}, and N_{1s} peaks as shown in Figure 2.6 and the assignment of the XPS peaks is shown in Table 2.5.

Table 2.4 IR assignments of functional groups on carbon surfaces (Fanning and Vannice, 1993 quoted in Figueiredo, Pereira, Freitas, and Orfao, 1999; Shen et al., 2008).

Functional group	**Assignment region (cm^{-1})**		
	1000 – 1500	**1500 – 2050**	**2050 – 3700**
C–O in ethers (stretching)	1000 – 1300		
Alcohols	1049 – 1276		3200 – 3640
Phenolic groups:			
C–OH stretch	1000 – 1220		
O–H bend/stretch	1160 – 1200		2500 – 3620
Carbonates: carboxyl-carbonates	1100 – 1500	1590 – 1600	
aromatic C=C stretching		1585 – 1600	
Quinones		1550 – 1680	
Carboxylic acids (–COOH)	1120 – 1200	1665 – 1760	2500 – 3300
Lactones	1160 – 1370	1675 – 1790	
Carboxylic anhydrides	980 – 1300	1740 – 1880	
C–H stretch			2600 – 3000
N–H, C=N		1560 – 1570	
C–N aromatic ring	1000, 1250, 1355		
C–N	1190		
C=C=N			2040 – 2070
N–O-	1000 – 1300		

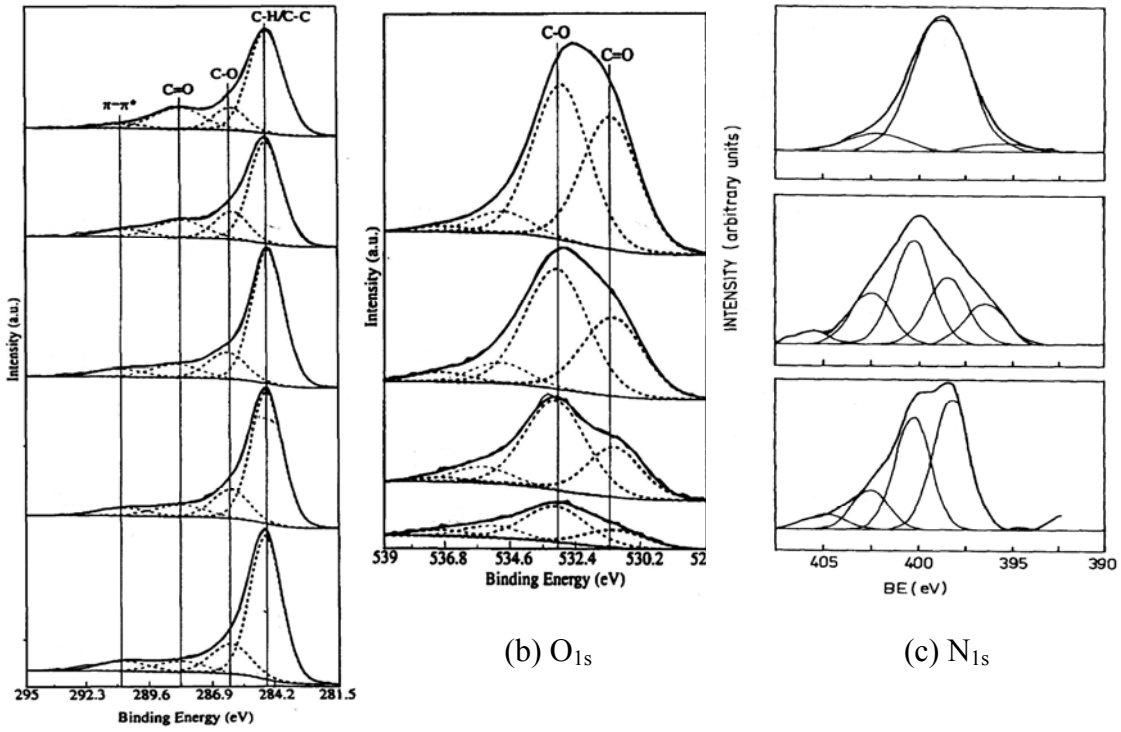

(a) C_{1s} (b) O_{1s} (c) N_{1s}

Figure 2.6 Deconvolution of XPS spectra of (a) C_{1s}, (b) O_{1s}, and (c) N_{1s} peaks (Puente, Pis, Menéndez, and Grange, 1997; Biniak, Szymański, Siedlewski, Swiatkowski, 1997).

Table 2.5 Position and assignments of the XPS peaks.

Spectral region	**Binding energy (eV)**	**Assignment surface group**	**References**
C_{1s}	284.6	Graphitic carbon (C)	Polovina, Babić, Kaluderović, and Dekanski (1997)
	286.0	Phenolic, alcoholic, etheric (C–O–)	
	287.3	Carbonyl or quinone (C=O)	
	288.9	Carboxyl or ether (COO)	
N_{1s}	398.9	Pyridine	Jansen and Bekkum (1995)
	399.9	Amine and amide	
	400.7	Pyrrole	
O_{1s}	531.3	Oxygen doubly bonded to carbon (C=O)	Hontoria-Lucas, López-Peinado, López-González, Rojas-Cervantes, and Martín-Aranda (1995)
	533.1	Oxygen singly bonded to carbon in aromatic rings, in phenols and ethers	Puente et al. (1997)

pH at the point of zero charge (pH_{pzc})

The pH_{pzc} is the pH at which activated carbon has equal amount of positive and negative charges on the surface, resulting in a net zero charge. In other word, the total charge from the cations and anions at the surface is equal to zero but this does not mean that the number of cations versus anions are equal. The surface charges on the activated carbon are important in determining particle interactions.

Figure 2.7 shows the influence of pH on the surface charge. When the pH value of the solution containing activated carbon is below the pH_{pzc} ($pH < pH_{pzc}$), the activated carbon surface becomes positively charged and exhibit an anion exchange capacity. This favors the adsorption of anionic species. When the pH of the solution equals to the pH_{pzc} ($pH = pH_{pzc}$), the activated carbon surface contains a balance of positive and negative charges and exhibit no exchange capacity. At the pH of the solution above the pH_{pzc} ($pH > pH_{pzc}$), the activated carbon surface becomes negatively charged and exhibit a cation exchange capacity. This favors the adsorption of cationic species (Radovic et al., 1997).

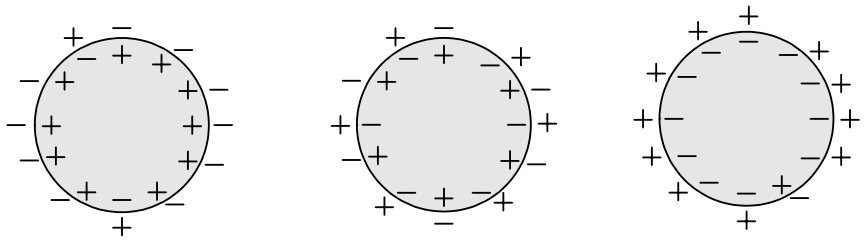

(a) $pH < pH_{pzc}$ (b) $pH = pH_{pzc}$ (c) $pH > pH_{pzc}$

Figure 2.7 The influence of pH on surface charge: (a) $pH < pH_{pzc}$, (b) $pH = pH_{pzc}$, and (c) $pH > pH_{pzc}$ (Leon and Radovic, 1994 quoted in Rodríguez-Reinoso, 1998).

2.4 Adsorption

Adsorption process involves the use of porous solid for removing substances from gas or liquid phase. The porous solid is called adsorbent while the substance which adsorbed is called adsorbate.

2.4.1 Type of adsorption

Adsorption is divided into two types i.e. physical adsorption or physisorption and chemical adsorption or chemisorption.

2.4.1.1 Physical adsorption

In physical adsorption process, the attraction between adsorbate molecules and adsorbent exists by the formation of intermolecular electrostatic i.e. van der Waals forces. These forces are relatively weak. During the process of physical adsorption, there is no breakage of the covalent structure of the adsorbate taking place so this adsorption process is very rapid with the equilibrium established quickly. Physical adsorption is an exothermic and reversible process.

2.4.1.2 Chemical adsorption

Chemical adsorption involves the transfer of electrons between adsorbent and adsorbate with the formation of chemical bonds by chemical reaction so these interactions are stronger than the force of physical adsorption. Chemical adsorption is more specific between adsorbate and surface site of adsorbent. Chemical adsorption is a slow reaction process for which the equilibrium may take a long time to achieve. The differences in the physical adsorption and chemical adsorption process are summarized in Table 2.6.

Table 2.6 Comparison of parameters of type of adsorption process (Ruthven, 1997).

Parameter	**Physical adsorption**	**Chemical adsorption**
Heat of adsorption	low	high
Nature of adsorbed phase	monolayer or multilayer	monolayer only
Temperature range	only significant at relative low temperatures	possible over a wide range of temperature
Temperature dependence of uptake (with increasing temperature)	decrease	increase
Forces of adsorption	no electron transfer although polarization of adsorbate may occur	electron transfer leading to bond formation between adsorbate and adsorbent
Rate of adsorption (at 273 K)	fast	slow
Desorption	easy by reduced pressure or increased temperature	difficult (high temperature required to break bonds)
Desorbed species	adsorbate unchanged	may be different to original adsorptive
Specificity	non-specific	very specific

2.4.2 Adsorption isotherms

The equilibrium relationship between an adsorbate and adsorbent is usually defined in terms of an adsorption isotherm which expresses the amount of adsorbate being adsorbed as a function of the fluid-phase concentration or partial pressure for gas and vapor at a constant temperature. IUPAC has extended the original adsorption isotherm classification proposed by Brunauer, Deming, Deming, and Teller (Type I – Type V) to give six classes of adsorption isotherms as shown in Figure 2.8 (Rouquerol, Rouquerol and Sing, 1999).

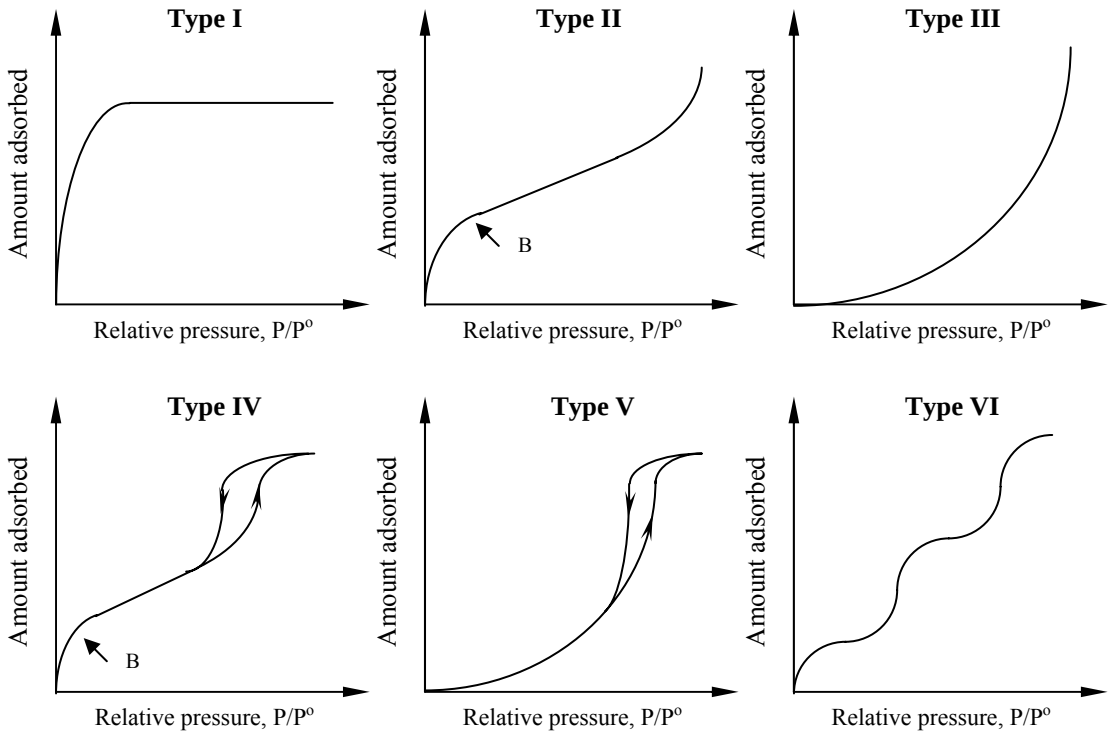

Figure 2.8 Types of adsorption isotherms according to the IUPAC classification.

Type I isotherm is concave to the relative pressure (P/P^o) axis. This isotherm rises sharply at low relative pressure and reaches a plateau as relative pressure approaches unity. Type I isotherm represents system where only monolayer adsorption occurs.

Type II isotherm is concave to the relative pressure axis then almost linear and finally convex to the relative pressure axis. At the knee of the isotherm (point B), the uptake is usually considered to represent the completion of the monolayer and the beginning of the formation of the multimolecular layer (multilayer). This isotherm is obtained with non-porous or macroporous adsorbents which allow unrestricted monolayer-multilayer adsorption to occur at high relative pressures.

Type III isotherm is convex to the relative pressure axis and therefore without the knee of the isotherm. This isotherm indicates the weak adsorbent-adsorbate interactions. Type III isotherm is not common.

Type IV isotherm is closely related to the Type II isotherm at low relative pressure but tends to level off at high relative pressure. This isotherm exhibits a hysteresis loop which is associated with the filling and emptying of the mesopores by capillary condensation.

Type V isotherm is initially convex to the relative pressure axis and also tends to level off at high relative pressure. This isotherm is similar to Type III isotherm except there is an existence of a hysteresis loop. Type V isotherm is relatively rare.

Type VI isotherm is a stepped isotherm. This isotherm is associated with layer-by-layer adsorption on a highly uniform surface. The sharpness of the steps is dependent on the system and the temperature. Type VI isotherm is also relatively rare.

2.5 Review of literatures

This part gives a review of past researches on the preparation, surface modification, and adsorption study of wood-based activated carbon.

2.5.1 Preparation of wood-based activated carbon

2.5.1.1 Physical activation

There is only two research groups that studied the preparation of activated carbon from eucalyptus wood by physical activation i.e. Tancredi, Cordero, Rodríguez-Mirasol, and Rodríguez in 1996 and Arriagada, García, Molina-Sabio, and Rodríguez-Reinoso in 1997. Tancredi et al. (1996) prepared activated carbon from *Eucalyptus grandis* sawdust. They compared the results of the activating agents used i.e. CO_2, CO_2–O_2 mixtures, and steam. The particle size of 0.5 – 1.6 mm of raw wood material was selected. The carbonization was performed at 400, 600, and 800^oC for 2 hours under N_2 flow (heating rate 10^oC/min). The carbonization temperature of 800^oC was selected for all activating agents because this temperature ensured extensive devolatilization of raw wood material and this char had high BET surface area. For CO_2 activation, the activation was performed at 800^oC with different periods of time (not reported) to obtain activated carbons with different burn-off level (CO_2 flow 200 cm^3/min and heating rate 10^oC/min). The results showed that CO_2 activation developed mainly microporous activated carbon and the BET surface area increased as burn-off was increased. For CO_2–O_2 activation, the activation was carried out at

800°C for 3 hours with different concentration of O_2 to obtain activated carbon with different burn-off (total CO_2–O_2 flow 200 cm^3/min and heating rate 10°C/min). They found that the presence of O_2 in the CO_2 atmosphere increased the mesopore and macropore volume of activated carbon compared to CO_2 activation. For steam activation, the activation was performed at 750°C and 800°C with different periods of time (not reported) to obtain activated carbon with different burn-off (steam flow 0.144 cm^3/min and heating rate 10°C/min). The obtained activated carbon indicated that steam activation gave higher development of mesopore and macropore volume than with CO_2 and CO_2–O_2 activation.

Arriagada et al. (1997) prepared activated carbon by carbonizing *Eucalyptus globulus* chip at 870°C for 2 hours. The char was crushed to particle size 1 – 2 mm and then activated at 800°C for 5 – 10 hours under steam flow of 140 cm^3/min. They found that the surface area of activated carbons increased as activation time was increased in the range of 658 – 801 m^2/g.

The research groups that prepared activated carbon by physical activation from other types of wood are Sánchez, Elguézabal, and Saenz in 2001, Zhang et al. in 2004, Ismadji, Sudaryanto, Hartono, Setiawan, and Ayucitra in 2005, and Kumar, Shivakamy, Miranda, and Velan in 2006. Sánchez, Elguézabal, and Saenz (2001) prepared activated carbon from *Quercus agrifolia* (oak) wood waste. The carbonization was performed at 450°C for 2 hours (heating rate 20°C/min). The char was crushed to obtain particle sizes of 0.5 – 1.4 mm. The activation was carried at 800, 840, and 880°C under CO_2 flow of 500 cm^3/min by changing holding time (not reported) to obtain activated carbon with different yield. Activated carbons with

predominantly microporous with BET surface area in the range of 510 – 1201 m^2/g were obtained.

Zhang et al. (2004) prepared activated carbon from oak wood waste by carbonization at 500°C under N_2 following by activation with CO_2 at 700°C and 800°C for 1 hour and 2 hours (CO_2 flow 24 cm^3/min). They found that BET surface area of the prepared activated carbons increased with increased activation temperature (at the same activation time) and activation time (at the same activation temperature). The activated carbons produced had the BET surface area ranging from 400 to 1000 m^2/g.

Ismadji et al. (2005) used teak sawdust as a starting material. They carbonized the sawdust at 600°C with the heating rate of 20°C/min and held at this temperature for 1 hour under N_2 flow of 150 cm^3/min and under vacuum condition (total pressure around 20 kPa). The activation was performed at 750 – 900°C and held for 2 – 10 hours under steam flow of 0.02 g/min. Activated carbons with BET surface area in the range of 438 – 1150 m^2/g were obtained.

Kumar et al. (2006) prepared activated carbon from rubber wood sawdust by steam activation. The starting wood materials with particle size 0.46, 0.93, and 1.31 mm were carbonized at 400°C for 1 hour. The activation was performed at 600, 700, and 750°C for 1 – 4 hours under steam atmosphere. The results showed that the iodine number and BET surface area decreased with increased in particle size (at the same activation temperature and activation time). The iodine number and BET surface area increased with increase of activation temperature (at same activation time) for all particle sizes. The iodine number also increased with increasing activation time (at the same activation temperature).

It can be seen that there are limited number of works on the preparation of eucalyptus wood-based activated carbon and no research has been reported on preparing wattle wood-based activated carbon by physical activation. Therefore, this research will be directed toward studying the preparation of activated carbon by physical activation from these woods to gain knowledge of the optimum preparation conditions. Moreover, there have been no reports on studying the effect of CO_2 concentration during the activation step, this aspect will be included and studied in the present work.

2.5.1.2 Chemical activation

There are some research groups that studied the preparation of activated carbon from wood by chemical activation. Díaz-Díez, Gómez-Serrano, Fernández-González, Cuerda-Correa, and Macías-García (2004) prepared activated carbons from chestnut, cedar, and walnut wood shavings by using H_3PO_4. The raw materials were impregnated with 36 wt% and 85 wt% H_3PO_4 for 4 hours. The impregnated samples were carbonized at 450^oC (heating rate 5^oC/min) for 4 hours under N_2 flow of 100 cm^3/min. The results showed that activated carbons activated with 36 wt% H_3PO_4 had higher BET surface area than activated carbons activated with 85 wt% H_3PO_4. This suggests that the effect of chemical activation with H_3PO_4 is better when lower acid concentration is used.

Gómez-Serrano, Cuerda-Correa, Fernández-González, Alexandre -Franco, and Macías-García (2005) prepared activated carbon from chestnut wood with particle size 3 – 5 mm. The wood material was impregnated with three different concentrations of solution of phosphoric acid i.e. 1:1, 1:2, and 1:3 water/H_3PO_4 proportions, for 1 – 4 hours. Then, the sample was carbonized at 500^oC

(heating rate 5°C/min) for 4 hours under N_2 flow of 100 cm^3/min. The results showed that BET surface area and total pore volume of the obtain activated carbons increased with increased acid concentration (at the same impregnation time). At the same acid concentration, BET surface area and total pore volume of the activated carbons also increased with the increase in impregnation time from 1 hour to 3 hours and then decreased with increased impregnation time from 3 hours to 4 hours.

López de Letona Sánchez et al. (2006) used cedar wood as a raw material for the preparation of activated carbon by H_2O_2 activation. The raw wood material was impregnated with 1 – 9 N H_2O_2 for 4 hours. The sample was then carbonized at 600, 700, and 800°C (heating rate 5°C/min) for 2 hours under N_2 flow of 100 cm^3/min. The sample prepared by 9 N H_2O_2 and carbonized at 600°C was subsequently activated under CO_2 flow of 100 cm^3/min at 700, 800, and 900°C (heating rate 5°C/min) for 4 hours. The results showed that the concentration of H_2O_2 did not significantly affect the BET surface area of the resulting activated carbons for all carbonization temperatures. At the same concentration of H_2O_2, BET surface area of the activated carbons increased with increased carbonization temperature from 600°C to 700°C and then decreased at higher temperatures from 700°C to 800°C. The results also showed that activated carbons subsequently activated with CO_2 showed much higher BET surface area than activated carbons without CO_2 activation.

Cuerda-Correa, Díaz-Díez, Macías-García, and Gañán-Gómez, (2006) used cedar wood as a raw material for the preparation of activated carbon by H_2SO_4 activation. The raw wood material was impregnated with 5, 7, and 10 M H_2SO_4 at 80°C under reflux for 8 hours. The sample was then carbonized at 600, 700, and 800°C (heating rate 5°C/min) for 2 hours under N_2 flow of 100 cm^3/min. The

sample prepared by 7 M H_2SO_4 and carbonized at 700^oC was subsequent activated under CO_2 flow of 100 cm^3/min at 700, 800, and 900^oC (heating rate 5^oC/min) for 2 hours and 4 hours. It was found that the BET surface area of the resulting activated carbons increased with increased concentration of H_2SO_4 from 5 M to 7 M, then the BET surface area decreased with increased acid concentration from 7 M to 10 M for all carbonization temperatures. The results also showed that activated carbons subsequently activated with CO_2 showed much higher BET surface area than activated carbons with no activation with CO_2.

Budinova et al. (2006) prepared activated carbon from birch wood by using H_3PO_4. The raw material with particle size 0.5 – 1 mm was impregnated with 20 wt% and 50 wt% H_3PO_4 at room temperature for overnight using weight ratio of acid solution:wood equal to 1, 1.5, and 2. The impregnated samples were carbonized under N_2 atmosphere at 600^oC (heating rate 3^oC/min) for 1 hour and steam at 700^oC for 2 hours. Increasing the concentration of H_3PO_4 (at constant weigh ratio of solution to raw material mass) resulted in an increase of iodine number of the obtained activated carbons for both carbonization conditions. The iodine number was found to increase with the increase in weight ratio of acid solution:wood from 1 to 1.5 then the iodine number decreased with higher weight ratio of acid solution:wood from 1.5 to 2. However, the activated carbons obtained from steam carbonization showed higher iodine number than those obtained from N_2 carbonization. The obtained activated carbons from N_2 carbonization were further activated under steam flow of 120 cm^3/min at 600^oC for 1 hour. These activated carbons showed higher iodine number than the activated carbons obtained from N_2

carbonization but lower iodine number than the activated carbons obtained from steam carbonization.

It is observed that that there have been no investigations on the preparation of eucalyptus or wattle wood-based activated carbon by chemical activation. Therefore, this research will focus on the preparation of activated carbon by chemical activation from these woods to gain better knowledge of the optimum preparation conditions. In addition, the preparation conditions such as carbonization temperature and carbonization time have not been systematically studied in the preparation of wood-based activated carbon. As a result of these shortcomings, this work will include the effects of these conditions on the preparation of wood-based carbons. Another topic of research interest is the combined use of chemical and physical activation i.e. impregnation of raw material with chemical agents and followed by activation in activating agent such as CO_2 or steam. However, this topic was not included in this work but warrants further investigation.

2.5.2 Surface modification of wood-based activated carbon

There have been a number of research groups which studied the surface modification of wood-based activated carbon. Salame and Bandosz (1999) used commercial wood-based activated carbon i.e. WVA 1100 (H_3PO_4 activation) oxidized with HNO_3, $(NH_4)_2S_2O_8$, and H_2O_2. The raw wood material was oxidized with 15 M HNO_3 for 24 hours at room temperature, saturated solution of $(NH_4)_2S_2O_8$ in 1 M H_2SO_4) for 18 hours at room temperature, and a mixture of 50 ml H_2O_2 and 50 ml 1 M H_2SO_4 for 1 hour at 50^oC. The results from Boehm titration showed that oxidation introduced a significant amount of oxygen functional groups on the activated carbons in the following order: HNO_3 oxidized carbon > $(NH_4)_2S_2O_8$ oxidized carbon > H_2O_2

oxidized carbon. The obtained FTIR results of the activated carbons after oxidation showed the peaks that were characteristic of oxygen functional groups. The porous structure parameters i.e. BET surface area and micropore volume of the activated carbon decreased after oxidation. The trend of the BET surface area of the activated carbon were original carbon > H_2O_2 oxidized carbon > $(NH_4)_2S_2O_8$ oxidized carbon > HNO_3 oxidized carbon and the trend of the micropore volume of the activated carbon were original carbon > H_2O_2 oxidized carbon ≅ $(NH_4)_2S_2O_8$ oxidized carbon > HNO_3 oxidized carbon.

Cordero et al. (2002) modified activated carbon prepared from carbonization of *Eucalyptus grandis* sawdust by HNO_3. The raw wood material was carbonized at 800^{o}C in N_2 atmosphere and then activated by CO_2 at 800^{o}C and air at 400^{o}C. Both activated carbons were oxidized with 70 wt% HNO_3 at 80^{o}C. For both activated carbons, the results from XPS showed that the surface atomic concentration obtained from O_{1s} spectral region increased (from 6.68% to 19.26% for CO_2 activation sample and 12.61% to 21.22% for air activation sample) while the surface atomic concentration obtained from C_{1s} spectral region decreased (from 93.32% to 79.66% for CO_2 activation sample and 87.12% to 77.37% for air activation sample) after oxidation. The porous properties i.e. BET surface area and micropore volume decreased after oxidation for both activated carbons. The BET surface area decreased from 890 m^2/g to 730 m^2/g and 600 m^2/g to 240 m^2/g for CO_2 and air activation samples, respectively. The micropore volume decreased from 0.41 cm^3/g to 0.34 cm^3/g and 0.26 cm^3/g to 0.11 cm^3/g for CO_2 and air activation samples, respectively.

Menéndez, Phillips, Xia, and Radovic (1996) studied the heat treatment process in order to remove the surface functional groups on activated carbon. The

commercial wood-based activated carbon i.e. NORIT C (H_3PO_4 activation) was used and then was heat treated under N_2 atmosphere at 950°C and H_2 atmosphere at 650, 800, and 950°C for 3 hours (flow 150 cm^3/min and heating rate 25°C/min). The results from electrophoretic mobility and microcalorimetric measurement techniques showed that heat treatment in an inert atmosphere was effective in removing oxygen functional groups on activated carbon surface. Elemental analysis results showed the decrease of oxygen content after heat treatment. For H_2 treatment, the oxygen content decreased as heat treatment temperature was increased. H_2 treatment decreased more oxygen content than N_2 treatment at the same temperature (950°C). The pH_{pzc} of the activated carbon increased after heat treatment because of the removing of acidic functional groups. The heat treatments did not produce any drastic changes in the textural properties of activated carbons.

Considine, Denoyel, Pendleton, Schumann, and Wong (2001) studied the modification of wood-based activated carbon by heat treatment process. The wood-based activated carbon which was activated by H_3PO_4 was heat treated under argon at 400 – 1000°C for 1 hour. The results from elemental analysis showed that oxygen content of heat treated activated carbons decreased with increased heat treatment temperature from 600°C to 1000°C. However, the oxygen content of activated carbon heat treated at 400°C still had the same value as that of the original activated carbon. The results from N_2 adsorption isotherm at −196°C showed that the micropore and total pore volume of heat treated activated carbon increased and higher than the original activated carbon until heat treatment temperature of 600°C was reached then the micropore and total pore volume decreased with further increase in heat treatment temperature.

It is observed that the effect of some conditions such as concentration of oxidizing agent and time of oxidation were not studied in the modification of wood-based activated carbon. Therefore, the study of influence of these modification conditions on the presence of oxygen functional groups is included in this research. It is also suggested that the effect of porous structure of the original activated carbon on the surface functional groups of the oxidized activated carbon be also studied. To complete the thesis work, gas phase oxidation as a mean to increase surface groups on carbon surface and the effect of heat treatment in controlling the amounts and types of oxygen functional groups are also carried out.

2.5.3 Adsorption on wood-based activated carbon

2.5.3.1 Liquid phase adsorption

The study of metal ion adsorption by using modified wood-based activated carbon is due to Cordero et al. (2002) who studied the adsorption of Cr(III) from aqueous solution. The activated carbons used in their work were prepared from carbonization of *Eucalyptus grandis* sawdust at 800^{o}C in N_2 atmosphere and then activated by CO_2 at 800^{o}C and air at 400^{o}C. Both activated carbons were treated with 70 wt% HNO_3 at 80^{o}C. The results indicated that oxidation of these activated carbons greatly enhanced the adsorption capacity of Cr(III) because the oxygen surface functional groups act as specific sites to Cr(III) adsorption.

The works on studying metal ion adsorption by using unmodified wood-based activated carbon include those by Bello, Cid, García, and Arriagada in 1999 (adsorption of Cr(VI) and Hg(II) on *Eucalyptus globulus* chip activated carbon), Mohan and Chander in 2001 (single metal adsorption of Fe(II) and Mn(II) and multi-component of Fe-Mn, Fe-Zn, Fe-Ca, Fe-Mn-Zn, and Fe-Mn-Zn-Ca on commercial

wood-based activated carbons), Karthikeyan, Rajgopal, and Miranda in 2005 (adsorption of Cr(VI) on *Hevea Brasilinesis* (rubber wood) sawdust activated carbon), Kalavathy, Karthikeyan, Rajgopal, and Miranda in 2005 (adsorption of Cu(II) on rubber wood sawdust activated carbon), and Budinova et al. in 2006 (adsorption of Hg(II) on birch wood-based activated carbon).

Previous investigations on studying adsorption from solution other than metal ions by modified wood-based activated carbon have been reported by Considine et al. in 2001 and Salame and Bandosz in 2003. Considine et al. (2001) studied the adsorption of 2-methylisoborneol (MIB), which is the most common odor found in water, on heat treated wood-based activated carbon (H_3PO_4 activation). The activated carbon was modified by heat treatment under argon at 400 – 1000^oC for 1 hour. The results showed that oxygen content of heat treated activated carbons decreased with increased heat treatment temperature. The MIB adsorption capacity increased as the oxygen content was decreased.

Salame and Bandosz (2003) used two commercial wood-based activated carbons i.e. WVA 1100 (H_3PO_4 activation at 627^oC) and UMC (further KOH activation of WVA carbon at 1027^oC) in adsorption of phenol from aqueous solution. Both activated carbons were oxidized activated carbons with $(NH_4)_2S_2O_8$ (saturated solution of $(NH_4)_2S_2O_8$ in 1 M H_2SO_4) for 18 hours at room temperature. Oxidation resulted in a decrease in the uptake of phenol. This is due to an increase in the amount of acidic groups on the activated carbon surface after oxidation and capable of removing π–electrons from the carbon aromatic ring matrix, thus causing a decrease in the strength of interactions between the benzene ring of phenol and the carbon's basal planes.

Therefore, this research will be directed toward studying the adsorption of several metal ions including Pb^{2+}, Zn^{2+}, Cu^{2+}, and Ca^{2+} on the modified eucalyptus wood-based activated carbon mainly because of the lack of results from previous investigations. To complete the role of oxygen functionalities on liquid adsorption, the adsorption of binary system of these metal ions are also studied.

2.5.3.2 Gas phase adsorption

To study the effect of surface functional groups of activated carbon on water and methanol vapors adsorption, Bandosz, Jagiello, and Schwarz (1996) used commercial wood-based activated carbon i.e. B4×14 oxidized with HNO_3 and H_2O_2. The raw wood material was oxidized with 15 N for 2 hours at 78^oC and 30% H_2O_2 for 2 hours at 50^oC. The results from Boehm titration indicated that HNO_3 oxidation introduced higher amount of acidic oxygen functional groups on the activated carbons than H_2O_2 oxidation. The results also showed that the water uptake increased after oxidation in the relative pressure (P/P^o) range of 0 – 0.4 for both activating agents with the following order: original carbon < H_2O_2 oxidized carbon < HNO_3 oxidized carbon, which was in agreement with the amount of acidic groups from Boehm titration results. For $P/P^o > 0.4$, the adsorption isotherm of both oxidized carbons showed the crossover of the adsorption isotherm of original carbon with the adsorption capacities at the relative pressure of about 0.9 followed the order: original carbon > H_2O_2 oxidized carbon > HNO_3 oxidized carbon. For methanol vapor, the adsorption uptake was decreased after oxidation in the relative pressure range 0 – 0.9 with the following descending order: original carbon > H_2O_2 oxidized carbon > HNO_3 oxidized carbon.

Salame and Bandosz (1999) used commercial wood-based activated carbon i.e. WVA 1100 (H_3PO_4 activation) oxidized with HNO_3, $(NH_4)_2S_2O_8$, and H_2O_2 to study the effect of surface functional groups on water vapor adsorption. The raw wood material was oxidized with 15 N HNO_3 for 2 hours at room temperature, saturated solution of $(NH_4)_2S_2O_8$ in 1 M H_2SO_4) for 18 hours at room temperature, and a mixture of 50 ml H_2O_2 and 50 ml 1 M H_2SO_4 for 1 hour at 50^oC. The results from Boehm titration showed that oxidation introduced a significant amount of oxygen functional groups on the activated carbons in the following order: HNO_3 oxidized carbon > $(NH_4)_2S_2O_8$ oxidized carbon > H_2O_2 oxidized carbon. They studied the water vapor adsorption in the relative pressure (P/P^o) range of 0 – 0.3. The results signified that the water uptake increased after oxidation in the following order: original carbon < H_2O_2 oxidized carbon < HNO_3 oxidized carbon < $(NH_4)_2S_2O_8$ oxidized carbon, which gave the same trend as the amount of carboxylic group in the oxidized carbons.

Salame and Bandosz (2000) used $(NH_4)_2S_2O_8$ as oxidizing agent for two commercial wood-based activated carbons i.e. WVA 1100 (H_3PO_4 activation at 627^oC) and UMC (further KOH activation of WVA carbon at 1027^oC) in studying adsorption of water and methanol vapors. The isotherms were measured at low relative pressure i.e. $P/P^o < 0.3$. The results showed that the water uptake increased after oxidation for both activated carbons. For methanol, oxidation did not significantly change the adsorption uptake. The adsorption on the oxidized activated carbon was only slightly higher than the original carbon. The adsorption isotherm of oxidized carbon showed the crossover with the adsorption isotherm of original carbon at P/P^o around 0.15. The difference in the uptake of water and methanol at low

relative pressures was related to different mechanisms of the adsorption processes. It was demonstrated that the effect of pore size and pore volume on adsorption uptake is more pronounced in the case of methanol, whereas water adsorption was governed mainly by surface chemistry of activated carbon.

The study of water, methanol, and ethanol vapors adsorption by using unmodified wood-based activated carbon are due to Harding, Foley, Norman, Francis, and Thomas (1998) who used commercial wood-based activated carbon i.e. BAX950 as an adsorbent for water vapor adsorption, Lee and Reucroft (1999) who used activated carbon prepared from white oak by H_3PO_4 activation as an adsorbent for water vapor adsorption, Fletcher and Thomas (2000) who used commercial wood-based activated carbon (BAX950) as an adsorbent for methanol and ethanol vapors adsorption, and Fletcher, Yüzak, and Thomas (2006) who used commercial wood-based activated carbon (BAX950) as an adsorbent for water and methanol vapors adsorption.

In the past researches of water vapor adsorption on modified activated carbon, the adsorption study was focused over the range of relative pressure (P/P^o) from 0 – 0.3, from which the adsorption uptake was increased significantly after oxidation in this range except the work of Bandosz, Jagiello, and Schwarz (1996) who studied the water adsorption over the full relative pressure range 0 – 0.9. However, the study of Bandosz et al. (1996) has shown that the water uptake was increased after oxidation in the relative pressure range of about 0 – 0.4. At higher relative pressure range ($P/P^o > 0.4$), the water uptake of oxidized carbon was found to decrease. Therefore, the present work will cover the study of water adsorption over full relative pressure range (P/P^o 0 – 0.9) using activated carbons that are modified

under suitable conditions. From the work of Salame and Bandosz (1999), they found that the water uptake depended on the amount of carboxylic group. Therefore, this research will use oxidized activated carbon with different distribution of surface functional groups (obtained from heat treatment process) as an adsorbent to verify the role of carboxylic group on water adsorption compared to other functional groups.

The study of adsorption from gas or vapor phase other than water vapor on modified wood-based activated carbon was under taken by Lillo-Ródenas, Cazorla-Amorós, and Linares-Solano (2005). They studied benzene adsorption on heat treated commercial wood-based activated carbon. The original wood-based activated carbon (H_3PO_4 activation) was heat treated with helium flow of 100 cm^3/min at 900^oC using a heating rate of 20^oC/min. This treatment temperature removed most of the surface oxygen functional groups of the activated carbon. The results showed that when reducing the content of surface oxygen functional groups, the activated carbon had higher adsorption capacity for benzene.

2.6 References

Arriagada, R., García, R., Molina-Sabio, M., and Rodríguez-Reinoso, F. (1997). Effect of steam activation on the porosity and chemical nature of activated carbons from *Eucalyptus globulus* and peach stones. **Micropor. Mater.** 8: 123-130.

Attia, A. A., Rashwan, W. E., and Khedr, S. A. (2006). Capacity of activated carbon in the removal of acid dyes subsequent to its thermal treatment. **Dyes Pigments** 69: 128-136.

Bandosz, T. J., Jagiello, J., and Schwarz, J. A. (1996). Effect of surface chemistry on sorption of water and methanol on activated carbons. **Langmuir** 12: 6480-6486.

Bansal, R. C., Donnet, J. B., and Stoeckli, F. (1988). **Active Carbon.** New York: Marcel Dekker.

Bansal, R. C., Donnet, J. B., and Stoeckli, F. (1988). **Active Carbon.** New York: Marcel Dekker. Quoted in Durán-Valle, C. J., Gómez-Corzo, M., Pastor-Villegas, J., and Gómez-Serrano, V. (2005). Study of cherry stones as raw material in preparation of carbonaceous adsorbents. **J. Anal. Appl. Pyrolysis** 73: 59-67.

Bello, G., Cid, R., García, R., and Arriagada, R. (1999). Retention of Cr(VI) and Hg(II) in *Eucalyptus globulus*- and peach stone-activated carbons. **J. Chem. Technol. Biotechnol.** 74: 904-910.

Biniak, S., Szymański, G., Siedlewski, J., Swiatkowski, A. (1997). The characterization of activated carbons with oxygen and nitrogen surface groups. **Carbon** 35: 1799-1810.

Boehm, H. P. (1994). Some aspects of the surface chemistry of carbon blacks and other carbons. **Carbon** 32: 759-769.

Brundle, C. R., Evans, C. A. Jr., and Wilson, S. (1992). **Encyclopedia of Materials Characterization.** Boston: Butterworth-Heinemann.

Budinova, T., Ekinci, E., Yardim, F., Grimm, A., Björnbom, E., Minkova, V., and Goranova, M. (2006). Characterization and application of activated carbon produced by H_3PO_4 and water vapor activation. **Fuel Process. Technol.** 87: 899-905.

Burchell, T. D. (1999). **Carbon Materials for Advanced Technologies.** Netherland: Pergamon.

Colman, J. (2001). **Acacia - Wattle** [Online]. Available: http://www.janinesgarden.com/plants/A/acacia.html

Considine, R., Denoyel, R., Pendleton, P., Schumann, R., and Wong, S.-H. (2001). The influence of surface chemistry on activated carbon adsorption of 2-methylisoborneol from aqueous solution. **Colloids Surf. A** 179: 271-280.

Cordero, T., Rodriguez-Mirasol, J., Tancredi, N., Piriz, J., Vivo, G., and Rodriguez, J. J. (2002). Influence of surface composition and pore structure on Cr(III) adsorption onto activated carbons. **Ind. Eng. Chem. Res.** 41: 6042-6048.

Cuerda-Correa, E. M., Díaz-Díez, M. A., Macías-García, A., and Gañán-Gómez, J. (2006). Preparation of activated carbons previously treated with sulfuric acid A study of their adsorption capacity in solution. **Appl. Surface Sci.** 252: 6042-6045.

Díaz-Díez, M. A., Gómez-Serrano, V., Fernández-González, C., Cuerda-Correa, E. M., and Macías-García, A. (2004). Porous texture of activated carbons prepared by phosphoric acid activation of woods. **Appl. Surface Sci.** 238: 309-313.

Fanning, P. E. and Vannice, M. A. (1993). A DRIFTS study of the formation of surface groups on carbon by oxidation. **Carbon** 31: 721-730. Quoted in Figueiredo, J. L., Pereira, M. F. R., Freitas, M. M. A., and Orfao, J. J. M. (1999). Modification of the surface chemistry of activated carbons. **Carbon** 37: 1379-1389.

Fletcher, A. J. and Thomas, K. M. (2000). Compensation effect for the kinetics of adsorption/desorption of gases/vapors on microporous carbon materials. **Langmuir** 16: 6253-6266.

Fletcher, A. J., Yüzak, Y., and Thomas, K. M. (2006). Adsorption and desorption kinetics for hydrophilic and hydrophobic vapors on activated carbon. **Carbon** 44: 989-1004.

Gardner, D. J. (2003). **Wood Cell Wall** [Online]. Available: http://www.umaine.edu/adhesion/gardner/5502002/wood%20cell%20wall.pdf

Gómez-Serrano, V., Cuerda-Correa, E. M., Fernández-González, M. C., Alexandre-Franco, M. F., and Macías-García, A. (2005). Preparation of activated carbons from chestnut wood by phosphoric acid-chemical activation. Study of microporosity and fractal dimension. **Mater. Lett.** 59: 846-853.

Harding, A. W., Foley, N. J., Norman, P. R., Francis, D. C., and Thomas, K. M. (1998). Diffusion barriers in the kinetics of water vapor adsorption/ desorption on activated carbons. **Langmuir** 14: 3858-3864.

Hon, D. N.-S. and Shiraishi, N. (2001). **Wood and Cellulosic Chemistry.** New York: Marcel Dekker, Inc.

Hontoria-Lucas, C., López-Peinado, A. J., López-González, J. De D., Rojas-Cervantes, M. L., and Martín-Aranda, R. M. (1995). Study of oxygen-containing groups in a series of graphite oxides: Physical and chemical characterization. **Carbon** 33: 1585-1592.

Howe-Grant, M. (1992). **Encyclopedia of Chemical Technology.** New York: John Wiley & Sons.

Ismadji, S., Sudaryanto, Y., Hartono, S. B., Setiawan, L. E. K., and Ayucitra, A. (2005). Activated carbon from char obtained from vacuum pyrolysis of teak sawdust: pore structure development and characterization. **Bioresour. Technol.** 96: 1364-1369.

Jagtoyen, M. and Derbyshire, F. (1998). Activated carbons from yellow poplar and white oak by H_3PO_4 activation. **Carbon** 36: 1085-1097.

Jankowska, H., Świątkowski, A., and Choma, J. (1991). **Active Carbon.** New York: Ellis Horwood.

Jansen, R. J. J. and Bekkum, H. V. (1995). XPS of nitrogen-containing functional groups on activated carbon. **Carbon** 33: 1021-1027.

Jonge, R. J., Breure, A. M., and Andel, J. G. (1996). Reversibility of adsorption of aromatic compounds onto powdered activated carbon (PAC). **Wat. Res.** 30: 883-892.

Kalavathy, M. H., Karthikeyan, T., Rajgopal, S., and Miranda, L. R. (2005). Kinetic and isotherm studies of Cu(II) adsorption onto H_3PO_4-activated rubber wood sawdust. **J. Colloid Interface Sci.** 292: 354-362.

Karthikeyan, T., Rajgopal, S., and Miranda, L. R. (2005). Chromium(VI) adsorption from aqueous solution by *Hevea Brasilinesis* sawdust activated carbon. **J. Hazard. Mater.** 124: 192-199.

Kent, J. A. (1992). **Riegel's Handbook of Industrial Chemistry.** New York: Van Nostrand Reinhold.

Kumar, B. G. P., Shivakamy, K., Miranda, L. R., and Velan, M. (2006). Preparation of steam activated carbon from rubberwood sawdust (*Hevea brasiliensis*) and its adsorption kinetics. **J. Hazard. Mater.** 136: 922-929.

Lahaye, J. (1998). The chemistry of carbon surfaces. **Fuel** 77: 543-547.

Lee, W. H. and Reucroft, P. J. (1999). Vapor adsorption on coal- and wood-based chemically activated carbons (I) Surface oxidation states and adsorption of H_2O. **Carbon** 37: 7-26.

Leon, C. A. and Radovic, L. R. (1994). **Chemistry and Physics of Carbon.** New York: Marcel Dekker. Quoted in Rodríguez-Reinoso, F. (1998). The role of carbon materials in heterogeneous catalysis. **Carbon** 36: 159-175.

Lillo-Ródenas, M. A., Cazorla-Amorós, D., and Linares-Solano, A. (2005). Behaviour of activated carbons with different pore size distributions and surface oxygen groups for benzene and toluene adsorption at low concentrations. **Carbon** 43: 1758-1767.

López de Letona Sánchez, M., Macías-García, A., Díaz-Díez, M. A., Cuerda-Correa, E. M., Gañán-Gómez, J., and Nadal-Gisbert, A. (2006). Preparation of activated carbons previously treated with hydrogen peroxide: Study of their porous texture. **Appl. Surface Sci.** 252: 5984-5987.

Menéndez, J. A., Phillips, J., Xia, B., and Radovic, L. R. (1996). On the modification and characterization of chemical surface properties of chemical surface properties of activated carbon: In the search of carbons with stable basic properties. **Langmuir** 12: 4404-4410.

Mohan, D. and Chander, S. (2001). Single component and multi-component adsorption of metal ions by activated carbons. **Colloids Surf. A** 177: 183-196.

Pereira, M. F. R., Soares, S. F., Órfão, J. J. M., and Figueiredo, J. L. (2003). Adsorption of dyes on activated carbons: influence of surface chemical groups. **Carbon** 41: 811-821.

Polovina, M., Babić, B., Kaluderović, B., and Dekanski, A. (1997). Surface characterization of oxidized activated carbon cloth. **Carbon** 35: 1047-1052.

Puente, G. de la, Pis, J. J., Menéndez, J. A., and Grange, P. (1997). Thermal stability of oxygenated functions in activated carbons. **J. Anal. Appl. Pyrolysis** 43: 125-138.

Radovic, L. R., Silva, I. F., Ume, J. I., Menéndez, J. A., Leon Y Leon, C. A., and Scaroni, A. W. (1997). An experimental and theoretical study of the adsorption of aromatics possessing electron-withdrawing and electron-donating functional groups by chemically modified activated carbons. **Carbon** 35: 1339-1348.

Rouquerol, F., Rouquerol, J., and Sing K. (1999). **Adsorption by Powders and Porous Solids.** London: Academic Press.

Rowell, R. M., Young, R. A., and Rowell, J. (1997). **Paper and Composites from Agro-based resources** New York: CRC Press, Inc.

Ruthven, D. M. (1997). **Encyclopedia of Separation Technology.** New York: John Wiley.

Salame, I. I. and Bandosz, T. J. (1999). Study of water adsorption on activated carbons with different degrees of surface oxidation. **J. Colloid Interface Sci.** 210: 367-374.

Salame, I. I. and Bandosz, T. J. (2000). Adsorption of water and methanol on micro- and mesoporous wood-based activated carbons. **Langmuir** 16: 5435-5440.

Salame, I. I. and Bandosz, T. J. (2003). Role of surface chemistry in adsorption of phenol on activated carbons. **J. Colloid Interface Sci.** 264: 307-312.

Sánchez, A. R., Elguézabal, A. A., and Saenz, L. L. T. (2001). CO_2 activation of char from *Quercus agrifolia* wood waste. **Carbon** 39: 1367-1377.

Seippel, J., Ulbig, P., and Schulz, S. (2000). Adsorption equilibrium data of binary liquid mixtures containing *n*-alkanes, cycloalkanes, and 1-alkanols on activated carbons. **J. Chem. Eng. Data** 45: 780-783.

Shen, W., Li, Z., and Liu, Y. (2008). Surface chemical functional groups modification of porous carbon. **Recent Patents on Chemical Engineering** 1: 27-40.

Society of Wood Science and Technology (2003). **Structure of Wood** [Online]. Available: http://www.swst.org/tech/tech1/structure1.ppt

Soerianegara, I. and Lemmens, R. H. M. J. (1999). **Plant Resources of South-East Asia 5(1) Timber trees: Major commercial timbers.** Bogor: ESCAP CGPRT Centre.

Tancredi, N., Cordero, T., Rodríguez-Mirasol, J., and Rodríguez, J. J. (1996). Activated carbons from Uruguayan eucalyptus wood. **Fuel** 75: 1701-1706.

The United States Department of Agriculture. Forest Products Laboratory. (1999). **Wood Handbook–Wood as an Engineering Material.** Wisconsin: Forest Service.

UC Forest Products Laboratory (2003). **Chemical constituents** [Online]. Available: http://www.ucfpl.ucop.edu/I-Zone/XX/biomass_ch4.pdf

UW Civil Engineering (2002). **Wood** [Online]. Available: http://www.civil.uwaterloo.ca/beg/CE265/Wood.pdf

Winfield Industries (2005). **Products** [Online]. Available: http://www.activatedcarbons.net/products_index.html

Zhang, T., Walawender, W. P., Fan, L. T., Fan, M., Daugaard, D., and Brown, R. C. (2004). Preparation of activated carbon from forest and agricultural residues through CO_2 activation. **Chem. Eng. J.** 105: 53-59.

CHAPTER III

PREPARATION OF ACTIVATED CARBON

ABSTRACT

This chapter focuses on the preparation of activated carbon from eucalyptus and wattle woods by chemical activation with H_3PO_4 and physical activation with CO_2. For chemical activation, the preparation conditions including chemical weight ratio of H_3PO_4 solution and wood, impregnation time, carbonization temperature, and carbonization time were studied to determine the optimal preparation conditions that gave the maximum in surface area. The preparation conditions such as carbonization temperature, carbonization time, activation temperature, activation time, and CO_2 concentration were investigated for the physical activation process. The porous properties of the prepared activated carbons were determined based on the analysis of N_2 adsorption isotherms measured at -196^oC. The maximum surface area of the obtained activated carbons using H_3PO_4 activation were 1857 m^2/g and 1550 m^2/g for eucalyptus and wattle woods, respectively. These activated carbons were obtained from the conditions: chemical weight ratio of H_3PO_4 solution and wood 1.5:1, impregnation time 1.5 hour, carbonization temperature 400^oC, and carbonization time 1 hour. For CO_2 activation, the activated carbons produced from eucalyptus and wattle woods had the maximum surface area of about 1490 m^2/g and 1030 m^2/g, respectively. The optimum activation conditions that gave the maximum surface area

occurred at 900^{o}C and 1 hour for eucalyptus wood and 800^{o}C and 5 hours for wattle wood. Under the conditions studied, the obtained activated carbons from physical activation consisted mainly of micropore structure (~80% of total pore volume), while the activated carbons prepared from chemical activation contained higher proportions of mesopore and macropore volume. The results also showed that the prepared activated carbons from H_3PO_4 activation had the surface area higher than that of the commercial activated carbons manufactured from woods and activated carbons prepared from other biomasses. However, the CO_2 activation gave activated carbon with comparable surface area to activated carbons prepared from other biomasses.

3.1 Introduction

Activated carbon which has large surface area and pore volume can be produced from a variety of carbonaceous materials including agricultural by-products, coal, petroleum coke, tyre, etc. There are generally two conventional processes for the preparation of activated carbon i.e. physical activation and chemical activation. There are two physical activation methods i.e. one-step procedure and two-step procedure. Two-step procedure involves the carbonization of a raw material in an inert atmosphere followed by the activation of the resulting char in CO_2, air, or steam. By eliminating the need for a separate carbonization process, the two steps can be combined into a one-step procedure. Chemical activation is performed in a single step of combined carbonization and activation by using chemical activating agents such as H_3PO_4, KOH, and $ZnCl_2$. H_3PO_4 and $ZnCl_2$ are used for the activation of lignocellulosic materials such as grain sorghum (Diao, Walawender, and Fan, 2002 with H_3PO_4 activation), peach stone (Molina-Sabio, Rodríguez-Reinoso, Caturla, and

Sellés, 1995 with H_3PO_4 activation), coffee bean husk (Baquero et al., 2003 with H_3PO_4 activation), apricot stone (Youssef, Radwan, Abdel-Gawad, and Singer, 2005 with H_3PO_4 and $ZnCl_2$ activation), corn cob (Tsai, Chang, and Lee, 1998 with $ZnCl_2$ activation), and pistachio-nut shell (Lua and Yang, 2005 with $ZnCl_2$ activation), whereas KOH is used for activation of coal (Zou and Han, 2001 using anthracite, bituminous, and lignite coal; Lozano-Castelló, Lillo-Ródenas, Cazorla-Amorós, and Linares-Solano, 2001 using anthracite coal; Teng and Hsu, 1999 using bituminous coal; Gañan et al., 2004 using bituminous coal pitch,). However, H_3PO_4 is more preferable than $ZnCl_2$ because of the problems of corrosion, inefficient chemical recovery, and environmental impact associated with the use of $ZnCl_2$ (Srinivasakannan and Bakar, 2004).

As described in section 2.5.1 (chapter II), only a few studies have been reported on preparing activated carbon from eucalyptus wood (Tancredi, Cordero, Rodríguez-Mirasol, and Rodríguez, 1996; Arriagada, García, Molina-Sabio, and Rodríguez-Reinoso, 1997) and there has been no study on the preparation of activated carbon from wattle wood. Therefore, this chapter has focused on the preparation of activated carbon from both woods by chemical activation with H_3PO_4 and two-step physical activation with CO_2. It is known that porous properties of the obtained activated carbon depend on the type of precursors as well as the method and conditions of preparation. Therefore, the effect of preparation conditions on the porous properties of activated carbon was also studied in details in this thesis work.

3.2 Apparatus and Methods

This section describes the apparatus, chemical, and methodology used for conducting the experiments on activated carbon preparation.

3.2.1 Apparatus and chemicals

1. Horizontal stainless steel tube furnace (VC TF4 with 4.5 cm diameter and 140 cm long, Vecstar) for chemical activation and horizontal ceramic tube furnace (CTF 12/75/700/201 with 7 cm diameter and 105 cm long, Carbolite) for physical activation
2. Sieves (ASTM11, Retsch) and sieve shaker (analysette, FRITSCH)
3. Rotor beater mill (SR 200, Retsch)
4. Oven (600, Memmert)
5. Analytical balance (BP221S, Sartorius)
6. pH meter (CG840, SCHOTT)
7. Automated adsorption apparatus (ASAP 2010, Micromeritics)
8. Thermogravimetric analyzer (SDT 2960 Simultaneous DSC–TGA, TA Instruments)
9. Scanning electron microscopy (JSM6400, JEOL)
10. Nitrogen gas (industrial grade with 99.9% purity for chemical activation and ultra high purity grade with 99.999% purity for physical activation, supplied by Thai Industrial Gases Public Company Limited)
11. Phosphoric acid (H_3PO_4) 85% by weight from Carlo Erba Reagenti
12. Carbon dioxide (high purity grade with 99.95% purity, supplied by Thai Industrial Gases Public Company Limited)

3.2.2 Methods

3.2.2.1 Chemical activation

1. Eucalyptus and wattle woods from a local sawmill in the form of shaving were milled by a rotor beater mill and sieved to obtain a size fraction of 20×30 mesh (average size 0.714 mm). Next, the wood samples were dried at 110^{o}C for 24 hours in an oven to remove excess moisture in the raw materials.

2. Seven grams of the wood sample was impregnated for 1 hour with 50 wt% H_3PO_4, prepared from 85 wt% H_3PO_4, using a 1:1 chemical weight ratio of H_3PO_4 solution and wood. Under this condition, the wood sample was completely soaked with acid solution.

3. The mixture of wood and H_3PO_4 solution was loaded into a ceramic boat and placed in the heated zone of the tube furnace with N_2 flowing through at a constant rate of 100 cm^3/min. The furnace was heated from room temperature to 400^{o}C at the heating rate of 25^{o}C/min and held at this temperature for 1 hour. After carbonization, the furnace was turned off and the activated carbon was allowed to cool down to room temperature under the flow of N_2. Figure 3.1 shows the schematic diagram of the experimental apparatus.

4. The obtained activated carbon was washed several times with distilled water to remove the remaining acid until the measured pH became constant and the final suspension was filtered through a filter paper. The washed product was dried at 110^{o}C in an oven and weighed to determine the yield of activated carbon. Table 3.1 summarizes the other preparation conditions used for chemical preparation of wood-based activated carbons.

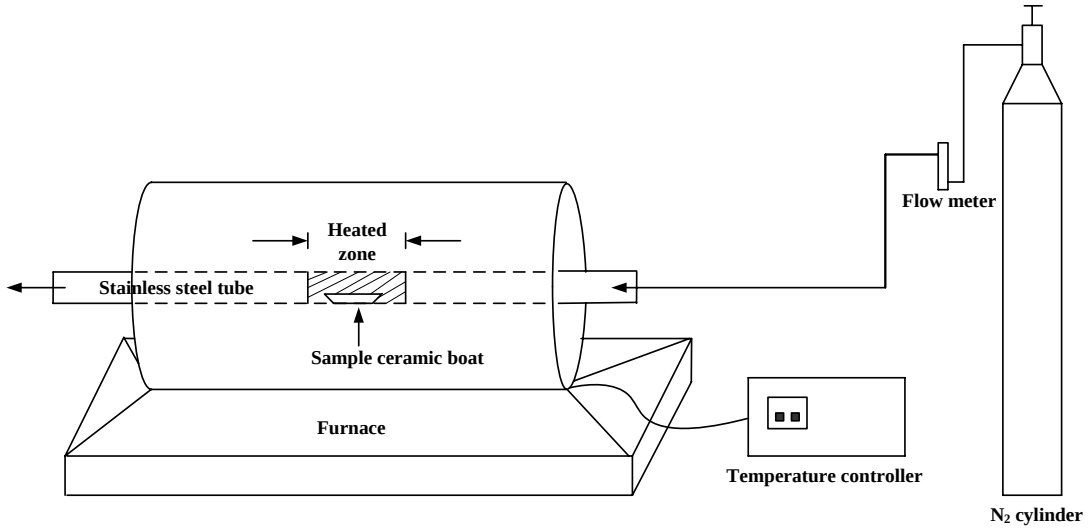

Figure 3.1 Schematic diagram of the experimental apparatus for preparing activated carbons by chemical activation.

Table 3.1 Preparation conditions used for prepare activated carbon by chemical activation with H_3PO_4.

Preparation parameters	**Conditions**
Carbonization temperature	$300^oC – 700^oC$
Chemical weight ratio (H_3PO_4 solution/wood)	0.5:1 – 3:1
Carbonization time	0.5 – 2 hour
Impregnation time	0.5 – 3 hour

3.2.2.2 Physical activation

1. Seven grams of the dried wood sample with an average size of 0.714 mm was loaded into the ceramic boat and placed in the heated zone of a horizontal ceramic tube furnace under a constant flow of N_2 at 100 cm^3/min. The furnace was heated from room temperature to 400^oC at the heating rate of 25^oC/min and held at this temperature for 1 hour. Then the furnace was shut down and the carbonized char was cooled down to room temperature under the flow of N_2.

2. The char derived from the carbonization step was further activated in a packed-bed reactor (2.5 cm diameter and 10 cm long) made of stainless steel. The reactor was packed with char particles, placed inside the horizontal ceramic tube furnace and heated from room temperature to 800^oC under the constant flow of N_2 at 100 cm^3/min using the heating rate of 25^oC/min. When the activation temperature was reached, the CO_2 was allowed to flow into the reactor at the rate of 100 cm^3/min, giving 50 vol% of CO_2 concentration in the gas mixture, and the furnace was operated at this set temperature for 1 hour. When the activation period was completed, the flow of CO_2 was stopped and the activated carbon product was cooled down to room temperature under the flow of N_2. Table 3.2 lists the other preparation conditions used for studying physical preparation of activated carbon.

Table 3.2 Preparation conditions used for prepare activated carbon by physical activation with CO_2.

Preparation parameters	Conditions
Carbonization temperature	$300^oC – 700^oC$
Carbonization time	1 – 4 hour
Activation temperature	$600^oC – 900^oC$
Activation time	1 – 5 hour
CO_2 concentration	25 – 100 vol%

3.2.2.3 Characterization of precursors and activated carbon

Precursors

The raw wood materials were characterized by using several techniques covering the analysis of lignocellulosic composition (cellulose, hemicellulose, and lignin), proximate analysis, and thermogravimetric analysis.

The cellulose and hemicelluloses contents were determined by using the method of Browing (Lee and Rowell, 2004). The lignin content was determined by using TAPPI Standard Test Method (T222-om-98), available from the Technical Association of the Pulp and Paper Industry (Jiménez, García, Pérez, Ariza, and López, 2001).

Proximate analysis was used to determine volatile matters, ash, fixed carbon, and moisture content. The proximate analysis was carried out by

employing a thermogravimetric analyzer as suggested by Lua and Guo (1998). Ten milligrams of the sieved wood (W_0) with average particle size 0.714 mm was heated to 110^{o}C under N_2 flow of 100 cm^3/min at the heating rate of 50^{o}C/min and held at this temperature for 5 minutes. The remaining weight at this temperature, W_{110}, was recorded and the percent of moisture content was calculated from the weight loss using the formula,

$$\% \text{ moisture content} = \frac{W_0 - W_{110}}{W_0} \times 100\% \tag{3.1}$$

Next, the sample was heated to 850^{o}C under N_2 flow of 100 cm^3/min at the heating rate of 50^{o}C/min and held at this temperature for 7 minutes. The sample weight at this temperature, W_{850}, was recorded and the percent of volatile matters was calculated as follows,

$$\% \text{ volatile matters} = \left[\frac{W_0 - W_{850}}{W_0} \right] \times 100\% - \% \text{ moisture content} \tag{3.2}$$

Then, the sample was cooled down to 800^{o}C under N_2 flow at the heating rate of 10^{o}C/min. At this temperature, the N_2 flow was switched to air flow and the sample was allowed to combust at this temperature for 25 minutes. The air flow was changed back to N_2 flow and the sample was cool down to room temperature. The final mass, W_F, of the ash sample was measured and the percent of ash content was calculated according to the following equation,

$$\% \text{ ash content} = \frac{W_F}{W_0} \times 100\% \quad (3.3)$$

Finally, the percent of fixed carbon content was found from the following relation

$$\% \text{ fixed carbon} = 100\% - \% \text{ moisture} - \% \text{ volatile matters} - \% \text{ ash} \quad (3.4)$$

Thermal analyses of both woods were performed using a thermogravimetric analyzer (TGA) under N_2 atmosphere. In this experiment, the temperature was programmed to increase from room temperature to 600^{o}C at the heating rate of 25^{o}C/min.

Char and activated carbon

The char and activated carbon product were characterized for the following properties: yield, burn-off, specific surface area, pore volume, pore size distribution, proximate analysis, and scanning electron micrograph.

The yield of activated carbon is defined as the ratio of the weight of resulting activated carbon, W, to that of the original wood, W_0, with both weights on a dry basis i.e.

$$\% \text{ yield} = \frac{W}{W_0} \times 100\% \quad (3.5)$$

The burn-off is defined for physical activation as the difference between the weight of the original char, W_1, and that of the activated carbon, W, divided by the weight of the original char, on a dry basis. That is,

$$\% \text{ burn-off} = \frac{W_1 - W}{W_1} \times 100\% \tag{3.6}$$

Specific surface area and pore volume of the resulting char and activated carbon were determined from N_2 gas adsorption data at –196^{o}C obtained by employing an automated adsorption apparatus. Prior to the adsorption measurement, the sample was first degassed at 300^{o}C under vacuum (< 50 μmHg) for 12 hours to remove moisture and other volatiles.

Specific surface area, S_{BET}, was estimated by applying the Brunauer-Emmett-Teller (BET) equation (Do, 1998). The BET equation is used for the multilayer adsorption. The basic assumptions of this equation are that the surface is energetically homogeneous or adsorption energy does not change with the progress of adsorption in the same layer and there is no interaction between the adsorbed molecules. The BET equation reads

$$\frac{\mathrm{P}}{n(\mathrm{P}^o - \mathrm{P})} = \frac{1}{n_m C} + \left(\frac{C-1}{n_m C}\right)\left(\frac{\mathrm{P}}{\mathrm{P}^o}\right) \tag{3.7}$$

where P is the pressure of gas adsorbed, P^o is the saturation vapor pressure of gas adsorbed at the temperature of adsorption, n is the amount of gas adsorbed at pressure P in mol/g, n_m is the monolayer amount adsorbed in mol/g, and C is the non-dimensional constant. A plot of the $\mathrm{P}/n(\mathrm{P}^o - \mathrm{P})$ versus $(\mathrm{P}/\mathrm{P}^o)$ give a straight line from which the slope and an intercept determine the values of n_m and C. The pressure range of validity of this equation is P/P^o = 0.05 – 0.3 (Do, 1998). For relative pressures

above, there exists capillary condensation, which is not amenable to multilayer analysis. The specific surface area is then calculated from

$$S_{\mathrm{BET}} = n_{\mathrm{m}} N_{\mathrm{A}} a_{\mathrm{m}} \times 10^{-20} \tag{3.8}$$

where S_{BET} is the specific surface area in m^2/g, n_{m} is the monolayer amount adsorbed in mol/g, N_{A} is the Avogadro number (6.023×10^{23} molecules/mole), and a_{m} is the molecular projected area (16.2 $Å^2$/molecule for N_2 at -196^oC).

Micropore volume, V_{mic}, was calculated by using Dubinin-Radushkevich (DR) equation (Do, 1998). This equation is based on the theory of micropore volume filling. The DR equation is as follows:

$$\log n = \log n_{\mathrm{o}} - \left[\frac{\mathrm{RT}}{\beta \mathrm{E}_{\mathrm{o}}}\right]^2 \left[\log \frac{\mathrm{P}^{\mathrm{o}}}{\mathrm{P}}\right]^2 \tag{3.9}$$

where n_{o} is the limiting micropore volume in cm^3/g, R is the gas constant (8.314 J/Kmol), β is the non-dimensional affinity coefficient (β = 0.33 for N_2), and E_{o} is the characteristic energy in J/mol. A plot of log n versus $[\log (\mathrm{P}^{\mathrm{o}} / \mathrm{P})]^2$ gives a straight line with an intercept equal to the micropore volume.

Total pore volume, V_{T}, was found from the amount of N_2 gas adsorbed at the relative pressure of 0.99 and converted to the corresponding volume of liquid state as follow

$$V_{\mathrm{T}} = V_{0.99} \times d \tag{3.10}$$

where V_T is the total pore volume in cm^3/g, $V_{0.99}$ is the amount of volume adsorbed at $P/P^o = 0.99$ in cm^3 STP/g, and d is the density conversion factor (0.0015468 cm^3 liquid/cm^3 STP for N_2 at -196^oC). The combined volume of mesopore and macropore, $V_{meso+mac}$, was found from the difference between total pore volume and micropore volume.

Pore size distributions were also computed by applying the Density Functional Theory (DFT) method (Olivier, 1995). Density functional theory describes the grand potential energy (Helmholtz free energy) as a function of the fluid particle density distribution. Therefore, the minimization of the grand potential energy gives the equilibrium density profile. The DFT model has been computed over the relative pressure range of 0.01 – 0.99.

Scanning electron microscopy (SEM) was used to study the structural features of the activated carbon surface. The sample was coated with gold by vacuum electroplating machine at 10 μA for 6 minutes.

3.3 Results and Discussion

3.3.1 Properties of raw materials

The proximate analysis and lignocellulosic composition of the wood samples are shown in Table 3.3. The results show that eucalyptus and wattle woods have fixed carbon content of 18.3% and 16.6%, respectively, and contain a high proportion of volatile matters but with low ash content. These fixed carbon contents are comparable with other biomass materials used to produce activated carbons such as corn cob (16.1%) (Chang, Chang, and Tsai, 2000), oil-palm stone (16.4%) (Lua and Guo, 2000), coconut shell (18.6%) (Daud and Ali, 2004), and pistachio-nut shell

(21.6%) (Yang and Lua, 2003). This indicates that both eucalyptus and wattle woods are potential precursors for the production of activated carbons. Both eucalyptus and wattle woods used in this work are hard wood type (Siamtree, 2003; Colman, 2001) with highest content of cellulose (57 – 62%), medium lignin content (25%), and lowest content of hemicellulose (12 – 16%).

Table 3.3 Analysis of raw materials (the values of proximate analysis in parentheses are moisture free basis).

	Eucalyptus wood	**Wattle wood**
Proximate analysis (wt%)		
Fixed carbon	18.3 (19.1)	16.6 (17.1)
Volatile matters	76.4 (79.7)	78.3 (80.9)
Ash	1.2 (1.2)	1.9 (2.0)
Moisture	4.1	3.2
Lignocellulosic composition (wt%)		
Cellulose	57.3	62.0
Hemicelluloses	16.8	12.6
Lignin	25.9	25.4

The thermogravimetric analysis (TGA) and differential thermo-gravimetric analysis (DTG) curves of both woods under N_2 atmosphere are presented in Figure 3.2. The DTG curves show an initial peak between 60^{o}C and 110^{o}C, which corresponds to the mass loss of absorbed moisture of approximately 3

wt% and 5 wt% for eucalyptus and wattle woods, respectively. These values are insignificantly different from the values of proximate analysis (Table 3.3). Following this peak, the DTG curves show two decomposition steps: the first decomposition shows a shoulder peak at about 280 – 340^{o}C (mass loss ~ 25 wt% for eucalyptus wood, ~ 22 wt% for wattle wood) and the major second decomposition peak at about 340 – 410^{o}C (mass loss ~ 40 wt% for eucalyptus wood, ~ 36 wt% for wattle wood). As described in section 2.1 (chapter II), hemicellulose has amorphous structure and rich of branches, therefore, it is very easy to remove at low temperature. Cellulose is consisted of a long polymer of glucose without branches, its structure is very strong, and the thermal stability is high. Lignin is full of aromatic rings with various branches and more difficult to decompose and the activity of the chemical bonds in lignin covered an extremely wide range (the degradation of lignin occurs in a wide temperature range of 100 – 900^{o}C) (Yang, Yan, Chen, Lee, and Zheng, 2007). Therefore, the first shoulder peak is probably attributed to the decomposition of hemicellulose and the major second decomposition peak should be ascribed to the decomposition of cellulose.

It should be also noted that the thermogravimetric analysis results can be used as primary data for the preparation of activated carbon. The TGA results showed that the complete devolatilization process occurred around 400^{o}C. Therefore, the carbonization temperatures of 400^{o}C and higher are suitable to produce char or activated carbon with high carbon content. However, too high of carbonization temperature will cause a shrinkage of char particle, hence giving a detrimental effect on pore development in the subsequent physical activation step.

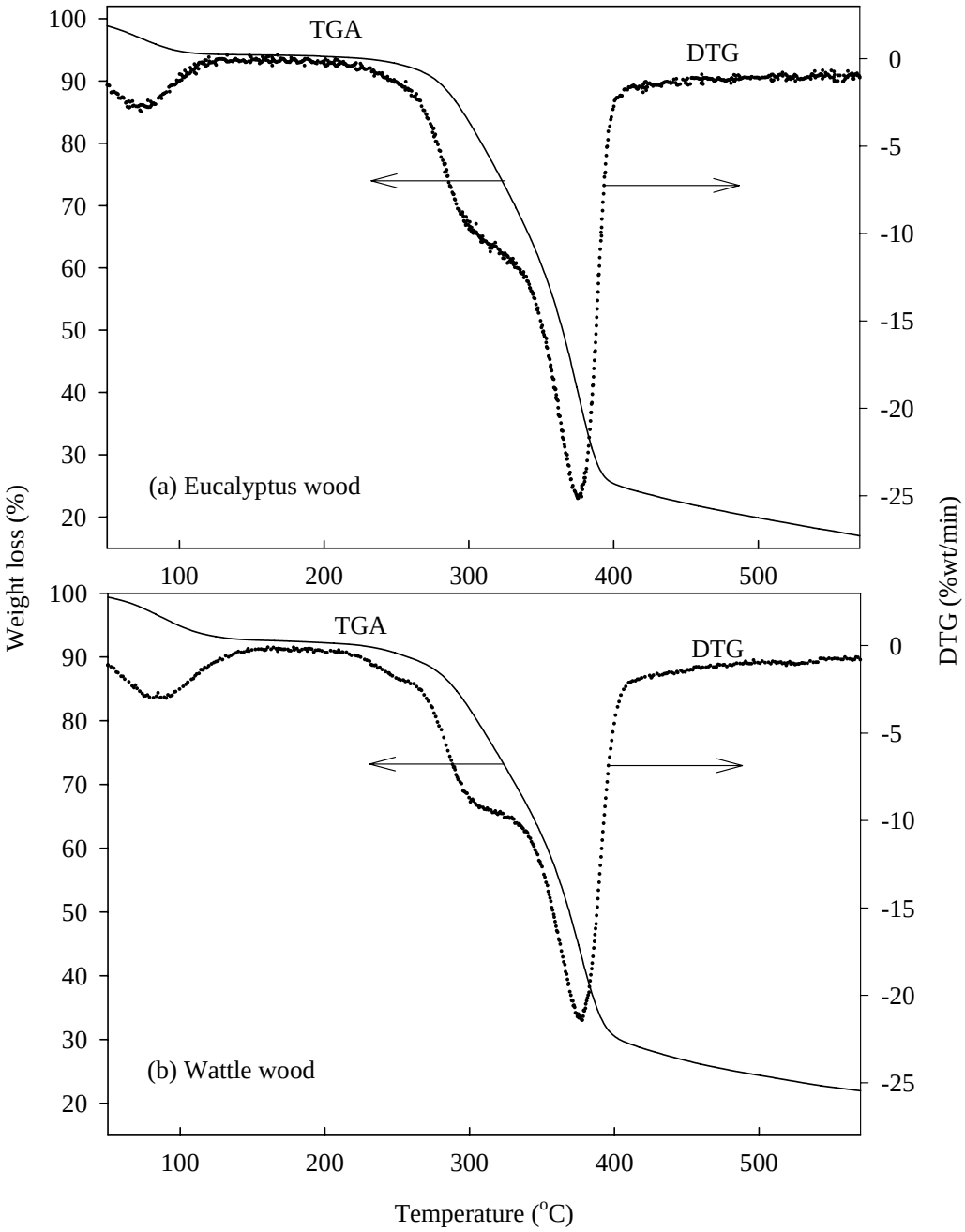

Figure 3.2 TGA and DTG curves of (a) eucalyptus and (b) wattle woods heated at 25°C/min under nitrogen atmosphere.

3.3.2 Chemical activation

This section presents the results on the effects of carbonization temperature, chemical weight ratio of H_3PO_4 solution and wood, carbonization time, and impregnation time on the porous properties of the prepared activated carbons.

3.3.2.1 Effect of carbonization temperature

In studying the effect of carbonization temperature, the following preparation conditions were kept constant: chemical weight ratio of H_3PO_4 solution and wood 1:1, impregnation time 1 hour, and carbonization time 1 hour. Table 3.4 and Figure 3.3 show the effect of the carbonization temperature on the product yield and porous properties of the derived activated carbons. The results show that the yield decreases continuously with an increase of carbonization temperature from 300^{o}C to 700^{o}C. Eucalyptus wood-based activated carbons give higher yield than wattle wood-based activated carbon at all carbonization temperatures.

The BET surface area and total pore volume increase sharply with carbonization temperature from 300^{o}C to 400^{o}C for both woods and pass through a maximum at 400^{o}C. The increase of carbonization temperature from 500^{o}C to 700^{o}C causes a slight decrease in the surface area and total pore volume. However, there is a small increase of total pore volume of eucalyptus wood-based activated carbon at carbonization temperature from 600^{o}C to 700^{o}C.

Eucalyptus wood shows a better pore development than wattle wood i.e. giving higher surface area and total pore volume at all carbonization temperatures. This difference in pore structure is possibly caused by the differences in the lignocellulosic compositions of both wood materials although they both are hardwood type.

Table 3.4 Effect of carbonization temperature on the porous properties of prepared activated carbons by chemical activation (chemical weight ratio of H_3PO_4 solution and wood 1:1, impregnation time 1 hour, and carbonization time 1 hour).

	Carbonization temperature (^oC)	**Yield (%)**	**S_{BET} (m^2/g)**	**V_{mic} (cm^3/g)**	**$V_{meso+mac}$ (cm^3/g)**	**V_T (cm^3/g)**
Eucalyptus wood	300	49.1	967	0.44 (89.8%)	0.05 (10.2%)	0.49
	400	45.3	1699	0.70 (73.7%)	0.25 (26.3%)	0.95
	500	43.4	1474	0.60 (74.1%)	0.21 (25.9%)	0.81
	600	41.4	1447	0.62 (83.8%)	0.12 (16.2%)	0.74
	700	35.2	1404	0.58 (76.3%)	0.18 (23.7%)	0.76
Wattle wood	300	47.2	717	0.33 (91.7%)	0.03 (8.3%)	0.36
	400	43.7	1094	0.49 (87.5%)	0.07 (12.5%)	0.56
	500	41.5	988	0.44 (86.3%)	0.07 (13.7%)	0.51
	600	38.3	938	0.41 (85.4%)	0.07 (14.6%)	0.48
	700	33.6	935	0.41 (87.2%)	0.06 (12.8%)	0.47

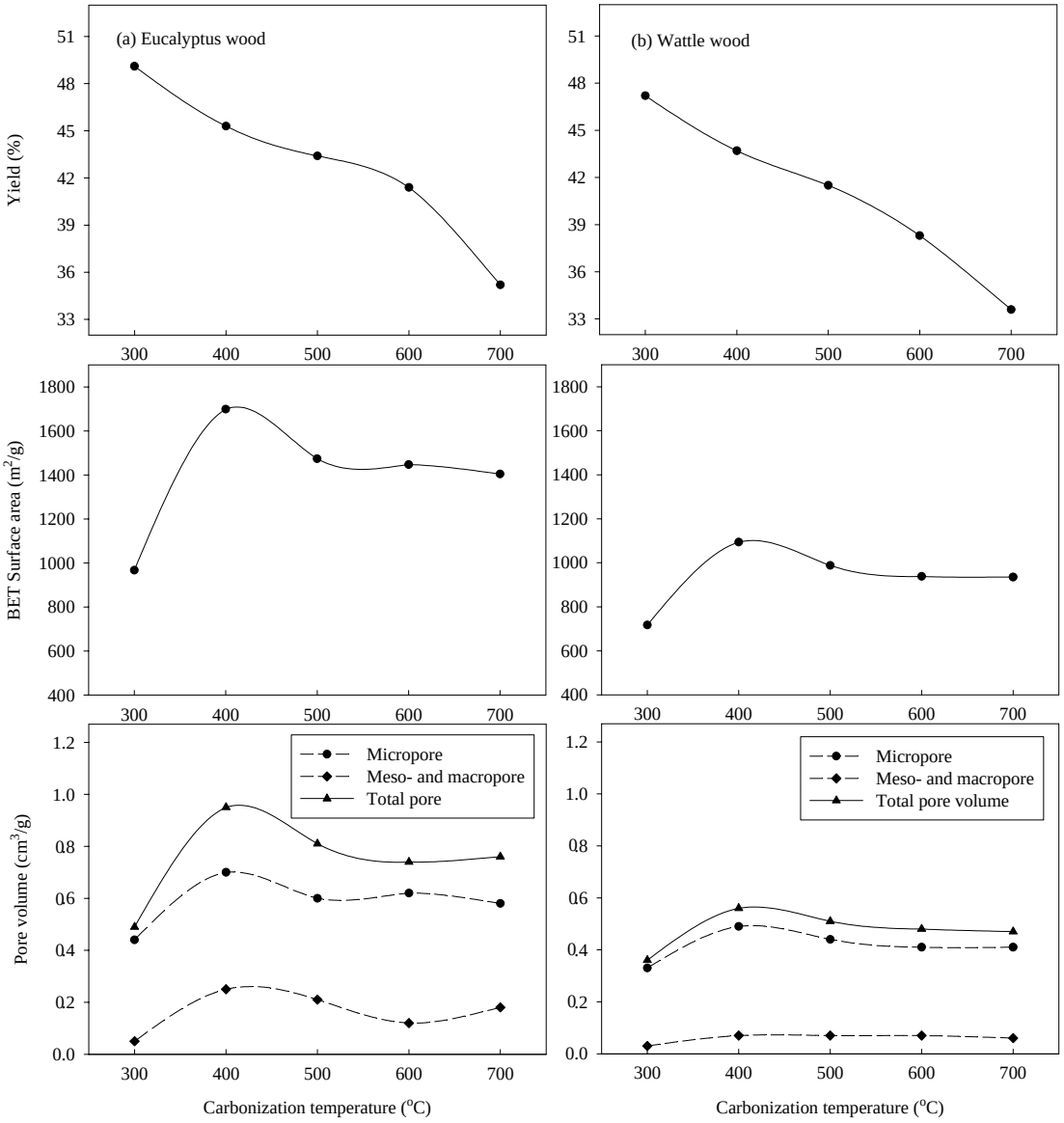

Figure 3.3 Effect of carbonization temperature on the porous properties of activated carbons prepared from (a) eucalyptus and (b) wattle woods by chemical activation (chemical weight ratio of H_3PO_4 solution and wood 1:1, impregnation time 1 hour, and carbonization time 1 hour).

The activated carbons obtained from both woods have the highest BET surface area and total pore volume at carbonization temperature of 400^{o}C which is approximately the highest temperature that complete devolatilization has occurred (see Figure 3.2). Therefore, the carbonization temperature is fixed at 400^{o}C for further studies of the effects of chemical weight ratio of H_3PO_4 solution and wood, carbonization time, and impregnation time on the preparation of activated carbon.

The effect of carbonization temperature on the micropore and larger pore volume follows approximately the same trend as that of total pore volume. It is further noted that eucalyptus wood-based carbons shows higher micropore volume and meso- and macropore volume than wattle wood-based carbons. However, wattle wood produced activated carbons with higher proportions of micropore volume than eucalyptus wood.

The reaction mechanisms of phosphoric acid and wood in relation to pore development during activation were suggested by Jagtoyen and Derbyshire (1998). They proposed that the reaction of wood with H_3PO_4 probably begins as soon as the components are mixed. At temperatures 50 – 200^{o}C, H_3PO_4 acts as an acid catalyst in promoting bond cleavage reactions. The acid first attacks hemicellulose and lignin possibly because of easier access to their amorphous structure of biopolymers than to the crystalline cellulose. The effects of acid attack are to hydrolyze glycosidic linkages in hemicellulose and cellulose and to split ether bonds in lignin. At temperature 200 – 450^{o}C, H_3PO_4 is able to combine with biopolymer fragments (from bond cleavage reaction at low temperature) to form

phosphate linkages such as phosphate and polyphosphate esters. The formation of phosphate linkages by the reaction of cellulose with H_3PO_4 is shown in Figure 3.4.

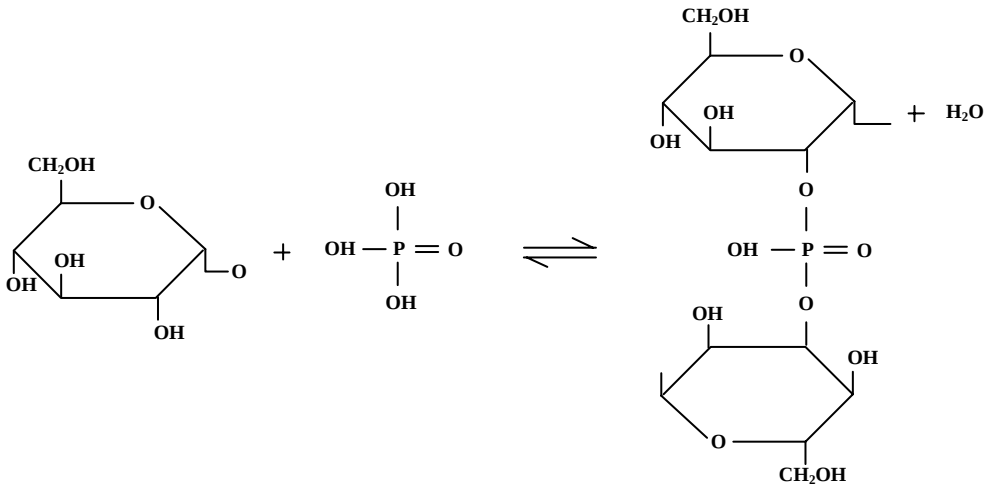

(a) formation of phosphate ester

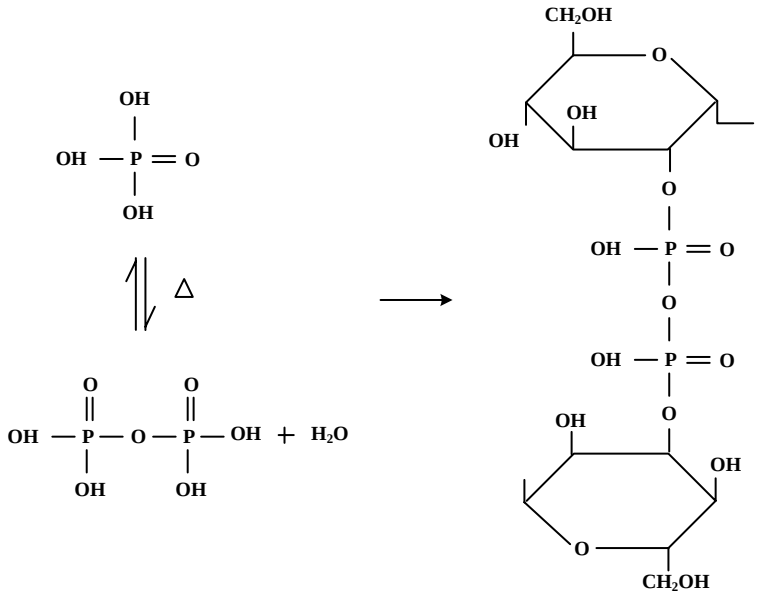

(b) formation of polyphosphate ester at higher temperatures

Figure 3.4 Mechanism of phosphate linkages (a) phosphate ester and (b) poly-phosphate ester formation by reaction of cellulose with H_3PO_4.

Phosphoric acid can insert between the cellulose chains by disrupting the existing hydrogen bonds and replace with phosphate linkage and simultaneously separate the chains and dilate the structure. Dilation can continue as more acid progressively incorporated and the phosphate crosslink may become more bulky at higher temperature due to polymerization of the phosphoric acid to form polyphosphate. In this temperature range, the structure dilates and cross-linking reactions dominate over bond cleavage reactions. The addition or insertion of phosphate groups affects the dilation of the structure so that after the removal of the acid will leave the matrix in an expanded state with and accessible pore structure. The removal of carbon during thermal treatment in the presence of H_3PO_4 in the form of CO, CO_2, and light hydrocarbon gases such as CH_4 also contribute to the creation of pore structure. This explains the development of porous structure of the activated carbon at carbonization temperature of 300^{o}C and 400^{o}C. The lower value of BET surface area and total pore volume of activated carbon prepared at 300^{o}C compared to activated carbon prepared at 400^{o}C may be due to the blockage of volatiles which are not removed completely at the temperature of 300^{o}C.

At temperature above 450^{o}C, the phosphate linkages become thermally unstable and breakdown, leading to the contraction of the structure. Figure 3.5 shows the breakdown mechanism of phosphate linkages in this temperature range. The collapse in crosslink density produces activated carbon with less porous structure. This reflected by the decrease of BET surface area and total pore volume of the activated carbon prepare from both woods at carbonization temperatures higher than 400^{o}C.

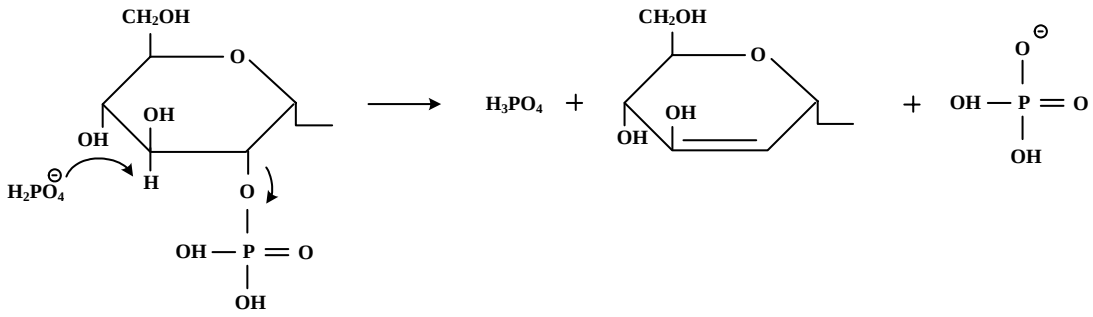

Figure 3.5 The breakdown of phosphate linkage at temperature above 450^{o}C.

The effect of carbonization temperature on the porous properties of activated carbon prepared from other biomass such as grain sorghum (Diao, Walawender, and Fan, 2002) showed that the BET surface area increased with an increase of carbonization temperature from 450^{o}C to 600^{o}C and slightly decreased with increase of carbonization temperature from 600^{o}C to 700^{o}C. However, the micropore volume, mesopore volume, and total pore volume all increased with an increase of carbonization temperature from 450^{o}C to 700^{o}C. For cherry stone (Olivares-Marín, Fernández-González, Macías-García, and Gómez-Serrano, 2005), the BET surface area, mesopore volume, macropore volume, and total pore volume progressively increased with an increase of carbonization temperature from 350^{o}C to 500^{o}C and then decreased with increasing of carbonization temperature from 500^{o}C to 550^{o}C, while micropore volume did not significantly change over this carbonization temperature range. However, for longan seed (Junpirom, Tangsathitkulchai, Tangsathitkulchai, 2007), the BET surface area, micropore volume, and total pore volume decreased with an increase of carbonization temperature from 400^{o}C to 700^{o}C and then increased again with increase of carbonization temperature from 700^{o}C to

900^{o}C, while meso- and macropore volume did not significantly alter over this carbonization temperature range.

Adsorption and desorption isotherms of N_2 at –196^{o}C of eucalyptus and wattle wood-based carbons are shown in Figure 3.6. The nitrogen uptake is significant only in the low relative pressures ($P/P^{o} < 0.2$). In the high relative pressure range, only slight increase in the amount adsorbed is observed. This shape of isotherm is of Type I according to the IUPAC classification (Patrick, 1995). For activated carbons prepared from eucalyptus wood, the adsorption-desorption curves show small hysteresis loops at the relative pressure higher than about 0.4 at carbonization temperatures of 400^{o}C and 500^{o}C indicating the presence of some mesopore volume. This is in agreement with the results of mesopore volume presented in Table 3.4 with carbons prepared at 400^{o}C and 500^{o}C having higher mesopore volume than carbons prepared at lower carbonization temperatures. This shape of isotherm can be approximated by Type IV isotherm. On the other hand, the activated carbons prepared from wattle wood show Type I isotherms for all carbonization temperatures which indicates that the porous structure is dominated with micropores. This is also in accord with the results from Table 3.4 from which wattle wood-based carbon contains micopore volume > 85%. The amounts of N_2 adsorbed of activated carbons follow the order: 300^{o}C < 600^{o}C < 500^{o}C < 400^{o}C for eucalyptus wood and 300^{o}C < 700^{o}C < 600^{o}C < 500^{o}C < 400^{o}C for wattle wood. These orders are in line with the results of surface area and total pore volume presented in Table 3.4. It is noted that, the adsorption and desorption isotherms of activated carbon prepared from eucalyptus wood at 700^{o}C are not shown in Figure 3.6 (a) because there are no significant differences between isotherms of this carbon with

carbon prepared at 600°C. Eucalyptus wood-based activated carbons show higher adsorbed amount of N_2 than wattle wood-based activated carbons for all carbonization temperatures, which is in agreement with the results shown previously that eucalyptus wood gives better pore development in activated carbon than wattle wood does.

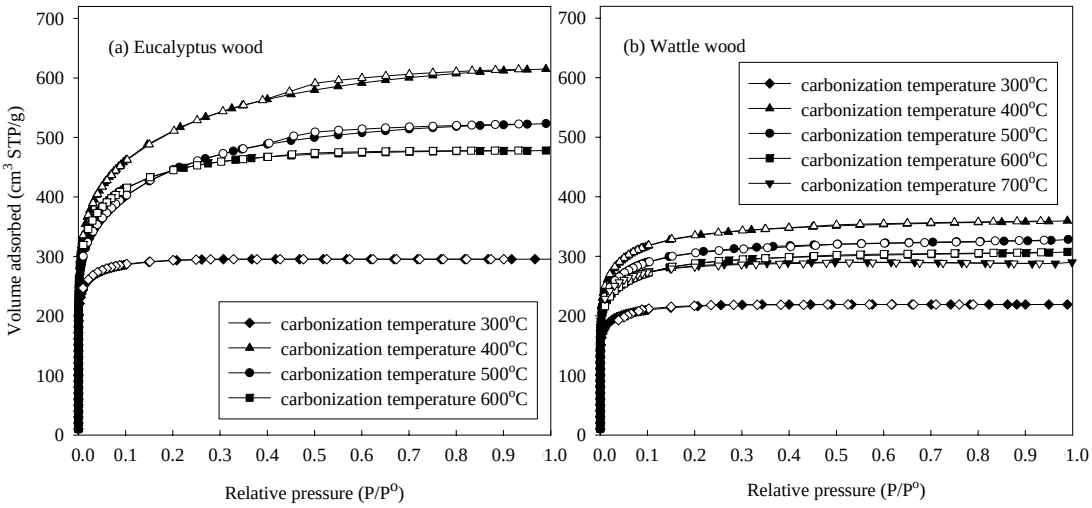

Figure 3.6 Adsorption (closed symbols) and desorption (open symbols) isotherms of N_2 at −196°C of activated carbons prepared from (a) eucalyptus and (b) wattle woods by chemical activation at different carbonization temperature (chemical weight ratio of H_3PO_4 solution and wood 1:1, impregnation time 1 hour, and carbonization time 1 hour).

Table 3.5 presents the results of proximate analysis of the prepared activated carbons from both woods. It can be seen that the prepared activated carbons have higher fixed carbon and ash contents but with lower volatile matters than the raw wood materials (Table 3.3). The prepared carbons also contain higher moisture content than the raw materials because carbons can adsorb extra

moisture due to their highly porous structure. It is noted that activated carbons prepared from both woods contain moisture content in following the order: 400^{o}C > 500^{o}C > 600^{o}C with eucalyptus wood-based carbons having higher moisture content than wattle wood-based carbons. This results follows the order of surface area and total pore volume (Table 3.4) and the fact that eucalyptus wood carbons have higher porous properties than wattle wood carbons. The ash content of activated carbons on a percentage basis increases with the carbonization temperature resulting from the decrease in volatile matters, although the actual amount of ash content should remain unchanged under any conditions.

Table 3.5 Proximate analysis of prepared activated carbons by chemical activation at different carbonization temperature (the values in parentheses are moisture free basis).

	Carbonization temperature (^{o}C)	**Fixed carbon (wt%)**	**Volatile matters (wt%)**	**Ash (wt%)**	**Moisture (wt%)**
Eucalyptus wood	400	71.8 (78.9)	13.4 (14.7)	5.8 (6.4)	9.0
	500	72.2 (79.1)	12.9 (14.1)	6.2 (6.8)	8.7
	600	71.6 (78.1)	12.7 (13.8)	7.4 (8.1)	8.3
Wattle wood	400	74.0 (80.1)	12.5 (13.5)	5.9 (6.4)	7.6
	500	75.6 (81.5)	10.7 (11.5)	6.5 (7.0)	7.2
	600	75.0 (80.4)	10.6 (11.4)	7.7 (8.2)	6.7

3.3.2.2 Effect of chemical weight ratio

From the previous section, the optimum carbonization temperature which gave activated carbon with highest surface area was 400^{o}C. Therefore, the carbonization temperature of 400^{o}C was selected as a base temperature to study the effect of chemical weight ratio of H_3PO_4 solution and the wood precursor. The chemical weight ratio of H_3PO_4 solution and wood studied in this section was 0.5:1, 1:1, 1.5:1, 2:1, and 3:1. The impregnation time and carbonization time were both kept at 1 hour as in the previous section.

Table 3.6 and Figure 3.7 show the effect of chemical weight ratio on the yield and porous properties of the prepared activated carbons. As shown, the yields of activated carbons for both woods increase with increasing chemical weight ratio from 0.5:1 to 1:1. At higher acid ratio, the yield drops continuously before approaching a constant value at the weight ratio of 3:1.

For eucalyptus wood, the surface area of the obtained carbons increases abruptly with an increase of chemical weight ratio from 0.5:1 to 1:1, slowly approaching a maximum value at 1.5:1 chemical weight ratio, followed by a slight decreasing at higher weight ratios. For wattle wood activated carbon, the surface area increases linearly with chemical weight ratio and passes through a maximum at weight ratio of 1.5:1 before decreasing in a linear fashion at higher values of chemical weight ratio. The chemical weight ratio 1.5:1 which gave the highest surface area was selected for further study of the effect of carbonization time and impregnation time. Again, eucalyptus wood shows better pore development than wattle wood at all chemical weight ratios studied.

Table 3.6 Effect of chemical weight ratio on the porous properties of prepared activated carbons by chemical activation (impregnation time 1 hour, carbonization temperature 400^{o}C, and carbonization time 1 hour).

	Chemical weight ratio (H_3PO_4 solution/wood)	**Yield (%)**	**S_{BET} (m^2/g)**	**V_{mic} (cm^3/g)**	**$V_{meso+mac}$ (cm^3/g)**	**V_T (cm^3/g)**
Eucalyptus wood	0.5:1	44.6	1200	0.55 (94.8%)	0.03 (5.2%)	0.58
	1:1	45.3	1699	0.70 (73.7%)	0.25 (26.3%)	0.95
	1.5:1	42.6	1764	0.70 (65.4%)	0.37 (34.6%)	1.07
	2:1	41.9	1688	0.61 (49.6%)	0.62 (50.4%)	1.23
	3:1	41.7	1664	0.68 (71.6%)	0.27 (28.4%)	0.95
Wattle wood	0.5:1	42.8	728	0.33 (89.2%)	0.04 (10.8%)	0.37
	1:1	43.7	1094	0.49 (87.5%)	0.07 (12.5%)	0.56
	1.5:1	42.1	1467	0.56 (61.5%)	0.35 (38.5%)	0.91
	2:1	41.9	1294	0.52 (69.3%)	0.23 (30.7%)	0.75
	3:1	41.2	1196	0.50 (76.9%)	0.15 (23.1%)	0.65

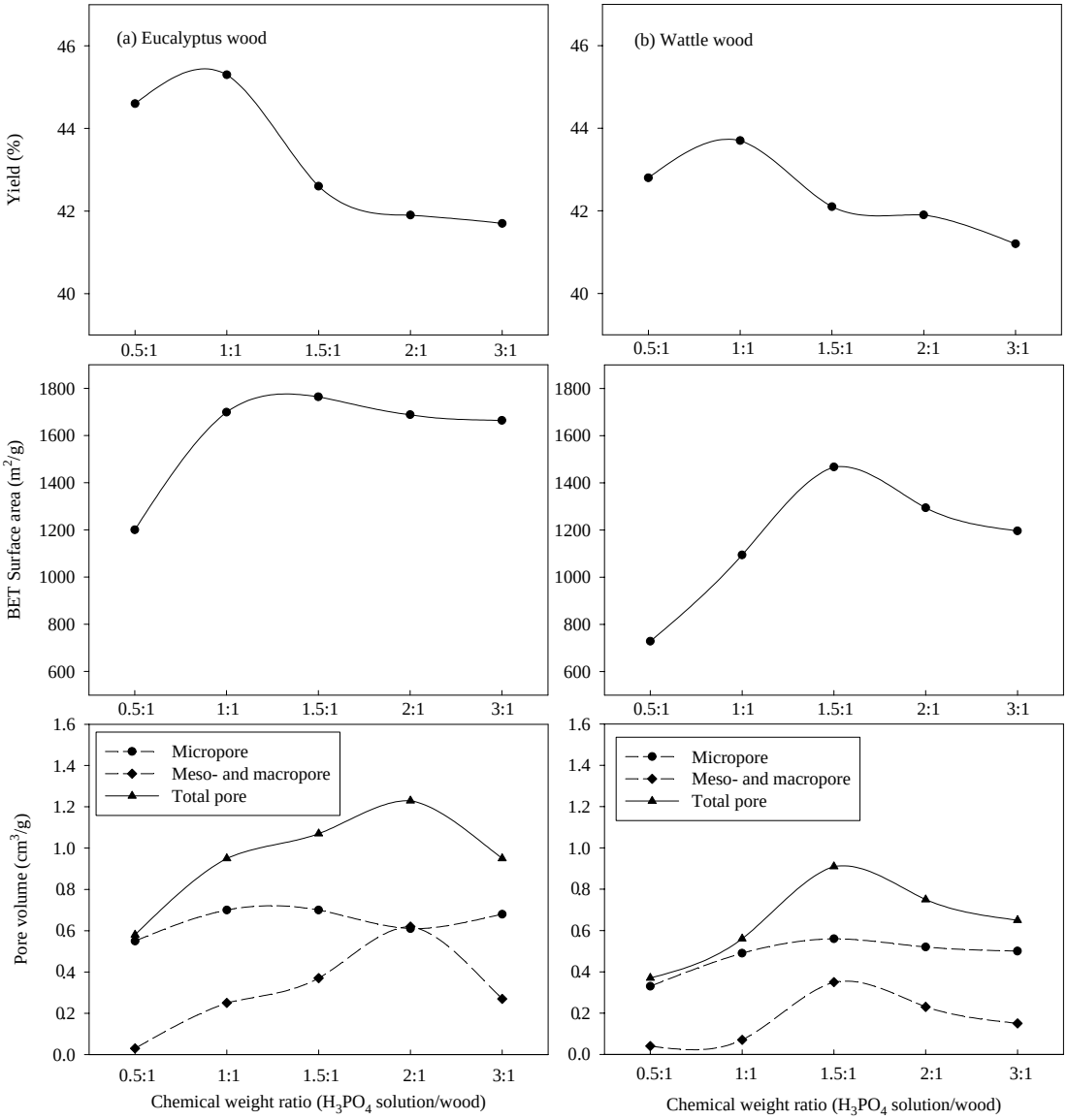

Figure 3.7 Effect of chemical weight ratio on the porous properties of activated carbons prepared from (a) eucalyptus and (b) wattle woods by chemical activation (impregnation time 1 hour, carbonization temperature 400^{o}C, and carbonization time 1 hour).

As observed in Figure 3.7, the chemical weight ratio shows an optimal effect on the total pore volume of activated carbons, with maximum pore volume occurring at weight ratios of 2:1 and 1.5:1 for eucalyptus and wattle woods, respectively. The effect on mesopore and macropore volume follows the same trend as the total pore volume, while micropore volume is less sensitive to the change in chemical weight ratio of acid. The drop in mesopore and macropore volume at high chemical weight ratio could be the collapse of these pores due to the strong action of the acid. This point will be elaborated later.

Figure 3.8 shows pore size distributions of activated carbons prepared from eucalyptus wood at chemical weight ratio 1.5:1 and 2:1 by applying the Density Functional Theory (DFT) method. For activated carbon prepared with chemical weight ratio 1.5:1, the pore size distribution show the main peak around 11 Å which corresponds to the micropore size. The main peak is shift to higher pore width (12 Å) for carbons prepared with chemical weight ratio 2:1 and this carbon shows smaller volume of this pore size. Both carbons show the creation of mesopore and macropore (pore width > 20 Å) with carbon prepared with chemical weight ratio 2:1 giving higher volume of this mesopore size than that prepared with chemical weight ratio of 1.5:1. This agrees with the results in Table 3.6, showing that the carbon prepared with chemical weight ratio 2:1 having lower micropore volume and higher meso- and macropore volume than carbon prepared with chemical weight ratio 1.5:1.

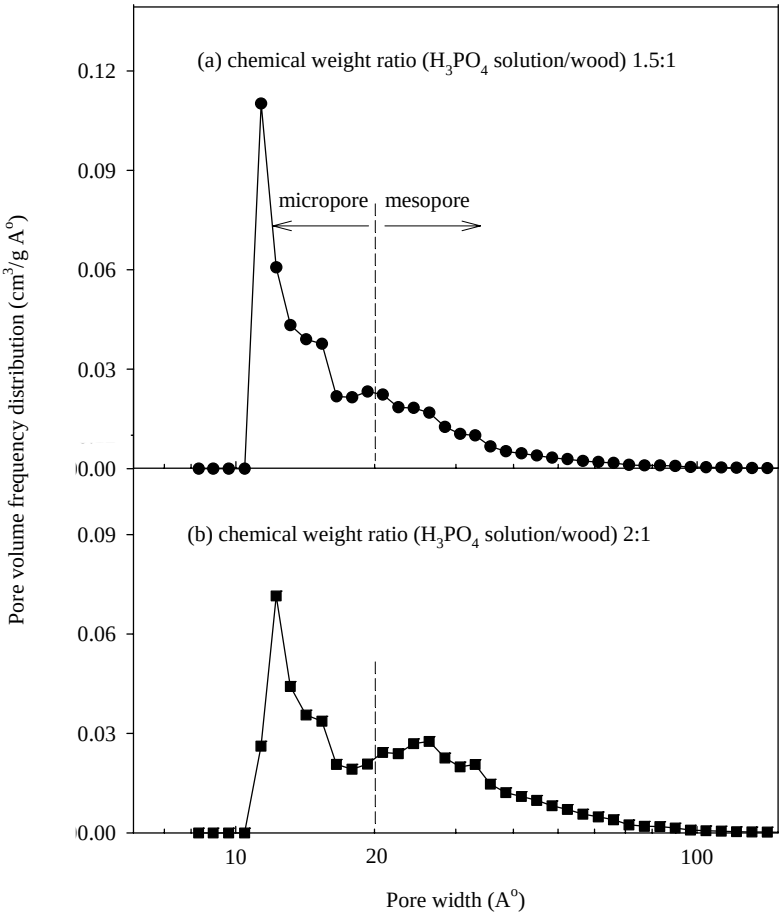

Figure 3.8 Pore size distribution of activated carbons prepared from eucalyptus wood by chemical activation at different chemical weight ratio (impregnation time 1 hour, carbonization temperature 400^{o}C, and carbonization time 1 hour).

It is noted that the progressive development of porosity appears to occur as more acid is incorporated into the raw wood materials, presumably due to increasing the degree of dilation of the structure by phosphate linkage until a limit is reached (chemical weight ratio 1.5:1). The excessive use of phosphoric acid has led to the reduction in porosity development. This might be attributed to the collapse of adjacent pores due to the weakness of the structure arising from the intensified

dilation. The collapse of the pores would lead to the decrease of surface area and the enlargement of pore size of the existing pore which is confirmed by the results of DFT. The DFT results (Figure 3.8) showed that the main peak of the obtained activated carbon with chemical weight ratio 2:1 shifts to the higher pore width (~ 10.5 Å) compared to activated carbon with chemical weight ratio 1:1 (~ 11 Å), and carbon with chemical weight ratio 2:1 shows the distribution of the pore width between 20 – 50 Å. Moreover, there appears a small distribution of pore width between 50 – 70 Å in the case of chemical weight ratio 2:1.

For other biomass such as peanut hull (Girgis, Yunis, and Soliman, 2002), the effect of impregnation ratio of H_3PO_4 solution/precursor (wt/wt) showed that the BET surface area, micropore volume, and total pore volume increased with an increase of impregnation ratio of H_3PO_4 solution/precursor from 0.5 to 1.0 but decreased with increasing of impregnation ratio from 1.0 to 1.6. However, the mesopore volume showed the reverse trend i.e. decreasing with an increase of impregnation ratio from 0.5 to 1.0 and increasing with higher impregnation ratios.

Figure 3.9 shows the adsorption and desorption isotherms of N_2 of activated carbons prepared from both woods. The shape of isotherm is of Type I. For activated carbons prepared from eucalyptus wood, the adsorption-desorption curves start to show hysteresis loops at chemical weight ratio 1:1, while wattle wood carbons start to show hysteresis loops at chemical weight ratio 1.5:1. The size of hysteresis loops follow the orders: 1:1 < 1.5:1 < 2:1 for eucalyptus wood and 3:1 < 2:1 < 1.5:1 for wattle wood. These results are consistent with those of mesopore volume presented in Table 3.6. The amount of N_2 adsorbed for obtained activated carbons follow the orders: 0.5:1 < 1:1 < 1.5:1 < 2:1 for eucalyptus wood and 0.5:1 <

1:1 < 3:1 < 2:1 < 1.5:1 for wattle wood. These orders match with the results of total pore volume presented in Table 3.6. It is noted that the adsorption and desorption isotherms of carbon prepared from eucalyptus wood at chemical weight ratio 3:1 are not included in the Figure 3.9 (a) because there are no significant differences between isotherms of this carbon with carbon prepared at chemical weight ratio 1:1. Again, eucalyptus wood-based carbons show higher amount of N_2 adsorbed than wattle wood-based carbons for all chemical weight ratios.

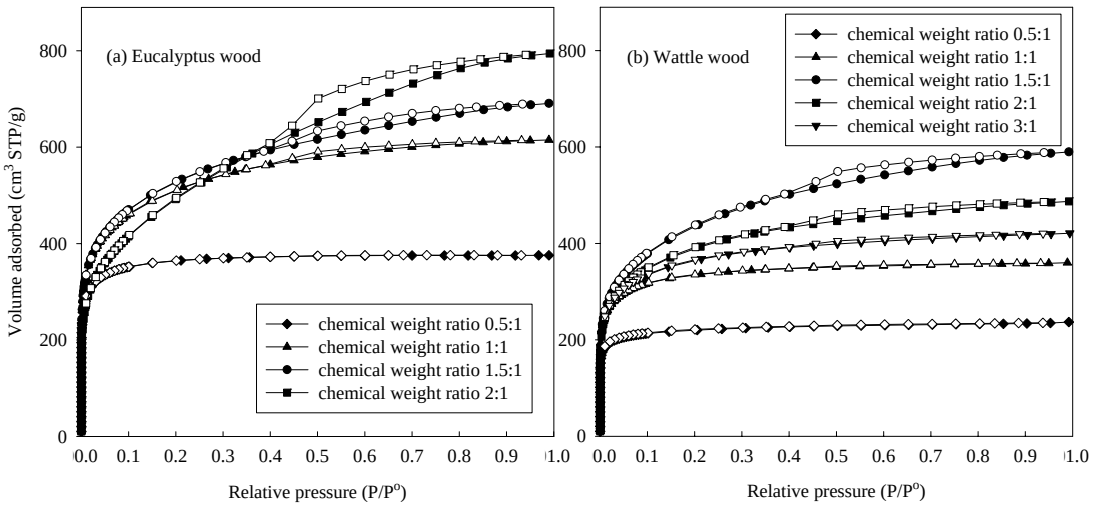

Figure 3.9 Adsorption (closed symbols) and desorption (open symbols) isotherms of N_2 at −196°C of activated carbons prepared from (a) eucalyptus and (b) wattle woods by chemical activation at different chemical weight ratio (impregnation time 1 hour, carbonization temperature 400°C, and carbonization time 1 hour).

3.3.2.3 Effect of carbonization time

As shown in the previous section, the activated carbon obtained at chemical weight ratio of H_3PO_4 solution and wood 1.5:1 has the highest surface area. Therefore, this section reports on the effect of carbonization time by fixing the chemical weight ratio at 1.5:1. The carbonization time was varied from 0.5 to 2 hours. The impregnation time used was 1 hour and carbonization temperature was 400^{o}C.

The yield and porous properties of the resulting activated carbons at different carbonization times are shown in Table 3.7 and Figure 3.10. The activated carbon yield decreases with the increase of carbonization time from 0.5 hour to 1 hour and increases at longer carbonization times for both woods. Eucalyptus wood shows higher carbon yield than wattle wood at all carbonization times.

For eucalyptus wood, the BET surface area and total pore volume increases with an increase of carbonization time from 0.5 hour to 1 hour followed by a linear decrease at longer times up to 2 hours. For wattle wood, the optimum carbonization time that produces maximum surface area also occurs at 1 hour, however, the degree of decrease in surface area at longer times becomes less.

For both woods, the effect of carbonization time on the micropore volume shows similar trend to that of total pore volume, but the variation of this porous property is not so significant over the carbonization time studied. The prepared activated carbons from both woods also show the variation of meso- and macropore volume in the same fashion as the effect on total pore volume.

Table 3.7 Effect of carbonization time on the porous properties of prepared activated carbons by chemical activation (chemical weight ratio of H_3PO_4 solution and wood 1.5:1, impregnation time 1 hour, and carbonization temperature 400^{o}C).

	Carbonization time (hour)	**Yield (%)**	S_{BET} **(m^2/g)**	V_{mic} **(cm^3/g)**	$V_{meso+mac}$ **(cm^3/g)**	V_T **(cm^3/g)**
Eucalyptus wood	0.5	44.7	1557	0.65 (77.4%)	0.19 (22.6%)	0.84
	1.0	42.6	1764	0.70 (65.4%)	0.37 (34.6%)	1.07
	1.5	44.4	1430	0.61 (79.2%)	0.16 (20.8%)	0.77
	2.0	44.6	1112	0.49 (89.1%)	0.06 (10.9%)	0.55
Wattle wood	0.5	43.2	858	0.36 (78.3%)	0.10 (21.7%)	0.46
	1.0	42.1	1467	0.56 (61.5%)	0.35 (38.5%)	0.91
	1.5	42.7	1266	0.52 (72.2%)	0.20 (27.8%)	0.72
	2.0	42.9	1216	0.50 (73.5%)	0.18 (26.5%)	0.68

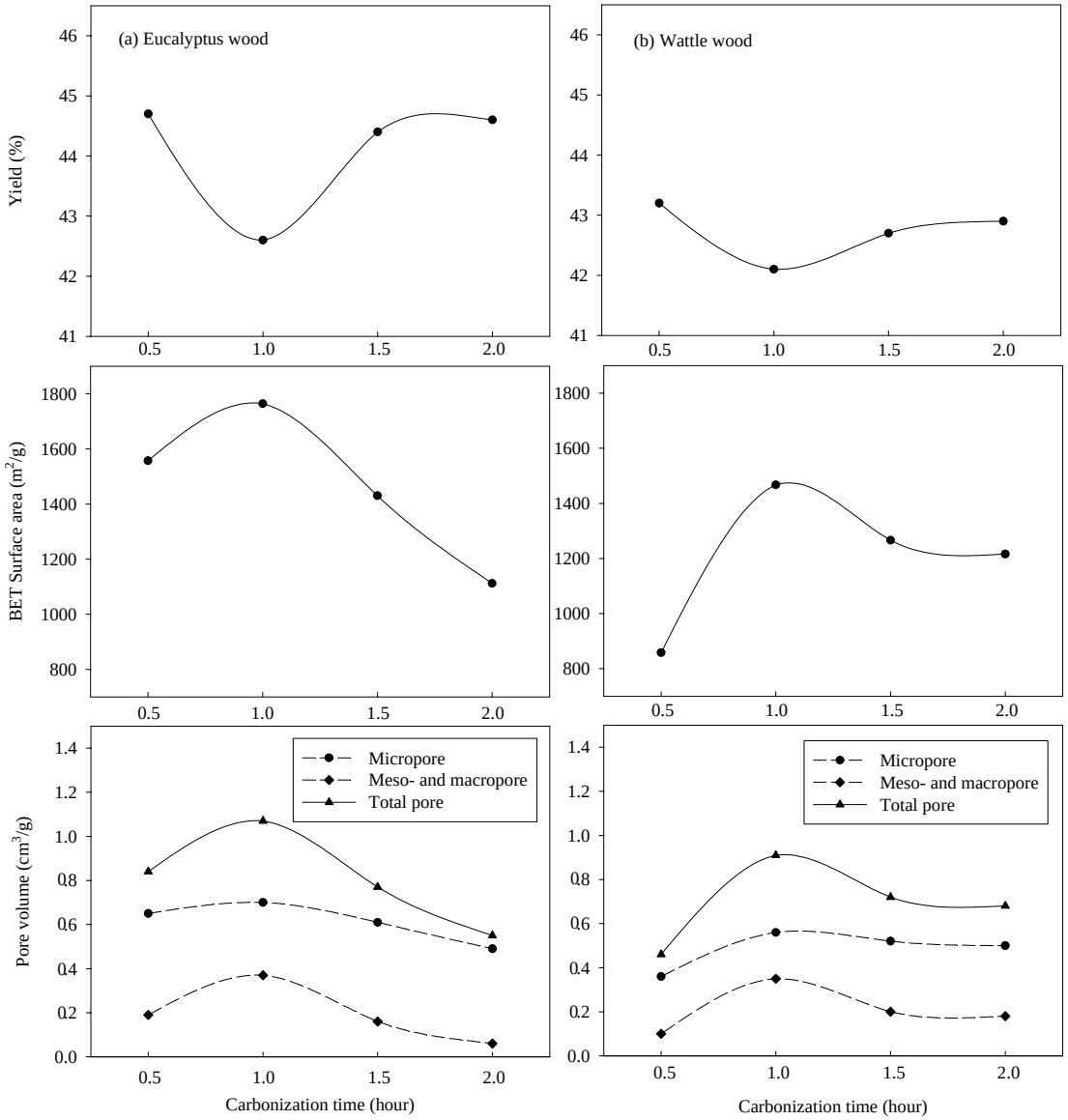

Figure 3.10 Effect of carbonization time on the porous properties of activated carbons prepared from (a) eucalyptus and (b) wattle woods by chemical activation (chemical weight ratio of H_3PO_4 solution and wood being 1.5:1, impregnation time 1 hour, and carbonization temperature 400^{o}C).

The progression of the structure dilation by phosphate linkage may lead to the increase of surface area and total pore volume when carbonization duration is increased from 0.5 hour to 1 hour, but these porous properties tend to decrease at longer carbonization times. This may be due to the collapse of weak pores caused by extreme dilation which could occur during long carbonization period. Again, eucalyptus wood shows better pore development than wattle wood i.e. higher surface area and total pore volume at all carbonization times. The carbonization time of 1 hour which gave the highest surface area and total pore volume was selected for further study of the effect of impregnation time on the properties of resulting activated carbons.

Figure 3.11 shows the adsorption and desorption isotherms of N_2 of eucalyptus and wattle wood-based activated carbons at different carbonization time. The shape of isotherm is also of Type I with the amount of N_2 adsorbed follow the orders: 2 hour < 1.5 hour < 0.5 hour < 1 hour for eucalyptus wood and 0.5 hour < 2 hour < 1.5 hour < 1 hour for wattle wood. These orders conform to the results of surface area and total pore volume presented in Table 3.7. Again, eucalyptus wood-based carbons show higher amount of N_2 adsorbed than wattle wood-based carbons at all carbonization times. For carbons prepared from eucalyptus wood, the adsorption-desorption curves show insignificant hysteresis loops at carbonization time 0.5 hour and 1.5 hours, while wattle wood carbons show almost no hysteresis loops at carbonization time 1.5 hours and 2 hours. However, at carbonization time of 1 hour, both woods show the clear existence of hysteresis loops. This result agrees with the result presented in Table 3.7 which indicates that carbonization time for 1 hour gave activated carbon with highest mesopore volume.

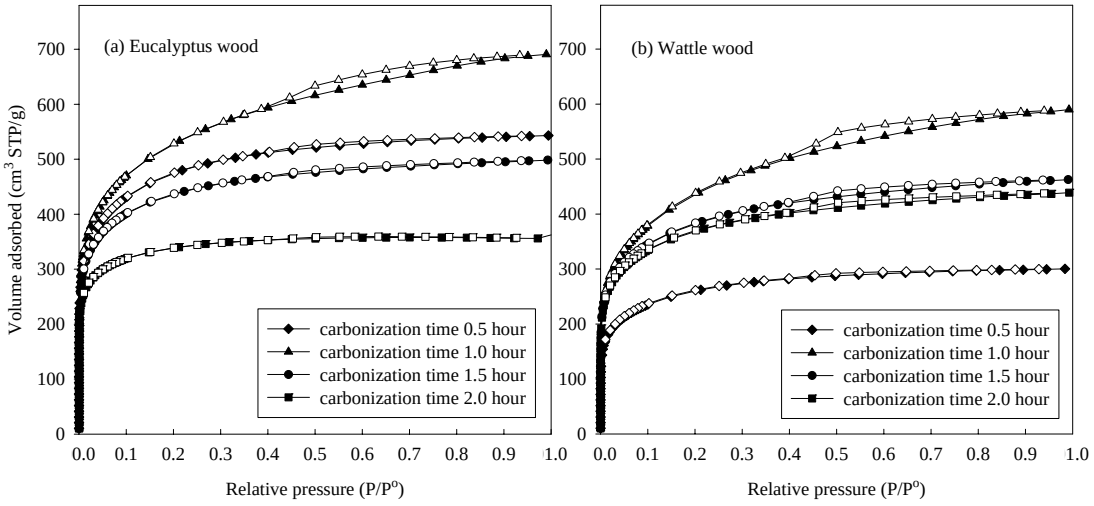

Figure 3.11 Adsorption (closed symbols) and desorption (open symbols) isotherms of N_2 at −196°C of activated carbons prepared from (a) eucalyptus and (b) wattle woods by chemical activation at different carbonization time (chemical weight ratio of H_3PO_4 solution and wood 1.5:1, impregnation time 1 hour, and carbonization temperature 400°C).

3.3.2.4 Effect of impregnation time

This section reports on the effect of impregnation time on the resulting activated carbon by varying this parameter from 0.5 to 3 hours. It can be seen from the previous section that the suitable carbonization time which produced carbons with highest surface area and total pore volume was 1 hour. Therefore, in studying the effect of impregnation time, the chemical weight ratio of H_3PO_4 solution and wood 1.5:1, carbonization temperature 400°C, and carbonization time 1 hour were chosen.

The effect of impregnation time on the yield and porous properties of the prepared activated carbons is shown in Table 3.8 and Figure 3.12.

There is a tendency for the product yield of activated carbons prepared from both woods to decrease as the impregnation time is increased. Eucalyptus wood shows higher carbon yield than wattle wood at all impregnation times.

For both woods, the BET surface area of the activated carbons increases with an increase of impregnation time up to 1.5 hours. The surface area then decreases with further increase in impregnation time from 1.5 hours to 2 hours. However, the surface area of eucalyptus wood-based carbon further decreases with increasing impregnation time from 2 hours on but there is no significant change for wattle-wood based carbon. The increase of surface area when increasing the impregnation time from 0.5 hour to 1.5 hours could be due to the ability of phosphoric acid to incorporate more into the raw material during long impregnation time, giving increased phosphate linkages at carbonization temperature of 400^{o}C. The decrease of surface area at longer impregnation time than 1.5 hours could be attributed to the collapse of pore due to extreme dilation of structure by phosphate linkages which could occur from the increasing amount of phosphoric acid inside the carbon structure during longer impregnation time. Therefore, the impregnation time of 1.5 hours which gave activated carbon with highest surface area is suitable for preparing activated carbon from both woods.

The total pore volume of activated carbon prepared from eucalyptus wood also shows the same trend as for the case of BET surface area. There is no significant change of micropore volume of the obtained carbons from both woods, while mesopore and macropore volume show similar variation to that observed with total pore volume. Again, at all impregnation time, eucalyptus wood shows higher total pore volume and surface area than wattle wood.

Table 3.8 Effect of impregnation time on the porous properties of prepared activated carbons by chemical activation (chemical weight ratio of H_3PO_4 solution and wood 1.5:1, carbonization temperature 400^oC, and carbonization time 1 hour).

	Impregnation time (hour)	**Yield (%)**	**S_{BET} (m^2/g)**	**V_{mic} (cm^3/g)**	**$V_{meso+mac}$ (cm^3/g)**	**V_T (cm^3/g)**
Eucalyptus wood	0.5	42.8	1508	0.64 (79.0%)	0.17 (21.0%)	0.81
	1.0	42.6	1764	0.70 (65.4%)	0.37 (34.6%)	1.07
	1.5	41.8	1857	0.70 (57.4%)	0.52 (42.6%)	1.22
	2.0	41.2	1714	0.66 (58.9%)	0.46 (41.1%)	1.12
	3.0	40.3	1543	0.64 (76.2%)	0.20 (23.8%)	0.84
Wattle wood	0.5	42.3	1164	0.51 (82.2%)	0.10 (17.8%)	0.61
	1.0	42.1	1467	0.56 (61.5%)	0.35 (38.5%)	0.91
	1.5	41.6	1550	0.64 (76.2%)	0.20 (23.8%)	0.84
	2.0	40.0	1444	0.60 (75.0%)	0.20 (25.0%)	0.80
	3.0	39.8	1440	0.59 (78.7%)	0.16 (21.3%)	0.75

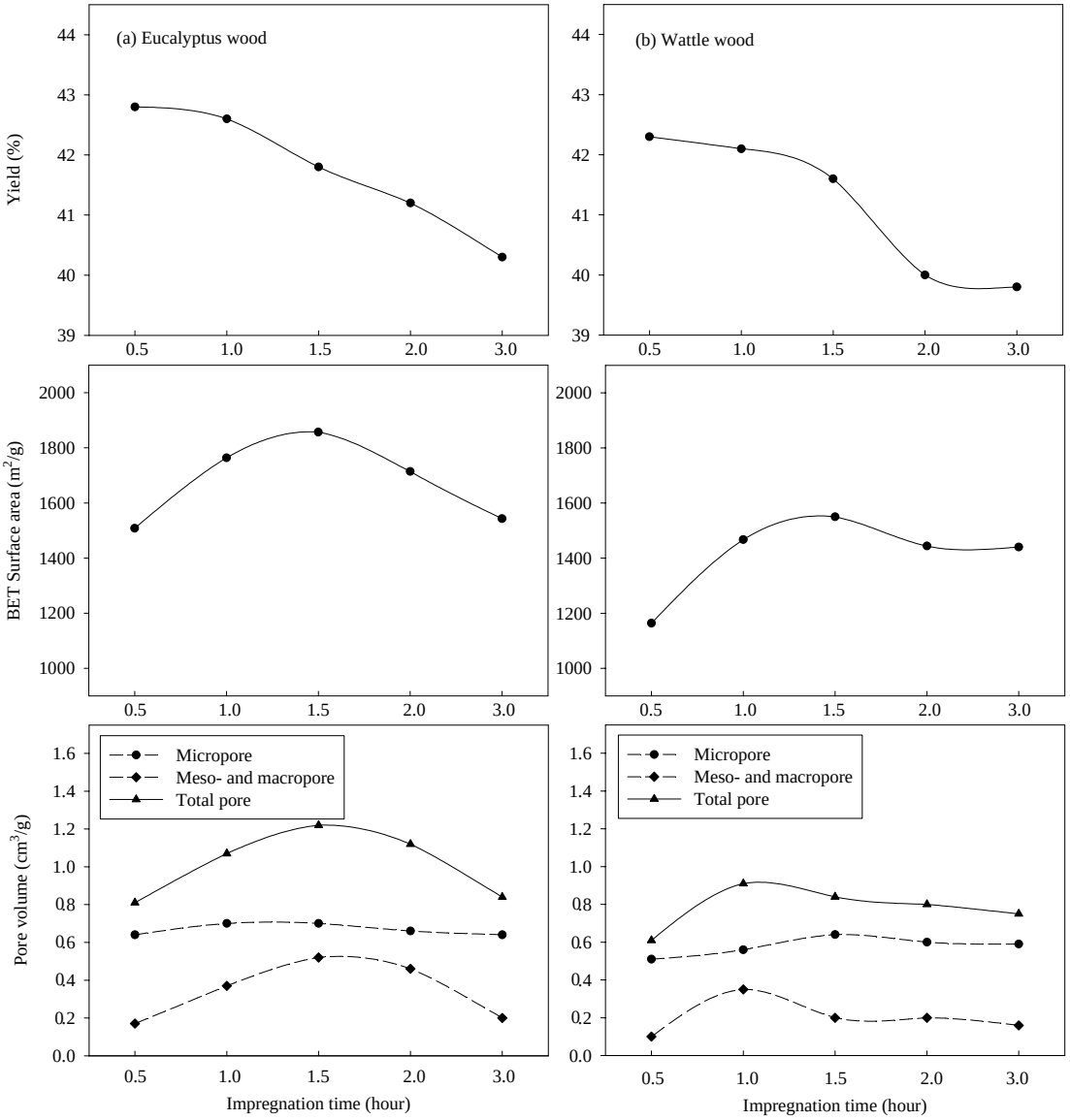

Figure 3.12 Effect of impregnation time on the porous properties of activated carbons prepared from (a) eucalyptus and (b) wattle woods by chemical activation (chemical weight ratio of H_3PO_4 solution and wood being 1.5:1, carbonization temperature 400^{o}C, and carbonization time 1 hour).

The optimal effect of impregnation time on the surface area and total pore volume of activated carbons from both woods was also observed in other works which used other different types of wood as raw materials. Gómez-Serrano, Cuerda-Correa, Fernández-González, Alexandre-Franco, and Macías-García (2005) found that surface area and total pore volume showed and increase with an increase of impregnation time from 1 hour to 3 hours for chestnut wood. The surface area decreased with further increase in impregnation time from 3 hours to 4 hours. The micropore volume also showed the same trend as that of surface area and total pore volume while mesopore and macropore volume reached a maximum value at impregnation time of 2 hours.

Figure 3.13 shows the adsorption and desorption isotherms of N_2 of eucalyptus and wattle wood-based carbons at different impregnation times. The shape of isotherm is of Type I with the amount of N_2 adsorbed follows the orders: 0.5 hour < 3 hour < 1 hour < 2 hour < 1.5 hour for eucalyptus wood and 0.5 hour < 3 hour < 2 hour < 1.5 hour < 1 hour for wattle wood. These orders match with the results of total pore volume presented in Table 3.8. Again, eucalyptus wood-based carbons show higher amount of N_2 adsorbed than wattle wood-based carbons at all impregnation times. The adsorption-desorption curves show significant hysteresis loops at impregnation time of 1 hour, 1.5 hours, and 2 hours for eucalyptus wood and impregnation time of 1 hour for wattle wood. This agrees with the results presented in Table 3.8 that the activated carbons prepared at theses conditions contain high proportion of mesopore volume (> 35%).

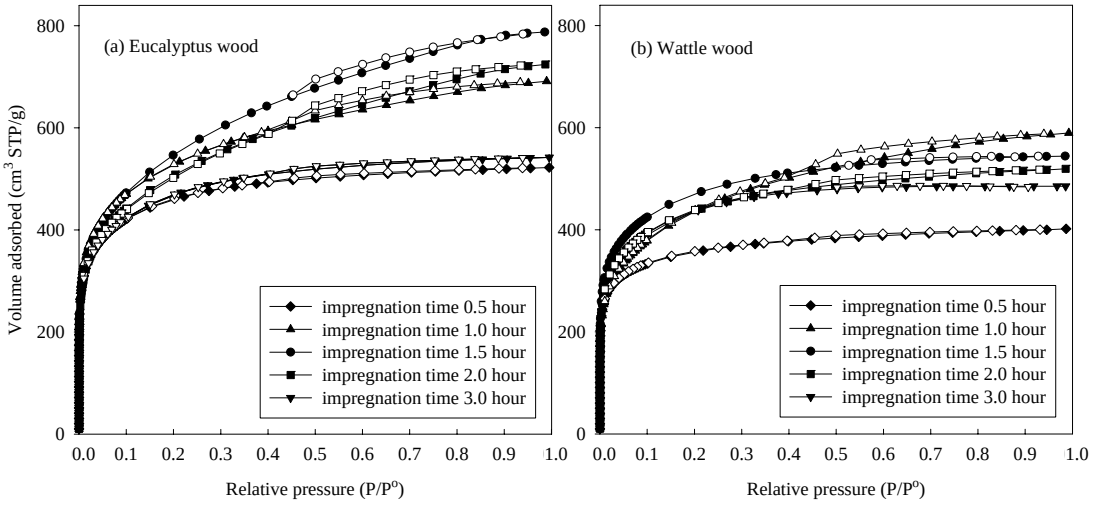

Figure 3.13 Adsorption (closed symbols) and desorption (open symbols) isotherms of N_2 at −196°C of activated carbons prepared from (a) eucalyptus and (b) wattle woods by chemical activation at different impregnation time (chemical weight ratio of H_3PO_4 solution and wood 1.5:1, carbonization temperature 400°C, and carbonization time 1 hour).

In this research, the highest surface area of the chemically prepared activated carbons were 1857 m^2/g and 1550 m^2/g for eucalyptus wood and wattle wood, respectively. These activated carbon have surface area higher than the commercial wood-based activated carbons i.e. BAX-1500 (1400 m^2/g), WVA-900 (1025 m^2/g), WVA-1100 (1110 m^2/g) which manufactured by using H_3PO_4 as chemical activating agent (Adib, Bagreev, and Bandosz, 1999). The prepared activated carbons also have the surface area higher than the activated carbons prepared from other biomasses such as coffee bean husk (1402 m^2/g) (Baquero et al., 2003), grain sorghum (1522 m^2/g) (Diao et al., 2002), bagasse (1574 m^2/g)

(Punsuwan, Tangsathitkulchai, and Tangsathitkulchai, 2006), and peach stone (1634 m^2/g) (Molina-Sabio et al., 1995) where H_3PO_4 was used as the activating agent.

3.3.3 Physical activation

In this section, the effects of carbonization conditions: temperature and time; and activation conditions: temperature, time, and CO_2 concentration on the porous properties of the prepared activated carbons were investigated.

3.3.3.1 Effect of carbonization temperature and time

In studying the effect of carbonization temperature on the porous properties of activated carbon, the char was prepared at the carbonization time of 1 hour. The activated carbon was prepared at the following conditions: activation temperature 800^oC, activation time 1 hour, and 50 vol% of CO_2 concentration. These preparation conditions were selected to first check the optimum carbonization temperature of both woods.

Table 3.9 and Figure 3.14 show the effect of carbonization temperature on the char yield and porous characteristics of prepared activated carbons. For both woods, the char yield rapidly decreases when increasing the carbonization temperature from 300^oC to 400^oC. Further increase in the carbonization temperature from 400^oC to 700^oC results in the decreased char yield but with lesser effect. However, for all carbonization temperatures, eucalyptus wood shows higher char yields compared to wattle wood except at the carbonization temperature of 700^oC.

Table 3.9 Effect of carbonization temperature on the porous properties of prepared activated carbons by physical activation (carbonization time 1 hour; activation conditions: temperature 800^{o}C, time 1 hour, and 50 vol% of CO_2 concentration).

	Carbonization temperature (^{o}C)	**Char yield (%)**	S_{BET} **(m^2/g)**	V_{mic} **(cm^3/g)**	$V_{meso+mac}$ **(cm^3/g)**	V_T **(cm^3/g)**
Eucalyptus wood	300	60.8	629	0.28 (87.5%)	0.04 (12.5%)	0.32
	400	34.2	651	0.29 (87.9%)	0.04 (12.1%)	0.33
	500	28.9	588	0.26 (86.7%)	0.04 (13.3%)	0.30
	600	25.2	574	0.26 (92.8%)	0.02 (7.2%)	0.28
	700	23.0	569	0.26 (89.6%)	0.03 (10.4%)	0.29
Wattle wood	300	60.1	585	0.26 (86.7%)	0.04 (13.3%)	0.30
	400	28.0	591	0.27 (93.1%)	0.02 (6.9%)	0.29
	500	24.1	548	0.24 (85.7%)	0.04 (14.3%)	0.28
	600	23.3	536	0.24 (85.7%)	0.04 (14.3%)	0.28
	700	23.1	535	0.24 (92.3%)	0.02 (7.7%)	0.26

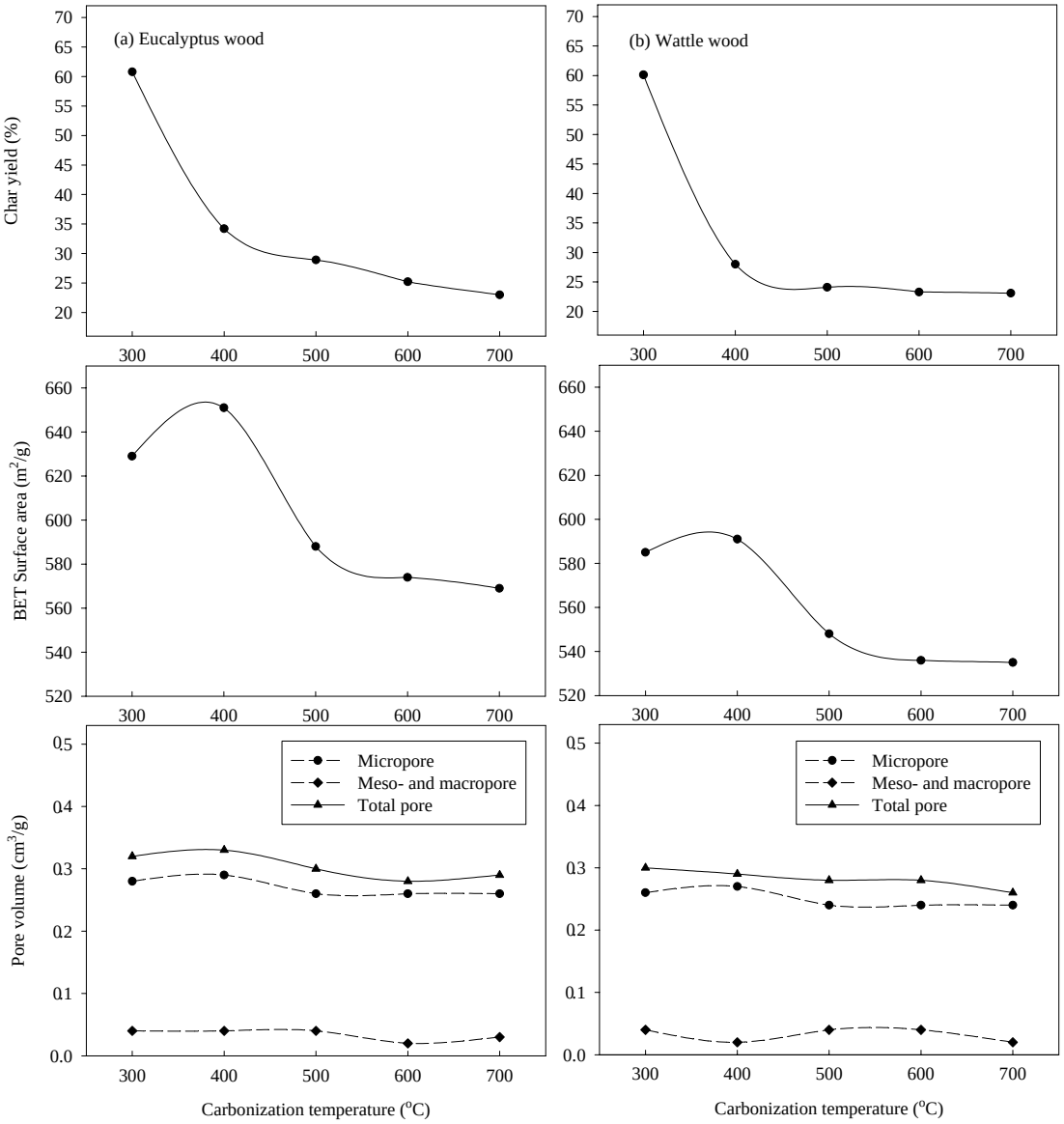

Figure 3.14 Effect of the carbonization temperature on the porous properties of the activated carbon prepared from (a) eucalyptus and (b) wattle woods by physical activation (carbonization time 1 hour; activation conditions: temperature 800^{o}C, time 1 hour, and 50 vol% of CO_2 concentration).

The porous properties of activated carbons presenting in Table 3.9 and Figure 3.14 show that increasing the carbonization temperature from 300^{o}C to 400^{o}C increases the BET surface area of both woods due to the increasing evolution of volatiles from the raw wood materials. Subsequent activation of these chars thus improved the formation and development of pores. However, the surface area decreases progressively when the carbonization temperature was further increased from 400^{o}C to 700^{o}C. This could be a consequence of decomposition of some volatile fractions to form an intermediate melt in the char structure. This melt probably closed some of the pores in the chars and subsequent activation of these chars may resulte in a decreased surface area of activated carbons (Lua, Yang, and Guo, 2004). Nevertheless, there are no significant change of the micropore volume, meso- and macropore volume, and total pore volume over the carbonization temperature studied. At all carbonization temperatures, eucalyptus wood shows higher surface area and pore volume than wattle wood.

Lua et al. (2004) studied the effect of the carbonization temperature on the porous properties of activated carbon prepared from pistachio-nut shell. They found that the BET surface area, micropore volume, meso- and macropore volume, and total pore volume increased with an increase of carbonization temperature from 250^{o}C to 500^{o}C and decreased with increasing of carbonization temperature from 500^{o}C to 800^{o}C.

The results show that carbonization temperature at 400^{o}C gave the highest BET surface area for both woods so that carbonization temperature of 400^{o}C was selected for subsequent study on the effect of carbonization time. It should be also noted from TGA results of Figure 3.2 that the carbonization temperature of

400^{o}C is the minimum temperature at which complete devolatilization is achievable, thus giving char with high carbon content. Higher carbonization temperature could give excessive volatile release, leading to the shrinkage of char. The optimum carbonization temperature for preparation of activated carbon also depends on the types of raw materials. For example, the complete devolatilization process of longan seed (Junpirom et al., 2007) and rice hull (Kim, Baek, Jeoung, and Park, 2003) occurred at 650^{o}C, while the complete removal of volatile matter for candlenut shell was 700^{o}C (Turmuzi, Daud, Tasirin, Takriff, and Iyuke, 2004).

In studying the effect of carbonization time, the carbonization temperature was maintained at 400^{o}C. Subsequent activation step was performed on this char for activation temperature of 800^{o}C, activation time 1 hour, and 50 vol% of CO_2 concentration.

Table 3.10 and Figure 3.15 show the effect of carbonization hold time on the char yield and porous properties of activated carbon prepared from both woods. For both woods, it is evident that the char yield decreases with increasing in carbonization time from 1 hour to 2 hours. The char yield remains almost unchanged after further increase in carbonization time from 2 hour to 4 hours. The results also indicate that for all carbonization times, eucalyptus wood carbons give higher char yield than wattle wood carbons.

Table 3.10 Effect of carbonization time on the porous properties of prepared activated carbons by physical activation (carbonization temperature 400^{o}C; activation conditions: temperature 800^{o}C, time 1 hour, and 50 vol% of CO_2 concentration).

	Carbonization time (hour)	**Char yield (%)**	S_{BET} **(m^2/g)**	V_{mic} **(cm^3/g)**	$V_{meso+mac}$ **(cm^3/g)**	V_T **(cm^3/g)**
Eucalyptus wood	1	34.2	651	0.29 (87.9%)	0.04 (12.1%)	0.33
	2	30.6	651	0.29 (85.3%)	0.05 (14.7%)	0.34
	3	30.4	651	0.29 (90.6%)	0.03 (9.4%)	0.32
	4	30.2	632	0.29 (96.7%)	0.01 (3.3%)	0.30
Wattle wood	1	28.0	591	0.27 (93.1%)	0.02 (6.9%)	0.29
	2	26.7	602	0.27 (87.1%)	0.04 (12.9%)	0.31
	3	26.7	600	0.27 (87.1%)	0.04 (12.9%)	0.31
	4	26.3	570	0.26 (89.6%)	0.03 (10.4%)	0.29

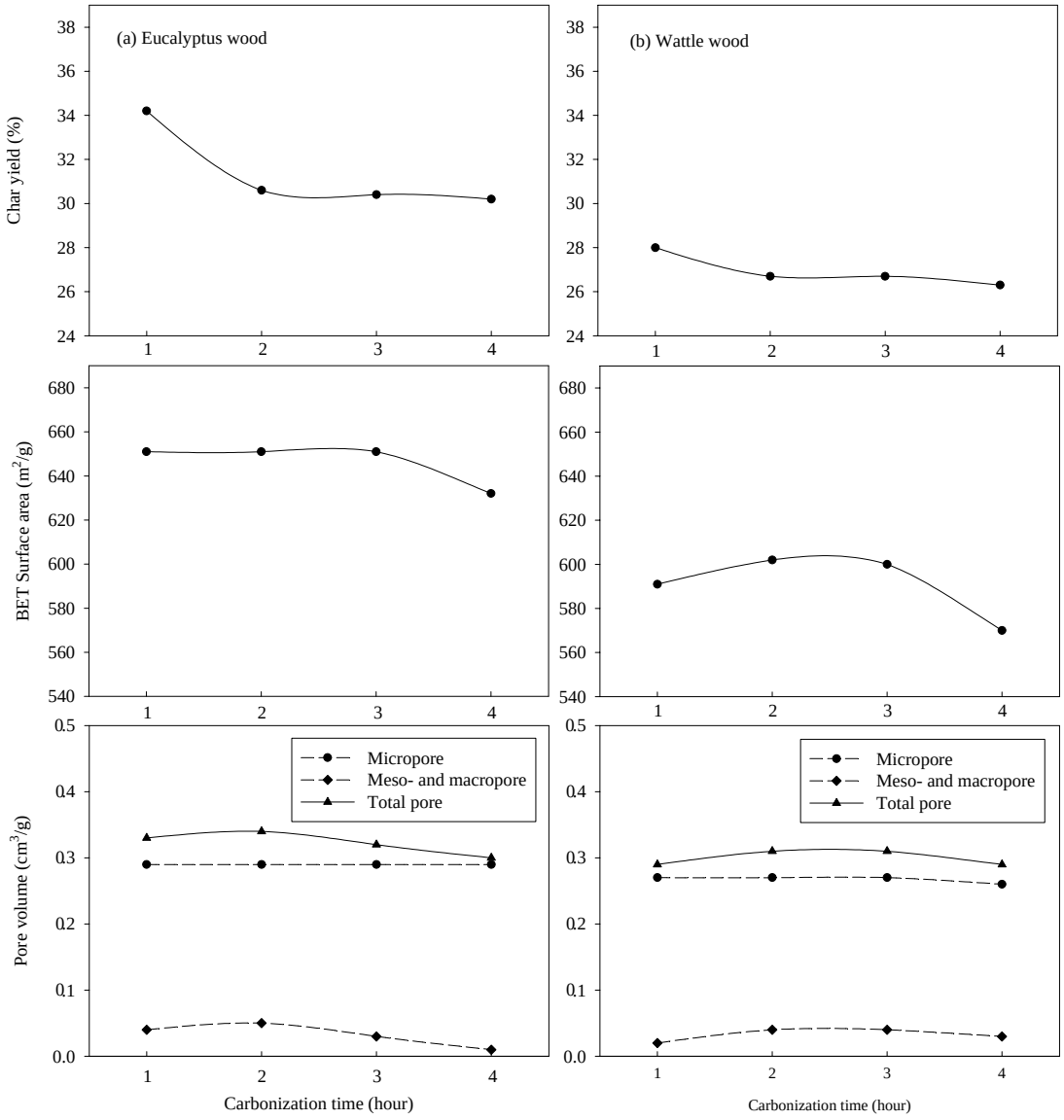

Figure 3.15 Effect of the carbonization time on the porous properties of the activated carbon prepared from (a) eucalyptus and (b) wattle woods by physical activation (carbonization temperature 400^{o}C; activation conditions: temperature 800^{o}C, time 1 hour, and 50 vol% of CO_2 concentration).

As shown in Table 3.10 and Figure 3.15, for eucalyptus wood, the carbonization time has no effect on the BET surface area up to 3 hours of carbonization but the surface area tends to decrease at the longer times. The mesopore volume and total pore volume slightly increase with an increase of carbonization time from 1 hour to 2 hours but to decrease with further increase of carbonization time from 2 hours to 4 hours, although these effects are not very pronounced. However, there is no effect of carbonization time on the micropore volume of the resulting eucalyptus-based carbons. For wattle wood, increasing the hold time during carbonization from 1 hour to 2 hours slightly increases the surface area, but thereafter this value decreases when the hold time is further increased up to 4 hours. Nevertheless, there is virtually no effect of carbonization time on the micropore volume, mesopore volume, and total pore volume of the wattle-based carbons. Again, at all carbonization times, eucalyptus wood shows better pore development than wattle wood.

Lua et al. (2004) also studied the effect of the carbonization time on the porous properties of activated carbon prepared from pistachio-nut shell. They reported that the BET surface area, micropore volume, meso- and macropore volume, and total pore volume increased with an increase of carbonization time from 1 hour to 2 hours but decreased at longer times from 2 hours to 3 hours.

As mentioned before, carbonization time almost had no effect on the surface area and pore volume development of activated carbons from both woods. Because of the highest char yield obtained and minimum time requirement, the carbonization time of 1 hour was thus selected for further investigation of the effect of activation conditions. Therefore, the char prepared at carbonization temperature

400°C, carbonization time 1 hour, and heating rate 25°C/min was selected for further study on the effects of activation temperature, activation time, CO_2 concentration and heating rate during the activation step with CO_2.

Table 3.11 shows the results of proximate analysis of the char obtained from each wood. It is clear that the fixed carbon content of char was significantly increased after carbonization (from 18.3 wt% and 16.6 wt% of raw eucalyptus and wattle wood materials). The volatile matters of both chars were decreased from 76.4 wt% of raw eucalyptus wood to 30.1 wt% and 78.3 wt% of raw wattle wood to 30.7 wt%. The surface area and pore volume of both chars before activation were extremely low as shown in Table 3.11, partly due to the pore blockage by tarry products resulting from the carbonization process.

Table 3.11 Properties of char prepared at carbonization temperature of 400°C for 1 hour using heating rate 25°C/min (the values of proximate analysis in parentheses are moisture free basis).

	Eucalyptus wood	**Wattle wood**
Proximate analysis (wt%)		
Fixed carbon	65.4 (68.3)	64.9 (67.0)
Volatile matters	30.1 (31.5)	30.7 (31.7)
Ash	0.2 (0.2)	1.3 (1.3)
Moisture	4.3	3.1
Porous property		
S_{BET} (m^2/g)	4.9	4.7
V_T (cm^3/g)	0.03	0.02

3.3.3.2 Effect of activation temperature and time

In studying the effect of activation temperature and time, the CO_2 concentration was used at 50 vol%. For activation temperature 600 – 800^oC, the effect of activation time was studied at 1 hour to 5 hours while for activation temperature between 850 – 900^oC the activation time of 1 hour was used. When activating at high temperatures (850 – 900^oC) and long activation time (> 1 hour), the activated carbon product turned into ash.

Figure 3.16 and Figure 3.17 shows, respectively, the effect of activation time and temperature on the extent of char burn-off due to C–CO_2 gasification reaction. For both woods, the burn-off increases linearly with increasing in the time of activation. Below 700^oC the char gasification rate, which is proportional to the slope of the curve, is relatively constant but at the higher temperature of 800^oC the rate increases by about twice for eucalyptus wood and three times for wattle wood. It also appears that the rate of gasification during activation at the same temperature is higher for wattle wood, although the lignocellulosic compositions of both woods are not so different. Figure 3.17 shows that temperature has a marked effect on the extent of burn-off, particularly at temperatures higher than 700^oC and activation time longer than two hours where the burn-off increases rapidly with increasing temperature. The removal of carbon atom by the effect of time and temperature during the activation step would lead to the creation of new pores and enlargement of existing pores, with temperature of activation exerting the most effect.

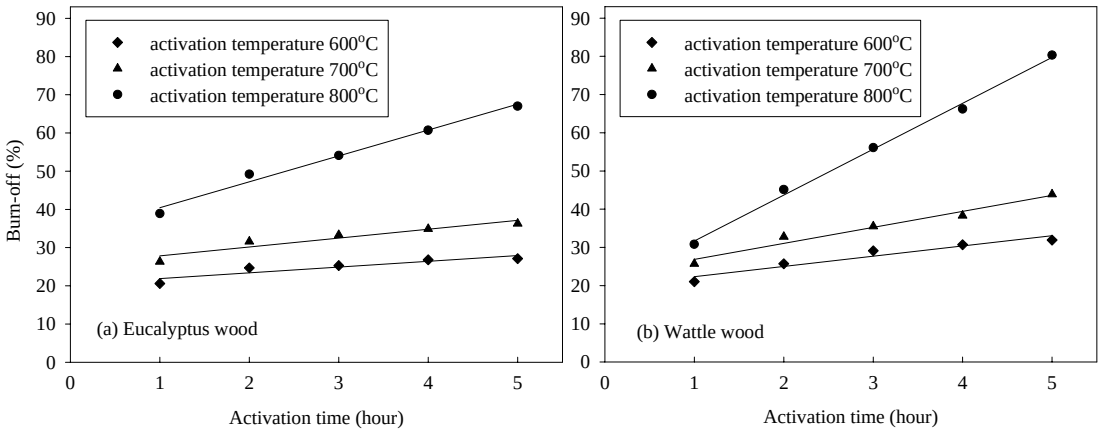

Figure 3.16 Burn-off of the chars at various times and temperatures of activation (a) eucalyptus and (b) wattle woods (carbonization conditions: temperature 400°C and time 1 hour; activation condition: 50 vol% of CO_2 concentration).

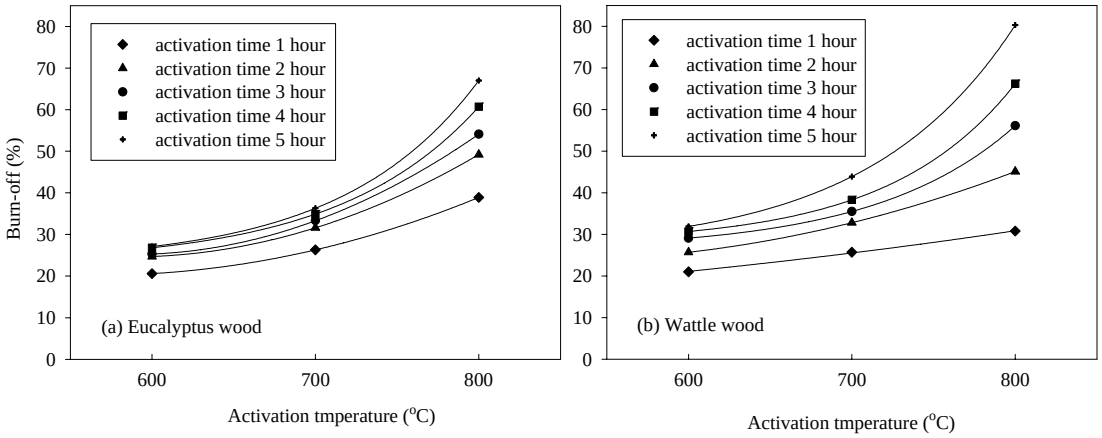

Figure 3.17 Burn-off of the chars at various temperatures and times of activation (a) eucalyptus and (b) wattle woods (carbonization conditions: temperature 400°C and time 1 hour; activation condition: 50 vol% of CO_2 concentration).

Figure 3.18 illustrates the dependence of char burn-off, which is indicative of extent of gasification reaction and hence the pore development, on the activation time and temperature for eucalyptus and wattle wood-derived chars. These burn-off contours were constructed directly from Figure 3.16 and Figure 3.17 by interpolation and are useful for the selection of activation conditions (activation time and activation temperature) to obtain the required level of char burn-off.

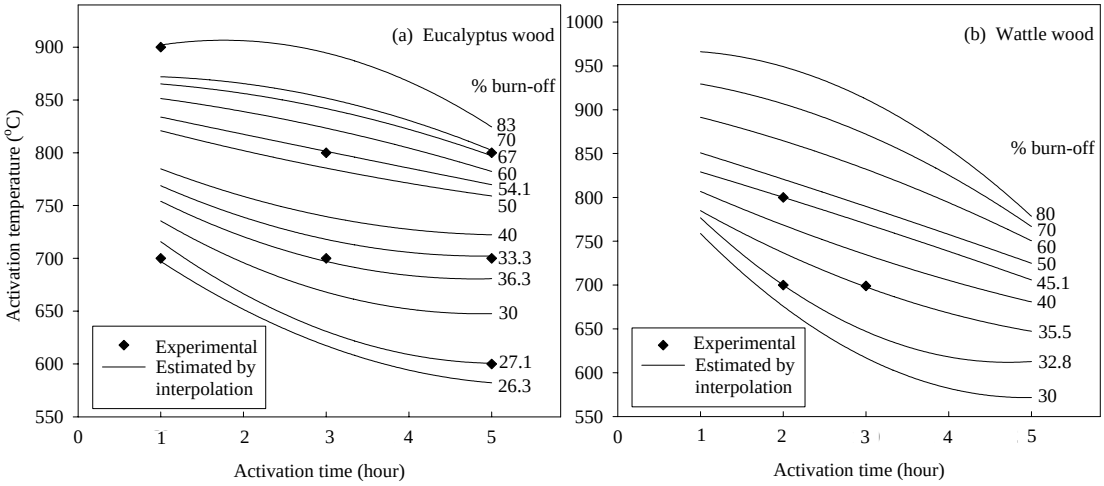

Figure 3.18 Contour of % burn-off as a function of activation time and temperature (a) eucalyptus and (b) wattle woods (carbonization conditions: temperature 400^{o}C and time 1 hour; activation condition: 50 vol% of CO_2 concentration).

Table 3.12, Table 3.13, Figure 3.19, and Figure 3.20 show the effect of the activation temperature and activation time on the porous properties of the prepared activated carbons. For both activated carbon series with activation time of 1 hour, the increase in activation temperature leads to an increase in BET surface area, micropore volume, meso- and macropore volume, and total pore volume. Increasing

in activation temperature from 600^{o}C to 700^{o}C leads to a slight increase in the percentage of micropore volume but the percentage of meso- and macropore volume shows the reverse trend. However, at temperatures higher than 700^{o}C, the percentage of micropore volume starts to decrease while BET surface area, micropore volume, meso- and macropore volume, percentage of meso- and macropore volume, and total pore volume tends to increase with the increase in activation temperature. This signifies that at higher temperatures there were not only the development of micropore by C–CO_2 reaction and the opening of blocked pores by devolatilization process, resulting in the formation of new micropores, but also the widening of existing micropore by gasification reaction and possibly by the collapse of adjacent pore walls.

For activated carbon samples with activation times longer than 1 hour, the BET surface area, micropore volume, meso- and macropore volume, percentage of meso- and macropore volume, and total pore volume also increases with activation temperature but the percentage of micropore volume decreases. This again is caused by the corresponding increase in the extent of gasification reaction for long activation time and also the widening of existing micropore by gasification reaction. It is also observed that at temperatures greater than 700^{o}C, the relative increase in the surface area with increasing temperature is higher for longer activation time.

Table 3.12 Effect of activation temperature and time on the porous properties of activated carbons prepared from eucalyptus wood by physical activation (carbonization conditions: temperature 400^{o}C and time 1 hour; activation condition: 50 vol% of CO_2 concentration).

Activation temperature (^{o}C)	**Activation time (hour)**	**Burn off (%)**	**S_{BET} (m^2/g)**	**V_{mic} (cm^3/g)**	**$V_{meso+mac}$ (cm^3/g)**	**V_T (cm^3/g)**
600	1	20.6	460	0.21 (91.3%)	0.02 (8.7%)	0.23
	2	24.7	463	0.21 (91.3%)	0.02 (8.7%)	0.23
	3	25.3	467	0.21 (91.3%)	0.02 (8.7%)	0.23
	4	26.8	471	0.21 (91.3%)	0.02 (8.7%)	0.23
	5	27.1	473	0.21 (91.3%)	0.02 (8.7%)	0.23
700	1	26.3	507	0.23 (92.0%)	0.02 (8.0%)	0.25
	2	31.6	556	0.25 (89.3%)	0.03 (10.7%)	0.28
	3	33.3	560	0.25 (89.3%)	0.03 (10.7%)	0.28
	4	34.9	577	0.26 (86.7%)	0.04 (13.3%)	0.30
	5	36.3	589	0.26 (84.0%)	0.05 (16.0%)	0.31
800	1	38.9	651	0.29 (87.9%)	0.04 (12.1%)	0.33
	2	49.2	828	0.36 (83.7%)	0.07 (16.3%)	0.43
	3	54.1	907	0.40 (80.0%)	0.10 (20.0%)	0.50
	4	60.7	1003	0.44 (78.6%)	0.12 (21.4%)	0.56
	5	67.0	1110	0.49 (77.8%)	0.14 (22.2%)	0.63
850	1	66.1	1016	0.44 (83.0%)	0.09 (17.0%)	0.53
900	1	83.0	1491	0.66 (82.5%)	0.14 (17.5%)	0.80

Table 3.13 Effect of activation temperature and time on the porous properties of activated carbons prepared from wattle wood by physical activation (carbonization conditions: temperature 400^{o}Cand time 1 hour; activation condition: 50 vol% of CO_2 concentration).

Activation temperature (^{o}C)	**Activation time (hour)**	**Burn off (%)**	**S_{BET} (m^2/g)**	**V_{mic} (cm^3/g)**	**$V_{meso+mac}$ (cm^3/g)**	**V_T (cm^3/g)**
600	1	21.0	433	0.20 (95.2%)	0.01 (4.8%)	0.21
	2	25.7	439	0.20 (95.2%)	0.01 (4.8%)	0.21
	3	29.1	451	0.21 (91.3%)	0.02 (8.7%)	0.23
	4	30.7	454	0.21 (91.3%)	0.02 (8.7%)	0.23
	5	31.9	512	0.23 (88.5%)	0.03 (11.5%)	0.26
700	1	25.7	473	0.22 (95.6%)	0.01 (4.4%)	0.23
	2	32.8	511	0.24 (92.3%)	0.02 (7.7%)	0.26
	3	35.5	548	0.25 (89.3%)	0.03 (10.7%)	0.28
	4	38.3	580	0.26 (86.7%)	0.04 (13.3%)	0.30
	5	43.9	606	0.27 (84.4%)	0.05 (15.6%)	0.32
800	1	30.8	591	0.27 (93.1%)	0.02 (6.9%)	0.29
	2	45.1	719	0.32 (86.5%)	0.05 (13.5%)	0.37
	3	56.1	823	0.37 (86.0%)	0.06 (14.0%)	0.43
	4	66.2	846	0.38 (84.4%)	0.07 (15.6%)	0.45
	5	80.3	1032	0.46 (82.1%)	0.10 (17.9%)	0.56
850	1	56.8	828	0.37 (84.1%)	0.07 (15.9%)	0.44
900	1	67.1	1000	0.44 (81.5%)	0.10 (18.5%)	0.54

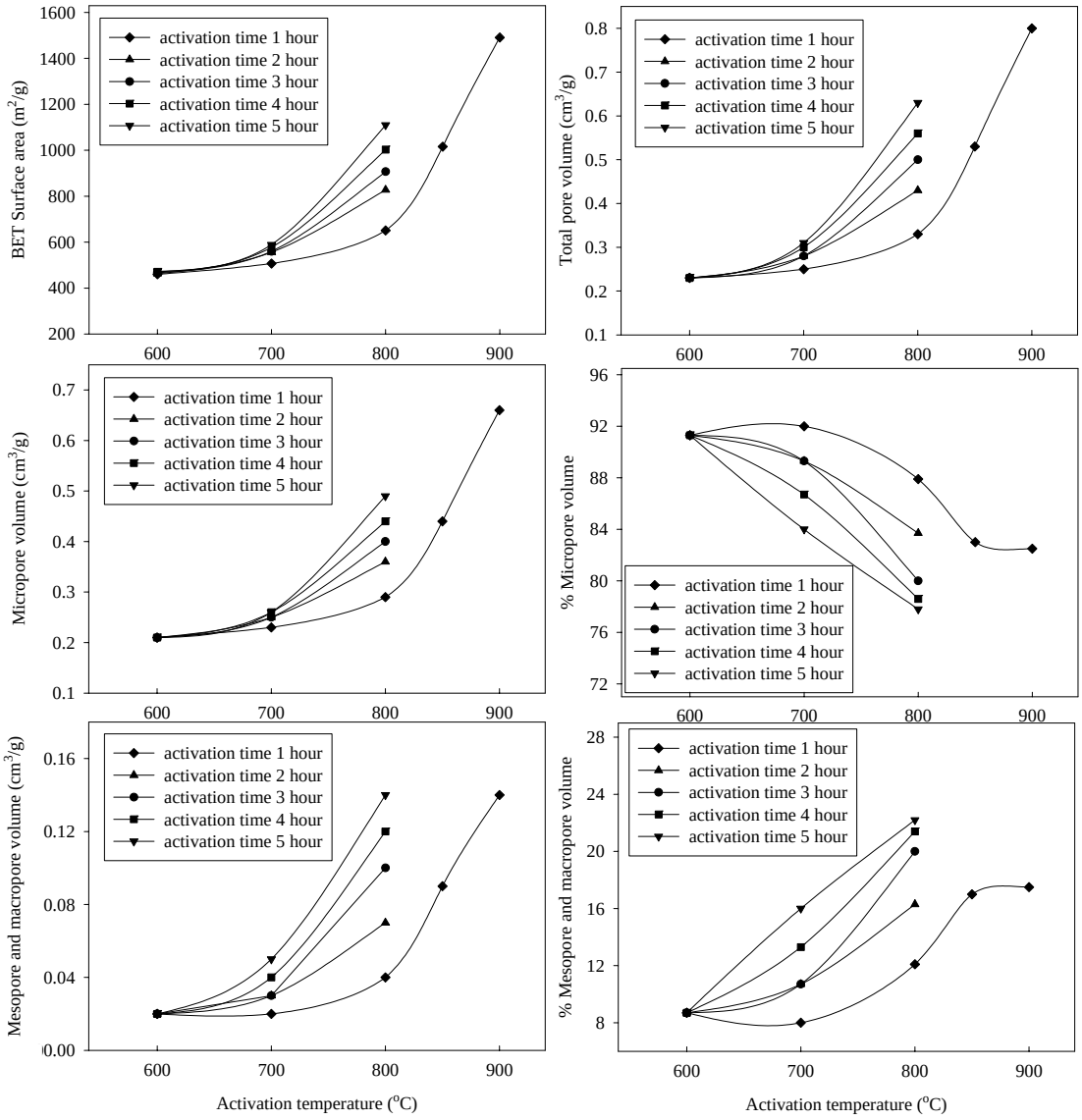

Figure 3.19 Effect of the activation temperature and activation time on the porous properties of the activated carbon prepared from eucalyptus wood by physical activation (carbonization conditions: temperature 400^{o}C and time 1 hour; activation condition: 50 vol% of CO_2 concentration).

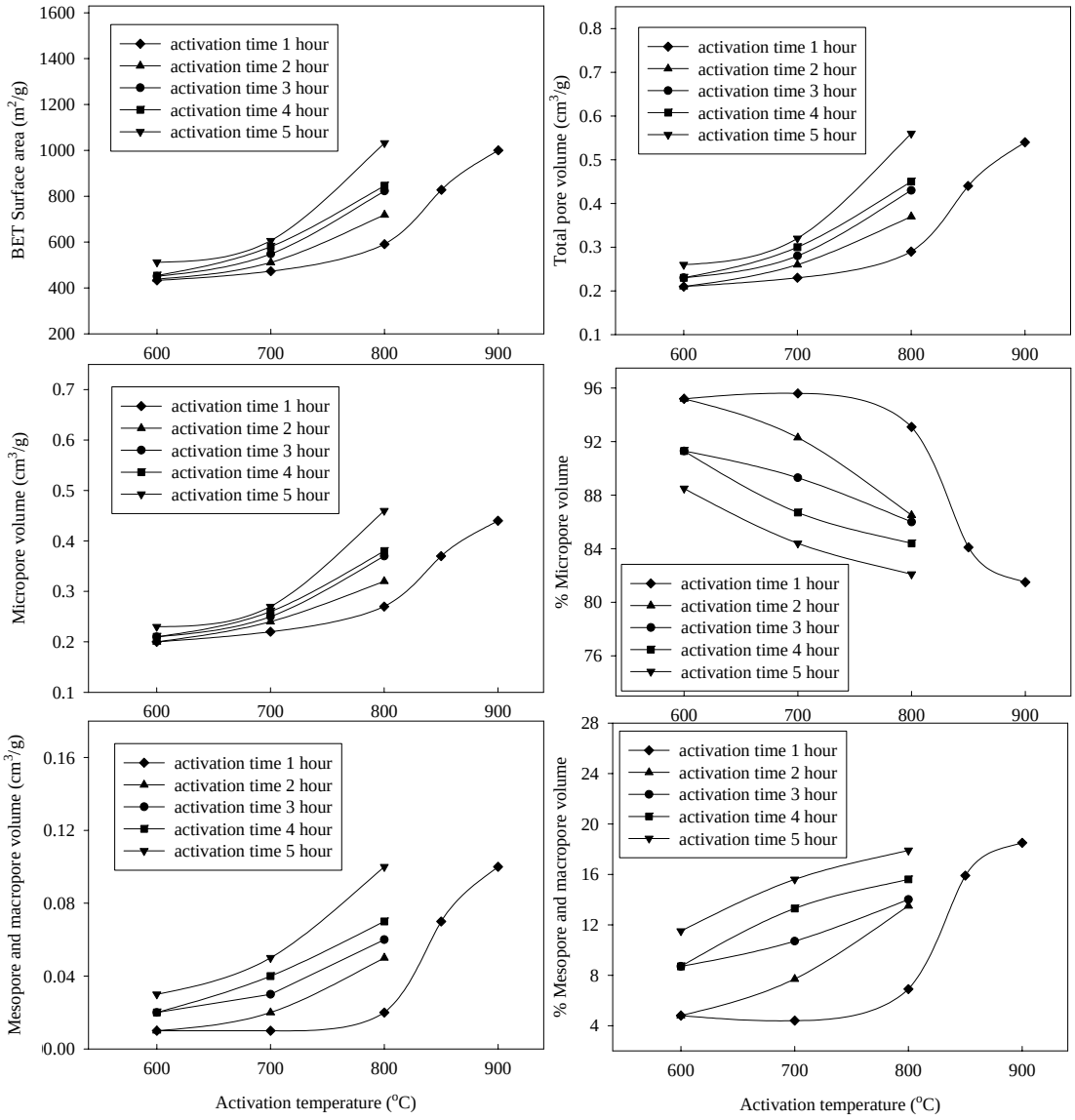

Figure 3.20 Effect of the activation temperature and activation time on the porous properties of the activated carbon prepared from wattle wood by physical activation (carbonization conditions: temperature 400^{o}C and time 1 hour; activation condition: 50 vol% of CO_2 concentration).

At any activation temperature, the effect of increasing activation time is to increase BET surface area, micropore volume, meso- and macropore volume, percentage of meso- and macropore volume, and total pore volume but the proportional increase is much greater at higher activation temperatures. There is also a tendency for the percentage of micropore volume to decrease as the time of activation is increased, with higher temperatures having the larger effect.

Under the same activation conditions, eucalyptus wood gave activated carbon with high surface area and pore volume than wattle wood. For eucalyptus wood, the activation conditions of 900^{o}C and 1 hour gave the highest surface area of 1491 m^2/g and total pore volume of 0.8 cm^3/g while wattle wood occurred at 800^{o}C and 5 hour (surface area of 1032 m^2/g and total pore volume of 0.56 cm^3/g).

The effect of activation temperature and time on the porous properties of activated carbon prepared from other lignocellulosic material such as longan seed (Junpirom et al., 2007) showed that BET surface area, micropore volume, meso- and macropore volume, percentage of meso- and macropore volume, and total pore volume increased with an increase of activation time from 0.5 hour to 3 hour while percentage of micropore volume decreased with an increase of activation time. At constant activation time, the surface area, micropore volume, meso- and macropore volume, percentage of meso- and macropore volume, and total pore volume increased with the increase of activation temperature from 800^{o}C to 900^{o}C. However, the percentage of micropore volume decreased with the increase activation temperatures over this temperature range. For oil-palm shell (Guo and Lua, 2002), the increase of activation temperature from 500^{o}C to 900^{o}C led to the increase of BET

surface area, micropore volume, percentage of micropore volume, and total pore volume while the percentage of meso- and macropore volume decreased. Nevertheless, the mesopore and macropore volume increased with an increase of activation temperature from 500^{o}C to 700^{o}C but there were no changes of these values at higher temperatures.

Figure 3.21 shows the correlation between the char burn-off and the BET surface area and total pore volume. It is observed that, both the BET surface area and total pore volume increase with the increase in the degree of burn-off as expected. Wattle wood-based activated carbon shows an approximate linear relationship over the entire range of burn-off up to 80%. The eucalyptus wood-based activated carbon gives approximately the same surface area and total pore volume as those of wattle wood-based activated carbon up to about 40% burn-off but gives higher porous property values at higher burn-off with the difference becoming greater at higher burn-off levels. Table 3.14 lists the fitted parameters for estimating the porous properties of activated carbons from both woods, using the following quadratic equation:

$$y = a_1 + a_2 x + a_3 x^2 \tag{3.11}$$

where y represents BET surface area or total pore volume and x is the % burn-off, covering burn-off up to about 80%.

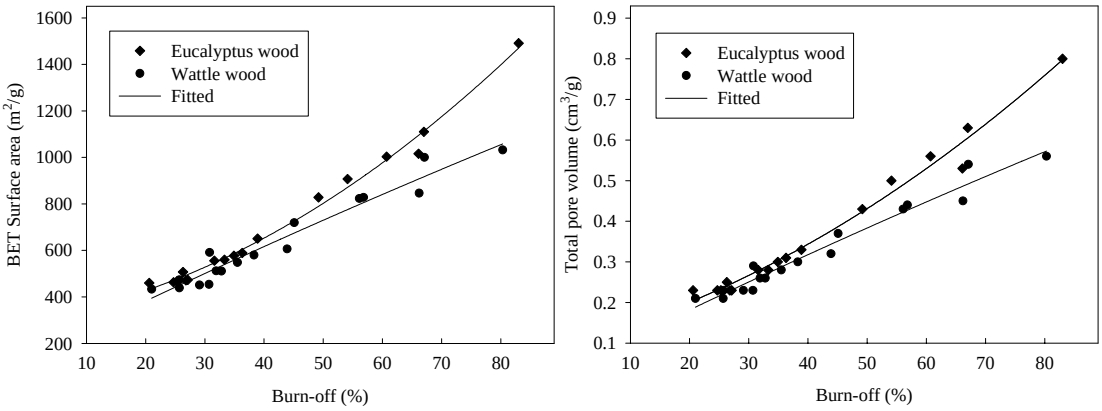

Figure 3.21 Effect of char burn-off on the porous properties of the activated carbon prepared by physical activation.

Table 3.14 Parameters of empirical equations (equation 3.11) for estimating porous properties of activated carbon from % burn-off.

	BET surface area (m^2/g)				**Total pore volume (cm^3/g)**			
	a_1	a_2	a_3	R^2	a_1	a_2	a_3	R^2
Eucalyptus wood	299.48	3.94	0.12	0.999	0.10	3.90×10^{-3}	5.41×10^{-5}	0.997
Wattle wood	138.54	12.45	-0.01	0.996	0.04	7.30×10^{-3}	-7.75×10^{-6}	0.996

Adsorption and desorption isotherms of N_2 at -196^oC for activated carbons prepared at different activation temperatures and activation times are shown in Figure 3.22 and Figure 3.23. As shown in Figure 3.22 and Figure 3.23, at activation time of 1 hour, the activated carbon prepared at 900^oC has the highest adsorption capacity for both woods. The amount of N_2 adsorbed at activation time 1 hour of both woods follows the order: $600^oC < 700^oC < 800^oC < 850^oC < 900^oC$ which is in agreement with the results of total pore volume presented in Table 3.12 and Table 3.13. It is obvious that eucalyptus wood-based carbons show higher amount of N_2 adsorbed than wattle wood-based carbons at all activation temperatures for activation time 1 hour. For the activated carbons prepared at $600 – 800^oC$ for 1 hour, the nitrogen uptake is significant only in the low-pressure range, i.e., for the relative pressure less than 0.2. In the high-pressure range, slight increase in adsorption is observed. According to the IUPAC classification (Patrick, 1995) this shape of isotherm is of Type I, indicating that the prepared activated carbons contain predominantly micropores. At higher activation temperatures ($> 800^oC$), the adsorption-desorption curves show closed hysteresis loops at relative pressure higher than about 0.4, indicating an increased proportion of mesopore volume.

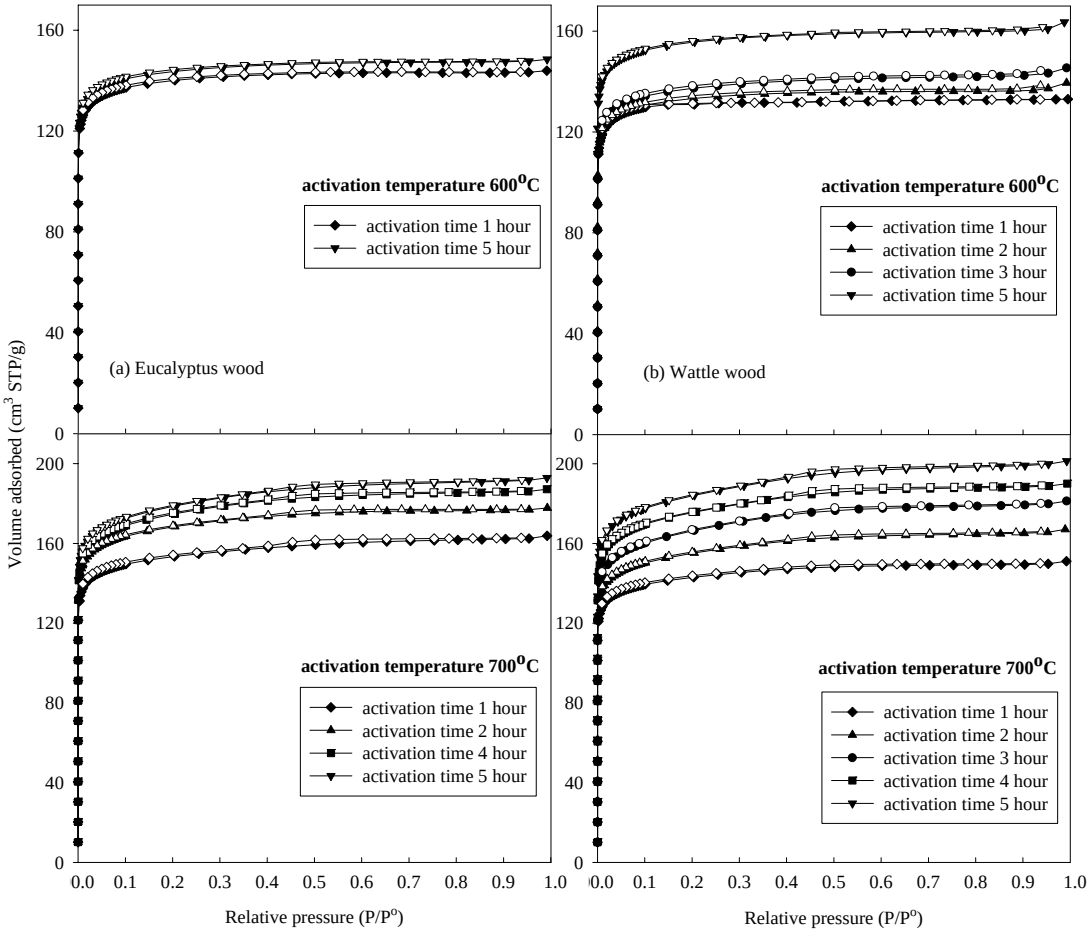

Figure 3.22 Adsorption (closed symbols) and desorption (open symbols) isotherms of N_2 at −196°C of activated carbons prepared from (a) eucalyptus and (b) wattle woods by physical activation at activation temperature 600°C and 700°C (carbonization conditions: temperature 400°C and time 1 hour; activation conditions: 50 vol% of CO_2 concentration).

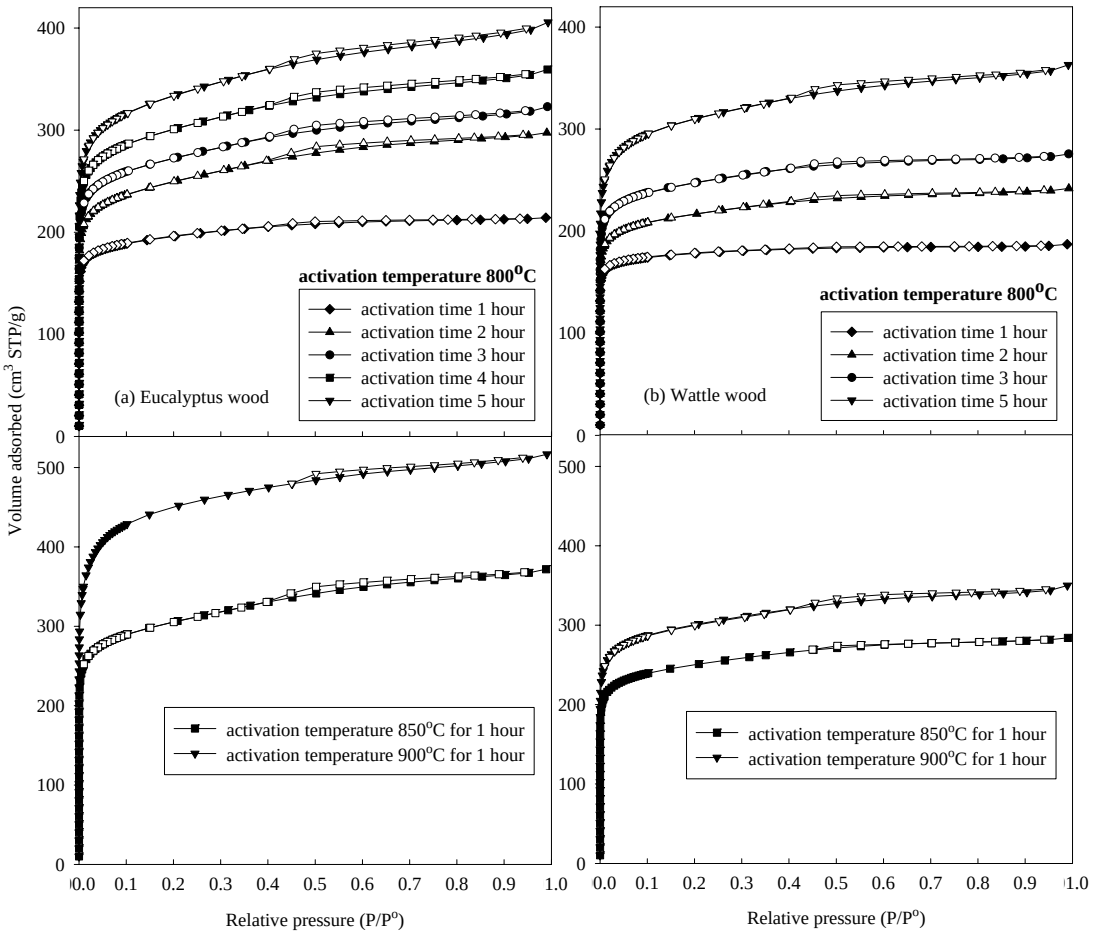

Figure 3.23 Adsorption (closed symbols) and desorption (open symbols) isotherms of N_2 at −196°C of activated carbons prepared from (a) eucalyptus and (b) wattle woods by physical activation at activation temperature 800°C, 850°C, and 900°C (carbonization conditions: temperature 400°C and time 1 hour; activation conditions: 50 vol% of CO_2 concentration).

It is noted that, the adsorption and desorption isotherms of activated carbons prepared from eucalyptus wood at activation temperature 600^{o}C for 2 hours, 600^{o}C for 3 hours and 4 hours, and 700^{o}C for 3 hours are not shown in Figure 3.22 (a) because there are no significantly different between the isotherms of these carbons with carbons prepared at activation temperature 600^{o}C for 1 hours, 600^{o}C for 5 hours, and 700^{o}C for 2 hours. The adsorption and desorption isotherms of activated carbons prepared from wattle wood at activation temperature 600^{o}C for 4 hours and 800^{o}C for 4 hours are also not shown in the Figure 3.22 (b) because these isotherms do not differ from those of carbons prepared at activation temperature 600^{o}C for 3 hours and 800^{o}C for 3 hours. Figure 3.22 and Figure 3.23 also reveals that at the same activation time, the increase in activation temperature for both woods can produce activated carbon with higher adsorption capacity. These results are consistent with the results of total pore volume in Table 3.12 and Table 3.13. At the same activation time, activated carbons from eucalyptus wood show higher volume of N_2 adsorbed than activated carbons obtained from wattle wood except for activation temperature 600^{o}C and 700^{o}C for 5 hours and this is in accord with the results of total pore volume (Table 3.12 and Table 3.13).

As shown in Figure 3.22 and Figure 3.23 for any activation temperature, the activated carbon prepared at 5 hours has the highest adsorption capacity for both woods. For the activated carbon prepared at 600^{o}C and 700^{o}C, the isotherm is of Type I at any activation time. For the activated carbon prepared at 800^{o}C and 1 hour, the isotherm is still of Type I isotherm. However, at higher activation times (> 2 hours), the adsorption-desorption curves for both woods start to

show small hysteresis loops at relative pressure greater than 0.4. This tends to change the isotherms from Type I to Type IV, although the effect is not so pronounced.

Figure 3.24 shows typical pore size distribution of activated carbon prepared from eucalyptus wood at activation time 1 hour and temperature varying from 600 – 900^{o}C by applying the Density Functional Theory (DFT) method. The curves of pore size distribution show the main peak around 7 Å for all carbons, which corresponds to the ultramicropore size (pore size ≤ 7 Å) (Lastoskie, Gubbins, and Quirke, 1993). The second smaller peak appears at 12 Å for 800^{o}C and 900^{o}C activation temperatures corresponding to the supermicropore (pore size between 7 to 20 Å) (Lastoskie, Gubbins, and Quirke, 1993). For activation temperatures of 600^{o}C and 700^{o}C, the second smaller peaks occur at 5 Å, which corresponds to the ultramicropore. The curves also show that the micropore volume (area under the curve) present in the activated carbon products varies in the sequence: 600^{o}C < 700^{o}C < 800^{o}C < 900^{o}C, which is in agreement with V_{mic} as shown in Table 3.12.

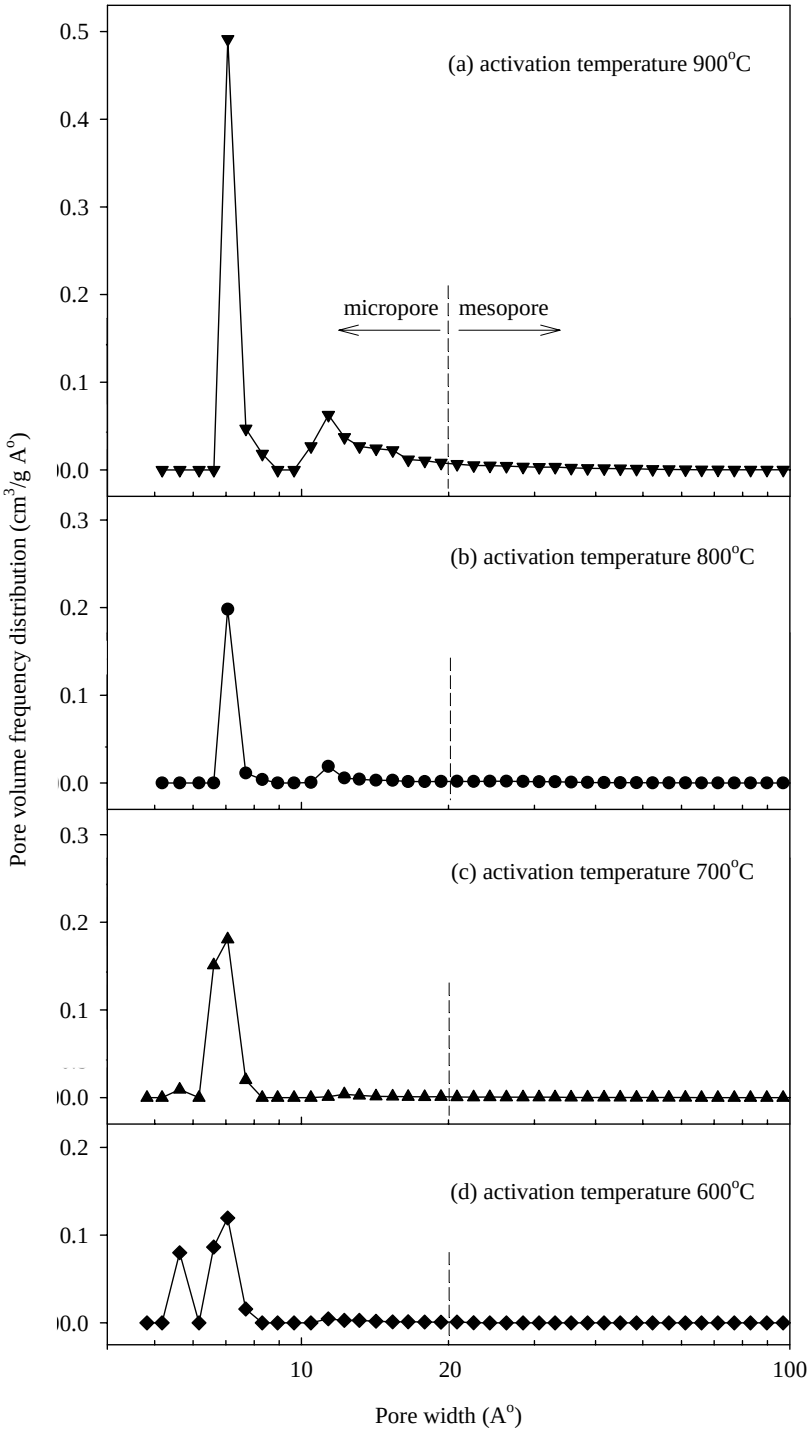

Figure 3.24 Pore size distribution of activated carbons prepared from eucalyptus wood by physical activation at activation temperature of (a) 900°C, (b) 800°C, (c) 700°C, and (d) 600°C for 1 hour.

Table 3.15 presents the results of proximate analysis of the prepared activated carbons of both woods. It can be seen that the prepared activated carbons have higher fixed carbon and moisture contents but lower volatile matters than the raw wood materials (Table 3.3) and chars (Table 3.11). This higher moisture content of the prepared activated carbons could result from their ability to adsorbed more moisture from air due to their highly porous structure. The activated carbons prepared from both woods contain moisture content with the amounts follow the order: $900^{o}C > 850^{o}C > 800^{o}C > 700^{o}C > 600^{o}C$, with eucalyptus wood having higher moisture content than wattle wood. This is in the same trend as the order of surface area and total pore volume as shown in Table 3.12 and Table 3.13, plus the fact that eucalyptus wood has higher porous properties than wattle wood.

Table 3.15 Proximate analysis of prepared activated carbons by physical activation at different activation temperature for 1 hour (the values in parentheses are moisture free basis).

	Activation temperature (^oC)	**Fixed carbon (wt%)**	**Volatile matters (wt%)**	**Ash (wt%)**	**Moisture (wt%)**
Eucalyptus wood	600	80.7 (83.8)	14.4 (15.0)	1.2 (1.2)	3.7
	700	82.2 (86.4)	11.8 (12.4)	1.1 (1.2)	4.9
	800	82.8 (87.6)	10.9 (11.5)	0.8 (0.9)	5.5
	850	81.7 (88.2)	10.2 (11.0)	0.7 (0.8)	7.4
	900	81.8 (88.7)	9.7 (10.5)	0.7 (0.8)	7.8
Wattle wood	600	81.1 (84.0)	13.0 (13.5)	2.4 (2.5)	3.5
	700	82.4 (85.7)	11.4 (11.9)	2.3 (2.4)	3.9
	800	83.6 (87.7)	10.2 (10.7)	1.5 (1.6)	4.7
	850	82.4 (87.8)	10.0 (10.6)	1.5 (1.6)	6.1
	900	81.8 (88.1)	9.7 (10.5)	1.3 (1.4)	7.2

3.3.3.3 Effect of CO_2 concentration

In studying the effect of CO_2 concentration, the activation was performed at 800^oC for 2 hours by varying the CO_2 concentration between 25 – 100 vol%. Although the suitable activation conditions that gave highest surface area were 900^oC and 1 hour for eucalyptus wood and 800^oC and 5 hours for wattle wood (burn-off ~ 80% for both woods), the activation temperature and time so selected were based on the consideration of higher carbon yield (burn-off ~ 45% and ~ 49% for eucalyptus and wattle woods, respectively).

Table 3.16 and Figure 3.25 show the effect of CO_2 concentration on the burn-off and porous properties of the resulting activated carbons prepared from both woods. The increase in CO_2 concentration from 25 – 100% by volume leads to an increase in burn-off, BET surface area, micropore volume, and total pore volume for both woods. There is no effect of CO_2 concentration on mesopore and macropore volume from 25 – 50% CO_2. However, their values increase with increase in CO_2 concentration from 50 – 100%. The percentage of micropore volume increases with increasing CO_2 concentration from 25% to 50% and then decreases with further increase in CO_2 concentration, while the percentage of mesopore and macropore show the opposite trend. The increased CO_2 concentration enhances the C–CO_2, resulting in an increase in the burn-off level and hence better pore development of the activated carbons. The increase of meso- and macropore volume at high CO_2 concentration may be due to the widening of existing micropore by C–CO_2 reaction and the collapse of adjacent pore walls. Again, eucalyptus wood could develop better porous properties than wattle wood.

Table 3.16 Effect of CO_2 concentration on the porous properties of prepared activated carbons by physical activation (carbonization conditions: temperature 400^{o}C and time 1 hour; activation conditions: temperature 800^{o}C and time 2 hours).

	CO_2 concentration (vol%)	**Burn off (%)**	**S_{BET} (m^2/g)**	**V_{mic} (cm^3/g)**	**$V_{meso+mac}$ (cm^3/g)**	**V_T (cm^3/g)**
Eucalyptus wood	25	44.4	753	0.33 (82.5%)	0.07 (17.5%)	0.40
	50	49.2	828	0.36 (83.7%)	0.07 (16.3%)	0.43
	75	54.8	841	0.37 (82.2%)	0.08 (17.8%)	0.45
	100	56.8	980	0.43 (78.2%)	0.12 (21.8%)	0.55
Wattle wood	25	44.0	684	0.30 (85.7%)	0.05 (14.3%)	0.35
	50	45.1	719	0.32 (86.5%)	0.05 (13.5%)	0.37
	75	52.0	806	0.36 (85.7%)	0.06 (14.3%)	0.42
	100	62.1	833	0.37 (82.2%)	0.08 (17.8%)	0.45

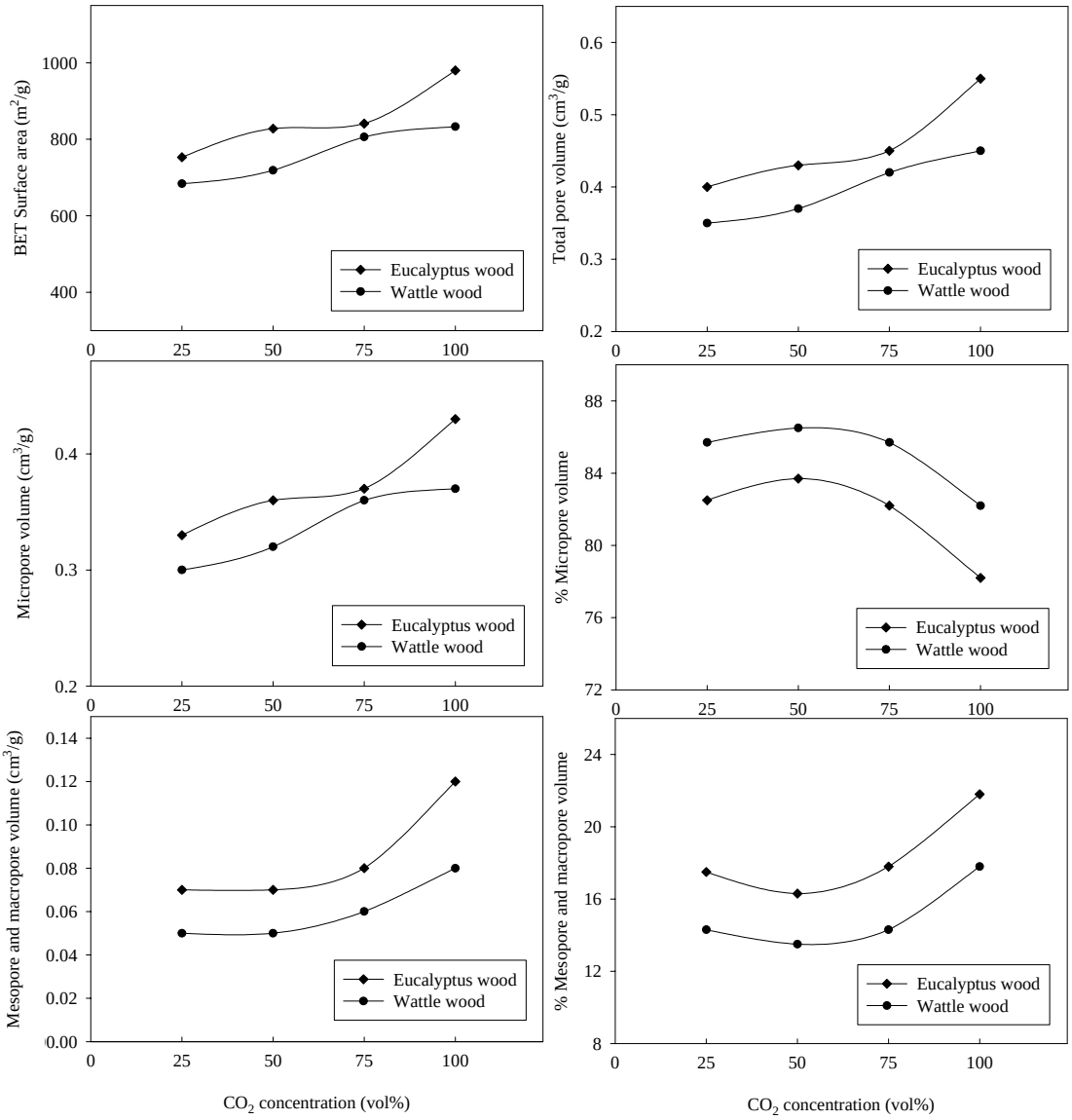

Figure 3.25 Effect of CO_2 concentration on the porous properties of activated carbons prepared from eucalyptus and wattle woods by physical activation (carbonization conditions: temperature 400^{o}C and time 1 hour; activation conditions: temperature 800^{o}C and time 2 hours).

Figure 3.26 shows the adsorption and desorption isotherms of N_2 of eucalyptus and wattle wood-based activated carbons for different CO_2 concentrations. The results show that the shape of all isotherms is of Type I. It is noted that, the adsorption and desorption isotherms of activated carbon prepared from eucalyptus wood at 75 vol% CO_2 does not appear in Figure 3.26 (a) because there are no significant difference between these isotherms and the isotherms which prepared at 50 vol% CO_2. The obtained activated carbons show the amount of N_2 adsorbed in the following order: 25% CO_2 < 50% CO_2 < 75% CO_2 < 100l% CO_2 for both woods. These orders match with the results of total pore volume presented in Table 3.16. For both woods, the adsorption-desorption curves show hysteresis loops with 100 vol% CO_2 giving the largest size of hysteresis loops. This is also consistent with the results of mesopore volume presented in Table 3.16. Eucalyptus wood-based carbons show higher amount of N_2 adsorbed than wattle wood-based carbons for all CO_2 concentrations.

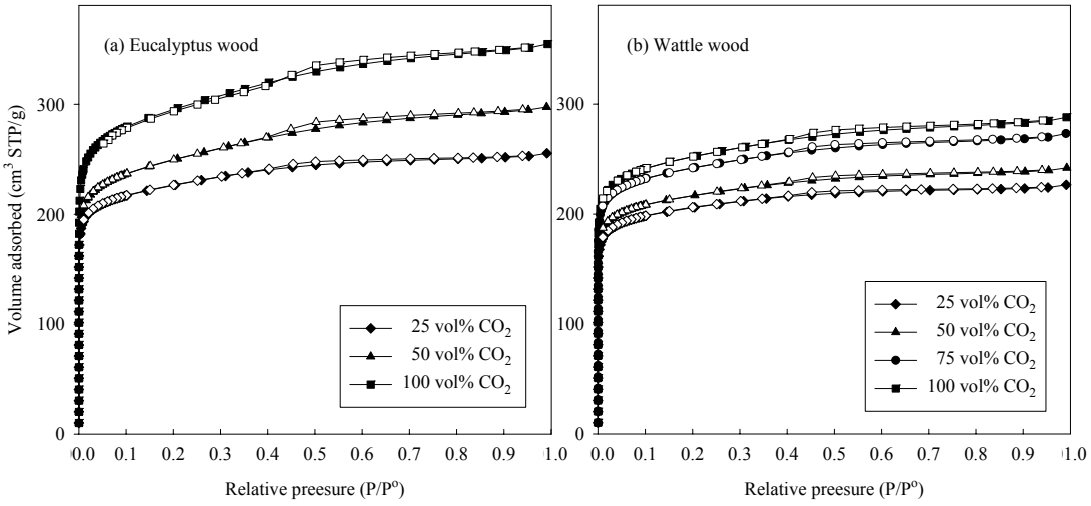

Figure 3.26 Adsorption (closed symbols) and desorption (open symbols) isotherms of N_2 at −196°C of activated carbons prepared from (a) eucalyptus and (b) wattle woods by physical activation different CO_2 concentration (carbonization conditions: temperature 400°C and time 1 hour; activation conditions: temperature 800°C and time 2 hours).

Figure 3.27 and Table 3.17 shows the correlation and the fitted parameters between the burn-off and the BET surface area and total pore volume by using a quadratic equation as shown in equation 3.11. This correlation covers all parameters studied in this research i.e. carbonization temperature 300°C – 700°C, carbonization time 1 – 4 hour, activation temperature 600°C – 900°C, activation time 1 – 5 hour, and CO_2 concentration 25 – 100 vol%. This correlation has advantage in predicting the surface area and total pore volume of the activated carbon with high accuracy (correlation coefficient $R^2 \geq 0.98$) and cover wide range of preparation conditions.

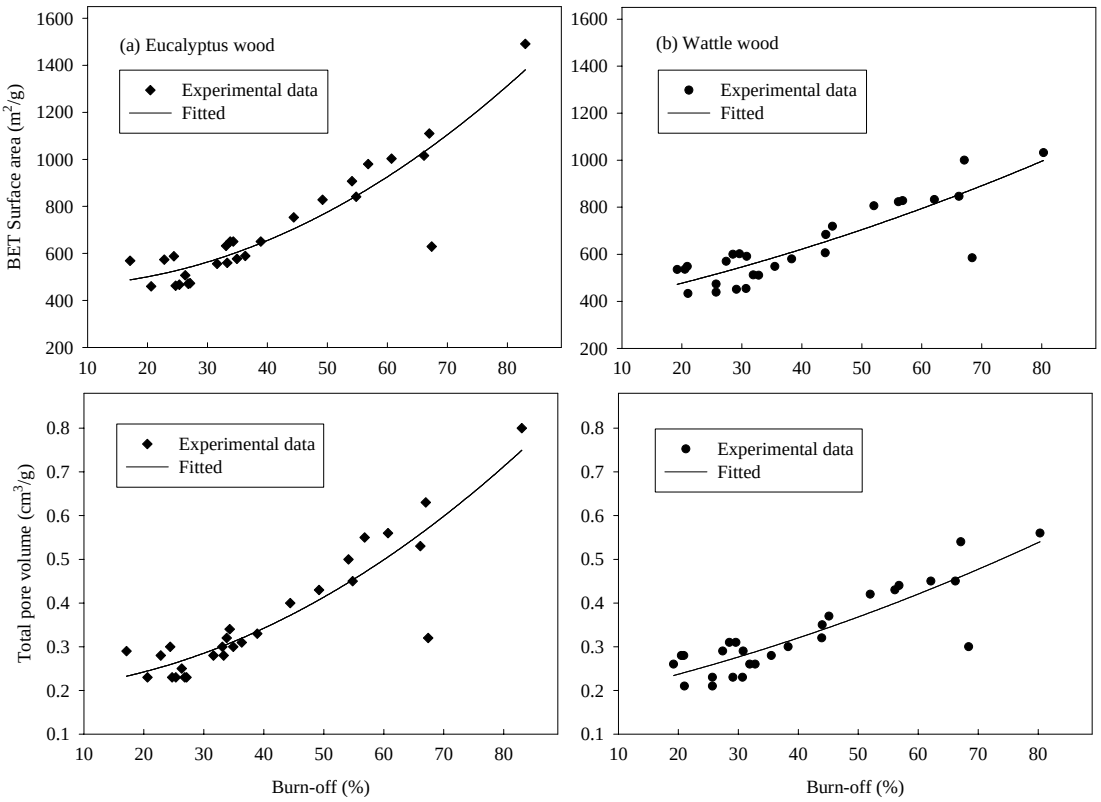

Figure 3.27 Effect of burn-off on the porous properties of the activated carbon prepared by physical activation covering all preparation conditions studied i.e. carbonization temperature, carbonization time, activation temperature, activation time, and CO_2 concentration.

Table 3.17 Parameters of empirical equations (equation 3.11) for estimating porous properties of activated carbon from % burn-off cover all preparation conditions studied i.e. carbonization temperature, carbonization time, activation temperature, activation time, and CO_2 concentration.

	BET surface area (m^2/g)				**Total pore volume (cm^3/g)**			
	a_1	a_2	a_3	R^2	a_1	a_2	a_3	R^2
Eucalyptus wood	462.22	-0.99	0.14	0.982	0.20	7.00×10^{-4}	7.10×10^{-5}	0.977
Wattle wood	360.62	5.13	0.04	0.984	0.17	2.80×10^{-3}	2.17×10^{-5}	0.982

In this research, activated carbon prepared from eucalyptus and wattle woods by CO_2 activation gave the highest BET surface area of 1491 m^2/g and 1032 m^2/g, respectively, and this occurred at the highest burn-off level for both woods (83% for eucalyptus and 80.3% for wattle wood). These surface area are comparable with those of other activated carbons prepared by CO_2 activation, for example, from corn hull (1010 m^2/g) (Zhang *et al*., 2004), candlenut shell (1050 m^2/g) (Turmuzi et al., 2004), pistachio-nut shell (1064 m^2/g) (Yang and Lua, 2003), longan seed (1278 m^2/g) (Junpirom et al., 2007), or oil-palm stone (1410 m^2/g) (Lua and Guo, 2000). In addition, as seen in Table 3.10, Table 3.11, and Table 3.14, the percentage of micropore volume of activated carbons is more than 78%. This indicates that CO_2 activation develops mostly micropores within wood-based activated carbon. This result is also in agreement with the work of Tancredi, Cordero, Rodríguez-Mirasol,

and Rodríguez (1996), Sainz-Diaz and Griffiths (2000), Sánchez, Elguézabal, and Saenz (2001), and Zhang *et al*. (2004).

3.3.4 General discussion

This section compares the properties of activated carbons obtained from chemical activation (section 3.3.2) and physical activation (3.3.3) methods. Figure 3.28 shows the yields of activated carbon products prepared from eucalyptus and wattle woods by the two activation methods versus activation temperature. The yield of final product was calculated based on the initial weight of dried wood. The yield for these two activation methods shows the same trend i.e. the yield decreases as the activation temperature is increased with chemical activation showing higher activated carbon yield or lower weight loss than physical activation. The weight loss during activation processes stems from the different reaction mechanisms for each activation method. For physical activation process, the loss of sample weight is due to $C–CO_2$ reaction, while the removal of carbon during thermal treatment in the presence of H_3PO_4 in the form of CO, CO_2, and light hydrocarbon gases such as CH_4 contributes to the weight loss.

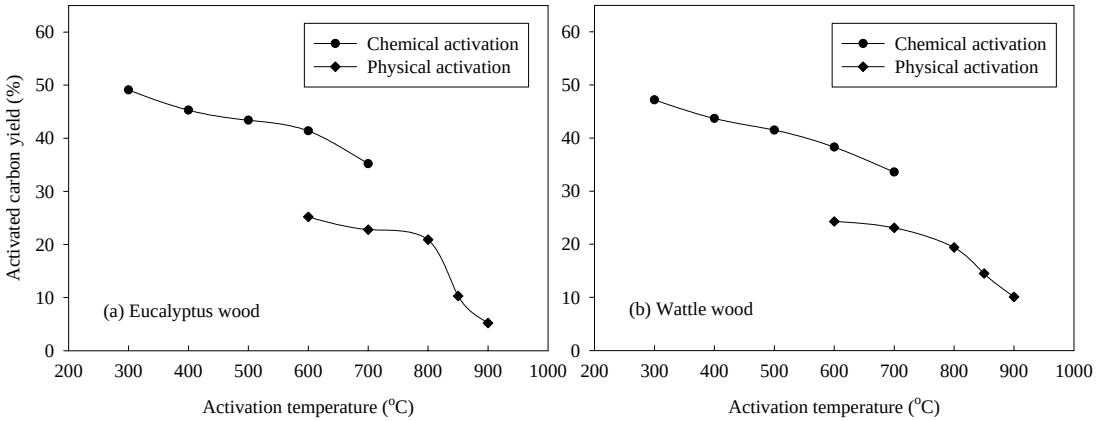

Figure 3.28 Yields of activated carbons prepared from (a) eucalyptus and (b) wattle woods by chemical activation and physical activation methods at different activation temperature (preparation conditions: chemical weight ratio of H_3PO_4 solution and wood 1:1, impregnation time 1 hour, carbonization time 1 hour for chemical activation; carbonization temperature 400°C, carbonization time 1 hour, activation time 1 hour, 50 vol% of CO_2 concentration).

The effect of activation temperature on the BET surface area and pore volume of activated carbons prepared by the two activation methods are shown in Figure 3.29. The results show that chemical activation produce activated carbon with higher surface area and pore volume than physical activation. Chemical activation also produced activated carbon with higher proportion of mesopore and macropore volume, while physical activation produced mainly micropore volume carbon.

A notable difference between both activation methods is that the pore evolution for chemical activation commences at a much lower temperature than physical activation which results in a higher yield of resulting activated carbons (Figure 3.28). Therefore, the major advantage of using chemical activation is that

activated carbon with very high surface area and pore volume, can be produced at lower energy cost, and higher product yield. However, a problem associated with chemical activation method is the incorporation of impurities in the activated carbon as a result of the impregnation with chemical agent.

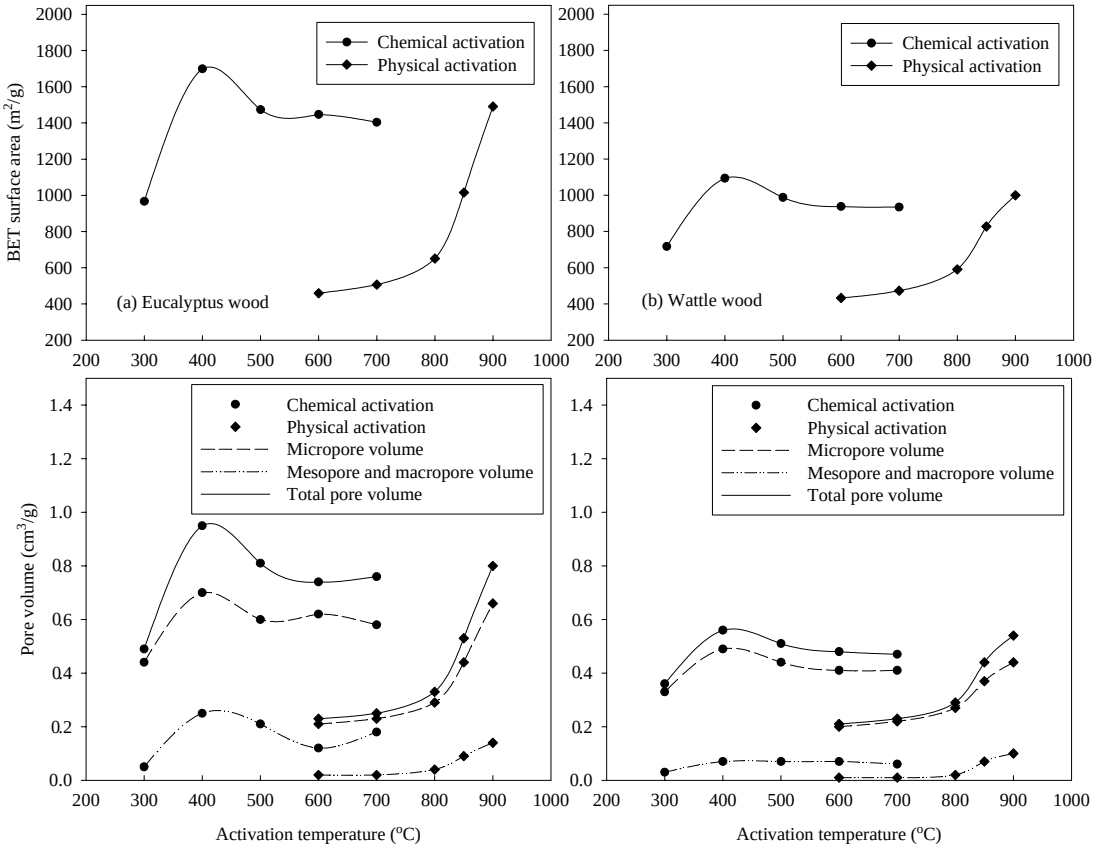

Figure 3.29 Comparison of the porous properties of activated carbons prepared from (a) eucalyptus and (b) wattle woods by chemical activation and physical activation methods at different activation temperature (preparation conditions: chemical weight ratio of H_3PO_4 solution and wood 1:1, impregnation time 1 hour, carbonization time 1 hour for chemical activation; carbonization temperature 400^oC, carbonization time 1 hour, activation time 1 hour, 50 vol% of CO_2 concentration).

The scanning electron micrographs of the external surface of the resulting activated carbons prepared from eucalyptus wood by different activation methods are compared in Figure 3.30. It can be seen from the micrographs that the external surface area of carbon activated with H_3PO_4 are full of cavities. It seems that the cavities on the surface of H_3PO_4 carbon could result from the dilation of structure by phosphate linkages, leaving the space after acid removal. As shown in Figure 3.30 (b), the external surface of CO_2 activated carbon is more intact than that of the H_3PO_4 activated carbon. There are small pits and tiny holes distributed over the surface, indicating the occurrence of $C–CO_2$ gasification on the external surface during activation. Both micrographs clearly show that H_3PO_4 activation produced wider pore than CO_2 activation. Due to the well developed pores, the H_3PO_4 carbon possessed higher surface area and pore volume than CO_2 carbon.

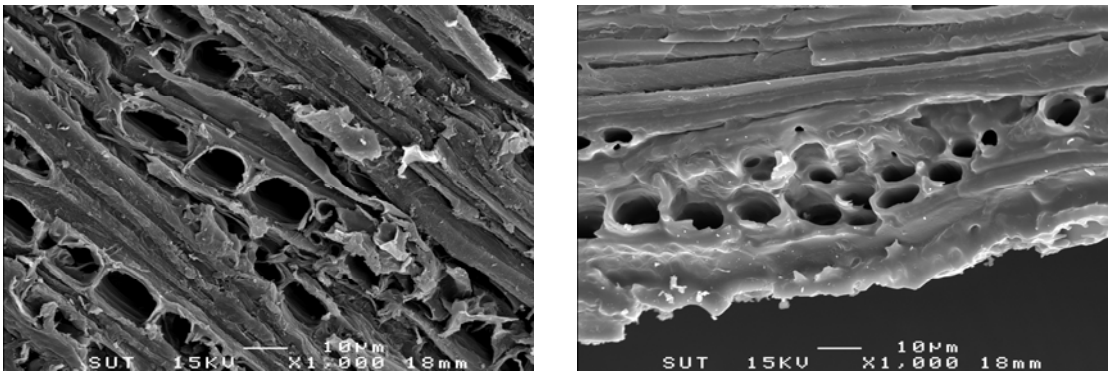

(a) chemical activation (b) physical activation

Figure 3.30 Scanning electron micrographs of activated carbons prepared from eucalyptus wood by (a) chemical activation and (b) physical activation methods by at activation temperature 600^{o}C.

Figure 3.31 shows the comparison of proximate analysis on the obtained activated carbons prepared by chemical activation and physical activation methods. It can be seen that there is no significantly difference between volatile matters for both activation methods. Physical activation shows higher fixed carbon content and lower moisture and ash contents than chemical activation. The higher moisture content of chemical activated carbon is due to its larger surface area and pore volume which can adsorb more moisture from air than physical activation.

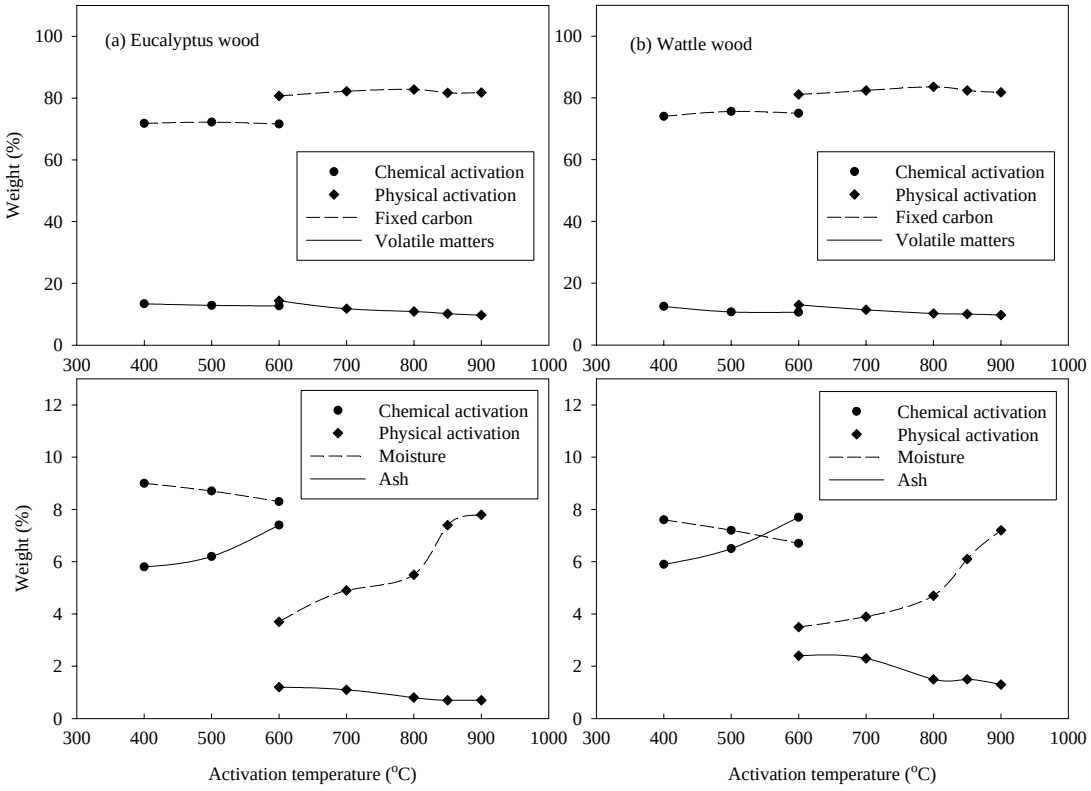

Figure 3.31 Comparison of the proximate analysis of activated carbons prepared from (a) eucalyptus and (b) wattle woods by chemical activation and physical activation methods at different activation temperature.

3.4 Conclusions

The results reported in this chapter showed that highly porous activated carbon can be produced from eucalyptus and wattle woods by chemical and physical activation. For chemical activation, the effects of chemical weight ratio, impregnation time, carbonization temperature, and carbonization time on the porous properties of activated carbon were investigated. The results indicated that activation at moderate temperature i.e. around 400^{o}C gave activated carbon with the highest surface area i.e. 1857 m^2/g and 1550 m^2/g for eucalyptus and wattle woods, respectively. The other optimum preparation conditions were chemical weight ratio of H_3PO_4 solution and wood 1.5:1, impregnation time 1.5 hours, and carbonization time 1 hour. For physical activation, the effects of carbonization temperature, carbonization time, activation temperature, activation time, and CO_2 concentration on the porous properties of activated carbon were investigated. The increase in activation temperature, activation time, and CO_2 concentration led to an increase in BET surface area and total pore volume with temperature showing the largest effect. The effects of activation time and temperature on these porous properties can be represented by the burn-off level of char during activation. Eucalyptus wood-based activated carbon gave maximum surface area and total pore volume of 1491 m^2/g and 0.80 cm^3/g, respectively, which occurred at 900^{o}C and 1 hour of activation conditions. In comparison, wattle wood-based activated carbon gave maximum BET surface area and total pore volume at 800^{o}C and 5 hour with corresponding values of 1032 m^2/g and 0.56 cm^3/g. The activated carbons derived from both eucalyptus and wattle woods by CO_2 activation produced internal pores mainly in the micropore size range, constituting about 80% of total pore volume. However, H_3PO_4 activation produced activated carbons with

higher proportions of mesopore and macropore volume. Overall, both eucalyptus and wattle wood-based activated carbons showed similar porous characteristics with eucalyptus giving relatively better pore development under the preparation conditions studied.

3.5 References

Adib, F., Bagreev, A., and Bandosz, T. J. (1999). Effect of surface characteristics of wood-based activated carbons on adsorption of hydrogen sulfide. **J. Colloid Interface Sci.** 214: 407-415.

Arriagada, R., García, R., Molina-Sabio, M., and Rodríguez-Reinoso, F. (1997). Effect of steam activation on the porosity and chemical nature of activated carbons from *Eucalyptus globulus* and peach stones. **Micropor. Mater.** 8: 123-130.

Baquero, M. C., Giraldo, L., Moreno, J. C., Suárez-García, F., Martínez-Alonso, A., and Tascón, J. M. D. (2003). Activated carbons by pyrolysis of coffee bean husks in presence of phosphoric acid. **J. Anal. Appl. Pyrolysis** 70: 779-784.

Chang, C. F., Chang, C. Y., and Tsai, W. T. (2000). Effects of burn-off and activation temperature on preparation of activated carbon from corn cob agrowaste by CO_2 and steam. **J. Colloid Interface Sci.** 232: 45-49.

Colman, J. (2001). **Acacia - Wattle** [Online]. Available: http://www.janinesgarden.com/plants/A/acacia.html

Daud, W. M. A. W. and Ali, W. S. W. (2004). Comparison on pore development of activated carbon produced from palm shell and coconut shell. **Bioresour. Technol.** 93: 63-69.

Diao, Y., Walawender, W. P., and Fan, L. T. (2002). Activated carbons prepared from phosphoric acid activation of grain sorghum. **Bioresour. Technol.** 81: 45-52.

Do, D. D. (1998). **Adsorption analysis: Equilibria and Kinetics.** Singapore: Imperial College Press.

Gañan, J., González-García, C. M., González, J. F., Sabio, E., Macías-García, A., and Díaz-Díez, M. A. (2004). Preparation of activated carbons from bituminous coal pitches. **Appl. Surface Sci.** 238: 347-354.

Girgis, B. S., Yunis, S. S., and Soliman, A. M. (2002). Characteristics of activated carbon from peanut hulls in relation to conditions of preparation. **Mater. Lett.** 57: 164-172.

Gómez-Serrano, V., Cuerda-Correa, E. M., Fernández-González, M. C., Alexandre-Franco, M. F., and Macías-García, A. (2005). Preparation of activated carbons from chestnut wood by phosphoric acid-chemical activation. Study of microporosity and fractal dimension. **Mater. Lett.** 59: 846-853.

Guo, J. and Lua, A. C. (2002). Characterization of adsorbent prepared from oil-palm shell by CO_2 activation for removal of gaseous pollutants. **Mater. Lett.** 55: 334-339.

Jagtoyen, M. and Derbyshire, F. (1998). Activated carbons from yellow poplar and white oak by H_3PO_4 activation. **Carbon** 36: 1085-1097.

Jiménez, L., García, J. C., Pérez, I., Ariza, J., and López, F. (2001). Acetone pulping of wheat straw. Influence of the cooking and beating conditions on the resulting paper sheets. **Ind. Eng. Chem. Res.** 40: 6201-6206.

Junpirom, S., Tangsathitkulchai, C., Tangsathitkulchai, M. (2007). Preparation of activated carbons from longan seed by physical and chemical activation method. **Suranaree J. Sci. Technol.** 14: 63-76.

Kim, T.-Y., Baek, I.-H., Jeoung, Y.-D., and Park, S.-C. (2003). Manufacturing activated carbon using various agricultural wastes. **J. Ind. Eng. Chem.** 9: 254-260.

Lastoskie, C., Gubbins, K. E., and Quirke, N. (1993). Pore size distribution analysis of microporous carbons: A Density Functional Theory approach. **J. Phys. Chem.** 97: 4786-4796.

Lee, B.- G. and Rowell R. M. (2004). Removal of heavy metal ions from aqueous solutions using lignocellulosic fibers. **Journal of Natural Fibers** 1: 97-108.

Lozano-Castelló, D., Lillo-Ródenas, M. A., Cazorla-Amorós, D., and Linares-Solano, A. (2001). Preparation of activated carbons from Spanish anthracite I. Activation by KOH. **Carbon** 39: 741-749.

Lua, A. C. and Guo, J. (1998). Preparation and characterization of chars from oil palm waste. **Carbon** 36: 1663-1670.

Lua, A. C. and Guo, J. (2000). Activated carbon prepared from oil palm stone by one-step CO_2 activation for gaseous pollutant removal. **Carbon** 38: 1089-1097.

Lua, A. C. and Yang, T. (2005). Characteristics of activated carbon prepared from pistachio-nut shell by zinc chloride activation under nitrogen and vacuum conditions. **J. Colloid Interface Sci.** 290: 505-513.

Lua, A. C., Yang, T., and Guo, J. (2004). Effects of pyrolysis conditions on the properties of activated carbons prepared from pistachio-nut shells. **J. Anal. Appl. Pyrolysis** 72: 279-287.

Molina-Sabio, M., Rodríguez-Reinoso, F., Caturla, F., and Sellés, M. (1995). Porosity in granular carbons activated with phosphoric acid. **Carbon** 33: 1105-1113.

Olivares-Marín, M., Fernández-González, C., Macías-García, A., and Gómez-Serrano, V. (2005). Porous structure of activated carbon prepared from cherry stones by chemical activation with phosphoric acid. **Energy & Fuels** Article In Press.

Olivier, J. P. (1995). Modeling physical adsorption on porous and nonporous solids using Density Functional Theory. **J. Porous Mater.** 2: 9-17.

Patrick, J. W. (1995). **Porosity in Carbons: Characterization and Applications.** London: Edward Arnold.

Punsuwan, N., Tangsathitkulchai, C., and Tangsathitkulchai, M. (2006). Activated carbon from bagasse and the removal of chromium from aqueous solution with activated carbon. **Suranaree J. Sci. Technol.** 13: 143-158.

Sainz-Diaz, C. I. and Griffiths, A. J. (2000). Activated carbon from solid wastes using a pilot-scale batch flaming pyrolyser. **Fuel** 79: 1863-1871.

Sánchez, A. R., Elguézabal, A. A., and Saenz, L. L. T. (2001). CO_2 activation of char from *Quercus Agrifolia* wood waste. **Carbon** 39: 1367-1377.

Siamtree (2003). **Known** [Online]. Available: http://www.siamtree.com/known.htm

Srinivasakannan, C. and Bakar, M. Z. A. (2004). Production of activated carbon from rubber wood sawdust. **Biomass and Bioenergy** 27: 89-96.

Tancredi, N., Cordero, T., Rodríguez-Mirasol, J., and Rodríguez, J. J. (1996). Activated carbons from Uruguayan eucalyptus wood. **Fuel** 75: 1701-1706.

Teng, H. and Hsu, L.-H. (1999). High-porosity carbons prepared from bituminous coal with potassium hydroxide activation. **Ind. Eng. Chem. Res.** 38: 2947-2953.

Tsai, W. T., Chang, C. Y., and Lee, S. L. (1998). A low cost adsorbent from agricultural waste corn cob by zinc chloride activation. **Bioresour. Technol.** 64: 211-217.

Turmuzi, M., Daud, W. R. W., Tasirin, S. M., Takriff, M. S., and Iyuke, S. E., (2004). Production of activated carbon from candlenut shell by CO_2 activation. **Carbon** 42: 453-455.

Yang, T. and Lua, A. C. (2003). Characteristics of activated carbons prepared from pistachio-nut shells by physical activation. **J. Colloid Interface Sci.** 267: 408-417.

Yang, H., Yan, R., Chen, H., Lee, D. H., and Zheng, C. (2007). Characteristics of hemicellulose, cellulose, and lignin pyrolysis. **Fuel** 86: 1781-1788.

Youssef, A. M., Radwan, N. R. E., Abdel-Gawad, I., and Singer, G. A. A. (2005). Textural properties of activated carbons from apricot stones. **Colloids Surf. A** 252: 143-151.

Zhang, T., Walawender, W. P., Fan, L. T., Fan, M., Daugaard, D., and Brown, R. C. (2004). Preparation of activated carbon from forest and agricultural residues through CO_2 activation. **Chem. Eng. J.** 105: 53-59.

Zou, Y. and Han, B.-H. (2001). High-surface-area activated carbon from Chinese coal. **Energy & Fuels** 15: 1383-1386.

CHAPTER IV

SURFACE MODIFICATION OF ACTIVATED CARBON

ABSTRACT

Activated carbons prepared from eucalyptus wood by chemical activation using phosphoric acid (H_3PO_4) were oxidized with nitric acid (HNO_3), hydrogen peroxide (H_2O_2), ammonium peroxydisulfate ($(NH_4)_2S_2O_8$), and air with the purpose to incorporate oxygen functional groups on their surfaces. In addition, activated carbons having different surface area and pore volume, prepared by physical activation with carbon dioxide, were oxidized with HNO_3 to investigate the effect of porous structure on the concentration and distribution of surface functional groups. In addition, the variation of types and contents of surface functional groups as controlled by high-temperature heating in an inert atmosphere of N_2 was also investigated. The surface chemistries of oxidized activated carbons were characterized by Boehm titration, Fourier Transform Infrared spectroscopy (FTIR), X-ray Photoelectron spectroscopy (XPS), elemental analysis, and pH at the point of zero charge (pH_{pzc}). The porous properties of oxidized activated carbons were determined by N_2 adsorption isotherms at –196^{o}C. Boehm titration results showed that the content of acidic oxygen functional groups increased after oxidation with all oxidants used. The results from FTIR, XPS, elemental analysis, pH_{pzc}, and N_2 adsorption isotherm confirmed the existence of oxygen functional groups. The percent increase in functional group concentration following the order: carboxylic acid > phenolic >

lactonic for all oxidation methods. The increasing of oxidation time, oxidation temperature, and acid concentration increased the total acid group and the amount of each acidic functional group, whereas the distribution of each functional group remains unchanged after oxidation treatments. Porous structure of activated carbon was found to affect the introduced functional groups distributing on its surfaces. The high surface area carbon had more area available for oxidizing agent to access and more functional groups could be formed compared to the lower surface area carbon. However, the functional groups development finally reached a constant with respect to increasing surface area. At the same oxidation conditions (oxidizing agent concentration, oxidation time, and oxidation temperature), it was found that activated carbon prepared from chemical activation with H_3PO_4 gave higher amount of acidic oxygen functional groups than activated carbon prepared from physical activation with CO_2. Thus, it may be concluded that the functional groups that were created after oxidation treatment not only depended on the activation method of the original sample (chemical activation or physical activation) but also on its available surface area. Heat treatment of oxidized carbons resulted in the removal of incorporated oxygen functional groups with carboxylic group being least stable followed by lactonic and phenolic groups.

4.1 Introduction

Activated carbon contains hydrophobic graphitic basal planes, which constitute the majority of the carbon surface (more than 90% of surface), and various hydrophilic surface functional groups, which are mainly located at the edges of the

carbon basal planes (Arafat, Franz, and Pinto, 1999). Its textural and surface properties depend on the raw material and the method used in its preparation.

Predominant types of surface functional group on activated carbon are surface oxygen functionality. Modification of the surface chemistry of activated carbon in order to increase the concentration of surface oxygen functional groups can be carried out by treating it with oxidizing agents either in the gas phase or in aqueous solution, namely dry and wet oxidations. A wide range of oxidizing agents such as HNO_3, H_2O_2, $(NH_4)_2S_2O_8$, H_2SO_4, $HClO_4$, and $KMnO_4$ have been used in liquid phase whereas air, O_2, and O_3 have been used in gas phase (Santiago, Stüber, Fortuny, Fabregat, and Font, 2005). The oxidation treatment produces two types of surface oxides: acidic and basic groups, with the latter presenting in a smaller amount. These groups are usually polar in nature and can interact with polar adsorbate species such as water vapor (Carrasco-Marin, Mueden, Centeno, Stoeckli, and Moreno-Castilla, 1997; Aharoni, 1997; Choma, Burakiewicz-Mortka, Jaroniec, Li, and Klinik, 1999), methanol vapor (Bandosz, Jagiello, Schwarz, and Krzyzanowski, 1996), and metal ions. The oxidation treatment can also affect the surface area and pore texture of the activated carbon (Moreno-Castilla et al., 1995).

Fixation of the acidic groups such as carboxylic, phenolic, and lactonic groups on the surface of activated carbon makes it more hydrophilic and increases the negative surface charge density. The changes in the surface chemistry of activated carbon induced by the formation of acidic oxygen functional groups will significantly affect the adsorptive behavior of the activated carbons when they are used as an adsorbent. For example, it could enhance the adsorption of aqueous metal cation species such as Pb^{2+} (El-Hendawy, 2003; Xiao and Thomas, 2005), Cu^{2+} (Biniak,

Pakuła, Szymański, and Świątkowski, 1999; Goyal, Rattan, Aggarwal, and Bansal, 2001; Chen, Wu, and Chong, 2003), Cd^{2+} (Jia and Thomas, 2000; Park, Lee, Ryu, and Kim, 2002), Cr^{3+} (Cordero et al., 2002; Rivera-Utrilla and Sánchez-Polo, 2003), Cr^{6+} (Liu, Chen, Chen, Liu, and Wang, 2007), Co^{2+} (Strelko and Malik, 2002), Zn^{2+} (Strelko and Malik, 2002), Ni^{2+} (Strelko and Malik, 2002), Mn^{2+} (Strelko and Malik, 2002), and Ca^{2+} (Xiao, 2004) with ion exchange playing an important role in the adsorption process. The acidic functional groups on activated carbon surface can also increase the adsorption capacities of basic dyes (basic red 14) (Soundping, 2002) and aniline (Radovic et al., 1997; Soundping, 2002).

Thermal treatment of activated carbon at high temperature can remove oxygen surface functional groups due to their thermal instability. Consequently, activated carbon exhibits more hydrophobic character after high temperature heat treatment in an inert atmosphere and thus the heat-treated carbon could increase the adsorption capacities of organic compounds such as phenol (Ania, Parra, and Pis, 2002; Nevskaia, Castillejos-Lopez, Guerrero-Ruiz, and Muñoz, 2004), 2-methylisoborneol (Considine, Denoyel, Pendleton, Schumann, and Wong, 2001), benzene (Wibowo, Setyadhi, Wibowo, Setiawan, and Ismadji, 2007), toluene (Wibowo et al., 2007), and dyes with anionic characteristics viz., reactive dyes such as reactive red 198, reactive yellow 3, and reactive blue 5 (Pereira, Soares, Órfão, and Figueiredo, 2003), direct dyes such as direct red 80, direct yellow 106, and direct blue 78 (Pereira et al., 2003), and acid dyes such as acid red 73 (Attia, Rashwan, Khedr, 2006), acid red 151 (Pereira et al., 2003), acid yellow 23 (Attia et al., 2006), acid yellow 49 (Pereira et al., 2003), and acid blue 113 (Pereira et al., 2003). The adsorption of these adsorbates

was generally determined by π–π dispersion interaction between the electron of activated carbon surface and the aromatic ring of the adsorbate.

Many researchers have illustrated that oxidation conditions such as types of oxidizing agents (Pradhan and Sandle, 1999; Salame and Bandosz, 1999; Moreno-Castilla, López-Ramón, and Carrasco-Marín, 2000), concentration of oxidizing agent (Tamon and Okazaki, 1996; Stavropoulos, Samaras, and Sakellaropoulos, 2007), oxidation temperature (Bandosz, Jagiełło, and Schwarz, 1993), and oxidation time (Carrasco-Marin et al., 1997; Pereira et al., 2003; Rivera-Utrilla and Sánchez-Polo, 2003) could affect the introduced surface functional groups. The present research proposes the hypotheses that, apart from the above oxidation conditions, (1) the oxidized activated carbons derived from activated carbons prepared by using different activation methods (i.e. chemical and physical activation) should exhibit different amounts and distribution of functional groups on the carbon surface and (2) porous structure of activated carbon should affect the amount and distribution of introduced functional groups.

Thus, this chapter reports on the investigation of the effect of oxidation conditions such as types of oxidizing agent, treatment time, treatment temperature, and concentration of oxidizing agent on the incorporated surface oxygen functional groups of activated carbon. The goal of the present study is not only to modify activated carbon to obtain high total acidic oxygen functional groups but also to achieve high content of carboxylic acid group which is the strongest introduced acid functional group. The experiments to verify the above two hypotheses were also performed. The techniques used to characterize the chemical characteristics of activated carbon surfaces include acid/base titration (Boehm's method), Fourier

Transform Infrared spectroscopy (FTIR), X-ray photoelectron spectroscopy (XPS), elemental analysis, and pH at the point of zero charge (pH_{pzc}). The measurement of N_2 adsorption isotherms was used for characterizing the porous properties of carbon samples.

4.2 Apparatus and Methods

4.2.1 Apparatus

1. Horizontal ceramic tube furnace (CTF 12/75/700/201, Carbolite)
2. Automated adsorption apparatus (ASAP 2010, Micromeritics)
3. Fourier Transform Infrared spectroscopy (FTS 175C, BIO-RAD)
4. C, H, N, and O analyzer (CHN/O-932, LECO)
5. X-ray Photoelectron spectroscopy (Siam National Synchrotron Research Center)
6. Platform shaker (2100, INNOVA)
7. Oven (600, Memmert)
8. Analytical balance (BP221S, Sartorius)
9. pH meter (CG840, SCHOTT)

4.2.2 Chemicals (Analytical grade)

1. Nitric acid (HNO_3) 69.5% by weight
2. Hydrogen peroxide (H_2O_2) 35% by weight
3. Ammonium peroxydisulfate ($(NH_4)_2S_2O_8$)
4. Sulfuric acid (H_2SO_4) 96% by weight
5. Hydrochloric acid (HCl) 37% by weight
6. Sodium hydroxide (NaOH)

7. Sodium carbonate (Na_2CO_3)

8. Sodium bicarbonate ($NaHCO_3$)

9. Sodium chloride (NaCl)

10. Air (zero grade, Thai Industrial Gases Public Company Limited)

11. Nitrogen gas (ultra high purity grade with 99.999% purity, Thai Industrial Gases Public Company Limited)

4.2.3 Methods

Eucalyptus wood-based activated carbons prepared by both chemical and physical activation were used in the study of surface modification and chemistry. Activated carbon prepared by chemical activation was used to study the effect of oxidizing agents and treatment conditions on the incorporation of surface functional groups. Activated carbons prepared by physical activation were selected to study the effect of porous structure on the amount and distribution of surface functional groups. The activated carbons prepared by physical activation were selected because physical activation could give activated carbons covering low to high range of surface area and total pore volume by controlling the char burn-off level (surface area 460 – 1491 m^2/g, total pore volume 0.23 – 0.80 cm^3/g) whereas chemical activation could provide activated carbons with only high range of surface area and total pore volume (surface area 967 – 1857 m^2/g, total pore volume 0.49 – 1.23 cm^3/g). The activated carbon prepared from physical activation was also used to study the effect of heat treatment process on the type and amount of surface functional groups.

The original activated carbons used for the study of surface modification were prepared under the conditions as shown in Table 4.1, along with their porous properties and designated codes.

Table 4.1 Preparation conditions and porous characteristics of original activated carbons.

Sample	S_{BET} (m^2/g)	V_{mic} (cm^3/g)	V_T (cm^3/g)	Sample code
Activated carbon from chemical activation with H_3PO_4 [1]	1200	0.55	0.58	AC
Activated carbon from physical activation with CO_2 [2]				
activation temperature at 600°C	460	0.21	0.23	AC600
activation temperature at 800°C	651	0.29	0.33	AC800
activation temperature at 900°C	1491	0.66	0.80	AC900

[1] Preparation conditions: chemical weight ratio of H_3PO_4 solution and wood 0.5:1, impregnation time 1 hour, and carbonization temperature 400°C for 1 hour

[2] Preparation conditions: carbonization temperature 400°C for 1 hour and activation time 1 hour

4.2.3.1 Liquid phase oxidation

The oxidizing agents used in the liquid phase oxidation for incorporating oxygen functional groups on activated carbon (sample AC) were H_2O_2, $(NH_4)_2S_2O_8$, and HNO_3.

For activated carbon oxidized with H_2O_2, two samples of 1 g each of original activated carbon were soaked with 10 cm^3 of 35 wt% H_2O_2 for 24 and 48 hours at room temperature. After oxidation, the oxidized activated carbons were washed thoroughly with hot water and dried at 110°C for overnight.

For activated carbon oxidized with $(NH_4)_2S_2O_8$, two samples of 1 g of original activated carbon were soaked with 10 cm^3 of saturated solution of $(NH_4)_2S_2O_8$ in 1 M H_2SO_4 for 24 and 48 hours at room temperature. After oxidation, the oxidized activated carbons were washed several times with hot water. Then the washed samples were dried at 110^oC for overnight and then heated at 400^oC for 1 hour under nitrogen flow to remove the remaining SO_2 gas.

For activated carbon oxidized with 1 M HNO_3 by the soaking method, three samples of 1 g of original activated carbon were soaked with 10 cm^3 of 1 M HNO_3 for 12, 24, and 48 hours at room temperature. After oxidation, the oxidized activated carbons were washed several times with hot water and further boiled in water by a reflux condenser to remove residual HNO_3 and other soluble materials until the pH of washed water remained constant. Finally, the washed activated carbons were dried at 110^oC for overnight.

For activated carbon oxidized with 1 M HNO_3 by the reflux method, three samples of 1 g of original activated carbon were refluxed in a reflux condenser at boiling point temperatures (~ 80 – 90^oC) for 12, 24, and 48 hours. The experiments by reflux method using 5 M and 10 M HNO_3 for 24 hours were also performed.

To study the effect of porous structure on the introduced surface functional groups, all three original activated carbons (AC600, AC800, and AC900) were oxidized with oxidizing agent to incorporate the highest amounts of surface functional groups. The experimental conditions of all liquid phase oxidations and the designated code of the samples are summarized in Table 4.2.

Table 4.2 The experimental conditions for studying the surface modification by liquid and gas phase oxidation.

Oxidizing agent	Conditions			Sample code
	Method	**Temperature**	**Treatment time (hour)**	
H_2O_2 (35 wt%)	Soaking	Room	24	H_2O_2 24h
			48	H_2O_2 48h
$(NH_4)_2S_2O_8$ (sat. in 1 M H_2SO_4)	Soaking	Room	24	$(NH_4)_2S_2O_8$ 24h
			48	$(NH_4)_2S_2O_8$ 48h
HNO_3 (1 M)	Soaking	Room	12	HNO_3 1M 12h
			24	HNO_3 1M 24h
			48	HNO_3 1M 48h
	Reflux	Boiling point (~ 80 – 90°C)	12	HNO_3 re 1M 12h
			24	HNO_3 re 1M 24h
			48	HNO_3 re 1M 48h
HNO_3 (5 M)	Reflux	Boiling point	24	HNO_3 re 5M 24h
HNO_3 (10 M)	Reflux	Boiling point	24	HNO_3 re 10M 24h
Air	Packed bed reactor	250°C	12	Air 250°C 12h
			24	Air 250°C 24h
			48	Air 250°C 48h
		350°C	24	Air 350°C 24h

4.2.3.2 Gas phase oxidation

About 1 g of original activated carbon (sample AC) was packed in a packed-bed reactor (2.5 cm diameter and 10 cm long of steel pipe). The reactor was placed inside a horizontal ceramic tube furnace and heated from room temperature to 250^{o}C under the constant flow of N_2 at the heating rate of 10^{o}C/min. When the final temperature was reached, the air was allowed to flow into the reactor at the rate of 100 cm^3/min for 12 hours. Then the furnace was cooled down to room temperature under the flow of N_2. Two more samples were oxidized in a similar way but with longer treatment times of 24 and 48 hours. The experiment was also conducted at another treatment temperature of 350^{o}C for 24 hours. The experimental conditions of gas phase oxidation and the sample codes are summarized in Table 4.2.

4.2.3.3 Characterization of modified activated carbons

The original activated carbons and the oxidized activated carbons were characterized using several techniques including Boehm titration, FTIR, XPS, elemental analysis, pH_{pzc}, and adsorption isotherm measurement.

Boehm titration (Boehm, 1994) is one of the most widely used method to quantify acidic groups with different strengths on activated carbon surfaces. The content and acidity strength can be determined by titration with basic solution of different base strengths. Based on this method, it is assumed that the following acidic groups on carbon surfaces become neutralized with basic: carboxylic group (relatively strongest acidic group) in a solution of $NaHCO_3$, carboxylic group and lactonic group (relatively weaker acidic group) in a solution of Na_2CO_3, and combined carboxylic group, lactonic group, and phenolic group (weakest acidic group) in a solution of NaOH. For the determination of basic groups on the carbon

surface, HCl is used to neutralize the basic groups. Boehm titration experiment was performed by the following procedure: one gram of activated carbon was mixed with each of the 100 cm^3 of 0.1 M solutions of HCl, NaOH, and $NaHCO_3$ and 0.05 M Na_2CO_3. Each vial was sealed, shaken for 24 hours and the suspensions filtered. 10 cm^3 of the filtrate solutions of NaOH, Na_2CO_3, and $NaHCO_3$ were pipetted and titrated with 0.1 M HCl, while the filtrate solution of HCl was titrated with 0.1 M NaOH. The titrant volumes of the various bases and acids were used to determine the amount of functional groups on the activated carbon surface.

The FTIR spectrometer was used to measure the infrared spectrum of the activated carbons and to identify their chemical functionality. The activated carbon was mixed with KBr powder and the pellet formed by compressing at 10 tons for 2 min in a hydraulic press. Before measurement, the instrument was run to collect the background, which was automatically subtracted from the sample spectrum.

The XPS spectra were collected using a Mg K_α x-ray source (1253.6 eV). The activated carbon samples were placed in the pretreatment chamber and degassed at 10^{-6} mbar. Then they were transferred to the ion-pumped analysis chamber, in which residual pressure is kept below 4×10^{-9} mbar during data acquisition. The C_{1s} peak of each sample was analyzed in the binding energy range of 275 – 295 eV. The O_{1s} peak of each sample was analyzed in the binding energy range of 525 – 545 eV. The accuracy of the binding energy is ± 0.1 eV.

Elemental analysis was used to determine C, H, N, and O contents by using a CHN/O analyzer.

The pH at the point of zero charge (pH_{pzc}) value was used to compare the extent of acidic surface functional groups of activated carbons. By definition, pH_{pzc} is the pH of the solution in contact with solid at which the net surface charge on the surface of an adsorbent particle is zero. Therefore, the activated carbon that contains acidic surface functional groups will exhibit a low value of pH_{pzc} whereas high value of pH_{pzc} is observed for the basic surface carbons. The pH_{pzc} of the activated carbon was measured by the pH drift method (Lopez-Ramon, Stoeckli, Moreno-Castilla, and Carrasco-Marin, 1999). In this method, at the solution pH above the pH_{pzc} the activated carbon with acidic functional groups on surface releases protons into a solution. If the solution pH is lower than the pH_{pzc} the activated carbon with acidic functional groups on surface receives protons from the solution. A point is reached at which the acidic functional groups are in equilibrium with protons in solution so that the final pH of solution does not change. This point is defined as the point of zero charge. Under this condition, all surface charges are effectively neutralized so that the net surface charge of the activated carbon is zero. The determination of pH_{pzc} was done by adjusting the pH of 0.01 M NaCl (50 cm^3) to values between 1 to 10 obtained by adding either 0.1 M HCl or NaOH. About 0.15 g of activated carbon was added into each solution at room temperature and then shaken for 48 hours. The final pH was measured and plotted against the initial pH. The pH at which the plotted curve intersects the line of pH (final) = pH (initial) was taken as the pH_{pzc} of the activated carbon surface.

Porous properties of the activated carbons were determined using N_2 adsorption isotherm data at -196^oC acquired by the automated adsorption apparatus. The activated carbon was first degassed at 300^oC under vacuum (< 50

μmHg) for 12 hours to remove moisture and other volatiles. From the obtained isotherm data, the specific surface area, S_{BET}, was estimated by applying Brunauer-Emmett-Teller (BET) equation (Do, 1998). The micropore volume, V_{mic}, was calculated by using Dubinin-Radushkevich (DR) equation (Do, 1998). The total pore volume, V_T, was found from the amount of N_2 gas adsorbed at the relative pressure of 0.99 and converted it to the corresponding volume in liquid state.

4.3 Results and Discussion

4.3.1 Original activated carbons

Table 4.3 and Figure 4.1 show the porous properties and amount of surface functional groups of original activated carbons prepared from chemical (AC) and physical activations (AC600, AC800, and AC900). As seen, the surface area and pore volume of the original carbons show the following order, AC600 < AC800 < AC < AC900 and the porous structure of all original carbons exhibits mainly microporosity (> 82%).

As to the surface functional groups, it is evident that the original carbon prepared by chemical activation (AC) contains much lower amount of total acidic groups compared to the physically activated carbons (AC600, AC800, and AC900). This difference should depends primarily on the differences in the two activation methods used, leading to different mechanisms of pore creation and fixation of functional groups on the activated carbon surfaces. In addition, higher temperatures of CO_2 activation should increase the incorporation of acidic surface groups compared to H_3PO_4 activation with the lower activation temperature of 400^oC.

Table 4.3 Porous properties and Boehm titration results of original activated carbons prepared from chemical (AC) and physical activations (AC600, AC800, and AC900).

Sample	S_{BET} (m^2/g)	V_{mic} (cm^3/g)	V_T (cm^3/g)	Acidic group					Basic group (mmol/g)
				Carboxylic (mmol/g)	Lactonic (mmol/g)	Phenolic (mmol/g)	Total (mmol/g)	Total ($mmol/m^2$)	
AC	1200	0.55 (95%)	0.58	0.06 (9%)	0.43 (65%)	0.17 (26%)	0.66	5.50×10^{-4}	0.63
AC600	460	0.21 (91%)	0.23	0.20 (17%)	0.36 (30%)	0.64 (53%)	1.20	2.61×10^{-3}	0.40
AC800	651	0.29 (88%)	0.33	0.19 (12%)	0.45 (28%)	0.95 (60%)	1.59	2.44×10^{-3}	0.45
AC900	1491	0.66 (82%)	0.80	0.16 (10%)	0.38 (24%)	1.06 (66%)	1.60	1.07×10^{-3}	1.17

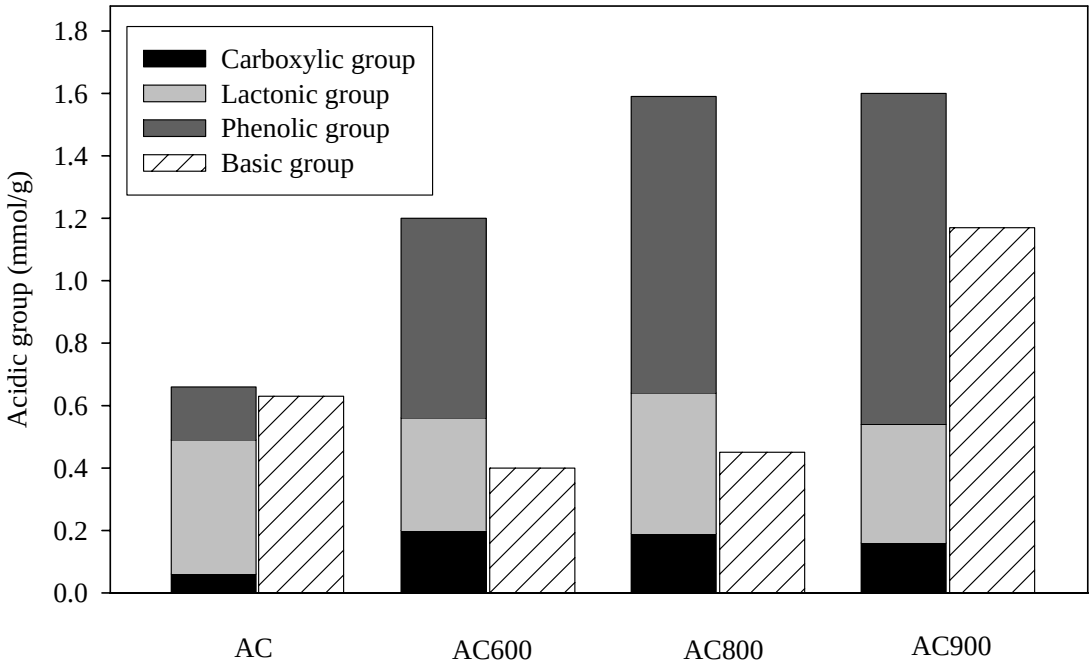

Figure 4.1 Content of surface functional groups of the original activated carbons prepared from chemical (AC) and physical activations (AC600, AC800, and AC900).

Table 4.3 also shows the presentation of acidic groups in terms of surface density in mmol/m^2. It is clear that sample AC gives the lowest acidic group density despite its relatively high surface area. For physically activated carbons, AC600 and AC800 show similar values of surface group density, indicating that at these activation temperatures the amount of acid groups created is proportional to the developed surface area. This is reasonable since the creation of surface acidic groups and pore development occur in parallel during the course of gasification reaction. However, too high activation temperature of 900^{o}C would cause the detachment of some acidic groups, hence lowering its surface density.

To test the hypothesis of surface group creation during gasification, it is suggested that an experiment be conducted as follows. Activated carbon is prepared at a selected activation condition as done before, say at 800^{o}C and 1 hour. However, now during the cooling period CO_2 is used instead of N_2 gas. When the furnace temperature is dropped to a low level (say 400^{o}C), where pore development is relatively unimportant, the system is maintained at this temperature for a certain period of time to allow the surface oxidation to take place and the final product determined for its acid group contents. If an increase in the surface acidic group is detected, it should prove that CO_2 is responsible for surface group creation during gasification and its amount is temperature dependent.

Apart from the differences in total acid quantity, the differences in the amount and distributions of acidic types of surface functional groups are also discernible. As seen in Figure 4.1, original activated carbon prepared from H_3PO_4 activation (AC) contains the highest amount of lactonic group (65%) followed by phenolic group (26%) and carboxylic group (9%), while all three original carbons prepared from CO_2 activation (AC600, AC800, and AC900) give the amounts of acidic groups in the following order, phenolic > lactonic > carboxylic. For original samples obtained from physical activation, the increasing of activation temperature also affects the quantity and distribution of each acidic functional group. There is a tendency that the percentages of carboxylic and lactonic groups decrease while phenolic group increase with increasing in activation temperature from 600^{o}C to 900^{o}C. The amount of basic groups also increases with increasing activation temperature.

It appears that both chemical and physical activation methods render the activated carbons with lowest amounts of carboxylic group. It has been established that the order of thermal stability of acidic functional groups is the following: carboxylic < lactonic < phenolic (Puente, Pis, Menéndez, and Grange, 1997). Therefore, it is likely that the high activation temperatures (400^{o}C for chemical activation and 600^{o}C – 900^{o}C for physical activation) could remove proportionally more carboxylic group compared to the other two surface groups during activation step, giving the least concentration of carboxylic acid in the final activated carbon products.

4.3.2 Effect of oxidizing agent on surface modification of activated carbon

4.3.2.1 N_2 adsorption results

Table 4.4 gives the porous properties of the original and oxidized activated carbons obtained from the analysis of N_2 adsorption isotherms. It is observed that all porous properties of the original activated carbon decrease after oxidation. This could arise from the inaccessibility of N_2 molecules into the internal adsorption sites due to the presence of increased functional groups at the pore entrance and possibly by the collapse of some thin pore walls caused by oxidizing agent during the oxidation treatment (Salame, Bagreev, and Bandosz, 1999). The lowering in the access amount of N_2 for the oxidized carbons is further evident from the adsorption isotherm data of N_2 at –196^{o}C, as shown in Figure 4.2. As a result, the porous properties of oxidized carbons with very high contents of acidic functional groups such as HNO_3 re 5M 24h, HNO_3 re 10M 24h, and air 350^{o}C 24h could not be readily determined from N_2 adsorption measurement.

Table 4.4 Porous characteristics obtained from N_2 adsorption isotherm of the original and oxidized activated carbons.

Sample	S_{BET} **(m^2/g)**	V_{mic} **(cm^3/g)**	V_T **(cm^3/g)**
AC (original activated carbon)	1200	0.55	0.58
H_2O_2 24h	689	0.34	0.35
$(NH_4)_2S_2O_8$ 24h	738	0.34	0.36
HNO_3 1M 24h	831	0.38	0.41
HNO_3 re 1M 12h	590	0.28	0.31
HNO_3 re 1M 24h	523	0.26	0.27
Air 250^{o}C 12h	794	0.37	0.39
Air 250^{o}C 24h	626	0.29	0.31
Air 250^{o}C 48h	585	0.27	0.28

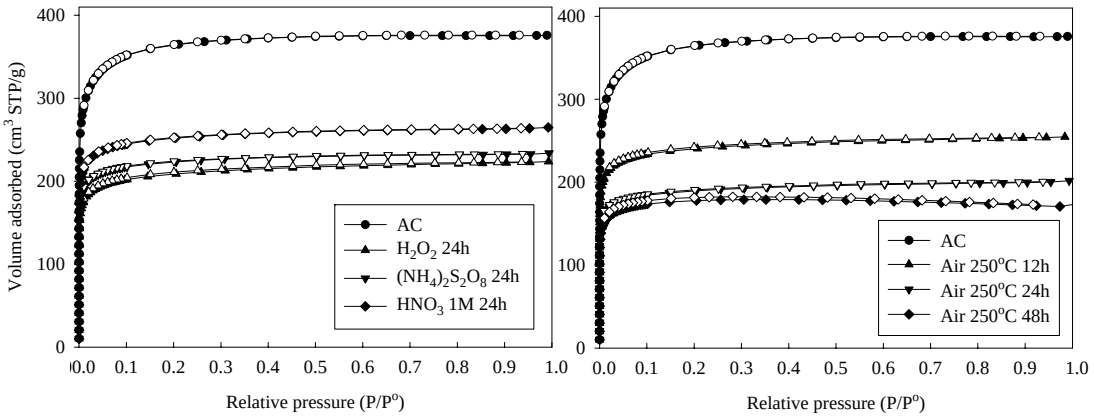

Figure 4.2 Adsorption (closed symbols) and desorption (open symbols) isotherms of N_2 at −196°C of original and oxidized activated carbons.

4.3.2.2 Boehm's results

The values of acidic and basic groups on activated carbon surfaces determined from Boehm titration of the H_2O_2 oxidation treatment are shown in Table 4.5 and Figure 4.3. Total acidic group increases after oxidation and increases with increasing in oxidation time from 24 hours to 48 hours. The H_2O_2 oxidation treatment gives the following order of percent increase in functional group concentration: carboxylic acid > phenolic > lactonic. However, the distribution of each functional group of oxidized samples is of the following order, carboxylic acid < phenolic < lactonic, which is the same order as the original sample. The increasing of oxidation time from 24 hours to 48 hours also affects the distribution of acidic functional group with the same order as above.

Table 4.5 Boehm titration results of original and H_2O_2 oxidized activated carbons (the value in square bracket [ ] is the percentage changes with reference to the original carbon, where "+" denotes % increasing and "–" denotes % decreasing).

Sample	Acidic group (mmol/g)				Basic group (mmol/g)
	Carboxylic	Lactonic	Phenolic	Total	
AC (original activated carbon)	0.06 (9%)	0.43 (65%)	0.17 (26%)	0.66	0.63
H_2O_2 24h	0.34 (20%) [+ 467%]	0.68 (41%) [+ 58%]	0.65 (39%) [+ 282%]	1.67 [+ 153%]	0.40 [– 36%]
H_2O_2 48h	0.61 (27%) [+ 917%]	0.87 (39%) [+ 102%]	0.77 (34%) [+ 353%]	2.25 [+ 241%]	0.35 [– 44%]

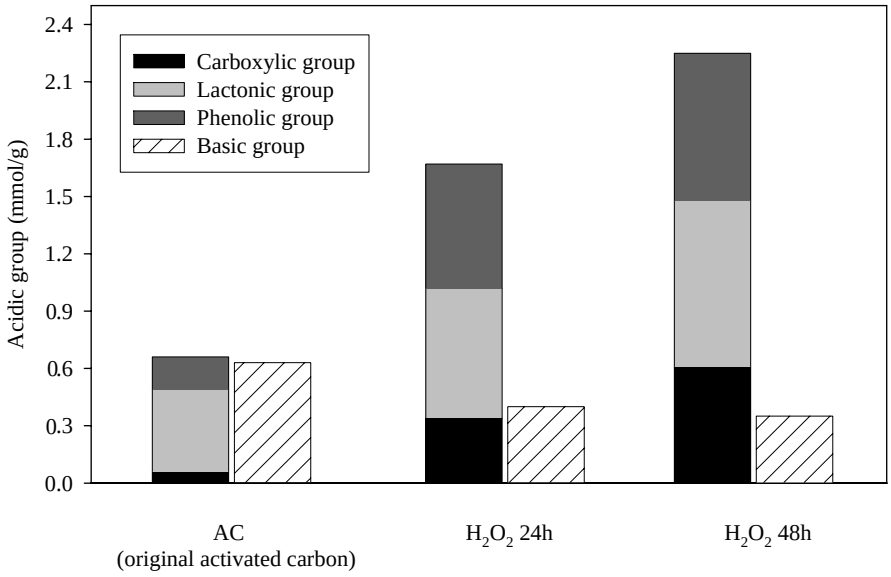

Figure 4.3 Contents of surface functional groups of the original activated carbon and activated carbons oxidized with H_2O_2.

When comparing with the original carbon, the basic group contents decrease by about 36% and 44% after H_2O_2 treatment for 24 and 48 hours, respectively, in consistent with the other reported results (Moreno-Castilla et al., 2000; Domingo-García, López-Garzón, Pérez-Mendoza, 2000). The decrease of basic groups (such as ketone) may be due to the conversion of this group to carboxylic acid and lactone, as suggested by the following reactions (Lebedev, 1984; Denisov and Afanas'ev, 2005; Smith and March, 2007):

$$\underset{\text{(ketone)}}{R^1C(O)CH_2R^2} \xrightarrow{+\,O_2} \underset{\text{(carboxylic acid)}}{R^1COOH} + \underset{\text{(aldehyde)}}{R^2CH(O)}$$

$$\underset{\text{(aldehyde)}}{R^2CH(O)} \xrightarrow{+\,O_2} \underset{\text{(per acid)}}{R^2C(O)OOH}$$

$$\underset{\text{(per acid)}}{R^2C(O)OOH} + \underset{\text{(ketone)}}{R^1C(O)CH_2R^2} \longrightarrow \underset{\text{(carboxylic acid)}}{R^2COOH} + \underset{\text{(lactone)}}{R^1C(O)OCH_2R^2}$$

The highest percent increase of carboxylic groups observed with the oxidized samples may partially come from the products of the above reactions.

The second oxidizing agent used to increase oxygen functional groups on activated carbon is ammonium peroxydisulfate ($(NH_4)_2S_2O_8$). The type and quantity of surface groups are summarized in Table 4.6 and Figure 4.4. It is seen that the oxidation results in an increase in the amount of total acidic groups which also increases with increasing of oxidation time. For both oxidation times, the percent increase and the distribution of functional groups show the same trend as the results of H_2O_2 oxidation. However, percent increase of total acid, carboxylic, and phenolic by $(NH_4)_2S_2O_8$ oxidation is less than H_2O_2 oxidation, due to the stronger oxidizing agent of H_2O_2 compared to $(NH_4)_2S_2O_8$ under the conditions studied.

Similar to the case of H_2O_2 oxidation, the treatment with $(NH_4)_2S_2O_8$ leads to the destruction of basic sites and there is a tendency to decrease with increased oxidation time. These results are also in agreement with those reported by several researchers using $(NH_4)_2S_2O_8$ as an oxidant (Moreno-Castilla, Carrasco-Marín, and Mueden, 1997; Salame and Bandosz, 2000).

Table 4.6 Boehm titration results of original and $(NH_4)_2S_2O_8$ oxidized activated carbons (the value in square bracket [ ] is the percentage changes with reference to the original carbon, where "+" denotes % increasing and "–" denotes % decreasing).

Sample	Acidic group (mmol/g)				Basic group (mmol/g)
	Carboxylic	Lactonic	Phenolic	Total	
AC (original activated carbon)	0.06 (9%)	0.43 (65%)	0.17 (26%)	0.66	0.63
$(NH_4)_2S_2O_8$ 24h	0.23 (14%) [+ 283%]	0.87 (54%) [+ 102%]	0.51 (32%) [+ 200%]	1.61 [+ 144%]	0.55 [– 13%]
$(NH_4)_2S_2O_8$ 48h	0.38 (19%) [+ 533%]	1.05 (51%) [+ 144%]	0.61 (30%) [+ 259%]	2.04 [+ 209%]	0.38 [– 40%]

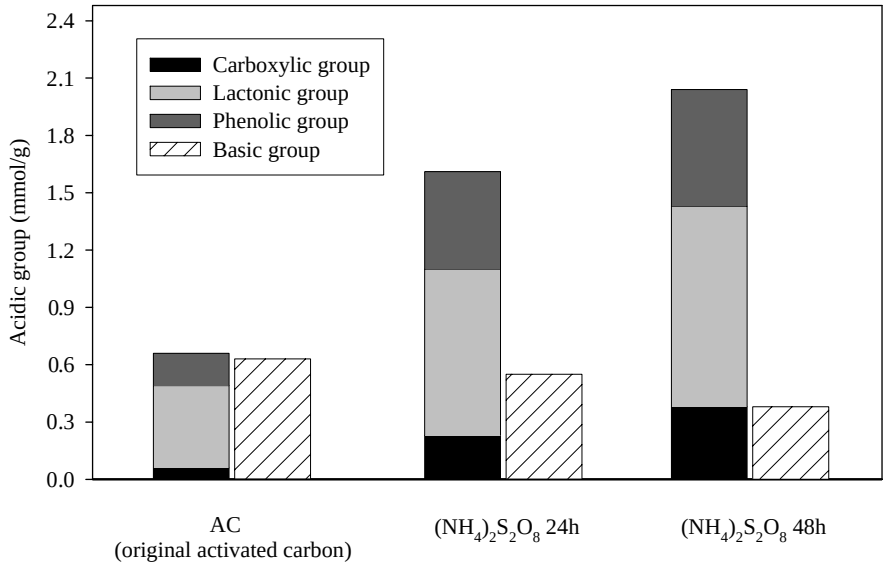

Figure 4.4 Contents of surface functional groups of the original activated carbon and activated carbons oxidized with $(NH_4)_2S_2O_8$.

One of the most widely used oxidizing agents to increase surface oxygen functional groups is nitric acid (HNO_3). It can be seen from Table 4.7 and Figure 4.5 that total acidic groups of all HNO_3 oxidized samples increase after the oxidation treatment. For both oxidation methods (soaking and reflux), at the same HNO_3 concentration (1 M), the oxidation by boiling in a reflux condenser gives much higher total acidic groups than oxidation by soaking at room temperature for all treatment times. This is due to the less efficiency of soaking method in creating functional groups of HNO_3 at room temperature as compared to fixation at the higher boiling temperature by reflux method. For samples oxidized by soaking and reflux methods, increasing in the treatment time and HNO_3 concentration lead to the increase of total acidic surface groups.

For the HNO_3 reflux method, the total acidic groups of oxidized samples is increased by about 27% (from 3.96 mmol/g to 5.03 mmol/g) when the acid concentration is increased from 1 M to 5 M. However, as the acid concentration is further increased from 5 M to 10 M only a 4% increase in acidic group (from 5.03 mmol/g to 5.23 mmol/g) is observed. This indicates that there exists a minimum HNO_3 concentration for the maximum development of acidic functional groups on a specific activated carbon. This critical concentration is 5 M HNO_3 for the sample AC (see Table 4.4 for the porous properties).

Table 4.7 Boehm titration results of original and HNO_3 oxidized activated carbons (the value in square bracket [ ] is the percentage changes with reference to the original carbon, where "+" denotes % increasing and "–" denotes % decreasing).

Sample	Acidic group (mmol/g)				Basic group (mmol/g)
	Carboxylic	**Lactonic**	**Phenolic**	**Total**	
AC (original activated carbon)	0.06 (9%)	0.43 (65%)	0.17 (26%)	0.66	0.63
HNO_3 1M 12h	0.14 (18%) [+ 133%]	0.28 (35%) [– 35%]	0.37 (47%) [+ 118%]	0.79 [+ 20%]	0.43 [– 32%]
HNO_3 1M 24h	0.19 (20%) [+ 217%]	0.32 (33%) [– 26%]	0.45 (47%) [+ 165%]	0.96 [+ 45%]	0.35 [– 44%]
HNO_3 1M 48h	0.39 (26%) [+ 550%]	0.49 (33%) [+ 14%]	0.60 (41%) [+ 253%]	1.48 [+ 124%]	0.25 [– 60%]
HNO_3 re 1M 12h	0.98 (30%) [+ 1553%]	1.09 (33%) [+ 153%]	1.24 (37%) [+ 629%]	3.31 [+ 402%]	1.25 [+ 98%]
HNO_3 re 1M 24h	1.01 (26%) [+ 1583%]	1.18 (30%) [+ 174%]	1.77 (44%) [+ 941%]	3.96 [+ 500%]	1.90 [+ 202%]
HNO_3 re 1M 48h	1.12 (26%) [+ 1767%]	1.40 (32%) [+ 226%]	1.79 (42%) [+ 953%]	4.31 [+ 553%]	1.95 [+ 210%]
HNO_3 re 5M 24h	1.24 (25%) [+ 1967%]	1.76 (35%) [+ 309%]	2.03 (40%) [+ 1094%]	5.03 [+ 662%]	2.16 [+ 243%]
HNO_3 re 10M 24h	1.26 (24%) [+ 2000%]	1.91 (37%) [+ 344%]	2.06 (39%) [+ 1112%]	5.23 [+ 692%]	2.30 [+ 265%]

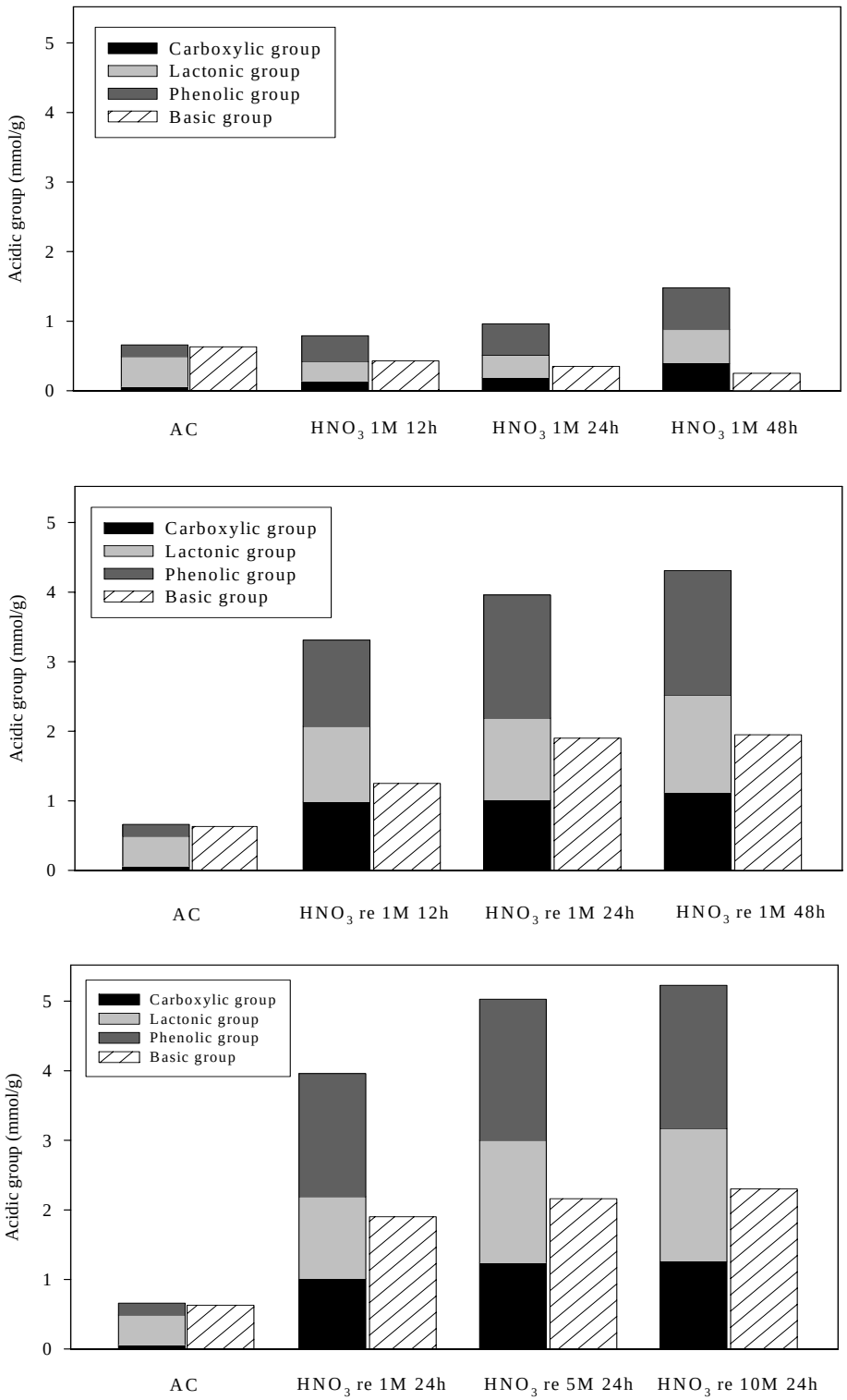

Figure 4.5 Contents of surface functional groups of the original activated carbon and activated carbons oxidized with HNO_3.

In all cases, the percent increase of acidic group employing HNO_3 reflux method follows the order, carboxylic > phenolic > lactonic. The distribution of each functional group of oxidized samples by soaking method follows the order, carboxylic acid << lactonic < phenolic, whereas the functional group distribution of oxidized samples by reflux method following the order, carboxylic acid < lactonic < phenolic. The increasing of oxidation time, oxidation temperature (room temperature and reflux temperature), and acid concentration increases the amount of all three functional group, and the distribution of each functional group remains the same as shown above.

The content of basic groups (such as ketone) decreases after oxidation by soaking method and decreases with increasing of oxidation time. The decrease of basic groups may be attributed to the conversion of these groups to carboxylic and lactonic as discussed in the case of H_2O_2 oxidation. However, the content of these basic groups increases for oxidation by reflux method. This could possibly be due to the higher oxidation temperature of reflux method and the intense mixing of boiling solution, leading to additional formation of ketone by the proposed reaction shown in Figure 4.6.

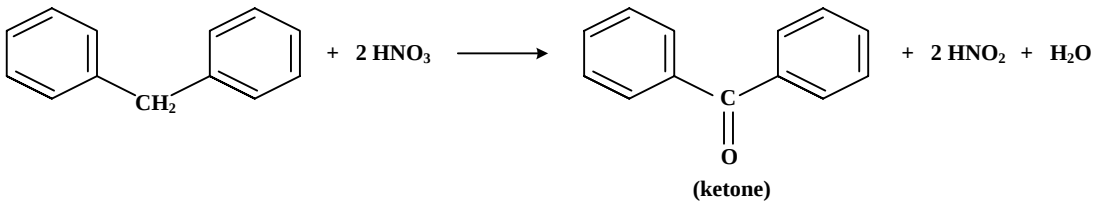

Figure 4.6 The formation of ketone involving in the oxidation with nitric acid by reflux method.

For gas phase oxidation, air was used as the oxidizing agent and the results of Boehm titration are given in Table 4.8 and Figure 4.7. The total acidic groups increase with the increase in both oxidation time and temperature. Although the oxidized activated carbon at oxidation temperature of 350^{o}C gives much higher total acidic groups than that at 250^{o}C, the yield of oxidized activated carbon at 350^{o}C is relatively low (i.e. 54%) when compared to the oxidized sample at 250^{o}C (i.e. 88%). The sample was converted into ash when the oxidation temperature is higher than 350^{o}C.

Table 4.8 Boehm titration results of original and air oxidized activated carbons (the value in square bracket [ ] is the percentage changes with reference to the original carbon, where "+" denotes % increasing and "–" denotes % decreasing).

Sample	**Acidic group (mmol/g)**				**Basic group (mmol/g)**	**Sample yield (%)**
	Carboxylic	**Lactonic**	**Phenolic**	**Total**		
AC	0.06 (9%)	0.43 (65%)	0.17 (26%)	0.66	0.63	–
Air 250^{o}C 12h	0.65 (53%) [+ 983%]	0.33 (27%) [– 23%]	0.25 (20%) [+ 47%]	1.23 [+ 86%]	0.40 [– 36%]	96
Air 250^{o}C 24h	1.53 (50%) [+ 2450%]	1.00 (33%) [+ 132%]	0.53 (17%) [+ 212%]	3.06 [+ 364%]	0.25 [– 60%]	88
Air 250^{o}C 48h	1.57 (41%) [+ 2517%]	1.41 (37%) [+ 228%]	0.87 (22%) [+ 412%]	3.85 [+ 483%]	0.13 [– 79%]	82
Air 350^{o}C 24h	3.54 (43%) [+ 5800%]	3.17 (39%) [+ 637%]	1.45 (18%) [+ 753%]	8.16 [+ 1136%]	0.05 [– 92%]	54

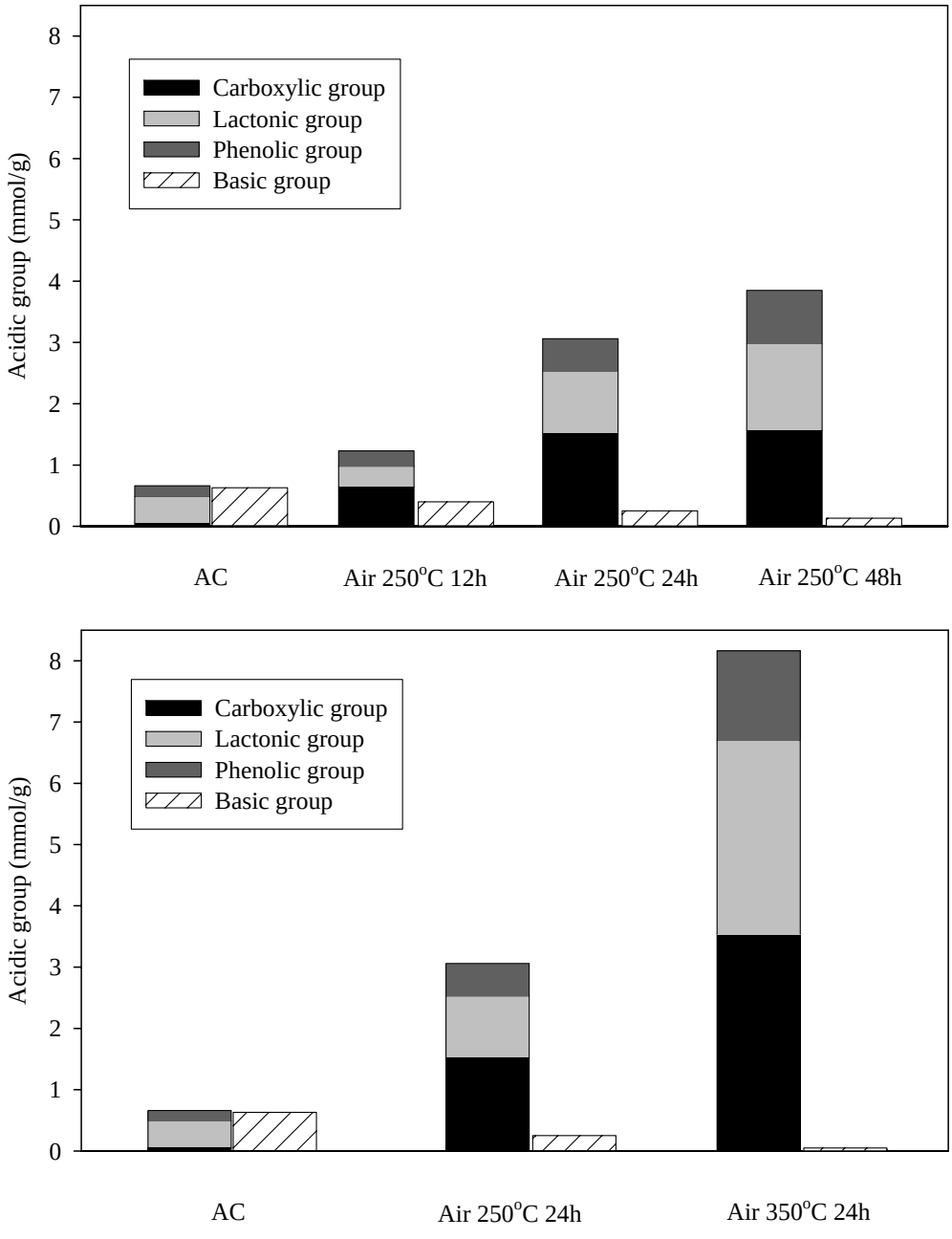

Figure 4.7 Contents of surface functional groups of the original activated carbon and activated carbons oxidized with air.

For all air oxidized carbons, the general order of percent increase of acidic groups is carboxylic > phenolic > lactonic, whereas the distribution of each functional group follows the order, carboxylic > lactonic > phenolic. The high content of carboxylic acid of air oxidation could result from the disruption of the carbon–carbon bond at high treatment temperature to form dicarboxylic group, as shown in following reaction:

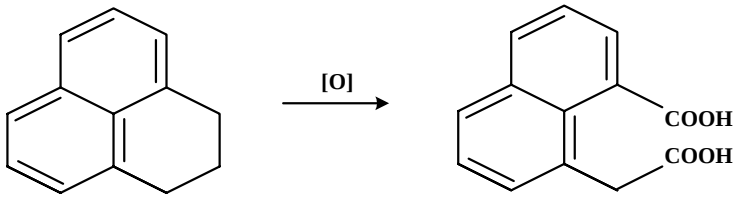

Therefore, this reaction could form more carboxylic group and its content is increased by 60 times when compared to the original sample, whereas the maximum increase of this group is only 20 times for liquid phase oxidation.

Data presented in Table 4.8 also shows that basic groups decrease after oxidation and with the increase in oxidation time and temperature. This may result from the high temperature effect of air oxidation that could disrupt the carbon–carbon bond but at the same time could also destroy some of the existing basic groups in the activated cabon structure.

In summary, for all oxidation methods, the percent increase in functional group concentration follows the order, carboxylic acid > phenolic > lactonic. The increasing of oxidation time, oxidation temperature, and acid concentration increases the total acid group and the amount of each acidic functional group, whereas the distribution of each functional group remains unchanged after oxidation treatments.

When comparing the maximum total acidic functional groups for each oxidation treatment (as shown in Table 4.9 and Figure 4.8), the following order is observed: air > HNO_3 by reflux method > H_2O_2 > $(NH_4)_2S_2O_8$ > HNO_3 by soaking method. Air oxidation has led to the formation of higher proportion of relatively stronger acidic group (i.e. carboxylic acid) with the following order: carboxylic acid > lactonic > phenolic. On the contrary, liquid phase oxidation resulted in the formation of higher proportion of relatively weaker acidic group (i.e. lactonic and phenolic) with the following order phenolic > lactonic > carboxylic acid for HNO_3 oxidation, and lactonic > phenolic > carboxylic acid for H_2O_2 and $(NH_4)_2S_2O_8$ oxidations. This could be the result of the stronger oxidant of O_2 (in air) and a higher temperature treatment of gas phase oxidation compared with the wet oxidation. Therefore, air is a suitable oxidizing agent to incorporate large amount of total acid group and carboxylic group. It is noted that no washing of sample is required for air oxidation and hence making the preparation step much simpler. However, the drawback of air oxidation is the relatively low yield of final oxidized carbon (54%).

Table 4.9 Comparison of Boehm titration results of original activated carbon and oxidized activated carbons with highest surface acidic functional groups obtained from each oxidizing agent (the value in square bracket [ ] is the percentage changes with reference to the original carbon, where "+" denotes % increasing and "–" denotes % decreasing).

Sample	Acidic group (mmol/g)				Basic group (mmol/g)	Sample yield (%)
	Carboxylic	Lactonic	Phenolic	Total		
AC	0.06 (9%)	0.43 (65%)	0.17 (26%)	0.66	0.63	–
HNO_3 1M 48h	0.39 (26%) [+ 550%]	0.49 (33%) [+ 14%]	0.60 (41%) [+ 253%]	1.48 [+ 124%]	0.25 [– 60%]	99
$(NH_4)_2S_2O_8$ 48h	0.38 (19%) [+ 533%]	1.05 (51%) [+ 144%]	0.61 (30%) [+ 259%]	2.04 [+ 209%]	0.38 [– 40%]	99
H_2O_2 48h	0.61 (27%) [+ 917%]	0.87 (39%) [+ 102%]	0.77 (34%) [+ 353%]	2.25 [+ 241%]	0.35 [– 44%]	95
HNO_3 re 10M 24h	1.26 (24%) [+ 2000%]	1.91 (37%) [+ 344%]	2.06 (39%) [+ 1112%]	5.23 [+ 692%]	2.30 [+ 265%]	93
Air 350^oC 24h	3.54 (43%) [+ 5800%]	3.17 (39%) [+ 637%]	1.45 (18%) [+ 753%]	8.16 [+ 1136%]	0.05 [– 92%]	54

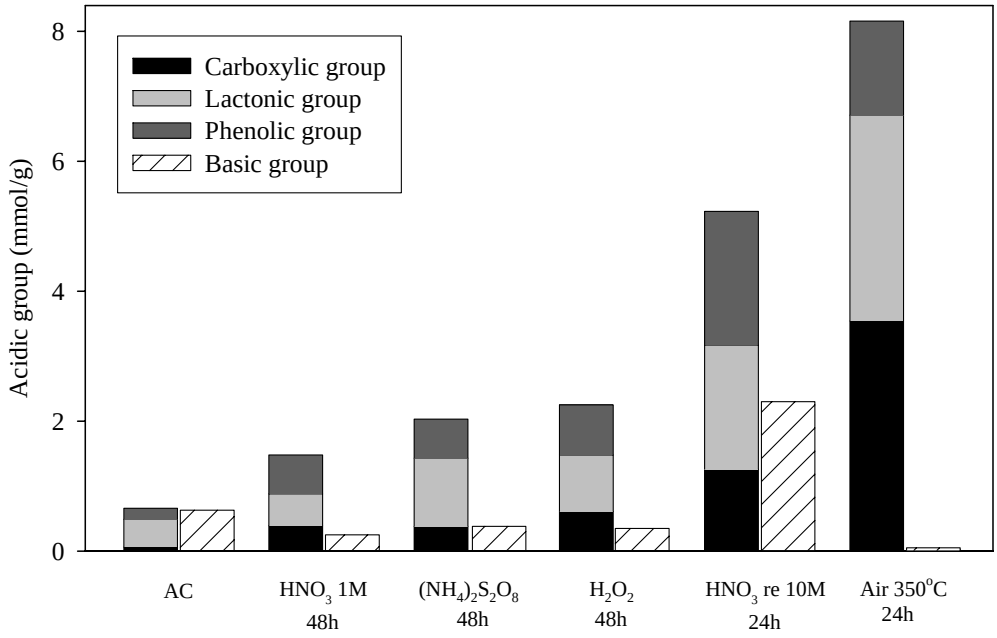

Figure 4.8 Contents of surface functional groups of the original activated carbon and oxidized activated carbons with maximum surface acidic functional groups obtained from each oxidizing agent.

Strelko, Malik, and Streat (2002) reported that the distribution of acidic surface groups was different between air and HNO_3 oxidized samples. Apparently, air oxidation led to the formation of a higher proportion of relatively weaker acid group (lactonic and phenolic groups), whereas HNO_3 oxidation gave relatively stronger acid group (carboxylic group) on the activated carbon surface. In their study, activated carbon derived from apricot stone by steam activation was used. Air oxidation was performed at 410 – 450^{o}C for 2 – 5 hours and HNO_3 oxidation was achieved at 90 – 95^{o}C for 2 – 15 hours. Differences in the raw material and oxidation conditions (time and temperature) probably give rise to the inconsistency between their results and those obtained in the present work. In the next sections (4.3.2.3 –

4.3.2.5), results from different analytical techniques are presented to substantiate the existence of surface functional groups previously reported.

4.3.2.3 FTIR results

The chemical nature of the oxygen surface functional groups formed on the activated carbons before and after oxidation treatment can be qualitatively compared using information from FTIR. Typical FTIR results of the original and some oxidized activated carbons are shown in Figure 4.9. Observation of the absorption bands shows that the differences between the original and oxidized activated carbons are mainly due to the formation of oxygen functional groups. The most characteristic changes with respect to increasing intensity of the bands are observed between two regions: around 1700 cm^{-1} and 1580 cm^{-1}. The band around 1700 cm^{-1} is ascribed to the stretching vibration of carboxyl groups on the edges of graphitic layer planes or to conjugated carbonyl groups (C=O in carboxylic acid and lactone groups). The band observed around 1580 cm^{-1} is assigned to phenolic O–H stretching vibrations conjugated with C=O stretching vibrations. In both regions, the pronounced bands follow the order HNO_3 re 1M 24h > H_2O_2 24h > $(NH_4)_2S_2O_8$ 24h > AC, and this order is also consistent with the results from Boehm titration (see Tables 4.5 – 4.7).

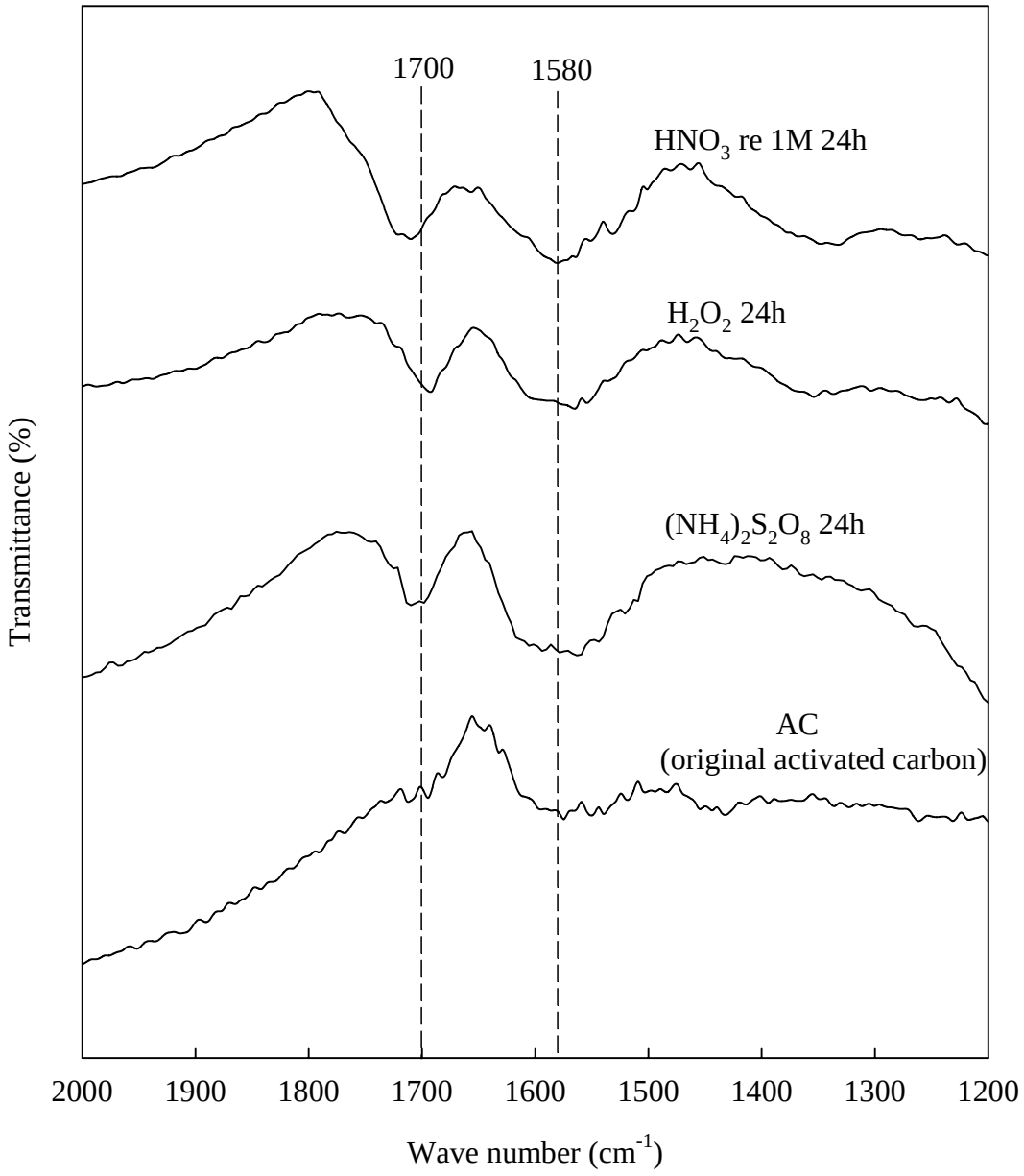

Figure 4.9 FTIR spectra of the original and oxidized activated carbons.

4.3.2.4 XPS and elemental results

The compositions of carbon and oxygen contents at the external surface of the activated carbon particles can be obtained from analyzing the spectra of X-ray Photoelectron spectroscopy (XPS). The O_{1s} and C_{1s} peaks are identified at the binding energy of about 533.2 and 284.6 eV, respectively. The O_{1s} and C_{1s} spectra of the original and oxidized activated carbons are illustrated in Figure 4.10. It can be observed that the peak area of O_{1s} spectra of the oxidized activated carbons are higher and the peak area of C_{1s} spectra of the oxidized activated carbons are lower than that of the original activated carbon. This indicates that there is higher oxygen content presenting on the surface of oxidized carbons than that observed in the original carbon. In order to calculate the percentage of surface atomic concentration, the peak areas of C_{1s} and O_{1s} were determined by applying the Gaussian equation and dividing by a sensitivity factor (0.205 for carbon and 0.63 for oxygen) (Cordero et al., 2002). Table 4.10 compares the surface atomic concentration for oxygen and carbon of the original and the oxidized activated carbons. The order of increasing in oxygen content in the samples, which supports the results from Boehm titration, is as follows: HNO_3 re 1M 24h > H_2O_2 24h > HNO_3 1M 24h > AC.

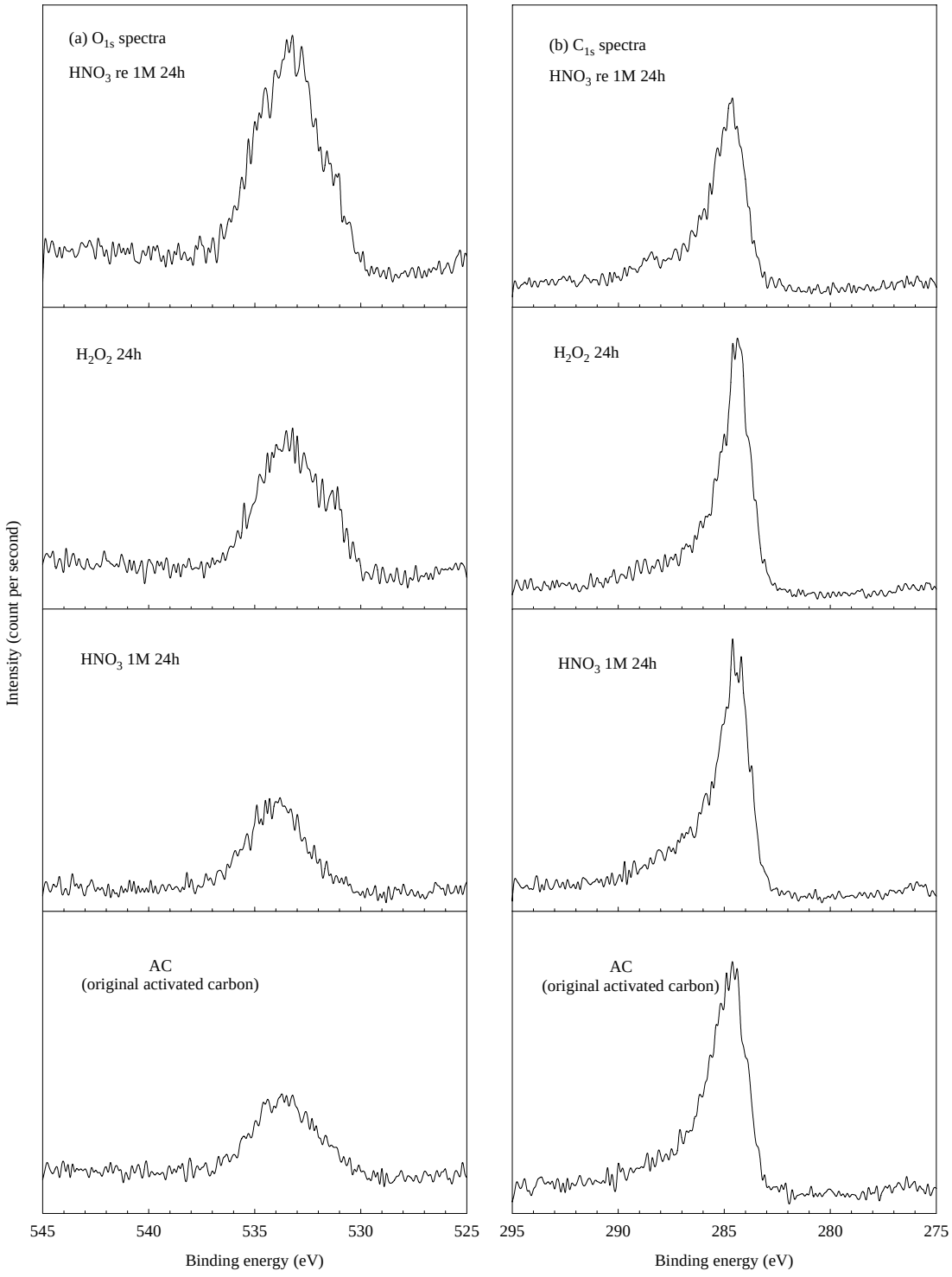

Figure 4.10 XPS spectra of (a) O_{1s} and (b) C_{1s} of the original and oxidized activated carbons.

Table 4.10 Surface atomic concentration obtained from the C_{1s} and O_{1s} XPS regions of original and oxidized activated carbons.

Sample	**C_{1s} (%)**	**O_{1s} (%)**
AC (original activated carbon)	83.36	16.64
H_2O_2 24h	71.14	28.86
HNO_3 1M 24h	81.72	18.28
HNO_3 re 1M 24h	56.77	43.23

To further confirm the existence of increased oxygen functional groups on the activated carbon surfaces, the elemental analyses were performed and the results are shown in Table 4.11. The results indicate that all oxidized activated carbons give significant increase in oxygen contents. Again, this demonstrates the increased amount of oxygen functional groups on the oxidized carbon surfaces as the consequence of oxidation treatment. It should be noted that the carbon content decreases due to the corresponding increase in the amount of oxygen after oxidation. From Table 4.11, the order of samples with decreasing in oxygen contents is that air 350^{o}C 24h > HNO_3 re 1M 24h > air 250^{o}C 24h > H_2O_2 24h > $(NH_4)_2S_2O_8$ 24h > HNO_3 1M 24h > AC. These results also are in line with those obtained by Boehm titration (Tables 4.5 – 4.8). Figure 4.11 shows the correlation between oxygen contents and the corresponding acidic groups concentration from Boehm's results.

This relationship can be approximated by the following quadratic equation of polynomial type:

$$y = 12.040 + 6.524x - 0.438x^2 \quad (4.1)$$

where y is the oxygen content in wt% and x is the concentration of acidic functional groups in mmol/g. The correlation coefficient (R^2) of this equation is 0.995. It is noted that the relationship is not linear because each oxidizing agent can incorporate different functional groups (carboxylic acid, lactonic, and phenolic) in different proportions as shown previously in Tables 4.5 – 4.8.

Table 4.11 Elemental analysis results of original and oxidized activated carbons.

Sample	**C (wt%)**	**H (wt%)**	**O (wt%)**	**N (wt%)**
AC (original activated carbon)	79.68	2.74	17.15	0.43
H_2O_2 24h	74.10	3.18	22.37	0.35
$(NH_4)_2S_2O_8$ 24h	75.29	2.86	21.42	0.43
HNO_3 1M 24h	79.57	2.56	17.32	0.55
HNO_3 re 1M 24h	61.43	2.82	33.98	1.77
HNO_3 re 5M 24h	60.98	2.76	34.41	1.85
Air 250^{o}C 24h	72.81	2.96	23.57	0.66
Air 350^{o}C 24h	61.50	1.83	35.75	0.92

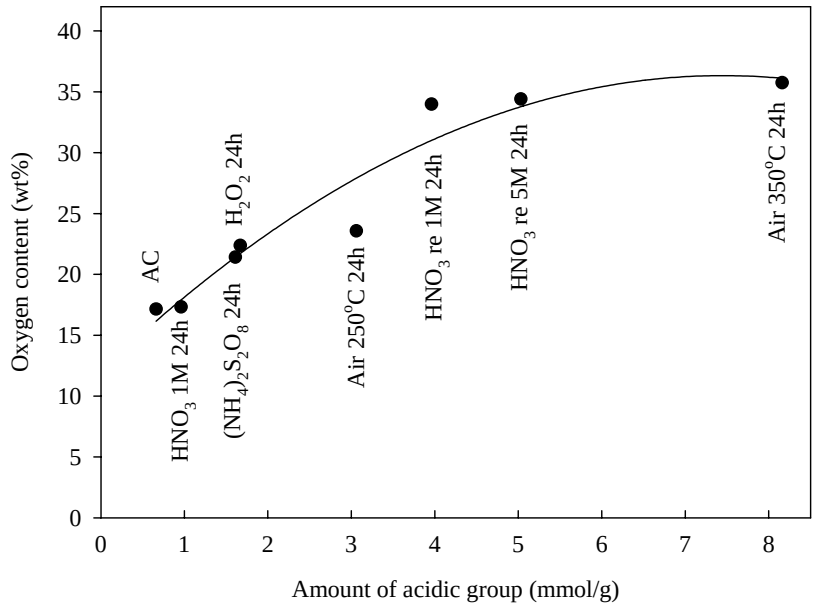

Figure 4.11 Relationship between oxygen content and amount of acidic functional groups of the original and oxidized activated carbons.

4.3.2.5 pH_{pzc} results

Figure 4.12 presents the results of the pH drift method to obtain the pH_{pzc} of the original and some oxidized carbons and Table 4.12 summarizes the pH_{pzc} values. As seen from Table 4.12, the oxidized carbons exhibit lower pH_{pzc} values than that of the original activated carbon. The order of the pH_{pzc} values is in agreement with the amount of acidic functional groups from Boehm titration (Tables 4.5 – 4.8) i.e. the higher content of acidic functional groups, the lower is the pH_{pzc}. Figure 4.13 shows the relationship between the pH_{pzc} values and the amount of acidic functional groups that can be represented as following quadratic equation of polynomial type:

$$y = 8.877 - 1.627x + 0.096x^2 \quad (4.2)$$

where y is the pH_{pzc} and x is the amount of acidic functional groups expressed as mmol/g. The correlation coefficient (R^2) of this equation is 0.998.

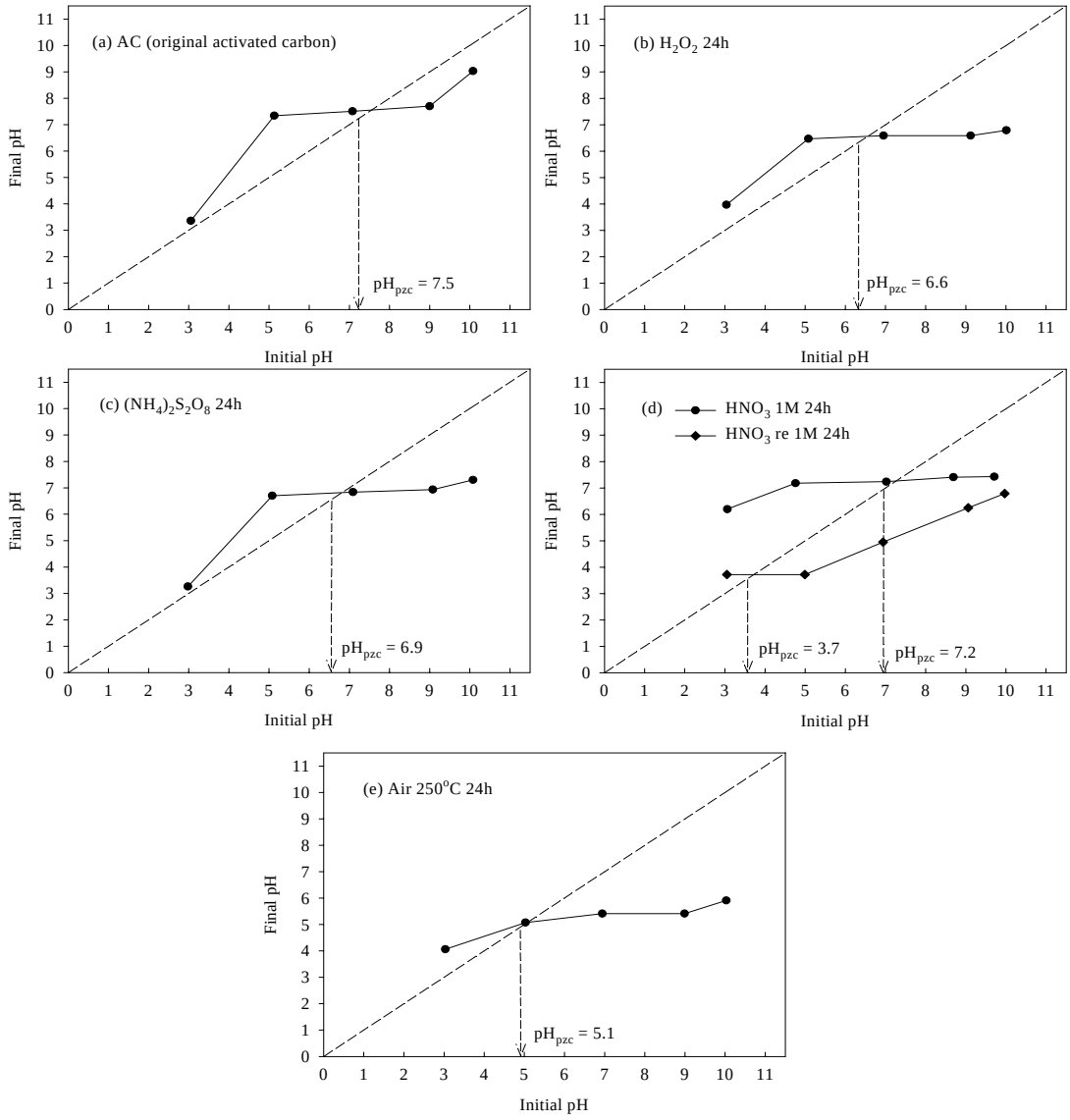

Figure 4.12 pH drift method to obtain the pH_{pzc} of the original and oxidized activated carbons.

Table 4.12 The results of pH_{pzc} of the original and oxidized activated carbons.

Sample	**pH_{pzc}**
AC (original activated carbon)	7.5
H_2O_2 24h	6.6
$(NH_4)_2S_2O_8$ 24h	6.9
HNO_3 1M 24h	7.2
HNO_3 re 1M 12h	4.9
HNO_3 re 1M 24h	3.7
HNO_3 re 5M 24h	2.8
HNO_3 re 10M 24h	2.7
Air 250^{o}C 12h	7.0
Air 250^{o}C 24h	5.1
Air 250^{o}C 48h	4.1
Air 350^{o}C 24h	2.2

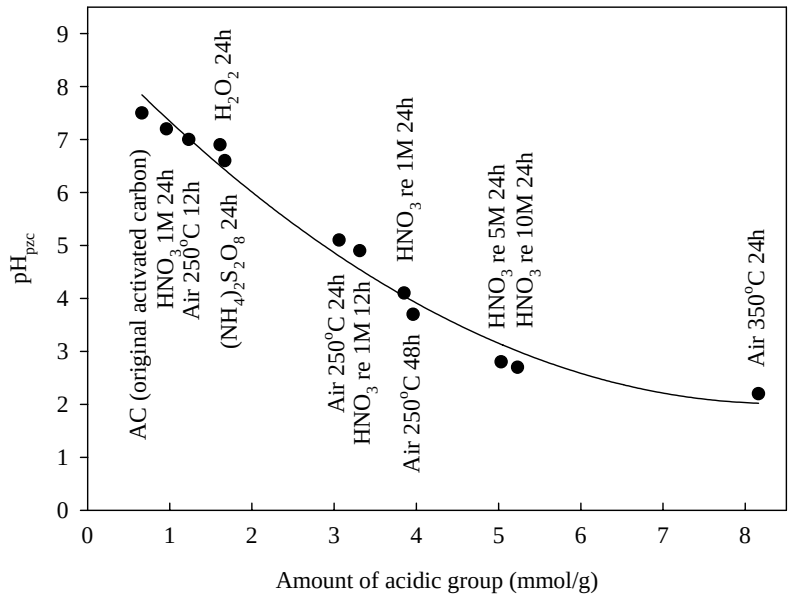

Figure 4.13 Relationship between pH_{pzc} and content of acidic functional groups of the original and oxidized activated carbons.

4.3.3 Effect of porous structure on the incorporation of surface functional groups

In an attempt to demonstrate the effect of carbon porous structure on the variation in the quantity and distribution of surface functional groups, three activated carbon samples prepared by physical activation i.e. AC600, AC800, and AC900 were oxidized with 1 M, 5 M, and 10 M HNO_3 by boiling in a reflux condenser for 24 hours. The oxidized activated carbons were designated as AC*X*-HNO_3 re *x*M 24h, where *X* is the activation temperature i.e. 600, 800, and 900°C and *x* is the concentration of HNO_3 i.e. 1, 5, and 10 M. It is important to note that HNO_3 treatment by reflux method was used in this study because this oxidant is the strongest oxidizing agent as compared to the other oxidizing agents used for liquid phase oxidation (H_2O_2 and $(NH_4)_2S_2O_8$). The treatment time of 24 hours was chosen to first

check the effect of porous structure on the introduced functional groups. The influence of oxidation time (for example 48 hours) on the incorporation of surface functional groups is suggested for future work.

The porous properties and amount of acidic and basic groups determined from Boehm titration are shown in Table 4.13 and Figure 4.14. In general, the total acidic groups increase after oxidation for all three original samples and the percent increase depends on both surface area of the original samples and concentration of HNO_3 used. For all oxidized carbons, the general orders of percent increase and percent distribution of acidic groups are the same with carboxylic > lactonic > phenolic. The decrease of phenolic group after oxidation may be due to the transformation of carboxylic and phenolic groups to lactonic group, as shown in Figure 4.15 (Puente, Pis, Menéndez, and Grange, 1997). Again, the increasing of acid concentration increases the amounts of all three functional group, and the distribution of each functional group still follows the above order.

The basic groups of all three original samples increase after oxidation and with increasing of acid concentration. The increase of these groups may be due to the formation of ketone as discussed earlier in section 4.3.2.2.

Table 4.13 Porous properties and Boehm titration results of original and oxidized activated carbons with different porous structure (the value in square bracket [ ] is the percentage changes with reference to the original carbon, where "+" denotes % increasing and "–" denotes % decreasing).

Sample	S_{BET} (m^2/g)	V_{mic} (cm^3/g)	V_T (cm^3/g)	Acidic group (mmol/g)				Basic group (mmol/g)
				Carboxylic	Lactonic	Phenolic	Total	
AC600	460	0.21	0.23	0.20 (17%)	0.36 (30%)	0.64 (53%)	1.20	0.40
AC600-HNO_3 re 1M 24h	405	0.20	0.23	1.10 (56%) [+ 450%]	0.52 (26%) [+ 44%]	0.36 (18%) [– 44%]	1.98 [+ 65%]	0.60 [+ 50%]
AC600-HNO_3 re 5M 24h	–	–	–	1.10 (55%) [+ 450%]	0.53 (26%) [+ 47%]	0.37 (19%) [– 42%]	2.00 [+ 67%]	0.62 [+ 55%]
AC800	651	0.29	0.33	0.19 (12%)	0.45 (28%)	0.95 (60%)	1.59	0.45
AC800-HNO_3 re 1M 24h	604	0.26	0.32	1.07 (49%) [+ 463%]	0.80 (37%) [+ 78%]	0.30 (14%) [– 68%]	2.17 [+ 36%]	0.93 [+ 107%]
AC800-HNO_3 re 5M 24h	–	–	–	1.21 (49%) [+ 537%]	0.85 (35%) [+ 89%]	0.40 (16%) [– 58%]	2.46 [+ 55%]	1.35 [+ 200%]
AC800-HNO_3 re 10M 24h	–	–	–	1.21 (49%) [+ 537%]	0.85 (35%) [+ 89%]	0.41 (16%) [– 57%]	2.47 [+ 55%]	1.36 [+ 202%]
AC900	1491	0.66	0.80	0.16 (10%)	0.38 (24%)	1.06 (66%)	1.60	1.17
AC900-HNO_3 re 1M 24h	1161	0.50	0.68	1.29 (60%) [+ 706%]	0.75 (34%) [+ 97%]	0.13 (6%) [– 88%]	2.17 [+ 36%]	1.58 [+ 35%]
AC900-HNO_3 re 5M 24h	–	–	–	1.91 (59%) [+ 1094%]	0.86 (26%) [+ 126%]	0.47 (15%) [– 57%]	3.24 [+ 102%]	1.65 [+ 41%]
AC900-HNO_3 re 10M 24h	–	–	–	2.19 (60%) [+ 1269%]	0.97 (26%) [+ 155%]	0.50 (14%) [– 53%]	3.66 [+ 129%]	1.70 [+ 45%]

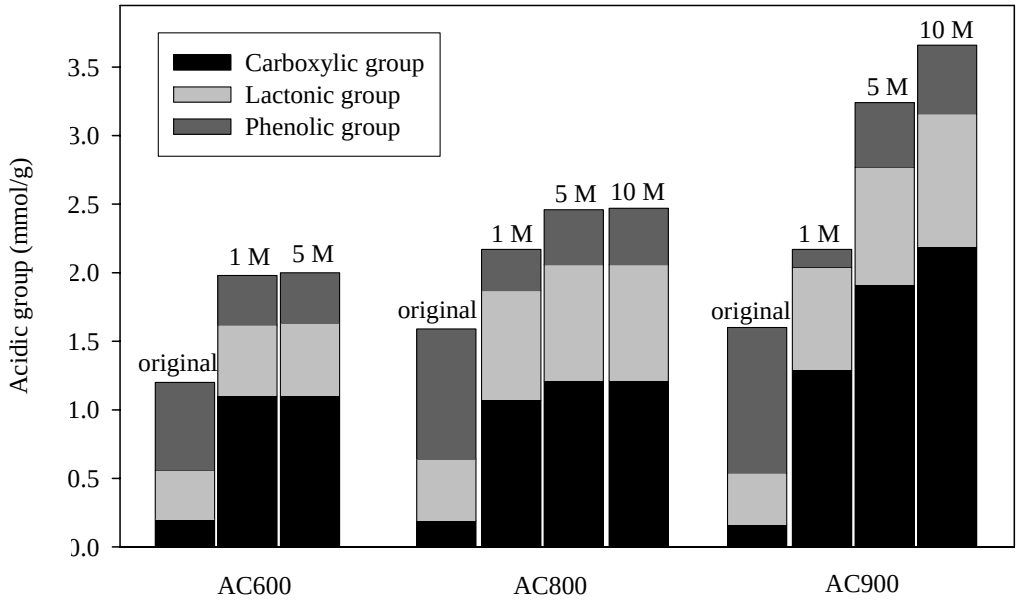

Figure 4.14 Contents of acidic functional groups of original and oxidized activated carbons with different porous structure.

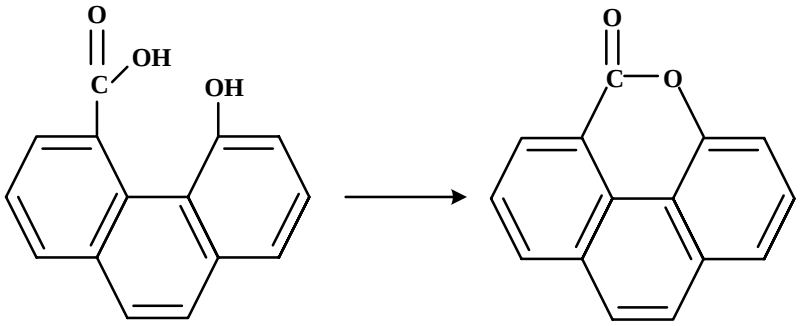

Figure 4.15 Possible formation of lactonic group from carboxylic acid and phenolic (Puente et al., 1997).

For activated carbon prepared at 600^{o}C (AC600) series, the amount of total acidic groups does not change appreciably when increasing the HNO_3 concentration from 1 M to 5 M. Similarly, activated carbon prepared at 800^{o}C (AC800), which has higher surface area, can accommodate the maximum amount of

acidic surface groups formed but with the use of a higher HNO_3 concentration of 5 M. Thus, we may conclude that there exists a minimum HNO_3 concentration that can create a maximum in acidic surface groups and this optimum acid concentration depends largely on the available surface area of the original carbons. Similar trend can also be observed for the case of AC900 sample.

Table 4.14 and Figure 4.16 shows the results of the introduced surface functional groups after HNO_3 oxidation by reflux method with different concentrations for 24 hours for activated carbons obtained from physical activation (AC600, AC800, and AC900) and activated carbon obtained from chemical activation (AC). As can be seen, after oxidation, the original carbons prepared from chemical activation and physical activation show the differences in both the amount of total acidic groups and the distribution of these groups. As previously described in section 4.3.1, the original carbon prepared from chemical activation (AC) contains lower amount of total acidic functional groups than all the three original carbons prepared from physical activation (AC600, AC800, and AC900). However, after oxidation under the same conditions, sample AC shows higher amount of total acidic groups than AC600, AC800, and AC900 samples, although sample AC has particularly less surface area than AC900. The amount of each acidic group of oxidized samples obtained from the original carbons prepared by physical activation was carboxylic > lactonic > phenolic, while the reverse order phenolic > lactonic > carboxylic was obtained for the original carbon prepared by chemical activation. This difference could be due to the surface characteristic of activated carbon prepared from physical activation has a high degree of surface rupture and defects to form carboxylic acid due to the higher activation temperature used. Therefore, it can be concluded that

under the same oxidation conditions the types and amounts of functional groups introduced after oxidation treatment depend not only on the available surface area of original carbon but also on the activation method (chemical or physical activation) used to prepare the original carbon.

Table 4.14 Comparison of acidic functional groups of original and oxidized activated carbons prepared by chemical and physical activations.

Sample	S_{BET} (m^2/g)	Acidic group (mmol/g)			
		Carboxylic	Lactonic	Phenolic	Total
AC	1200	0.06	0.43	0.17	0.66
HNO_3 re 1M 24h		1.01	1.18	1.77	3.96
HNO_3 re 5M 24h		1.24	1.76	2.03	5.30
HNO_3 re 10M 24h		1.26	1.91	2.06	5.23
AC600	460	0.20	0.36	0.64	1.20
HNO_3 re 1M 24h		1.10	0.52	0.36	1.98
HNO_3 re 5M 24h		1.10	0.53	0.37	2.00
AC800	651	0.19	0.45	0.95	1.59
HNO_3 re 1M 24h		1.07	0.80	0.30	2.17
HNO_3 re 5M 24h		1.21	0.85	0.40	2.46
HNO_3 re 10M 24h		1.21	0.85	0.41	2.47
AC900	1491	0.16	0.38	1.06	1.60
HNO_3 re 1M 24h		1.29	0.75	0.30	2.17
HNO_3 re 5M 24h		1.91	0.86	0.40	3.24
HNO_3 re 10M 24h		2.19	0.97	0.41	3.66

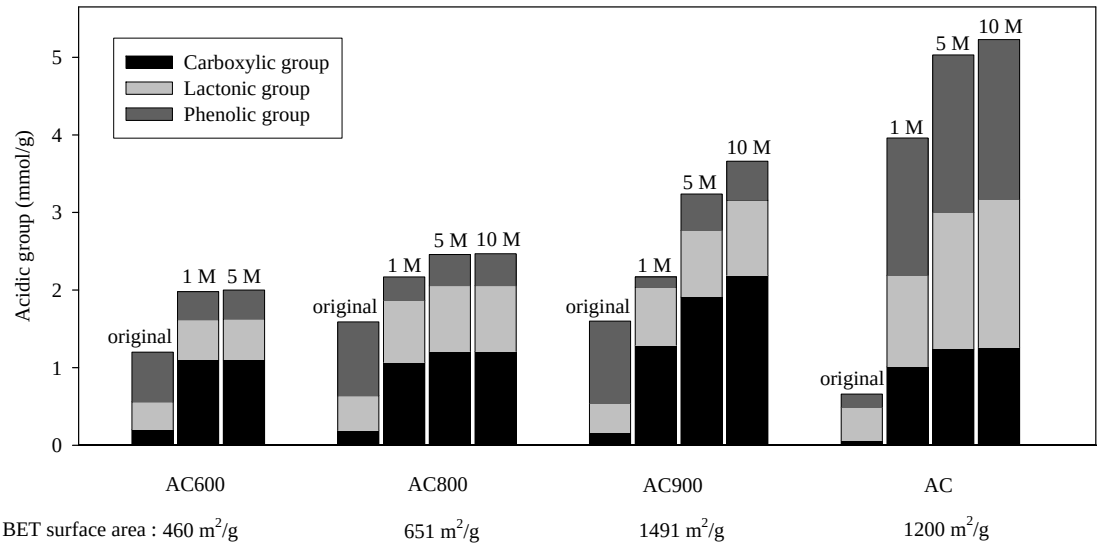

Figure 4.16 Comparison of acidic functional groups obtained from HNO_3 oxidation by reflux method for 24 hours of original activated carbons prepared by chemical and physical activations.

4.3.4 Effect of heat treatment on surface functional groups

The purpose of this section is to study the effect of heat treatment process on the variation of concentration and distribution of oxygen functional groups. The distribution of each acidic functional group can affect the adsorption process of polar molecules, for example, each type of acidic functional group was capable of forming a certain maximum number of hydrogen bonds directly with water molecules. Carrasco-Marin et al. (1997) evaluated the number of water molecules interacting with each type of functional groups and suggested that there are 3 water molecules interacting with the carboxylic and lactone groups and 1.5 water molecules with the phenol group. To further understand this phenomenon, the activated carbon prepared by physical activation at the activation temperature 800^{o}C and oxidized with 1 M HNO_3 (AC800-HNO_3 re 1M 24h) was subsequently heat treated in a packed-bed

reactor (2.5 cm diameter and 10 cm long of steel pipe) at 600^{o}C and 800^{o}C for 12 hours under the flow of N_2 at 100 cm^3/min. Heat treated carbons at 600^{o}C and 800^{o}C were designated as AC800-HNO_3-HT600^{o}C and AC800-HNO_3-HT800^{o}C, respectively.

Table 4.15 and Figure 4.18 show that when the oxidized samples (AC800-HNO_3 re 1M 24h) are heat treated to high temperatures of 600^{o}C and 800^{o}C, their total acidic functional groups are found to decrease. The higher heat treatment temperature of 800^{o}C decreases higher amount of the total acidic groups (45%) compared to the lower heat treatment temperature of 600^{o}C (26%). These results agree with those of other researchers (Pradhan and Sandle, 1999; Bagreev, Adib, and Bansosz, 2001; László, 2005; Shin, Yoo, Park, and Song, 2006).

Table 4.15 Boehm titration results of original, oxidized, and heat treated activated carbons (the value in square bracket [ ] is the percentage changes with reference to the original carbon, where "+" denotes % increasing and "–" denotes % decreasing).

Sample	Acidic group (mmol/g)				Basic group (mmol/g)
	Carboxylic	Lactonic	Phenolic	Total	
AC800	0.19 (12%)	0.45 (28%)	0.95 (60%)	1.59	0.45
AC800-HNO_3 re 1M 24h	1.07 (49%)	0.80 (37%)	0.30 (14%)	2.17	0.93
AC800-HNO_3-HT600^oC	0.39 (24%) [– 64%]	1.01 (63%) [+ 26%]	0.20 (13%) [– 33%]	1.60 [– 26%]	0.54 [– 42%]
AC800-HNO_3-HT800^oC	0.27 (22%) [– 75%]	0.73 (61%) [– 9%]	0.20 (17%) [– 33%]	1.20 [– 45%]	0.45 [– 52%]

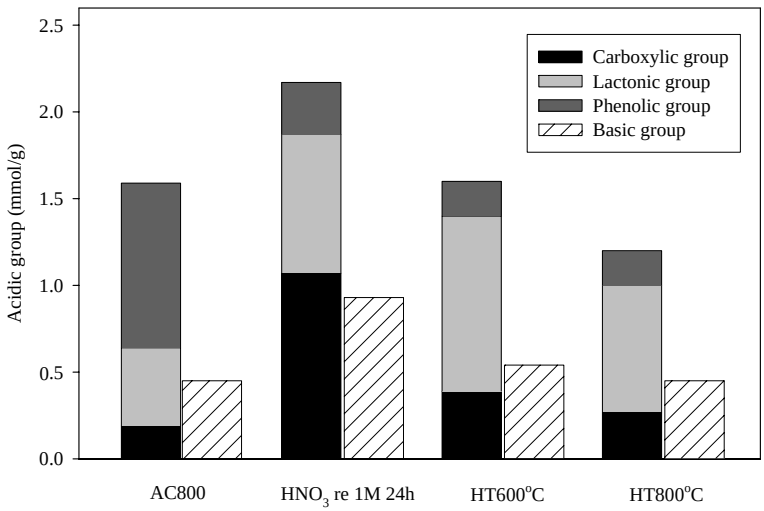

Figure 4.17 Contents of surface functional groups of the original, oxidized, and heat treated activated carbons.

For treatment temperature of 600^{o}C, the heat-treated sample (AC800-HNO_3-HT600^{o}C) has the total acidic groups comparable to the original carbon. The original AC800 has high phenolic group followed by lactonic and carboxylic groups while the heat-treated sample has high lactonic group followed by carboxylic and phenolic groups. This indicates that heat treatment process can reduce the amount and change the distribution of acidic groups of activated carbon. In comparison with the modified carbon (AC800-HNO_3 re 1M 24h) large decrease of carboxylic group can be observed, whereas the phenolic and lactonic contents show relatively small variation during the heat treatment. The lowering in the amount of total acidic functional groups of AC800-HNO_3-HT800^{o}C (1.20 mmol/g) than AC800 (1.59 mmol/g) indicates that heat treatment at 800^{o}C not only removed the acidic groups incorporated by HNO_3 oxidation but it also removed the inherent acidic groups being introduced by CO_2 activation during the preparation step of the original carbon.

As can be observed from Table 4.15, carboxylic acid group is most sensitive to heat treatment i.e. this group decreases in largest amount at both treatment temperatures. At heat treatment temperature of 600^{o}C, more than half of carboxylic acid group was removed (64%) followed by phenolic group (33%), whereas lactonic group showed about 26% increase. An increase in lactonic group content may arise from the transformation of lactonic group from carboxylic and phenolic groups during heat treatment as shown in Figure 4.15 in section 4.3.3. At higher heat treatment temperature (800^{o}C), carboxylic acid group was largely removed (75%) and lactonic group showed a small decrease (9%). The phenolic group remained relatively unchanged in its amount at this temperature. This indicates that phenolic and lactonic groups are more stable than the carboxylic group. Salame and Bandosz (2000) studied

the thermal analysis of activated carbon in nitrogen atmosphere and indicated that the weight loss at temperatures lower than 527^{o}C is attributed to the decomposition of carboxylic acid and lactone. The weight loss at a temperature higher than 527^{o}C is due to the decomposition of phenol. Therefore, according to the results obtained in the present work along with other works (Xiao, 2004; Bagreev et al., 2001), the order of thermal stability of oxygen functional groups is the following: carboxylic < lactonic < phenolic.

As noticed from Table 4.15 and Figure 4.17, thermal treatments also removed the basic groups on carbon and gave much decrease of these values with increasing in heat treatment temperature. These results were also observed in the work of Shin et al. (2006).

Table 4.16 gives the porous properties of the original, oxidized, and heat treated activated carbons. It is observed that heat treatment process increases all porous properties of heat treated carbons. Upon the removal of surface functional groups being formed at the pore entrance during heat treatment, the N_2 molecules can thus get access into the internal adsorption sites. The increasing of porous properties of the heat treated carbons is consistent with the decreasing amount of surface functional groups, as shown in Table 4.15.

Table 4.16 Porous characteristics results of original, oxidized, and heat treated activated carbons.

Sample	S_{BET} (m^2/g)	V_{mic} (cm^3/g)	V_T (cm^3/g)
AC800	651	0.29	0.33
AC800-HNO_3 re 1M 24h	604	0.26	0.32
AC800-HNO_3-HT600^oC	647	0.29	0.34
AC800-HNO_3-HT800^oC	774	0.35	0.40

4.4 Conclusions

Eucalyptus wood-based activated carbon was modified by oxidative liquid treatment (H_2O_2, $(NH_4)_2S_2O_8$, and HNO_3) and gas treatment (air). The treatment conditions such as concentration, time, and temperature were investigated. The effect of porous structure on the amount and distribution of functional groups was also studied. The surface chemistries of oxidized activated carbons were characterized by various analytical methods.

The results can be summarized as follows:

- In all cases, oxidative treatments of activated carbons resulted in the increase in the number of total acidic oxygen functional groups.

- Air oxidation gave the highest total acidic groups and highest amount of carboxylic acid in the carbon as compared with the wet oxidation method. However, the yield of oxidized carbon by air oxidation was lower.

- The percent increase of acidic types in the oxidized activated carbon as compared to the original activated carbon was highest for carboxylic acid group followed by phenolic and lactonic for all the oxidation treatment in the present study.

- The preparation method of activated carbon had a direct effect on the amount and distribution of functional groups. For HNO_3 by reflux method treatment, the original activated carbon prepared by chemical method gave higher total acidic groups but created less carboxylic acid group as compared to the original activated carbon prepared by physical method.

- Porous structure of the original activated carbon had an effect on the introduction of oxygen functional groups. The highest amounts of acidic functional groups were obtained in the activated carbon having highest surface area. There exists a minimum oxidant concentration corresponding to the available surface area that can produce maximum amount of acidic surface group.

- Under all the conditions used in the present study, air is the suitable oxidizing agent capable of incorporating high content of strong acid group i.e. carboxylic acid on activated carbon prepared from chemical activation, whereas high surface area sample (AC900) oxidized with high concentration of HNO_3 (10 M) gave high amount of carboxylic acid for activated carbon prepared from physical activation.

- Heat treatment process reduced the amount and changed the distribution of oxygen functional groups on activated carbon and increased the surface area. The content of each functional groups was changed in the same way as the order of thermal stability i.e. carboxylic < lactonic < phenolic.

4.5 References

Aharoni, C. (1997). The solid-liquid interface in capillary condensation. Sorption of water by active carbons. **Langmuir** 13: 1270-1273.

Ania, C. O., Parra, J. B., and Pis, J. J. (2002). Influence of oxygen-containing functional groups on active carbon adsorption of selected organic compounds. **Fuel Process. Technol.** 79: 265-271.

Arafat, H. A., Franz, M., and Pinto, N. G. (1999). Effect of salt on the mechanism of adsorption of aromatics on activated carbon. **Langmuir** 15: 5997-6003.

Attia, A. A., Rashwan, W. E., and Khedr, S. A. (2006). Capacity of activated carbon in the removal of acid dyes subsequent to its thermal treatment. **Dyes Pigments** 69: 128-136.

Bagreev, A., Adib, F., and Bandosz, T. J. (2001). pH of activated carbon surface as an indication of its suitability for H2S removal from moist air streams. **Carbon** 39: 1897-1905.

Bandosz, T. J., Jagiełło, J., and Schwarz, J. A. (1993). Effect of surface chemical groups on energetic heterogeneity of activated carbons. **Langmuir** 9: 2518-2522.

Bandosz, T. J., Jagiello, J., Schwarz, J. A., and Krzyzanowski A., (1996). Effect of surface chemistry on sorption of water and methanol on activated carbons. **Langmuir** 12: 6480-6486.

Biniak, S., Pakuła, M., Szymański, G. S. and Świątkowski, A. (1999). Effect of activated carbon surface oxygen- and/or nitrogen-containing groups on adsorption of copper(II) ions from aqueous solution. **Langmuir** 15: 6117-6122.

Boehm, H. P. (1994). Some aspects of the surface chemistry of carbon blacks and other carbons. **Carbon** 32: 759-769.

Carrasco-Marin, F., Mueden, A., Centeno, T. A., Stoeckli, F., and Moreno-Castilla, C. (1997). Water adsorption on activated carbons with different degrees of oxidation. **J. Chem. Soc., Faraday Trans.** 93: 2211-2215.

Chen, J. P., Wu, S., and Chong, K.-H. (2003). Surface modification of a granular activated carbon by citric acid for enhancement of copper adsorption. **Carbon** 41: 1979-1986.

Choma, J., Burakiewicz-Mortka, W., Jaroniec, M., Li, Z., and Klinik, J. (1999). Monitoring changes in surface and structural properties of porous carbons modified by different oxidizing agents. **J. Colloid Interface Sci.** 214: 438-446.

Considine, R., Denoyel, R., Pendleton, P., Schumann, R., and Wong, S.-H. (2001). The influence of surface chemistry on activated carbon adsorption of 2-methylisoborneol from aqueous solution. **Colloids Surf. A** 179: 271-280.

Cordero, T., Rodriguez-Mirasol, J., Tancredi, N., Piriz, J., Vivo, G., and Rodriguez, J. J. (2002). Influence of surface composition and pore structure on Cr(III) adsorption onto activated carbons. **Ind. Eng. Chem. Res.** 41: 6042-6048.

Denisov, E. T. and Afanas'ev, I. B. (2005). **Oxidation and Antioxidations in Organic Chemistry and Biology.** CRC Press.

Do, D. D. (1998). **Adsorption analysis: Equilibria and Kinetics.** Singapore: Imperial College Press.

Domingo-García, M., López-Garzón, F. J., Pérez-Mendoza, M. (2000). Effect of some oxidation treatments on the textural characteristics and surface chemical nature of an activated carbon. **J. Colloid Interface Sci.** 222: 233-240.

El-Hendawy, A.-N. A. (2003). Influence of HNO_3 oxidation on the structure and adsorptive properties of corncob-based activated carbon. **Carbon** 41: 713-722.

Goyal, M., Rattan, V. K., Aggarwal, D., and Bansal, R. C. (2001). Removal of copper from aqueous solutions by adsorption on activated carbons. **Colloids Surf. A** 190: 229-238.

Jia, Y. F. and Thomas, K. M. (2000). Adsorption of cadmium ions on oxygen surface sites in activated carbon. **Langmuir** 16: 1114-1122.

László, K. (2005). Adsorption from aqueous phenol and aniline solutions on activated carbons with different surface chemistry. **Colloids Surf. A** 265: 32-39.

Lebedev, N. N. (1984). **Chemistry and Technology of Basic Organic and Petrochemical Synthesis.** Moscow: MIR Publishers.

Liu, S. X., Chen, X., Chen, X. Y., Liu, Z. F., and Wang, H. L. (2007). Activated carbon with excellent chromium(VI) adsorption performance prepared by acid–base surface modification. **J. Hazard. Mater.** 141: 315-319.

Lopez-Ramon, M. V., Stoeckli, F., Moreno-Castilla, C., and Carrasco-Marin, F. (1999). On the characterization of acidic and basic surface sites on carbons by various techniques. **Carbon** 37: 1215-1221.

Moreno-Castilla, C., Ferro-García, M. A., Joly, J. P., Bautista-Toledo, I., Carrasco-Marín, F., and Rivera-Utrilla, J. (1995). Activated carbon surface modifications by nitric acid, hydrogen peroxide, and ammonium peroxydisulfate treatments. **Langmuir** 11: 4386-4392.

Moreno-Castilla, C., Carrasco-Marín, F., and Mueden, A. (1997). The creation of acid carbon surface by treatment with $(NH_4)_2S_2O_8$. **Carbon** 35: 1619-1626.

Moreno-Castilla, C., López-Ramón, M. V. and Carrasco-Marín, F. (2000). Changes in surface chemistry of activated carbons by wet oxidation. **Carbon** 38: 1995-2001.

Nevskaia, D. M., Castillejos-Lopez, E., Guerrero-Ruiz, A., and Muñoz, V. (2004). Effects of the surface chemistry of carbon materials on the adsorption of phenol-aniline mixtures from water. **Carbon** 42: 653-665.

Park, G. I., Lee, J. K., Ryu, S. K., and Kim, J. H. (2002). Effect of two-step surface modification of activated carbon on the adsorption characteristics of metal ions in wastewater I. Equilibrium and batch adsorptions. **Carbon Science** 3: 219-225.

Pereira, M. F. R., Soares, S. F., Órfão, J. J. M., and Figueiredo, J. L. (2003). Adsorption of dyes on activated carbons: influence of surface chemical groups. **Carbon** 41: 811-821.

Pradhan, B. K. and Sandle, N. K. (1999). Effect of different oxidizing agent treatments on the surface properties of activated carbons. **Carbon** 37: 1323-1332.

Puente, G. de la, Pis, J. J., Menéndez, J. A., and Grange, P. (1997). Thermal stability of oxygenated functions in activated carbons. **J. Anal. Appl. Pyrolysis** 43: 125-138.

Radovic, L. R., Silva, I. F., Ume, J. I., Menéndez, J. A., Leon Y Leon, C. A., Scaroni, A. W. (1997). An experimental and theoretical study of the adsorption of aromatics possessing electron-withdrawing and electron-donating functional groups by chemically modified activated carbons. **Carbon** 35: 1339-1348.

Rivera-Utrilla, J. and Sánchez-Polo, M. (2003). Adsorption of Cr(III) on ozonised activated carbon: importance of Cπ–cation interactions. **Wat. Res.** 37: 3335-3340.

Salame, I. I., Bagreev, A., and Bandosz, T. J. (1999). Revisiting the effect of surface chemistry on adsorption of water on activated carbons. **J. Phys. Chem. B** 103: 3877-3884.

Salame, I. I. and Bandosz, T. J. (1999). Study of water adsorption on activated carbons with different degrees of surface oxidation. **J. Colloid Interface Sci.** 210: 367-374.

Salame, I. I. and Bandosz, T. J. (2000). Comparison of the surface features of two wood-based activated carbons. **Ind. Eng. Chem. Res.** 39: 301-306.

Santiago, M. S., Stüber, F., Fortuny, A., Fabregat, A., and Font, J. (2005). Modified activated carbons for catalytic wet air oxidation of phenol. **Carbon** 43: 2134-2145.

Shin, J. W., Yoo, K. S., Park, S. Y., and Song, K. S. (2006). Characteristics of *n*-hexane adsorption over heat-treated activated carbon. **J. Ind. Eng. Chem.** 12: 418-424.

Smith, M. B. and March, J. (2007). **March's Advanced Organic Chemistry: Reactions, Mechanisms, and Structure.** John Wiley & Sons, Inc.

Soundping, C. (2002). **Surface modification of activated carbon by oxidation reaction for adsorption capacity study of aniline, dyes and chromium(III) ion.** M. thesis, King Mongkut's University of Technology Thonburi, Thailand.

Stavropoulos, G. G., Samaras, P., and Sakellaropoulos, G. P. (2007). Effect of activated carbons modification on porosity, surface structure and phenol adsorption. **J. Hazard. Mater.** In Press, Corrected Proof.

Strelko, V. Jr. and Malik, D. J. (2002). Characterization and metal sorptive properties of oxidized active carbon. **J. Colloid Interface Sci.** 250: 213-220.

Strelko, V. Jr., Malik, D. J., and Streat, M. (2002). Characterisation of the surface of oxidized carbon adsorbents. **Carbon** 40: 95-104.

Tamon, H. and Okazaki, M. (1996). Influence of acidic surface oxides of activated carbon on gas adsorption characteristics. **Carbon** 34: 741-746.

Wibowo, N., Setyadhi, L., Wibowo, D., Setiawan, J., and Ismadji, S. (2007). Adsorption of benzene and toluene from aqueous solutions onto activated carbon and its acid and heat treated forms: Influence of surface chemistry on adsorption. **J. Hazard. Mater.** 146: 237-242.

Xiao, B. (2004). **Characterisation of functionalised nanoporous carbon materials & adsorption of aqueous metal ions.** Ph.D. thesis, University of Newcastle upon Tyne, United Kingdom.

Xiao, B. and Thomas, K. M. (2005). Adsorption of aqueous metal ions on oxygen and nitrogen functionalized nanoporous activated carbons. **Langmuir** 21: 3892-3902.

CHAPTER V

ADSORPTION STUDY OF SURFACE-MODIFIED ACTIVATED CARBON

ABSTRACT

This chapter focuses on the equilibrium adsorption of vapors (water, methanol and ethanol) and heavy metal ions (Pb^{2+}, Zn^{2+}, Cu^{2+}, and Ca^{2+}) on modified activated carbons obtained by oxidation method. In addition, the effects of porous structure and heat treatment process on the variation of surface functional groups and water vapor adsorption were also investigated. The experimental results illustrated that the adsorption of polar molecules with higher polarizability and smaller molecular size (water vapor) depended on both porous structure and surface functional groups of the carbon while the adsorptions of lower polarizability and larger molecular size (methanol and ethanol vapors) depended only on the porous structure of carbons. The amount of water adsorbed was found to increase with carbon having higher surface area and pore volume as well as higher carboxylic acid group. Heat treatment process which decreased the highest amount of carboxylic acid group decreased the amount of water adsorbed. For heavy metal ions adsorption, the uptake for all metal ions increased with the increase in oxygen functional groups on the activated carbon surfaces with the following order $Pb^{2+} > Zn^{2+} > Cu^{2+} > Ca^{2+}$, and Langmuir model was found to describe well the equilibrium adsorption of these ions from solution.

Competitive adsorptions in binary systems decreased the amount of individual metal ions adsorbed with the maximum amount adsorbed follow the order $Pb^{2+} > Zn^{2+} \sim Cu^{2+} >> Ca^{2+}$. The presence of Ca^{2+} in the binary system did not affect the adsorption of the other ion in the solution.

5.1 Introduction

Activated carbons are widely used as adsorbents for adsorbing a wide range of species from both gas and liquid phases. The high adsorption capacity of activated carbons is associated with their well developed porous structure and large internal surface areas. In addition to the physical structure, activated carbons possess a chemical structure as well. The surface chemistry of activated carbons involves both hydrophobic graphene layers and hydrophilic surface functional groups. These properties make activated carbons a versatile adsorbent. That is, organic compounds are largely adsorbed on the hydrophobic graphene layer, whereas other polar species are selectively adsorbed on the hydrophilic functional groups.

Activated carbons are widely applied for the removal of gases and vapors from air. When activated carbons are used to remove toxic species from air containing water vapor, there is a competition between the material to be adsorbed on the activated carbon surface and water vapor in air. Water vapor is known to have an appreciable effect on the adsorption of contaminants from air or gas streams resulting in a decrease in the breakthrough time for the activated carbon bed and is therefore detrimental to the performance of the activated carbon adsorption bed (Foley, Thomas, Forshaw, Stanton, and Norman, 1997). The adsorption of water molecules on activated carbon surface is strongly influenced by the presence of hydrophilic

functional groups which play the role of primary adsorption centers by forming the bonds between the adsorbed molecules and the functional groups, and the uptake of water vapor is thus enhanced by theses functional groups.

Heavy metals are among the most important pollutants in the environment. They are extremely toxic elements, which can seriously affect plants, animals and causing a large number of afflictions (Ricordel, Taha, Cisse, and Dorange, 2001). Chemical precipitation, membrane filtration, ion exchange and electrochemical methods can be used to remove aqueous heavy metal pollutants present in high concentrations. However, the final low concentrations of metal species not being removed by these treatment processes must also be removed, and this can be achieved by adsorption on activated carbons (Xiao and Thomas, 2005). The adsorption process of metal ion species from aqueous solution depends on the surface chemistry of activated carbon, the nature of the chemical interaction between metal ion species and the surface groups, the speciation of the metal ion solution and the adsorption conditions (e.g. pH, temperature, etc). These affecting factors complicate the adsorption of chemical species from aqueous solution. There have been many reports on the modification of activated carbons to enhance the adsorption of aqueous metal species as reviewed in section 4.1 of chapter 4. The most common procedure is chemical oxidation, which can incorporate large quantities of oxygen functional groups on the surface of activated carbon.

Therefore, to study the role of incorporated surface groups by oxidation method, the equilibria adsorption of water vapor, volatile organic compounds (methanol and ethanol vapors) were carried out as well as the adsorption of heavy metal ions (Pb^{2+}, Zn^{2+}, Cu^{2+}, and Ca^{2+}) both in the single component and binary

systems. The three cations, Pb^{2+}, Zn^{2+}, and Cu^{2+}, were selected for the present study because they are typical toxic heavy metal species present in wastewater, whereas Ca^{2+} was chosen because this metal usually contains in hard water and often present in real problem situations as a background ion.

5.2 Apparatus and Methods

5.2.1 Apparatus and chemicals (analytical grade)

1. Intelligent gravimetric analyzer (IGA 002, Hiden Analytical, UK) for adsorption studies

2. Inductively Coupled Plasma (ICP) atomic emission spectrometer (701, Unicam)

3. Water bath (OR, Unitronic)

4. Analytical balance (BP221S, Sartorius)

5. pH meter (CG840, SCHOTT)

6. Lead (II) nitrate ($Pb(NO_3)_2$) 99%

7. Zinc nitrate ($Zn(NO_3)_2.6H_2O$) 99%

8. Copper (II) nitrate ($Cu(NO_3)_2.3H_2O$) 99.6%

9. Calcium nitrate tetrahydrate ($Ca(NO_3)_2.4H_2O$) 99%

10. Methanol (99.9% v/v)

11. Ethanol (99.8% v/v)

5.2.2 Methods

5.2.2.1 Vapor adsorption

Adsorptions of water, methanol, and ethanol vapors were carried out by using an Intelligent Gravimetric Analyzer. This apparatus (Figure 5.1) is fully

computer controlled and measures the amount adsorbed via a microbalance. Prior to the adsorption measurement, the activated carbon sample was first outgassed at 250^{o}C at least for 5 hours until the weight became constant, at a vacuum pressure (75 mmHg). The liquid used to generate the vapor was degassed fully by repeated evacuation of the liquid reservoir. Adsorption of water vapor was studied at 20, 25, and 30^{o}C while the adsorptions of methanol and ethanol vapors were studied at 10, 20, and 30^{o}C. Sample temperature was maintained with the aid of a sample chamber jacket and a temperature control system. Mass uptake was measured as a function of time, and after equilibrium was established, the pressure was increased to the next set value and the uptake was again measured when equilibrium was established. The adsorptions of all three vapors were studied over the relative pressure range from 0 – 0.94.

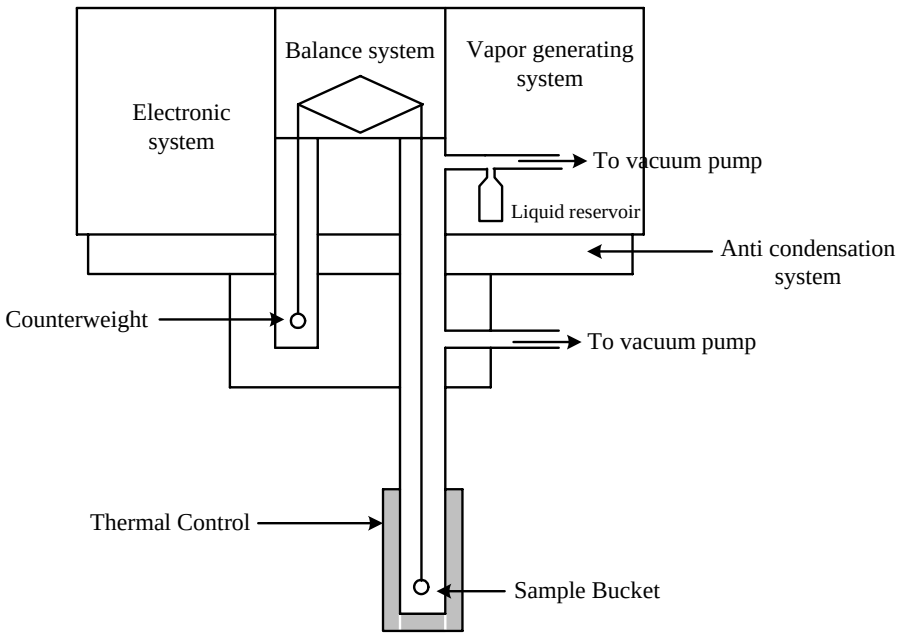

Figure 5.1 Diagrammatic of Intelligent Gravimetric Analyzer for vapor adsorption experiment.

5.2.2.2 Heavy metal ions adsorption

Batch adsorptions of metal cations in aqueous solution by activated carbons were conducted according to the following procedures. Each stock solutions of 10 mM of Pb^{2+}, Zn^{2+}, Cu^{2+}, and Ca^{2+} were prepared from $Pb(NO_3)_2$, $Zn(NO_3)_2.6H_2O$, $Cu(NO_3)_2.3H_2O$, and $Ca(NO_3).4H_2O$, respectively. Aqueous solutions with different concentrations were prepared by diluting the initial stock solution and 0.1 g of carbon sample was added into 50 cm^3 of respective solution. The mixture was shaken and allowed to equilibrate at 30^oC for 72 h without adjusting the pH. This contact time was sufficient to achieve equilibrium in the system (Xiao and Thomas, 2004). The pH values of the solution before and after adsorption were measured. It is noted that the initial pH values were in the range 5.26 – 5.97, 6.79 – 7.05, 5.17 – 5.95, and 6.06 – 6.64 for Pb^{2+}, Zn^{2+}, Cu^{2+}, and Ca^2, respectively. It seems likely that the adsorption experiments were performed in the narrow range of pH for all four metal ions and these pH variation should not greatly affect the adsorption capacities as noted in the previous works (Srivastava, Gupta, and Mohan, 1996; Chen, Wu, and Chong, 2003; Gerçel and Gerçel, 2007; Rao, Rao, Seshaiah, Choudary, and Wang, 2007). The effect of pH on the adsorption is suggested to study in future work.

Competitive adsorption is the usual situation encountered in real applications and therefore the competitive adsorption of binary aqueous metal ions in mixtures of Pb^{2+}/Cu^{2+}, Pb^{2+}/Ca^{2+}, Pb^{2+}/Zn^{2+}, Zn^{2+}/Cu^{2+}, and Cu^{2+}/Ca^{2+} were investigated under the molar ratio of 1:1.

The concentrations of aqueous metal ions in solutions were measured by Inductively Coupled Plasma (ICP) atomic emission spectrometer. The

amount of metal ion retained in the adsorbent phase was estimated by the following mass balance equation,

$$q_e = \frac{(C_o - C_e)V}{W} \tag{5.1}$$

where q_e is the amount of metal ion adsorbed in mmol/g, C_o and C_e are the initial and final equilibrium metal ion concentrations in solution in mM, respectively, V is the solution volume (50 cm^3), and W is the adsorbent weight (0.1 g).

5.3 Results and Discussion

5.3.1 Equilibria of vapor adsorption

5.3.1.1 Vapor adsorption on unmodified activated carbon

This section describes the adsorption characteristic of molecules with different polarities viz., water and alcohol vapors (methanol and ethanol) on unmodified activated carbons and compares the adsorption characteristic of molecule with higher polarity (water vapor; dipole moment = 1.85 Debye) and lower polarity (methanol and ethanol vapors; dipole moment = 1.69 Debye). Two eucalyptus wood-based activated carbons prepared by chemical activation (H_3PO_4 activation) with different porous structure were used in this study. Table 5.1 lists the preparation conditions and porous properties of both carbons. As seen, sample AC1 has high surface area and total pore volume with high proportion of meso- and macropore volume (43%), whereas sample AC gives lower surface area and total pore volume, consisting mainly of micropores (95%).

Table 5.1 Preparation conditions and porous characteristics of unmodified activated carbons used to study the adsorption of water, methanol, and ethanol vapors.

Sample	**Preparation conditions**	S_{BET} **(m^2/g)**	V_{mic} **(cm^3/g)**	$V_{meso+mac}$ **(cm^3/g)**	V_T **(cm^3/g)**	**Average pore width (nm)**
AC1	• chemical weight ratio of H_3PO_4 solution and wood 1.5:1 • impregnation time 1.5 hrs • carbonization temperature 400^oC for 1 hour	1857	0.70 (57%)	0.52 (43%)	1.22	2.63
AC	• chemical weight ratio of H_3PO_4 solution and wood 0.5:1 • impregnation time 1 hour • carbonization temperature 400^oC for 1 hour	1200	0.55 (95%)	0.03 (5%)	0.58	1.93

A widely accepted generalization of the mechanism of water adsorption includes the following consecutive steps (Brennan, Bandosz, Thomson, Gubbins, 2001): (1) the adsorption of water on surface functional groups; (2) the adsorption of water on previously adsorbed water molecules and subsequent cluster formation via hydrogen bonds; and (3) pore filling by growing clusters. In principle,

the adsorption should occur first in micropores at low pressure, mainly due to the stronger interaction forces induced by the narrow pore walls, then adsorption will proceed into the larger pores at a higher pressure once the micropores are completely filled with an adsorbate (Rouquerol, Rouquerol, and Sing, 1999). The surface functional groups of both carbons were determined by Boehm titration and presented in Table 5.2. The results showed that sample AC1 has higher acidic oxygen functional groups than sample AC. Both carbons show the same distribution of acid group concentration in the following order: lactonic > phenolic > carboxylic.

Table 5.2 Surface functional groups of unmodified activated carbons obtained from Boehm titration.

Sample	**Acidic group (mmol/g)**				**Basic group (mmol/g)**
	Carboxylic	**Lactonic**	**Phenolic**	**Total**	
AC1	0.28 (12%)	1.25 (54%)	0.77 (34%)	2.30	0.30
AC	0.06 (9%)	0.43 (65%)	0.17 (26%)	0.66	0.63

Figure 5.2 (a) and (b) show the water vapor adsorption and desorption isotherms at 20 – 30^{o}C of sample AC1 and sample AC, respectively. For sample AC1, the isotherms are of Type V whereas the isotherms of sample AC are Type III (S-shaped) according to the IUPAC classification (Patrick, 1995). Significant hysteresis is observed for sample AC1 (typical character of a mesoporous adsorbent)

but sample AC does not exhibit hysteresis (the desorption branch approximately coincide with the adsorption branch).

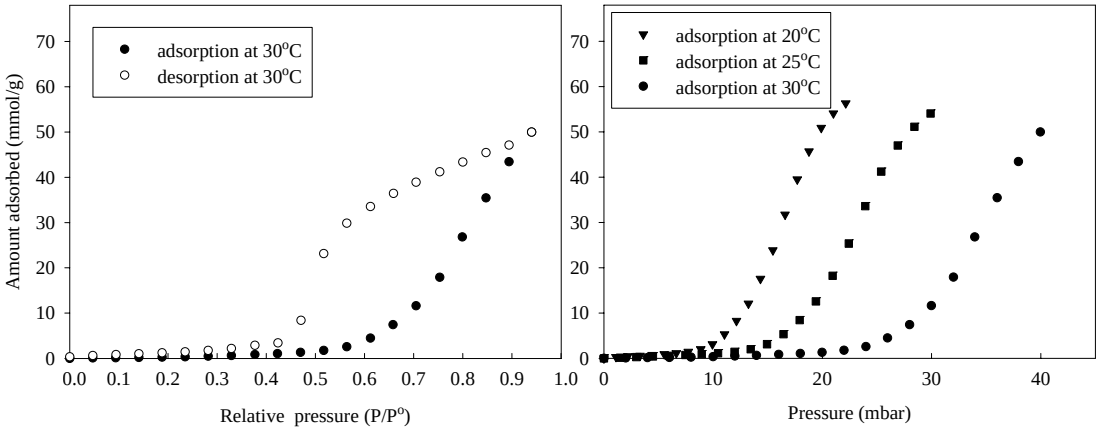

(a) AC1

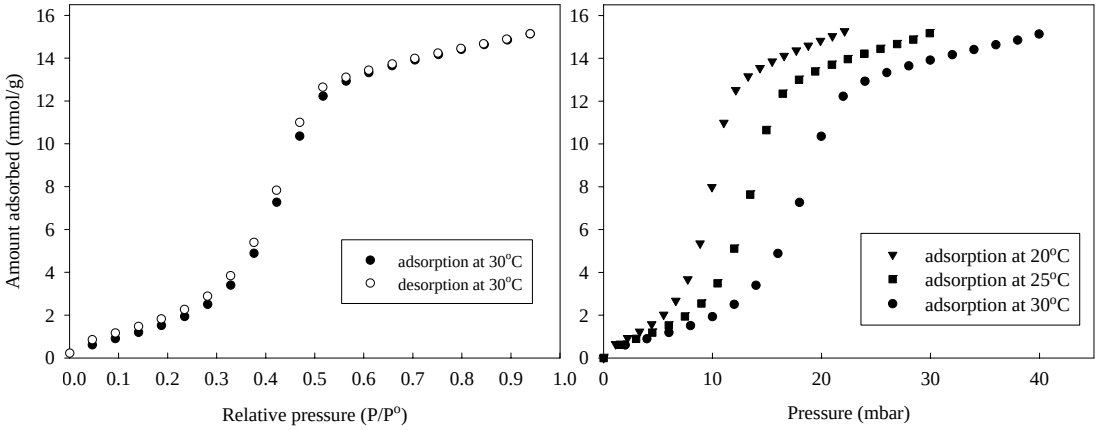

(b) AC

Figure 5.2 Water vapor adsorption-desorption isotherms at 20 – 30°C of (a) sample AC1 and (b) sample AC.

The water adsorption isotherm of sample AC1 (Figure 5.2 (a)) shows low adsorbed amount for low range of relative pressures ($P/P^o < 0.5$) followed by a rapid rise in the adsorbed amount at higher pressures ($P/P^o > 0.5$). Three regions of isotherm curve can be observed for sample AC: the adsorbed amount increases almost linearly with increasing relative pressure up to $P/P^o = 0.3$ (region I). In the range of relative pressure $P/P^o = 0.3 – 0.5$, a marked increasing of the amount adsorbed (region II), and region III showing a linear increase of adsorbed amount for $P/P^o > 0.7$ with approximately the same slope as region I.

The hysteresis exists as the result of differences in pore filling (adsorption) and emptying (desorption) mechanisms. The pore emptying involves the removal of adsorbed molecules that form a stable phase in pores which would be a more liquid-like phase in the central layer as the pore width is increased. Therefore, the desorption process in large pores is difficult to remove from the adsorbed phase (Rouquerol, Rouquerol, and Sing, 1999). As a result, the size of adsorption hysteresis will depend on the pore width. As mentioned above, sample AC1 has high meso- and macropore volume with average pore width of 2.63 nm (Table 5.1). Therefore, remarkable hysteresis loop is observed with sample AC1. On the other hand, sample AC contains mainly micropore volume with smaller average pore width of 1.93 nm, and thus this carbon does not show the hysteresis loop.

For both samples, water uptake appears to decrease with increasing in adsorption temperature. This is reasonable since the increasing of temperature tends to weaken the intermolecular force of hydrogen bonds between water–water molecules. Therefore, adsorption at higher temperatures will lead to the lower amount of water adsorbed.

In order to obtain a clearer comparison between water vapor adsorption isotherms of both samples, only the adsorption branches are re-plotted and shown in Figure 5.3 at various temperatures. It can be observed from Figure 5.3 that the adsorbed amount of AC with lower surface area and pore volume is somewhat higher than that of AC1 at the relative pressure $P/P^o < 0.58$, $P/P^o < 0.6$, and $P/P^o < 0.7$ for adsorption temperature of 20^{o}C, 25^{o}C, and 30^{o}C, respectively. At higher values of these relative pressures, the crossing of isotherm curves can be observed with those of AC1 being on top of AC curves.

For sample AC, over the relative pressure $P/P^o \sim 0 – 0.5$, water is first adsorbed on surface oxygen functional groups followed by adsorption of water–water molecules via hydrogen bonds and the increase in relative pressure results in more water adsorbed. At $P/P^o > 0.5$, where the functional groups are totally used and the pores (micropore in this case) are completely filled so that a plateau of amount of water adsorbed can be observed. For sample AC1, the amount of water adsorbed increased continuously with increasing relative pressure. The low adsorped amount at low relative pressures ($P/P^o < 0.5$) is attributed to the adsorption in micropores whereas the rapid rise in the amount adsorbed at $P/P^o > 0.5$ is probably due to the adsorption in mesopores and macropores, where larger pore sizes are capable of accommodating larger amounts of adsorbate. Although sample AC1 has higher micropore volume and total surface functional groups, sample AC1 adsorbs lesser amount of water than sample AC over the relative pressure up to 0.5. It is likely that the distribution of functional groups in micropore of sample AC1 is much less than that of sample AC. In other words, active surface functional groups of AC1 probably

concentrated more in the larger pore sizes. This behavior could be affected by the preparation conditions of activated carbon, the mechanism of which is not yet known.

As shown in Figure 5.3 (d) the water adsorption isotherms of sample AC at various temperatures fall on top of one another on a relative pressure basis whereas on the same plot the isotherms of sample AC1 shifts systematically toward higher relative pressure as the temperature is increased.

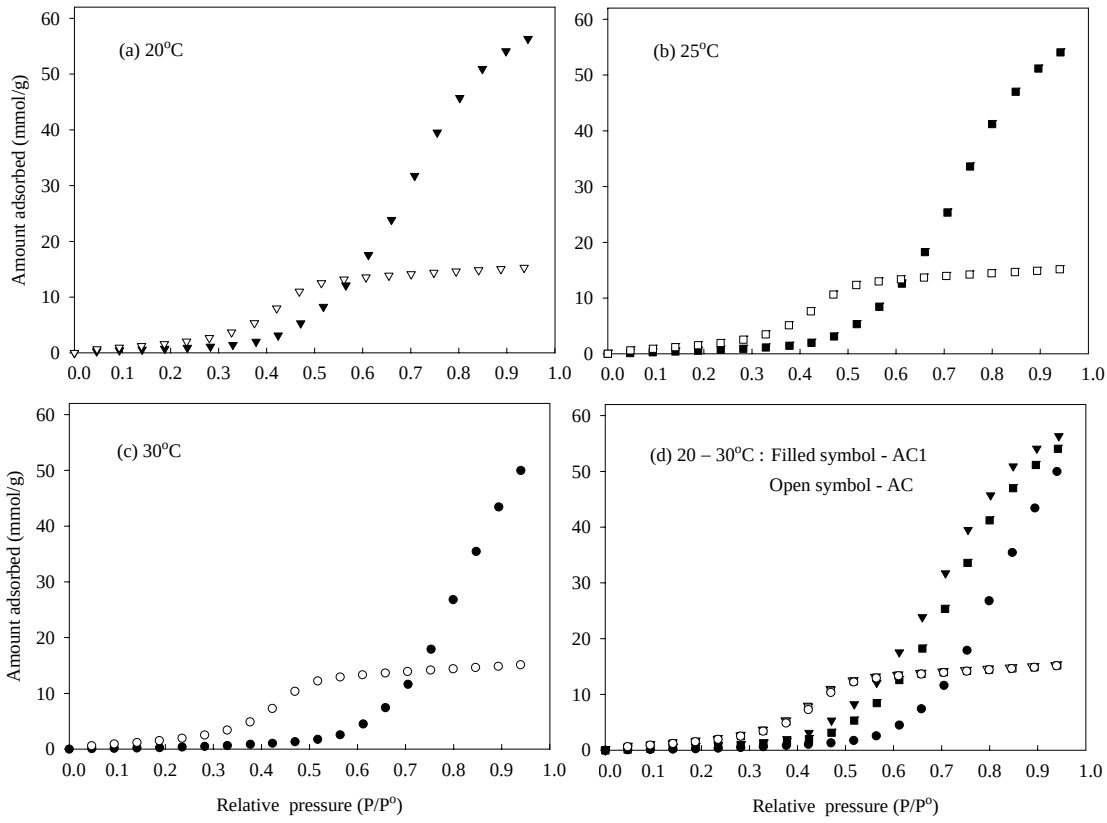

Figure 5.3 Comparison of water vapor adsorption isotherms between sample AC1 and sample AC at (a) 20°C, (b) 25°C, (c) 30°C, and (d) 20 – 30°C.

Several isotherm models for water adsorption on activated carbons have been proposed. One of the well-known models to explain the mechanism of water adsorption on carbonaceous materials is due to Dubinin and Serpinsky (DS) (Dubinin and Serpinsky, 1981). Although the fundamental assumptions of the model were introduced almost fifty years ago, it is still widely applied due to its simplicity and giving reliable results. This phenomenological model treats the adsorption of water molecules to start from specific energy sites which acts as primary adsorption centers for water attachment on predominantly hydrophobic carbon surface. Water molecules adsorbed on these sites further create some new centers, called secondary centers, for adsorption of the subsequent molecules via the cluster formation. The original DS equation can be written as,

$$C_{\mu} = c(C_{\mu o} + C_{\mu})x \qquad (5.2)$$

where C_{μ} is the water adsorbed amount, $C_{\mu o}$ is the concentration of the primary sites, c is the ratio of the rate constants describing the kinetics of adsorption and desorption (k_{ads}/k_{des}), and x is the relative pressure (P/P^{o}). It is well known that this original equation describes well only the data measured on non-porous adsorbents and on strongly hydrophobic carbons. Therefore, the main disadvantage of this simple model is the assumption of unlimited adsorption space or the lack of saturation of secondary adsorption centers. The applicability of this original DS model is limited to the hyperbolic behavior of the adsorption isotherms i.e. the water adsorption generated on the basis of this equation leads to infinity if the relative pressure tends to $1/c$. With this limitation, the original DS concept was later improved by Dubinin and co-worker (Dubinin and Serpinsky, 1981). The initial stages of water adsorption mechanism on

carbonaceous solids are similar to that assumed in the original DS equation i.e. water molecules are initially strongly adsorbed via hydrogen bonding on surface sites considered as specific or active groups (oxygen groups). However, the further adsorption causes the creation of water clusters at larger relative pressures and this process decreases the number of secondary adsorption sites (taking limited adsorption space or pore volume). Thus, Dubinin and Serpinsky (1981) proposed the following equation:

$$C_{\mu} = c(C_{\mu o} + C_{\mu})(1 - k\,C_{\mu})x \tag{5.3}$$

where k represents the loss of the secondary sites in the course of adsorption due to the finiteness of the adsorption volume and thus this constant value affects the maximum adsorption capacity. This equation is a quadratic equation in terms of C_{μ} and it can be solved to obtain C_{μ} explicitly as

$$C_{\mu} = \frac{-\frac{1}{k}\left(\frac{1}{cx} + kC_{\mu o} - 1\right) + \sqrt{\frac{1}{k^2}\left(\frac{1}{cx} + kC_{\mu o} - 1\right)^2 + \frac{4C_{\mu o}}{k}}}{2} \tag{5.4}$$

The basic quantity derived using this model is the number of primary adsorption sites ($C_{\mu o}$) which can be easily determined by fitting the experimental data to the proposed isotherm. Therefore, the DS equation was first adopted in this section to check the model validity in predicting the water isotherms. Figure 5.4 shows the fitting of the DS model to the water vapor adsorption isotherms of both activated carbon samples. The model parameters are given in Table 5.3 and the results of total acidic oxygen functional groups from Boehm titration were also

given in this table for comparison. According to the results, DS model can fit the isotherm of sample AC1 better than sample AC. The concentrations of primary sites ($C_{\mu o}$) or surface oxygen groups predicted from this model show the lower and higher values than the concentration of functional groups determined from Boehm titration for sample AC1 and sample AC, respectively.

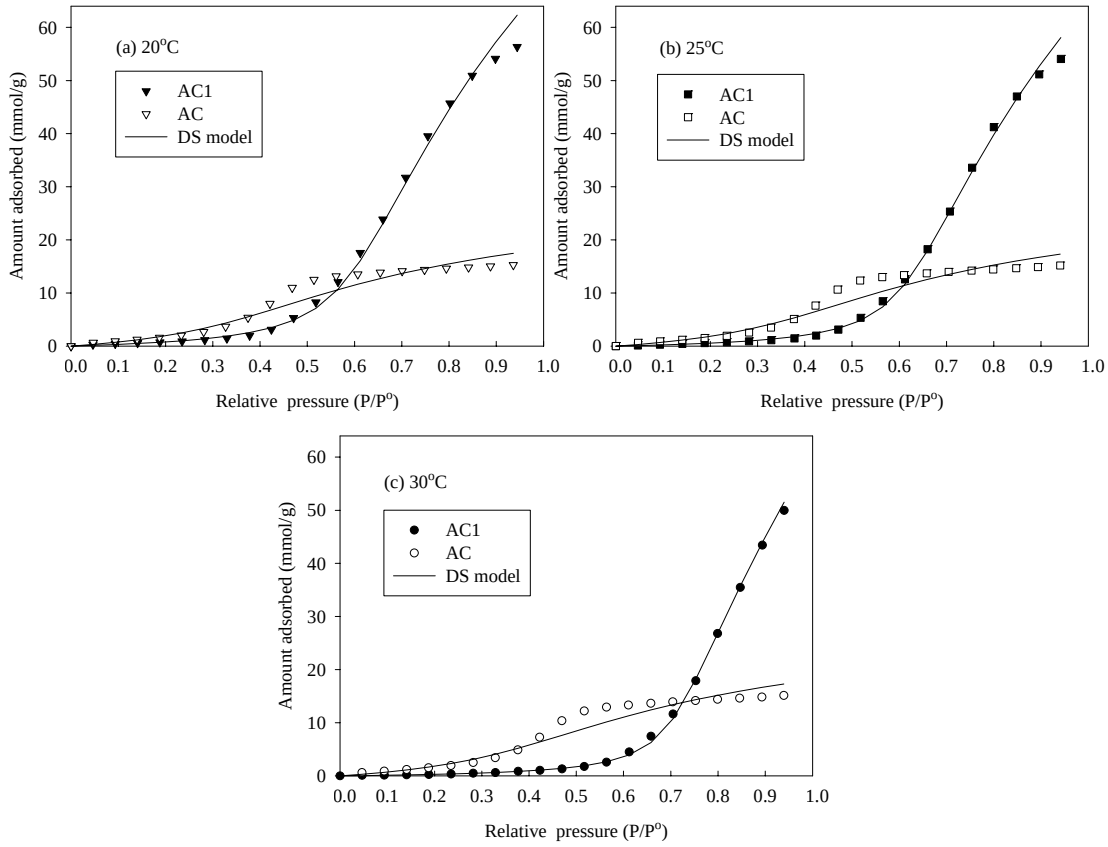

Figure 5.4 Fitting of the Dubinin-Serpinsky (DS) model to the water vapor adsorption isotherms of unmodified activated carbons at (a) 20°C, (b) 25°C, and (c) 30°C.

Table 5.3 Parameters obtained from Dubinin-Serpinsky (DS) equation of unmodified activated carbons and amount of total acidic oxygen functional groups from Boehm titration.

Sample	DS model parameters				Total acidic group from Boehm titration (mmol/g)
	$C_{\mu o}$ (mmol/g)	k (g/mmol)	c	R^2	
AC1					2.30
20°C	1.63	0.006	1.64	0.995	
25°C	1.21	0.006	1.59	0.997	
30°C	0.75	0.005	1.40	0.999	
AC					0.66
20°C	2.96	0.032	2.11	0.937	
25°C	2.84	0.032	2.09	0.936	
30°C	2.91	0.032	2.04	0.936	

Do and Do (2000) have proposed another water adsorption model which is more flexible in dealing with different shapes of water isotherm curves of carbonaceous materials. In this model, at the first stage, water molecules are first bonded to the primary adsorption sites and form conglomerates of molecules via hydrogen bonds. If the number of molecules is equal to six, the conglomerate of five molecules (pentamer) can tear away from the cluster and filled in the micropores.

Thus, the Do and Do model can be considered as the so called “hybrid”, one in which the first term describes the adsorption on the primary sites and the second term accounts for the desorption from these sites followed by the adsorption of the pentamer into the micropores, thus this term describes the micropore filling. The final form of the adsorption isotherm equation is

$$C_{\mu} = S_{o} \frac{K_{f} \sum_{n=1} n x^{n}}{1 + K_{f} \sum_{n=1} x^{n}} + C_{\mu s} \frac{K_{\mu} \sum_{n=6} x^{n}}{K_{\mu} \sum_{n=6} x^{n} + \sum_{n=6} x^{n-5}} \tag{5.5}$$

where C_{μ} is the water adsorbed concentration, S_o is the concentration of surface active groups, $C_{\mu s}$ is the saturation concentration in the micropore, K_f is the chemisorption equilibrium constant, K_{μ} is the micropore equilibrium constant, n is the number of water molecules in a cluster taken as 5, and x is the relative pressure (P/P^{o}). This model is able to describe most of water adsorption behaviors of non-polar surface activated carbon as well as highly oxidized activated carbon.

Fitting of Do and Do model, as shown in Figure 5.5 , shows that this model provides better description of isotherm data than DS model for sample AC. However, this model fails to fit the isotherms of sample AC1 at the relative pressure higher than 0.66 for all three temperatures. The fitted parameters shown in Table 5.4 demonstrates that the concentrations of functional group (S_o) predicted from this model show the same trend as those obtained from DS model viz., lower value than the concentration of functional groups determined from Boehm titration for AC1 and higher value for AC. The saturation concentration in the micropore values ($C_{\mu s}$) are reasonable for sample AC while these values exceed the adsorbed amount obtained from experimental data for sample AC1.

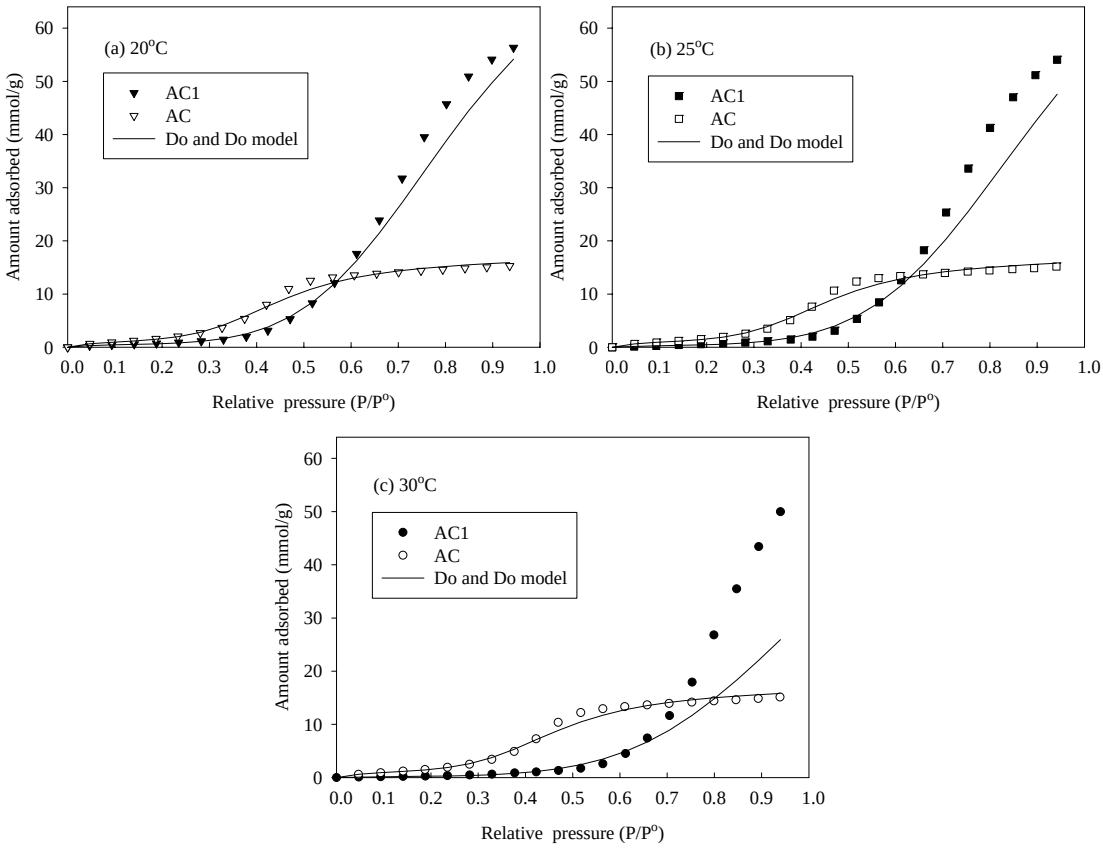

Figure 5.5 Fitting of the Do and Do model to the water vapor adsorption isotherms of unmodified activated carbons at (a) 20°C, (b) 25°C, and (c) 30°C.

Table 5.4 Parameters obtained from Do and Do model of unmodified activated carbons and amount of total acidic oxygen functional groups from Boehm titration.

Sample	Do and Do model parameters					Total acidic group from Boehm titration (mmol/g)
	S_o (mmol/g)	K_f	$C_{\mu s}$ (mmol/g)	K_μ	R^2	
AC1						2.30
20°C	0.59	19.64	77.25	2.83	0.975	
25°C	0.54	7.76	82.14	1.72	0.973	
30°C	0.29	7.45	67.86	0.80	0.962	
AC						0.66
20°C	1.34	17.72	12.43	61.01	0.987	
25°C	1.28	17.75	12.46	55.40	0.986	
30°C	1.31	16.63	12.42	51.29	0.986	

Recent work of Junpirom (2006) suggested that the number of water molecules in the cluster (n) in the original Do and Do model can be adjusted from five to an arbitrary number to cover the adsorption that occurs in the mesopore and macropore size range. They suggested that the increasing of cluster size for high relative pressure range, where the adsorption taking place in the mesopore and macropore, is the result of the lower interaction energy of solid surface and adsorbate

molecules in mesopore as compared to that in the micropore. This model was referred to as "modified Do and Do model". Therefore, for the present work, the ranges of relative pressure (P/P^o) of sample AC1 are estimated and divided into two regions based on the adsorption into micropore (pore size ≤ 20 Å) and meso- and macropore (pore size > 20 Å) by using volumetric amount of water adsorbed corresponding to the volume of various pore sizes (obtained from density functional theory (DFT)) and Table 5.5 shows the results of isotherm at 20°C. Further, this modified model was also applied to adsorption isotherms at 25°C and 30°C. It is noted that the amount of water adsorbed is slightly lower than pore volume obtained from nitrogen adsorption at –196°C. Lower values for the water vapor pore volume compared with N_2 pore volume have been reported in previous studies (Foley et al., 1997; Fletcher, Yüzak, Thomas, 2006).

Table 5.5 Estimated relative pressure range from volumetric amount of water adsorbed corresponding to volume of various pore sizes for sample AC1 at 20°C.

Pore zize	**Pore volume from DFT (cm^3/g)**	**Amount of water adsorbed (cm^3/g)**	**P/P^o of water isotherm**
≤ 20 Å (micropore)	0.51	0.48	0 – 0.66
> 20 Å (meso- and macropore)	0.56	0.53	0.66 – 0.94

Figure 5.6 shows the fitting of this modified Do and Do model with the cluster size (n) being determined by a trial and error search procedure to give the best fit between experimental data and data predicted by the model and Table 5.6 gives the model parameters. The results show that this modified model can fit the experimental data well for relative pressure range $P/P^o > 0.66$ for all three adsorption temperatures. It can be seen from Table 5.6 that the cluster size (n) is higher than 5 at $P/P^o > 0.66$ for all adsorption temperatures, which represent the adsorption in meso- and macropore, and the cluster size shows a decrease with the increase in temperature. These results primarily confirm that the cluster size in larger pores should be greater than 5 and the increasing of temperature tends to decrease the intermolecular force of hydrogen bonds between water–water molecules resulting in the decrease of water uptake with increasing temperature as discussed before. The total values of S_o for both micopores and larger pores predicted from this modified model are closer to the values obtained from Boehm titration than the original Do and Do model for all three temperatures. The saturation concentration in the micropore values ($C_{\mu s}$) are not reasonable, exceeding the adsorbed amount obtained from experimental data for $P/P^o \leq 0.66$. However, for $P/P^o > 0.66$, this modified model gives reasonable values of $C_{\mu s}$ lying in the range of adsorbed amount obtained from experimental data.

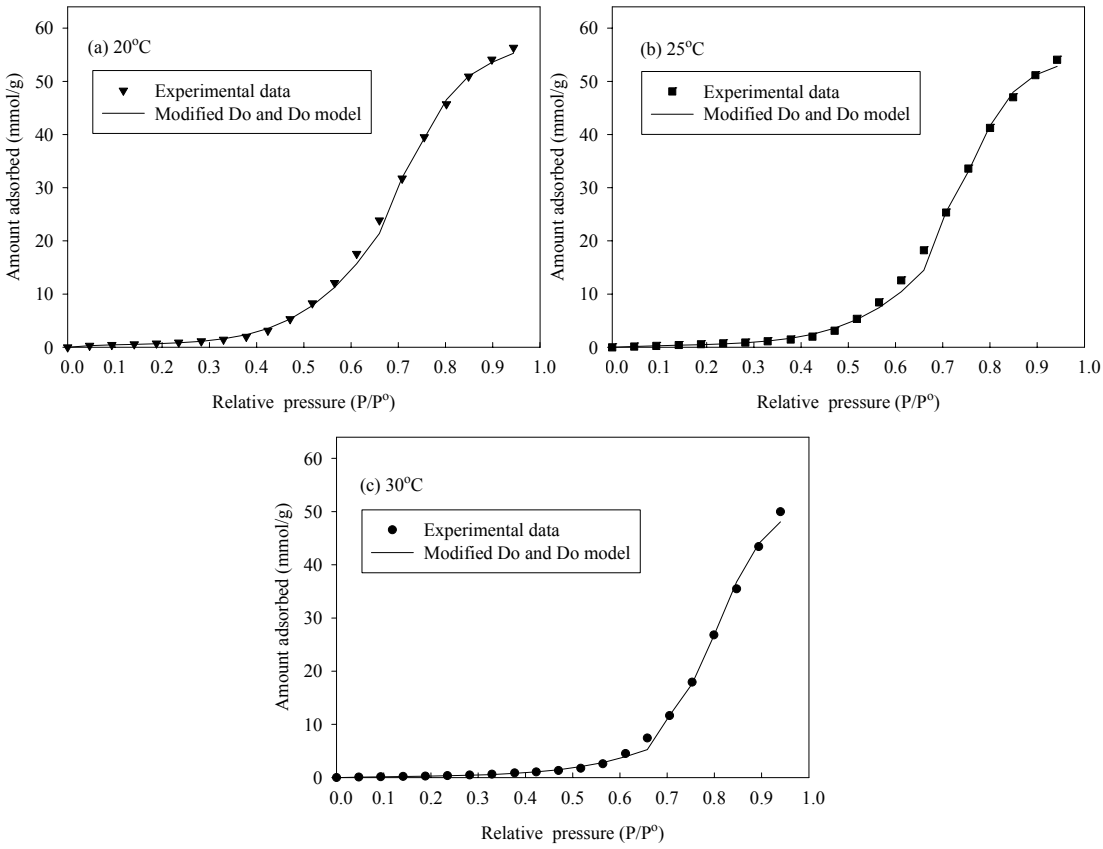

Figure 5.6 Fitting of the modified Do and Do model to the water vapor adsorption isotherms for sample AC1 at (a) 20°C, (b) 25°C, and (c) 30°C.

Table 5.6 Parameters obtained from the modified Do and Do model for sample AC1 and amount of total acidic oxygen functional groups from Boehm titration.

Adsorption temperature	Modified Do and Do model parameters						Total acidic group from Boehm titration (mmol/g)
	S_o (mmol/g)	K_f	$C_{\mu s}$ (mmol/g)	K_μ	n	R^2	
20°C							2.30
$P/P^o \leq 0.66$	0.64	16.68	130.61	1.44	5	0.998	
$P/P^o > 0.66$	0.87	12.56	24.26	270.55	20	0.996	
25°C							
$P/P^o \leq 0.66$	0.69	5.37	195.83	0.57	5	0.992	
$P/P^o > 0.66$	0.45	47.62	31.84	111.95	18	0.995	
30°C							
$P/P^o \leq 0.66$	0.47	3.39	78.28	0.48	5	0.958	
$P/P^o > 0.66$	0.04	24.55	44.30	27.37	16	0.995	

One of the basic quantities in adsorption studies is the isosteric heat of adsorption, Q_{st}, which can be calculated from the van't Hoff equation (Do, 1998). The integrated form of this equation is,

$$(\ln P)_n = \frac{-Q_{st}}{RT} + C \tag{5.6}$$

where P, T, R, and C are the pressure, temperature, universal gas constant (8.314×10^{-3} J/mol K), and integration constant, respectively. The plot of ln P versus 1/T at a given amount adsorbed (n) from the isotherms for a series of adsorption temperatures should

give a straight line from which Q_{st} can be estimated from the slope of the line. The isosteric heat of adsorption for water vapor of sample AC is shown in Figure 5.7 as a function of amount adsorbed. Almost all Q_{st} values in the whole range of amount adsorbed are greater than the heat of condensation of water vapor (45.05 kJ/mol), as shown by a dash line. The values obtained are in the range 45.0 – 52.9 kJ/mol and these values are close to the heat of condensation which support the likely interaction between water–water molecules. Kimura et al. (2004) suggested that surface functional groups should raise the Q_{st} values higher than heat of condensation.

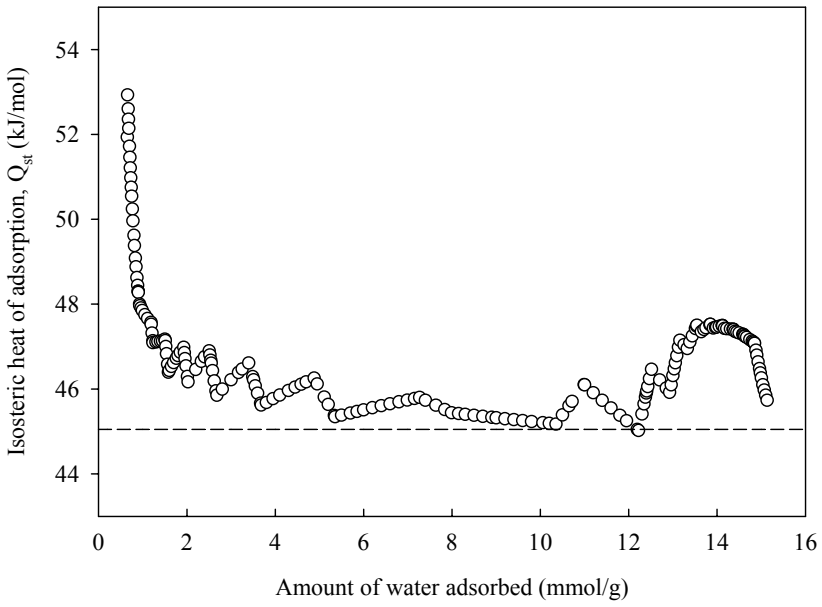

Figure 5.7 Isosteric heat of water vapor adsorption with relative pressure of sample AC.

Adsorption and desorption isotherms of methanol vapor at 10 – 30^{o}C of sample AC1 and sample AC are shown in Figure 5.8 (a) and Figure 5.8 (b), respectively. In order to compare the effect of porous structure on the adsorption, the isotherms were re-plotted and shown in Figure 5.9. Adsorption isotherms for sample AC1 show Type II isotherm, typical adsorption in meso- and macropore whereas isotherms of sample AC give Type I, a characteristic of adsorption in micropore, with both samples not showing hystereses. For sample AC1, the methanol uptake rises continuously with increasing relative pressure whereas sample AC shows a rapid increase over the low relative pressures from 0 to 0.2 and approach a constant value at higher relative pressures. Methanol uptake shows a decrease with increasing in the temperature for both samples as expected for physical adsorption with relatively weak van der Waals forces. Figure 5.9 indicates that the amount adsorbed of sample AC are slightly higher than those of sample AC1 for the low relative pressure range ($P/P^{o} <$ 0.1) but the uptake becomes less at higher relative pressures. In addition, sample AC shows much lower maximum uptake (8 mmol/g) than sample AC1 (26 mmol/g). This is obviously due to the lower surface area and total pore volume which limits the adsorption capacity of sample AC.

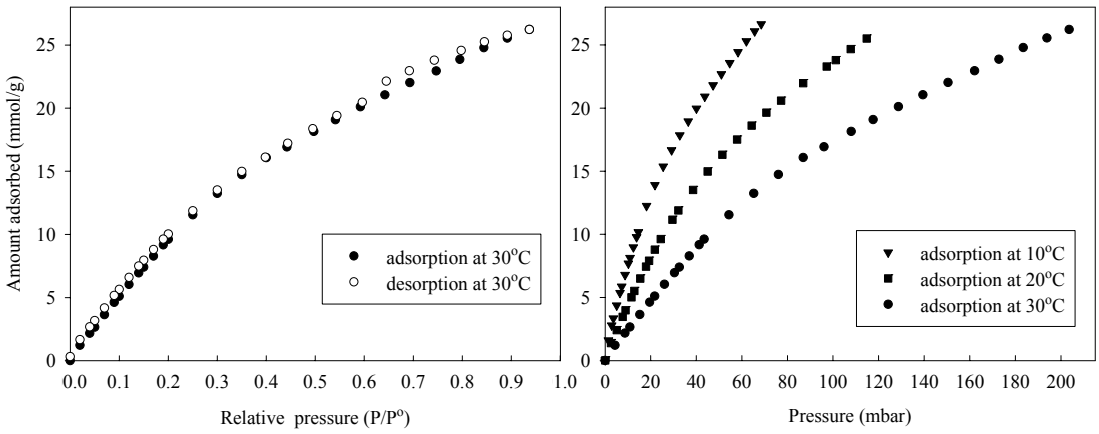

(a) AC1

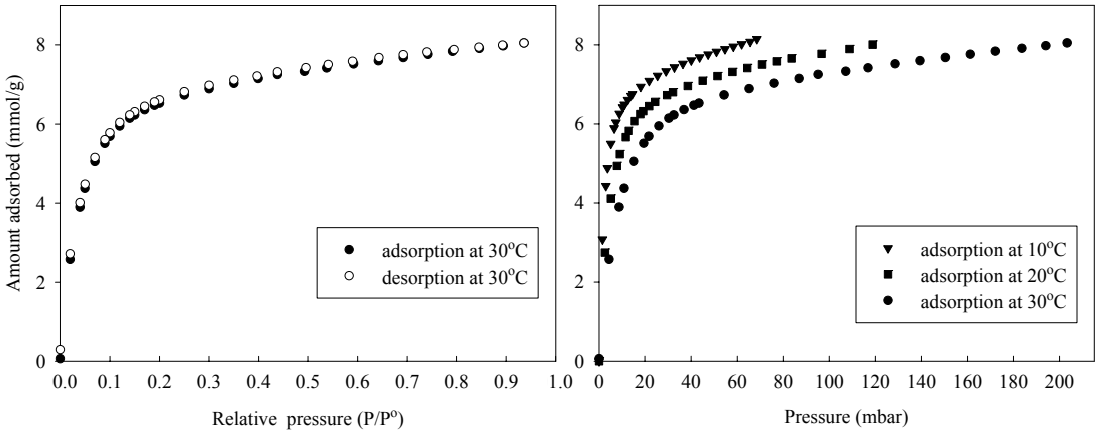

(b) AC

Figure 5.8 Methanol vapor adsorption-desorption isotherms at 10 – 30°C of (a) sample AC1 and (b) sample AC.

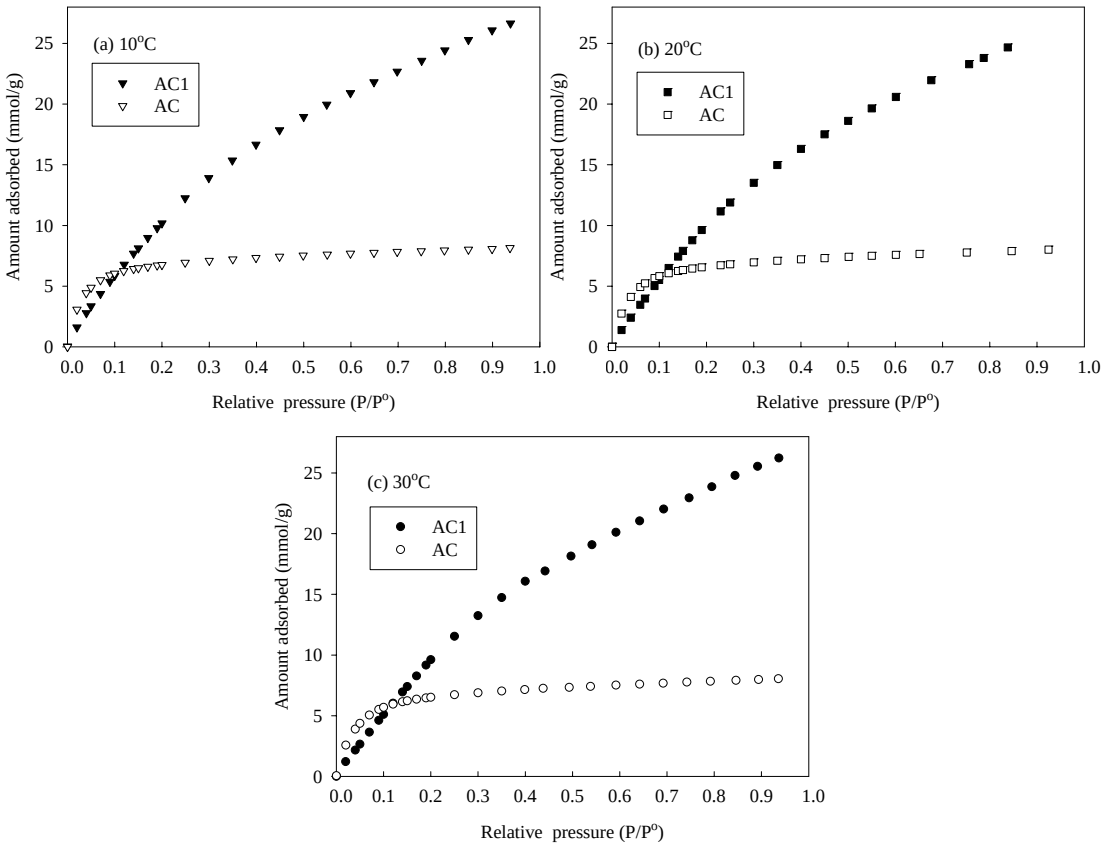

Figure 5.9 Comparison of methanol vapor adsorption isotherms between sample AC1 and sample AC at (a) 10°C, (b) 20°C, and (c) 30°C.

Ethanol adsorption and desorption isotherms at 10 – 30°C of sample AC1 and sample AC are presented in Figure 5.10 (a) and Figure 5.10 (b), respectively, and Figure 5.11 compares the isotherms of the two carbon samples. Again, for sample AC1, the adsorption isotherms of ethanol are Type II whereas isotherms of sample AC are Type I with both samples showing small hysteresis. The isotherms show the hysteresis which extends to very low relative pressure. This behavior was also observed by Gales, Mendes, and Costa (2000) who studied the ethanol adsorption on activated carbon. They reported that the relationship between micropore size and shape and adsorptive molecular diameter seems to be the reason

for this abnormal behavior. The ethanol isotherm shows similar characteristic with methanol isotherm viz., the ethanol uptake increased continuously with increasing relative pressure for sample AC1 and the ethanol uptake increases sharply at low narrow range of relative pressure (0 to 0.2) before attending a plateau region at higher pressures for sample AC. As with methanol adsorption, ethanol uptake also decreases with increasing of temperature for both samples, as expected for physical adsorption. As Figure 5.11 shows, both samples adsorb the same amount of ethanol in the relative pressure range of 0 – 0.1. At higher relative pressures, sample AC1 shows much higher adsorbed amount than sample AC with the former and the latter giving maximum uptakes of 18 mmol/g and 5.5 mmol/g, respectively.

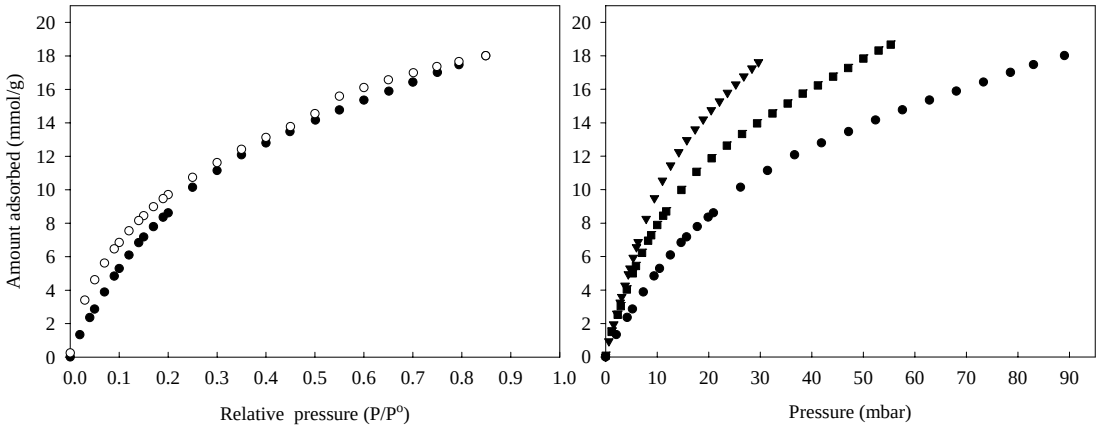

(a) AC1

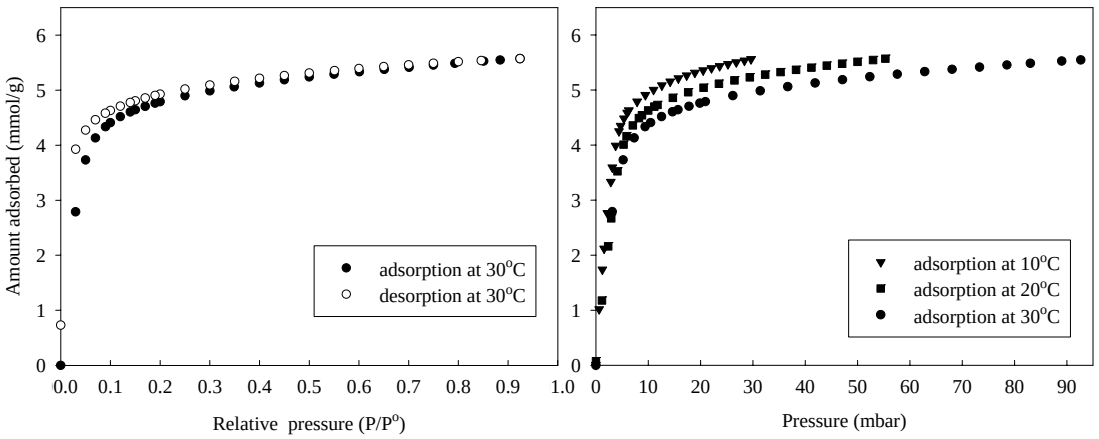

(b) AC

Figure 5.10 Ethanol vapor adsorption-desorption isotherms at 10 – 30°C of (a) sample AC1 and (b) sample AC.

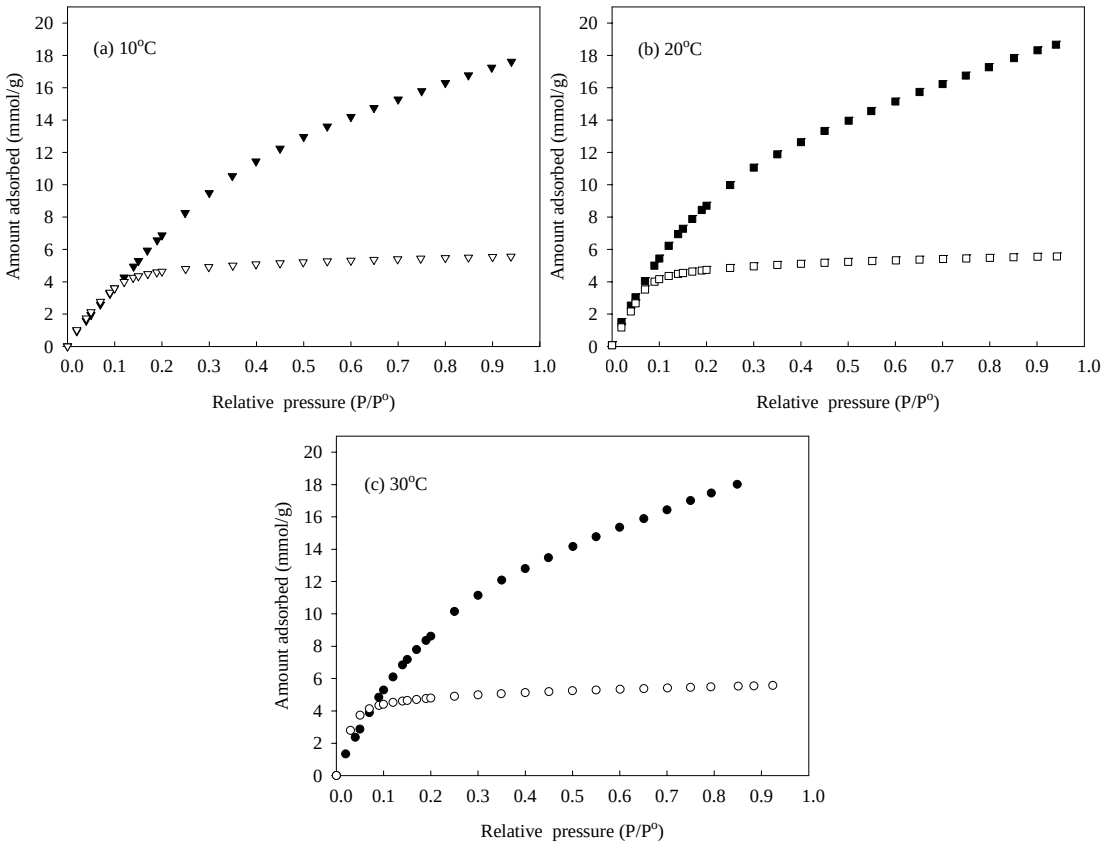

Figure 5.11 Comparison of ethanol vapor adsorption isotherms between sample AC1 and sample AC at (a) 10°C, (b) 20°C, and (c) 30°C.

Isosteric heat of adsorption for methanol and ethanol vapors of sample AC are shown in Figure 5.12. The Q_{st} values for both vapors show different pattern viz., Q_{st} of methanol tends to decrease with increased amount adsorbed whereas Q_{st} of ethanol gives the opposite trend. The values obtained for methanol and ethanol vary in the range 41.8 – 50.6 kJ/mol and 28.8 – 41.6 kJ/mol, respectively. The corresponding values for the heat of condensation of methanol and ethanol are 35.2 and 38.6 kJ/mol (dash line), respectively. Sun and Satyapal (1999, quoted in Salame and Bandosz, 2000) reported the heat of methanol adsorption on activated carbons is equal to about 55 kJ/mol which is higher than its heat of condensation.

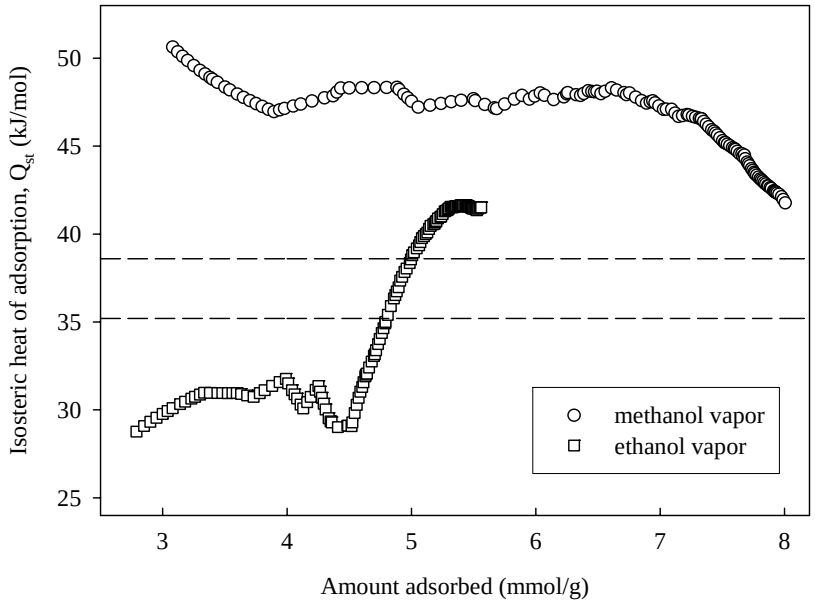

Figure 5.12 Isosteric heat of methanol and ethanol vapors adsorption with amount adsorbed of sample AC.

Adsorption isotherms of all three vapors are compared in Figure 5.13. For both carbon samples, the maximum uptake (amount adsorbed at $P/P^o = 0.9$) increases in the order water > methanol > ethanol. This behavior may be attributed to the difference in adsorption mechanisms of these vapors viz., water molecules can adsorbed first at available active sites (surface functional groups) followed by self-adsorption with stronger hydrogen bonds particularly at high pressures where the adsorption takes place in larger pores, giving high adsorption capacity. For the case of methanol and ethanol molecules, being less polar than water, they will adsorbs more on hydrophobic part of the surface which constitutes the micropores but self-adsorption in larger pores is much less because of the lower polarity. The lower amount adsorbed of ethanol compared to methanol could be due to the larger size of

ethanol molecule than methanol molecule, as shown in Figure 5.14, which could create the hindrance effect among the adsorbed molecules.

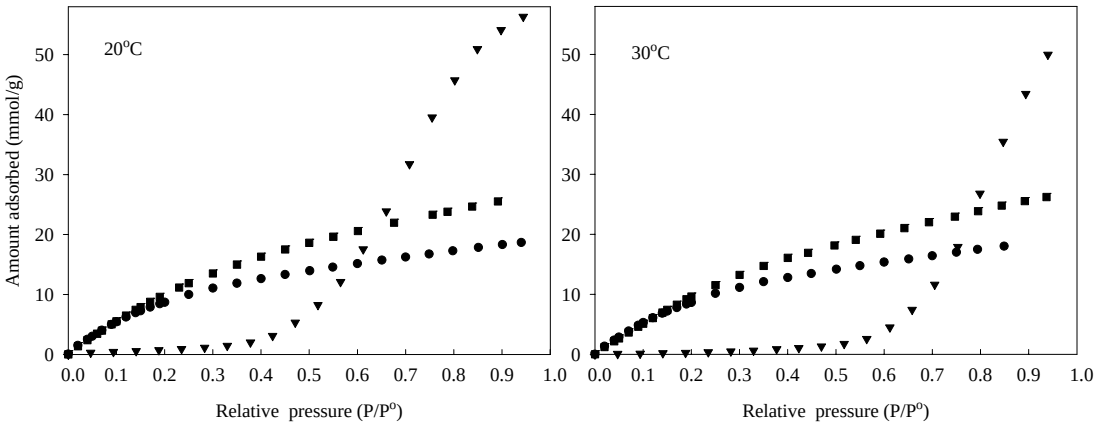

(a) AC1

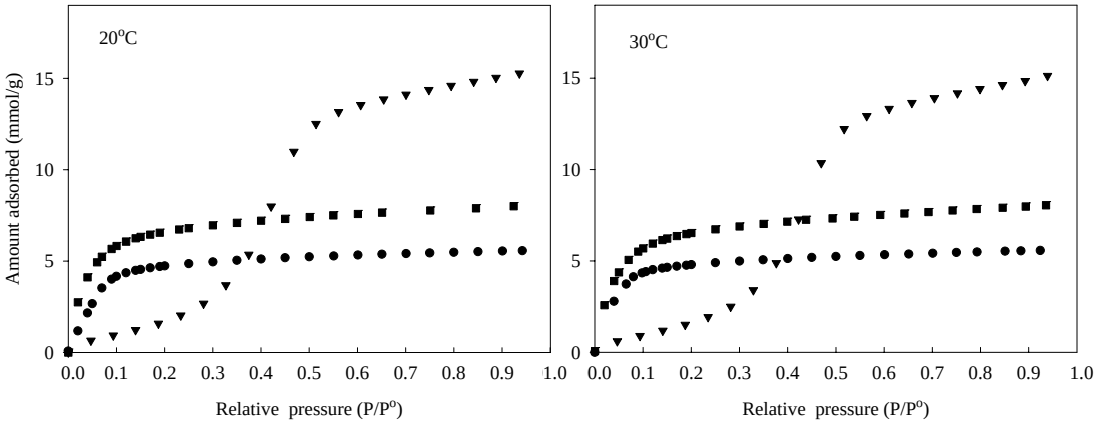

(b) AC

Figure 5.13 Comparison of water, methanol, and ethanol vapor adsorption isotherms at 20 and 30°C of (a) sample AC1 and (b) sample AC.

(a) methanol (b) ethanol

Figure 5.14 Chemical structure of (a) methanol and (b) ethanol.

5.3.1.2 Vapor adsorption on modified activated carbon

Eucalyptus wood-based activated carbons prepared by physical and chemical activations were used in this section to study the effect of surface functional groups on vapor adsorptions of water, methanol, and ethanol. The activated carbon prepared by physical activation was also selected to study the effect of heat treatment process on the adsorption of water vapor.

Three original activated carbons prepared by CO_2 activation (AC600, AC800, and AC900) and one original activated carbon prepared by H_3PO_4 activation were used. The three original carbons from CO_2 activation were oxidized with 1, 5, and 10 M HNO_3 by boiling in a reflux condenser for 24 hours for AC600, AC800, and AC900, respectively. The oxidized samples were designated as AC600-HNO_3 re 1M 24h, AC800-HNO_3 re 5M 24h, and AC900-HNO_3 re 10M 24h. The amount of surface functional groups and porous properties of these carbons are shown in Table 5.7.

Table 5.7 Porous properties and surface functional groups of original and oxidized activated carbons prepared by CO_2 activation (the value in square bracket [ ] is the percentage changes of functional groups with reference to the original carbon, where "+" denotes % increasing and "–" denotes % decreasing).

Sample	S_{BET} (m^2/g)	V_{mic} (cm^3/g)	$V_{meso+macro}$ (cm^3/g)	V_T (cm^3/g)	Acidic group (mmol/g)				Basic group (mmol/g)
					Carboxylic	Lactonic	Phenolic	Total	
AC600	460	0.21 (91%)	0.02 (9%)	0.23	0.20 (17%)	0.36 (30%)	0.64 (53%)	1.20	0.40
AC600-HNO_3 re 1M 24h	405	0.20 (87%)	0.03 (13%)	0.23	1.10 (56%) [+ 450%]	0.52 (26%) [+ 44%]	0.36 (18%) [– 44%]	1.98 [+ 65%]	0.60 [+ 50%]
AC800	651	0.29 (88%)	0.04 (12%)	0.33	0.19 (12%)	0.45 (28%)	0.95 (60%)	1.59	0.45
AC800-HNO_3 re 5M 24h	–	–	–	–	1.21 (49%) [+ 537%]	0.85 (35%) [+ 89%]	0.40 (16%) [– 58%]	2.46 [+ 55%]	1.35 [+ 200%]
AC900	1491	0.66 (82%)	0.14 (18%)	0.80	0.16 (10%)	0.38 (24%)	1.06 (66%)	1.60	1.17
AC900-HNO_3 re 10M 24h	–	–	–	–	2.19 (60%) [+ 1269%]	0.97 (26%) [+ 155%]	0.50 (14%) [– 53%]	3.66 [+ 129%]	1.70 [+ 45%]

In order to demonstrate the effect of heat treatment on the adsorption of water vapor, sample AC800 was used as the original carbon. This original carbon was oxidized with 1 M HNO_3 by boiling in a reflux condenser for 24 hours (AC800-HNO_3 re 1M 24h) and then the oxidized sample was subsequently heat treated at 600^oC and 800^oC for 12 hours under the flow of N_2 at 100 cm^3/min using the heating rate of 10^oC/min (AC800-HNO_3-HT600^oC and AC800-HNO_3-HT800^oC). The amount of surface functional groups and porous properties of these samples are shown in Table 5.8.

For activated carbon prepared from H_3PO_4 activation, sample AC was used as the original carbon. Three samples of surface modified carbons were prepared from this original carbon by oxidizing with 1 M and 5 M HNO_3 by boiling in a reflux condenser for 24 hours (HNO_3 re 1M 24h and HNO_3 re 5M 24h) and in air by heating at 250^oC for 48 hours (Air 250^oC 48h). The amount of surface functional groups and porous properties of these activated carbons are summarized in Table 5.9.

Table 5.8 Porous properties and surface functional groups of original, oxidized, and heat treated activated carbons (the value in square bracket [ ] is the percentage changes of functional groups with reference to the original carbon, where "+" denotes % increasing and "–" denotes % decreasing).

Sample	S_{BET} (m^2/g)	V_{mic} (cm^3/g)	$V_{meso+macro}$ (cm^3/g)	V_T (cm^3/g)	Acidic group (mmol/g)				Basic group (mmol/g)
					Carboxylic	Lactonic	Phenolic	Total	
AC800	651	0.29 (88%)	0.04 (12%)	0.33	0.19 (12%)	0.45 (28%)	0.95 (60%)	1.59	0.45
AC800-HNO_3 re 1M 24h	604	0.26 (81%)	0.06 (19%)	0.32	1.07 (49%)	0.80 (37%)	0.30 (14%)	2.17	0.93
AC800-HNO_3-HT600^oC	647	0.25 (74%)	0.05 (26%)	0.34	0.39 (24%) [– 64%]	1.01 (63%) [+ 26%]	0.20 (13%) [– 33%]	1.60 [– 26%]	0.54 [– 42%]
AC800-HNO_3-HT800^oC	774	0.35 (88%)	0.05 (12%)	0.40	0.27 (22%) [– 75%]	0.73 (61%) [– 9%]	0.20 (17%) [– 33%]	1.20 [– 45%]	0.45 [– 52%]

Table 5.9 Porous properties and surface functional groups of original and oxidized activated carbons prepared by H_3PO_4 activation (the value in square bracket [ ] is the percentage changes of functional groups with reference to the original carbon, where "+" denotes % increasing and "–" denotes % decreasing).

Sample	S_{BET} (m^2/g)	V_{mic} (cm^3/g)	V_T (cm^3/g)	Acidic group (mmol/g)				Basic group (mmol/g)
				Carboxylic	Lactonic	Phenolic	Total	
AC (original activated carbon)	1200	0.55 (95%)	0.58	0.06 (9%)	0.43 (65%)	0.17 (26%)	0.66	0.63
Air 250°C 48h	585	0.27 (96%)	0.28	1.57 (41%) [+ 2517%]	1.41 (37%) [+ 228%]	0.87 (22%) [+ 412%]	3.85 [+ 483%]	0.13 [– 79%]
HNO_3 re 1M 24h	523	0.26 (96%)	0.27	1.01 (26%) [+ 1583%]	1.18 (30%) [+ 174%]	1.77 (44%) [+ 941%]	3.96 [+ 500%]	1.90 [+ 202%]
HNO_3 re 5M 24h	–	–	–	1.24 (25%) [+ 1967%]	1.76 (35%) [+309%]	2.03 (40%) [+ 1094%]	5.03 [+ 662%]	2.16 [+ 243%]

Effect of surface functional groups on water vapor adsorption

Water vapor adsorption isotherms at 30°C of the three physically activated carbons (AC600, AC800, and AC900) as compared to the respective oxidized carbons are shown in Figure 5.15 and the replotting of isotherms are presented in Figure 5.16. As seen in Figure 5.15, the amount of water adsorbed increase after oxidation for all three samples. It should be noted that each oxidized carbon contains the maximum amount of incorporated total acidic groups. As a result, the behavior of water adsorption should be largely determined by the role of surface functionality.

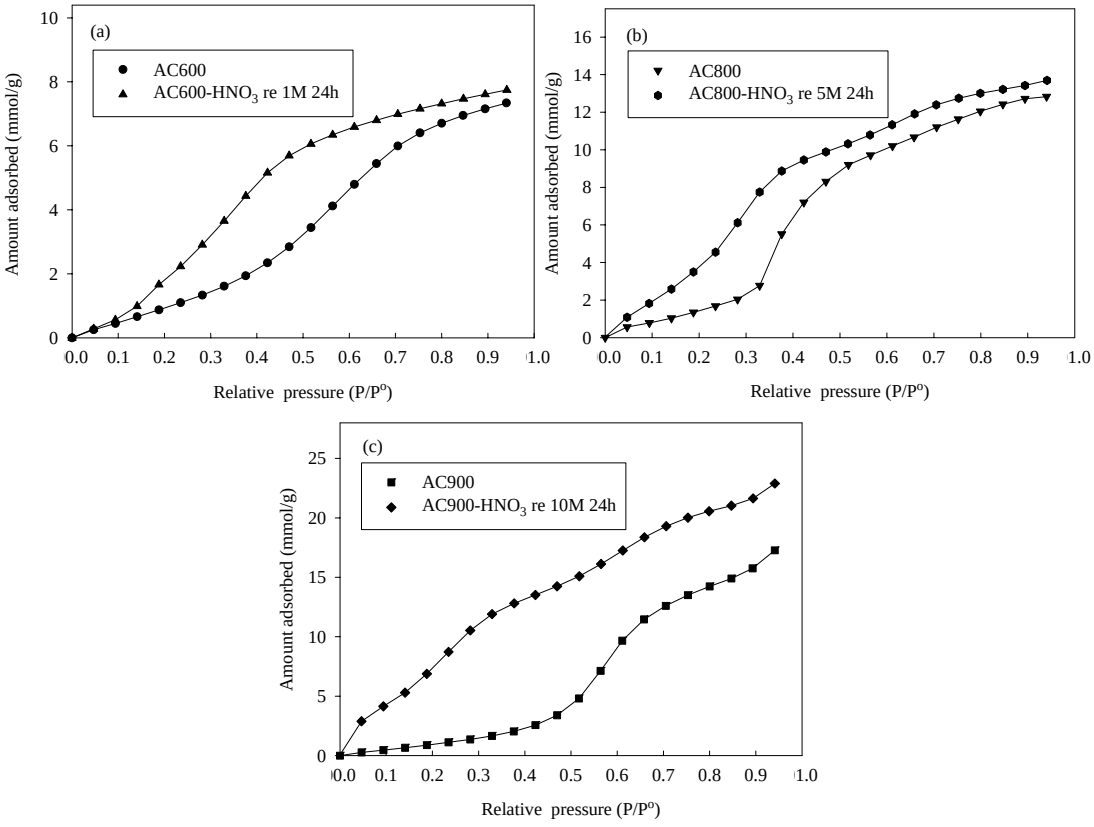

Figure 5.15 Water vapor adsorption isotherms at 30°C of original and oxidized activated carbons prepared by CO_2 activation.

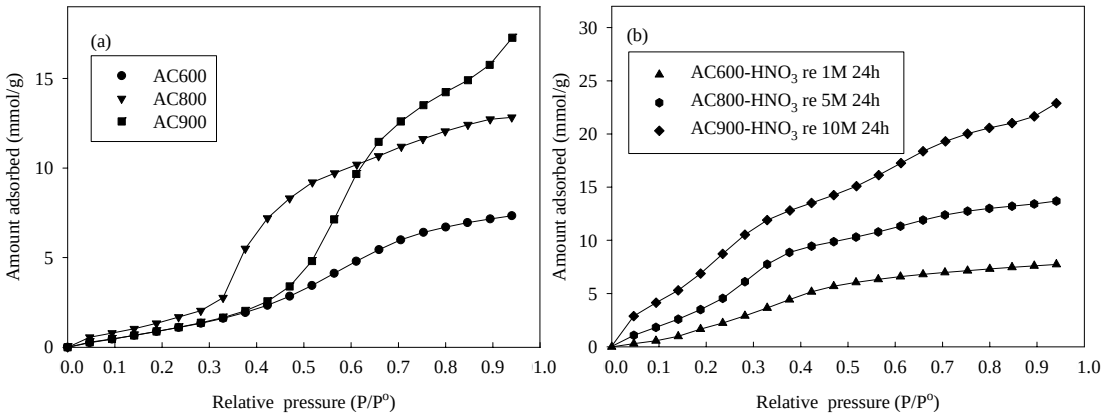

Figure 5.16 Water vapor adsorption isotherms at 30°C of original and oxidized activated carbons prepared by CO_2 activation.

As Figure 5.16 (a) shows, the amount of water adsorbed over the relative pressure of 0 – 0.3 increases approximately linearly with pressure and is the same for all original carbons. This behavior may be explained that all three original carbons probably contain the same amount of acidic functional groups which concentrates in these small pore sizes for adsorption at $P/P^o < 0.3$. In the range of relative pressure 0.3 – 0.6, the amount adsorbed increases steadily with the following order of amount adsorbed: AC800 > AC900 > AC600. For adsorption at $P/P^o > 0.6$, where the adsorption occurs in larger pore sizes, it is believed that the concentration of surface group is low and the adsorption then occurs by weak physical adsorption on non-polar carbon surface where the amount adsorbed is proportional to the available surface area, hence AC900 > AC800 > AC600. Figure 5.16 (b) shows that the amount of water adsorbed follow the order of total acidic functional groups, that is AC600-HNO_3 re 1M 24h < AC800-HNO_3 re 5M 24h < AC900-HNO_3 re 10M 24h. Further examination of Table 5.7 for the three oxidized carbon on the concentration of acidic group tends to indicate that the increased amount of adsorbed water is

probably due to the role of carboxylic acid group since the content of this group increases significantly compared to lactonic and phenolic groups.

Water vapor adsorption isotherms of the original activated carbon prepared by H_3PO_4 activation and the three oxidized carbons are shown in Figure 5.17. At low relative pressure range ($P/P^o < 0.45$), the amount of water adsorbed on all three oxidized carbons are higher than the original carbon with the following order: HNO_3 re 5M 24h > HNO_3 re 1M 24h > air 250°C 48h > AC, showing the same order as the total amount of acidic oxygen functional groups from Boehm titration results (Table 5.9). However, at higher relative pressure ($P/P^o > 0.45$), the adsorption capacities of HNO_3 re 1M 24h and air 250°C 48h samples are lower than the original sample.

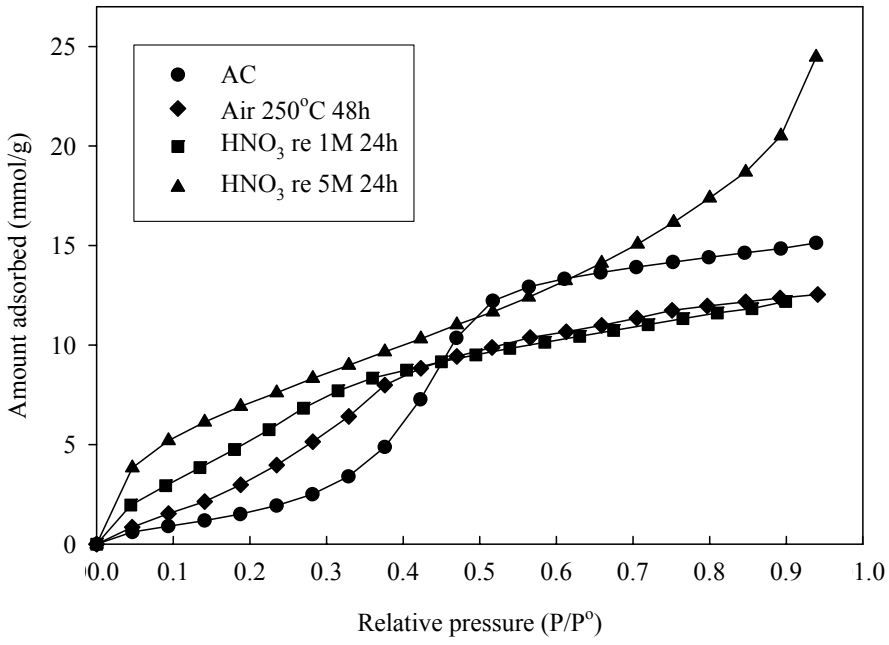

Figure 5.17 Water vapor adsorption isotherms at 30°C of original and oxidized activated carbons prepared by H_3PO_4 activation.

It could be possible that, for HNO_3 re 1M 24h and air 250^oC 48h samples, the type of active functional groups that assists in the process of water adsorption may not evenly distribute over the entire pore size range and could concentrate more in micropore, that is at $P/P^o < 0.45$, hence giving higher amount of water adsorbed proportionally to the amounts of functional groups which locate at the edge of basal plane. At $P/P^o > 0.45$, the lesser amount of water adsorbed may be due to the presence of smaller amount of functional groups at the pore entrance which could further prevent the water molecules to be adsorbed inside the pores. Therefore, at $P/P^o < 0.45$ surface functional groups play an important role in adsorption in small pores whereas at higher relative pressure the adsorption occurs by self-adsorption between water molecules inside a larger pore if there is insufficient acidic group available at the edge of carbon planes. For sample HNO_3 re 5M 24h, the surface functional groups may still exist for all pore sizes, thus giving a steady increase in the amount adsorbed by the role of functional group only.

The result that the water adsorption isotherm of oxidized activated carbon is higher than the isotherm of original activated carbon at low relative pressures and becomes lower at higher relative pressures has also been found by other researchers (Bandosz, Jagiello, Schwarz, and Krzyzanowski, 1996; Goworek, Świątkowski, and Biniak, 1997; Choma, Burakiewicz-Mortka, Jaroniec, Li, and Klinik, 1999).

Figure 5.18 compare the water adsorption of sample AC900-HNO_3 re 10M 24h and sample HNO_3 re 5M 24h which have comparable surface area of the original samples (S_{BET} = 1491 m^2/g for AC900 and 1200 m^2/g for AC) but have significant difference in surface functional groups (total acidic groups = 3.66 mmol/g

for AC900-HNO_3 re 10M 24h and 5.03 mmol/g for HNO_3 re 5M 24h). It is seen that sample AC900-HNO_3 re 10M 24h has higher amount of water adsorbed than sample HNO_3 re 5M 24h although it has lower total acidic, lactonic, and phenolic groups. However, sample AC900-HNO_3 re 10M 24h has higher amount of carboxylic acid group than sample HNO_3 re 5M 24h (see Table 5.7 and 5.9). This evidence thus further indicates that carboxylic acid group plays an important role in water vapor adsorption.

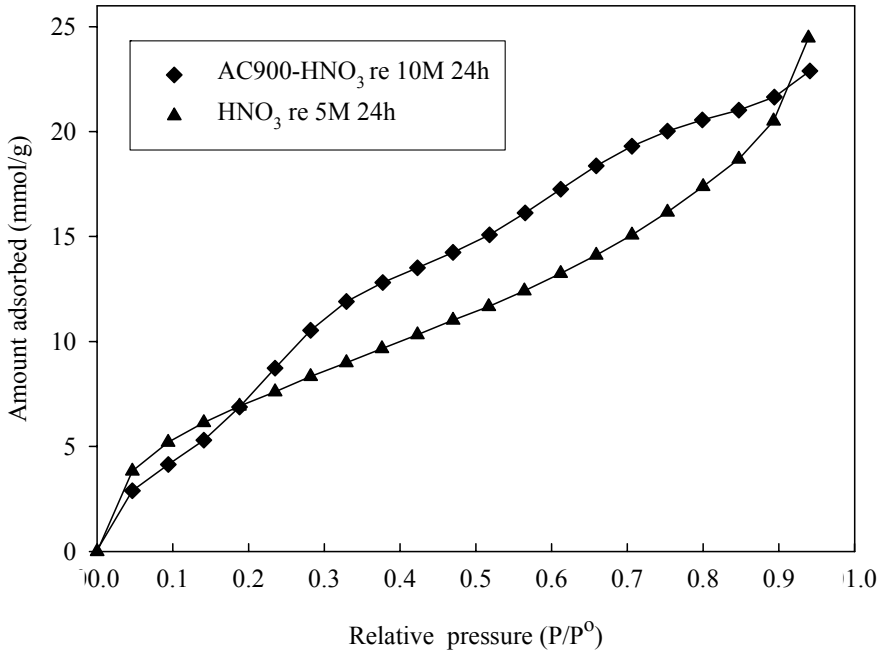

Figure 5.18 Comparison of water vapor adsorption isotherms at 30°C of samples with have comparable surface area of the original samples but have significant difference in surface functional groups.

Figure 5.19 shows the water vapor adsorption isotherms at 30^{o}C of the original, oxidized, and heat treated activated carbons. Heat treatment process which significantly decrease the amount of carboxylic acid group (see Table 5.8) causes a decrease in the amount of water adsorbed at $P/P^{o} < 0.4$ for heat-treated sample at 600^{o}C and at $P/P^{o} < 0.6$ for heat-treated sample at 800^{o}C. This confirms that carboxylic acid group plays an important role in water vapor adsorption.

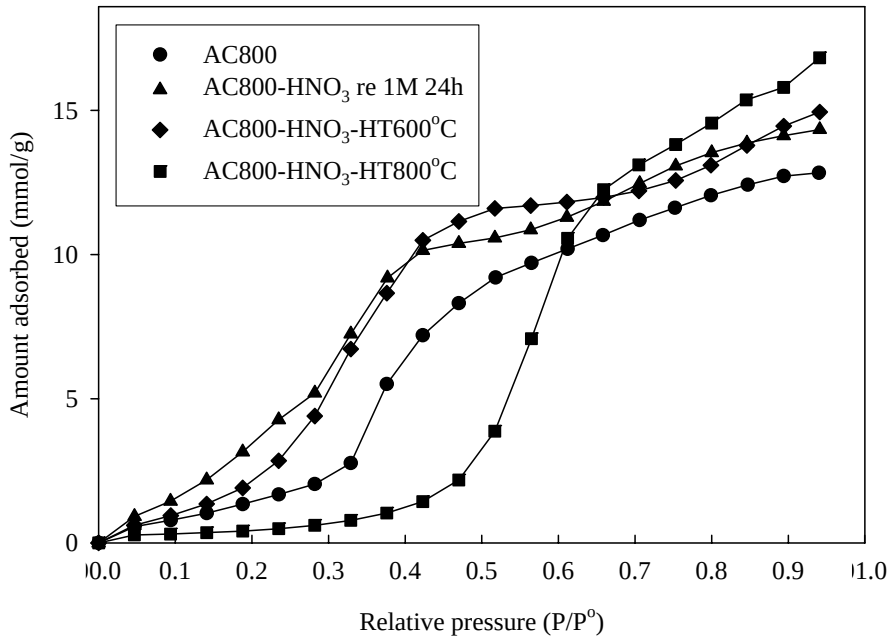

Figure 5.19 Water vapor adsorption isotherms at 30^{o}C of original, oxidized, and heat treated activated carbons.

At relative pressures higher than 0.4, there is not much difference in the amount of water adsorbed for sample heat treated at 600^{o}C compared to the oxidized carbon (AC800-HNO_3 re 1M 24h). However, the isotherm of heat-treated sample at 800^{o}C starts to rise sharply at $P/P^{o} > 0.4$ and surpass both AC800 and AC800-HNO_3-HT600^{o}C at $P/P^{o} \approx 0.6$. The higher adsorption capacity of AC800-

HNO_3-HT800^oC at higher relative pressure range is believed to be dominated by the consequence of physical adsorption on hydrophobic surfaces and pore filling effect in the larger pore sizes, due to a large reduction of surface groups in smaller pores.

Figure 5.20 shows the fitting of DS and Do and Do models to the water vapor adsorption isotherms of original and oxidized activated carbons prepared by H_3PO_4 activation and Table 5.10 gives the model parameters. According to the results, DS model can fit the isotherm of activated carbons oxidized with 1 M HNO_3 and air quite well but this model fails to fit the isotherm of original sample at the relative pressures higher than 0.4 and sample HNO_3 re 5M 24h at all relative pressure range. On the other hand, the Do and Do model provide better fitting of isotherms than DS model for these samples. This indicates that Do and Do model is able to describe water adsorption behaviors for most of activated carbons with low and high concentrations of surface functional groups. The concentrations of functional group predicted from DS model ($C_{\mu o}$) give significantly higher values than those determined from Boehm titration whereas the predicted values from Do and Do model (S_o) are closer to the values from Boehm titration. The $C_{\mu o}$ and S_o values also show the same trend of surface functional groups determined from titration viz., AC < air 250^oC 48h < HNO_3 re 1M 24h < HNO_3 re 5M 24h. The obtained saturation concentration in the micropore values ($C_{\mu s}$) from Do and Do model are reasonable for all samples.

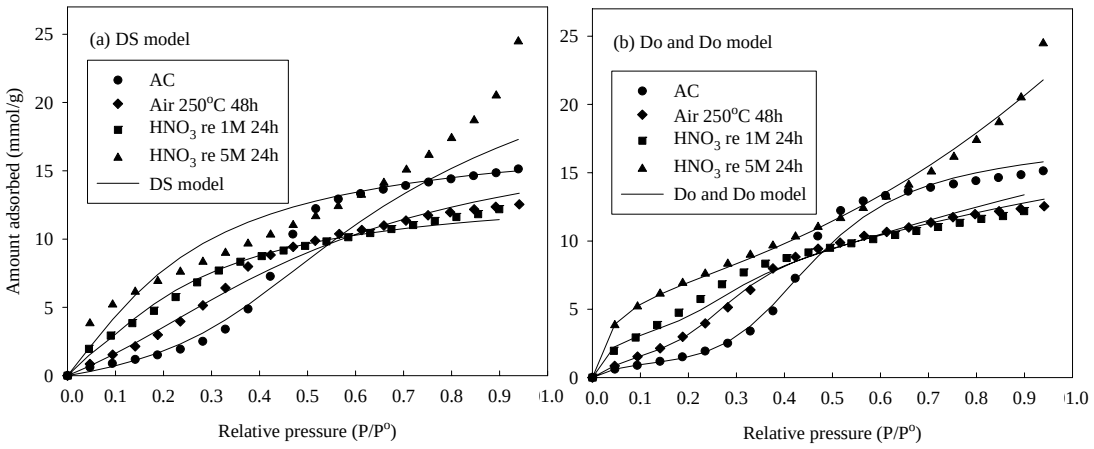

Figure 5.20 Fitting of (a) Dubinin-Serpinsky (DS) and (b) Do and Do models to the water vapor adsorption isotherms at 30°C of original and oxidized samples prepared by H_3PO_4 activation.

Table 5.10 Parameters obtained from Dubinin-Serpinsky (DS) and Do and Do models of original and oxidized activated carbons prepared by H_3PO_4 activation and amount of total acidic oxygen functional groups from Boehm titration.

Sample	DS model parameters				Do and Do model parameters					Total acidic group from Boehm titration (mmol/g)
	$C_{\mu o}$ (mmol/g)	k (g/mmol)	c	R^2	S_o (mmol/g)	K_f	$C_{\mu s}$ (mmol/g)	K_μ	R^2	
AC	2.91	0.03	2.04	0.936	1.31	16.63	12.42	51.29	0.986	0.66
Air 250^{o}C 48h	7.46	0.05	1.95	0.983	2.87	8.45	5.05	499.97	0.996	3.85
HNO_3 re 1M 24h	8.18	0.07	3.46	0.990	3.83	23.65	2.85	500.07	0.975	3.96
HNO_3 re 5M 24h	15.12	0.05	2.93	0.753	6.35	28.86	19.84	0.32	0.984	5.03

Figure 5.21 (a) and (b) show the fitting of DS and Do and Do models to the water vapor adsorption isotherms of the original, oxidized, and heat treated activated carbons and Table 5.11 lists the obtained model parameters. According to these figures, DS model fails to fit the isotherm of sample AC800-HNO_3-HT600^oC whereas both DS and Do and Do models fail to fit the isotherm of sample AC800-HNO_3-HT800^oC.

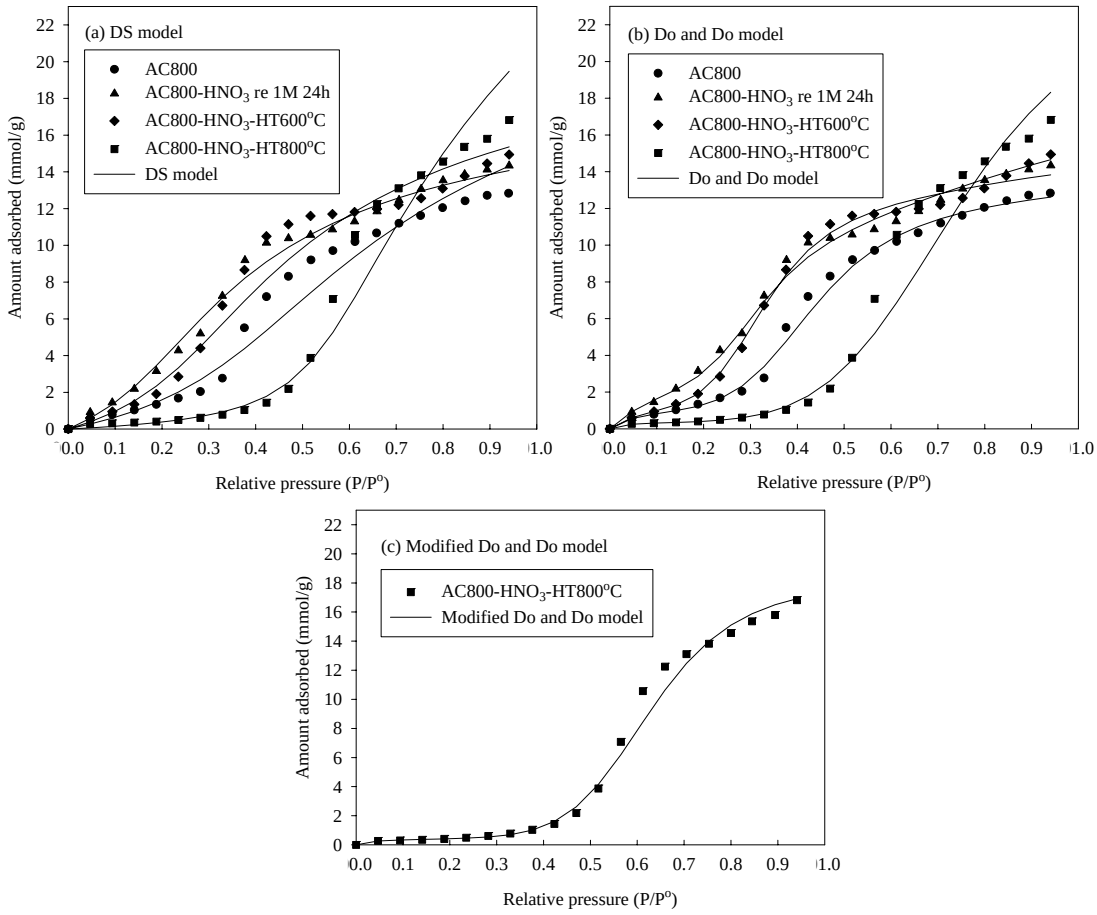

Figure 5.21 Fitting of (a) Dubinin-Serpinsky (DS), (b) Do and Do, and (c) modified Do and Do models to the water vapor adsorption isotherms at 30^oC of original, oxidized, and heat treated activated carbons.

Table 5.11 Parameters obtained from Dubinin-Serpinsky (DS), Do and Do, and modified Do and Do models of original, oxidized, and heat treated activated carbons and amount of total acidic oxygen functional groups from Boehm titration.

Sample	DS model parameters				Do and Do model [Modified Do and Do model] parameters						Total acidic group from Boehm titration (mmol/g)
	$C_{\mu o}$ (mmol/g)	k (g/mmol)	c	R^2	S_o (mmol/g)	K_f	$C_{\mu s}$ (mmol/g)	K_μ	n	R^2	
AC800	2.62	0.04	2.00	0.959	1.06	20.49	9.81	65.30	5	0.993	1.59
AC800-HNO_3 re 1M 24h	3.20	0.05	3.37	0.990	2.98	8.54	6.33	299.88	5	0.993	2.17
AC800-HNO_3-HT600^{o}C	2.65	0.04	2.77	0.960	1.48	12.98	9.71	251.20	5	0.991	1.60
AC800-HNO_3-HT800^{o}C	0.71	0.02	1.76	0.954	0.32 [0.36]	63.14 [47.87]	22.84 [16.46]	4.33 [26.77]	5 [7]	0.953 [0.989]	1.20

Neitsch, Heschel, and Suckow (2001) indicated that in carbon with a small density of primary adsorption sites, the cluster size should be greater than in carbon with a higher concentration of these sites. So, the modified Do and Do model was applied to sample AC800-HNO_3-HT800^oC which contains the lowest surface functional groups, according to Boehm's result. It is noted that this modified model was applied to all range of relative pressure (P/P^o 0 – 0.94) and without the need to divided the adsorption into different pressure range since this sample consists mainly of micropores (see Table 5.8). Figure 5.21 (c) shows that the modified Do and Do model can provide the better fit of isotherm of sample AC800-HNO_3-HT800^oC than the original Do and Do model with cluster size equal to 7, proving that the cluster size of carbon with small density of primary adsorption sites is greater than that of carbon with high concentration of these sites.

The concentrations of functional group ($C_{\mu o}$, S_o) predicted from Do and Do model have the values closer to the values obtained from Boehm titration than with the DS model, except sample AC800-HNO_3-HT800^oC. However, the order of these values derived from both models still follows the Boehm titration results i.e. AC800-HNO_3 re 1M 24h > AC800-HNO_3-HT600^oC > AC800 > AC800-HNO_3-HT800^oC. The saturation concentration in the micropore values ($C_{\mu s}$) obtained from Do and Do and modified Do and Do model seem reasonable for all samples except sample AC800-HNO_3-HT800^oC for which Do and Do model predicts the values slightly higher than experimental data.

Effect of surface functional groups on methanol and ethanol vapors adsorption

Methanol and ethanol vapors adsorption isotherms of the original activated carbon (AC) and sample HNO_3 re 1M 24h are shown in Figure 5.22. According to the results, the oxidation decreases the amount of methanol and ethanol adsorbed with much decrease for ethanol vapor. Although methanol and ethanol are polar molecules, the surface oxygen functional groups of activated carbon do not contribute to the increased adsorption capacity. On the contrary, the adsorption capacity decreases with the increase of theses functional groups. It is likely that the increased surface functional groups which located at the pore entrance may have blocked and prevented the methanol and ethanol molecules from transporting into the internal pore. It is noted that, the larger decrease of adsorption capacity in the case of ethanol vapor may be also due to the larger molecular size of ethanol than methanol which makes it even more difficult to enter the pores. The decrease of methanol adsorption on activated carbon after oxidation has also been found in the work of Bandosz et al. (1996).

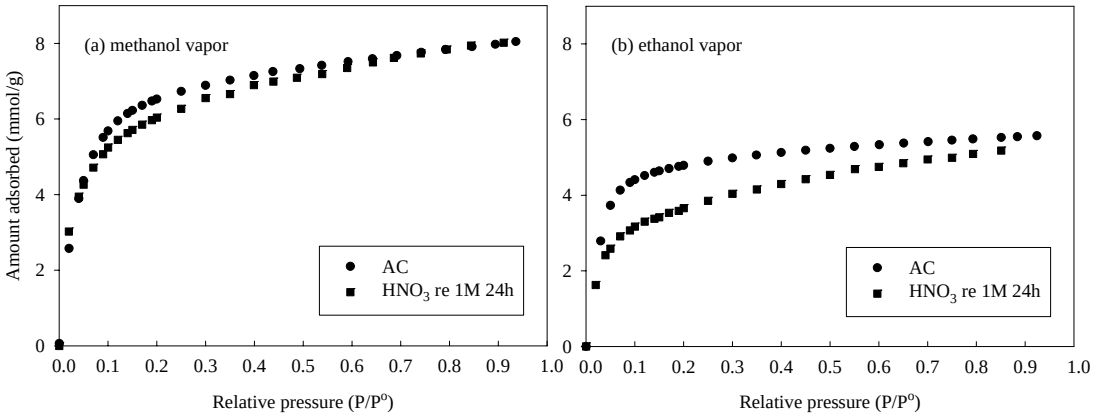

Figure 5.22 Adsorption isotherms of (a) methanol and (b) ethanol vapors at 30°C of original activated carbon (AC) and sample HNO_3 re 1M 24h.

5.3.2 Equilibria of heavy metal ions adsorption on modified activated carbon

To study the effect of surface functional groups on the heavy metal ions adsorption in both single and binary mixture, the sample AC was used as the original activated carbon. This original carbon was oxidized with 1 M HNO_3 by boiling in a reflux condenser and 35 wt% H_2O_2 by soaking at room temperature for 24 hours (HNO_3 re 1M 24h and H_2O_2 24h). The amount of surface functional groups and porous properties of these activated carbons are summarized in Table 5.12. Oxidation gave rise to the increase of acidic oxygen functional groups with the following order: HNO_3 re 1M 24h > H_2O_2 24h > AC.

Table 5.12 Porous properties and surface functional groups of original and oxidized activated carbons for study the effect of surface functional groups on the heavy metal ions adsorption (the value in square bracket [ ] is the percentage changes of functional groups with reference to the original carbon, where "+" denotes % increasing and "–" denotes % decreasing).

Sample	S_{BET} **(m^2/g)**	V_{mic} **(cm^3/g)**	V_T **(cm^3/g)**	**Acidic group (mmol/g)**				**Basic group (mmol/g)**
				Carboxylic	**Lactonic**	**Phenolic**	**Total**	
AC (original activated carbon)	1200	0.55	0.58	0.06 (9%)	0.43 (65%)	0.17 (26%)	0.66	0.63
H_2O_2 24h	689	0.34	0.35	0.34 (20%) [+ 467%]	0.68 (41%) [+ 58%]	0.65 (39%) [+ 282%]	1.67 [+ 153%]	0.40 [– 36%]
HNO_3 re 1M 24h	523	0.26	0.27	1.01 (26%) [+ 1583%]	1.18 (30%) [+ 174%]	1.77 (44%) [+ 941%]	3.96 [+ 500%]	1.90 [+ 202%]

5.3.2.1 Single ion adsorption

Adsorption isotherms of heavy metal ions are presented for each metal ion and each activated carbon as shown in Figure 5.23 and Figure 5.24, respectively. As seen in Figure 5.23, the adsorption isotherms of all metal ions display Type I according to the IUPAC classification system. The results show that all oxidized carbons enhance the adsorption capacity of the four metal ions as compared to the adsorption of original carbon. According to Figure 5.23 (e), sample HNO_3 re 1M 24h gives the highest increase of the maximum adsorption of all metal ions compared with the original sample (350% for Pb^{2+}, 500% for Zn^{2+}, 700% for Cu^{2+}, and 600% for Ca^{2+}). The sample H_2O_2 24h helps increase the maximum adsorption capacities by 50% for Pb^{2+}, 100% for Zn^{2+}, 180% for Cu^{2+}, and 100% for Ca^{2+}.

The results from Figure 5.24 show that the amount of metal ions adsorbed by the original and oxidized samples follows the following order: $Ca^{2+} < Cu^{2+} < Zn^{2+} < Pb^{2+}$. It was reported that metal ion with higher electronegativity demonstrate higher affinities for adsorption sites on the activated carbon (Dastgheib and Rockstraw, 2002). The values of electronegativities are in the following : 1.00 for Ca^{2+} < 1.65 for Zn^{2+} < 1.90 for Cu^{2+} < 2.33 for Pb^{2+} (Dastgheib and Rockstraw, 2002; Han et al., 2006). However, the adsorption of Zn^{2+} and Cu^{2+} obtained from the present study did not follow the same trend as electronegativities. The level of metal ion uptake $Zn^{2+} > Cu^{2+}$ obtained from this work has also been observed by other researchers (Chubar, Carvalho, and Correia, 2004).

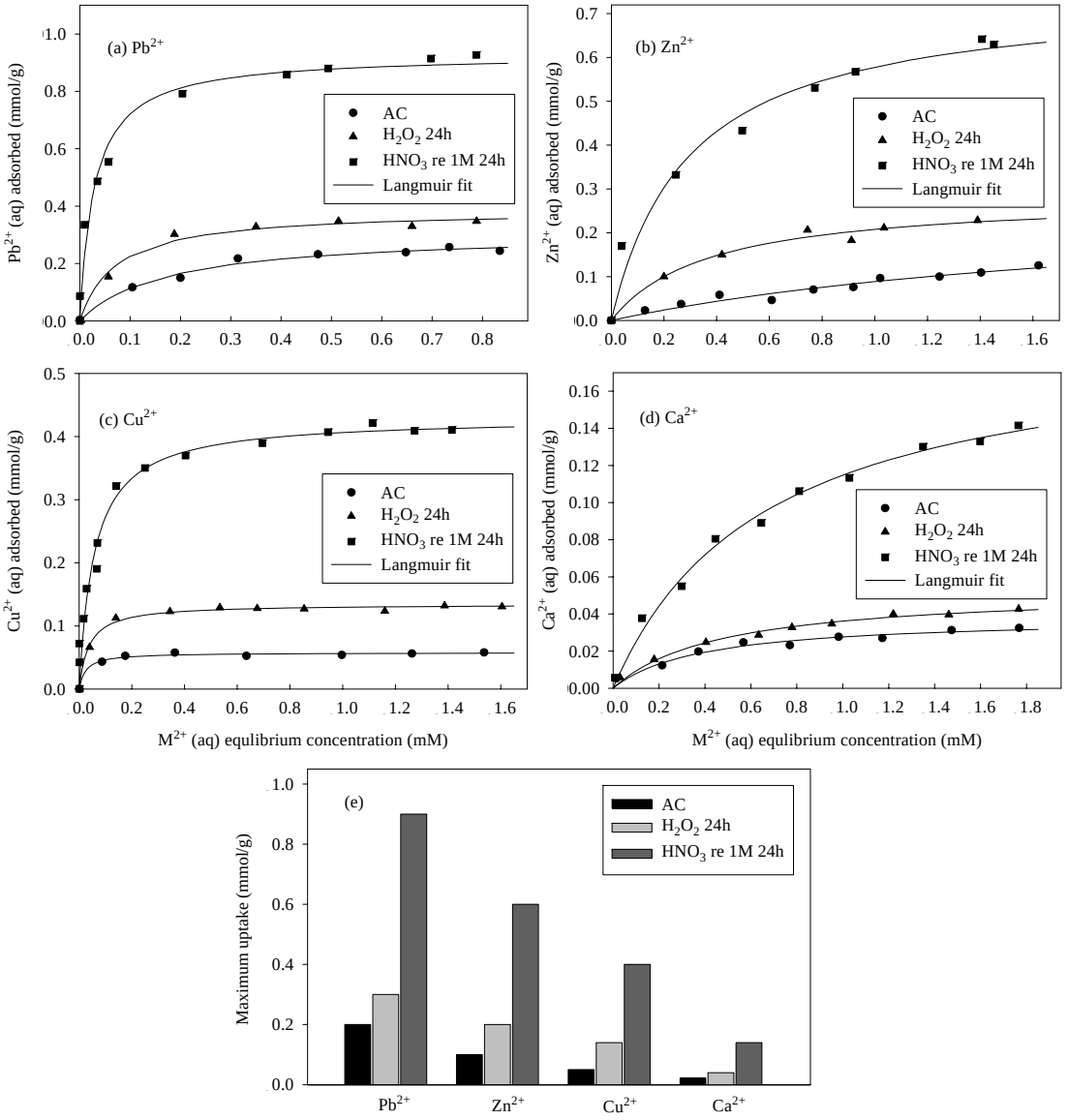

Figure 5.23 Adsorption isotherms at 30°C of (a) Pb^{2+}, (b) Zn^{2+}, (c) Cu^{2+}, and (d) Ca^{2+} on original and oxidized activated carbons and (e) maximum uptake of all four metal ions on each carbon sample.

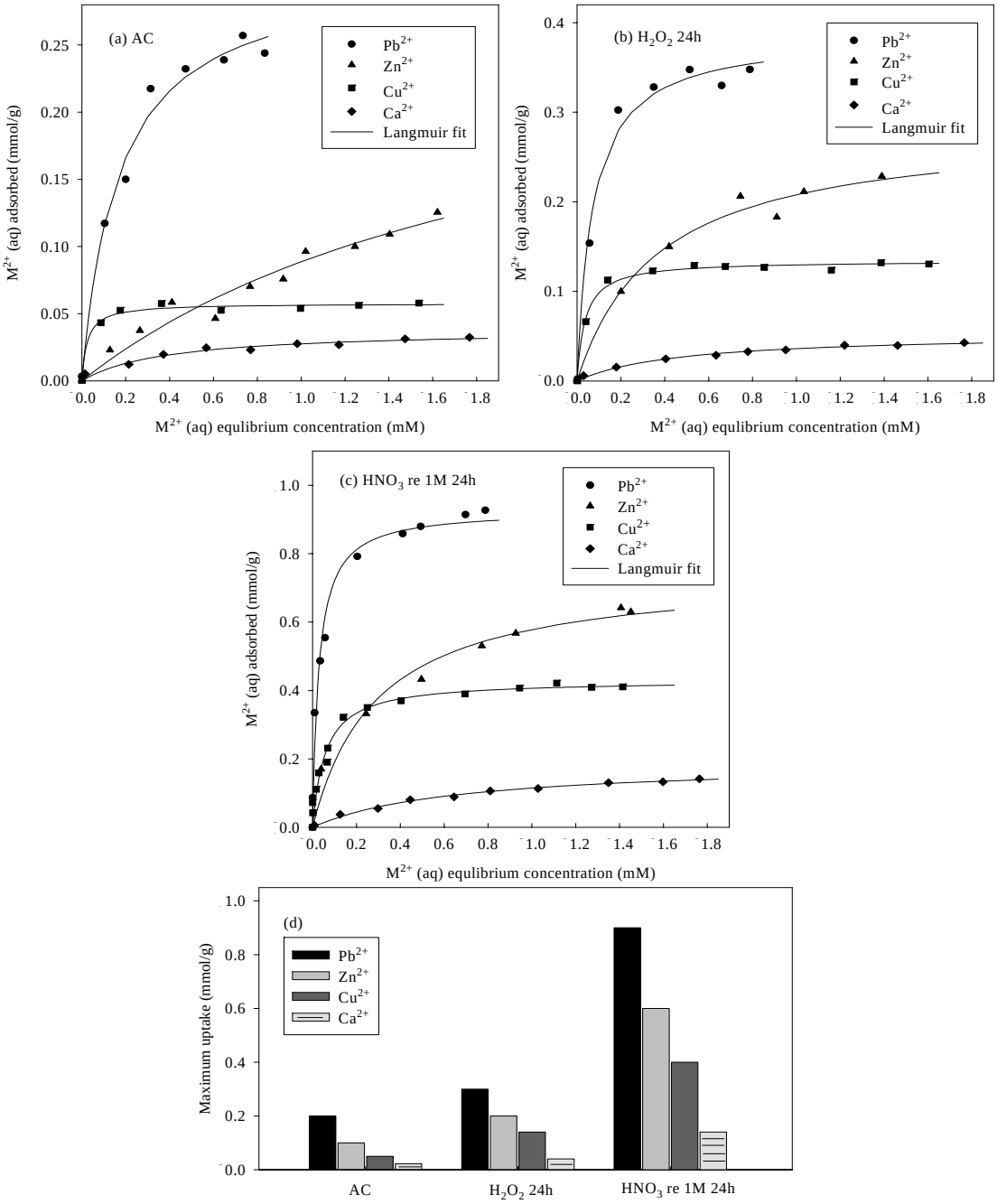

Figure 5.24 Adsorption isotherms at 30^{o}C of heavy metal ions on (a) original sample, (b) sample H_2O_2 24h, and (c) sample HNO_3 re 1M 24h and (d) maximum uptake on all three samples.

Experimental isotherms of all metal ions were modeled by employing the Langmuir isotherm which reads

$$q_e = \frac{q_m b C_e}{1 + b C_e} \tag{5.7}$$

where q_e is the adsorbed amount of metal ion at equilibrium, q_m is the maximum amount adsorbed in mmol/g, b is the Langmuir constant in L/mmol, and C_e is the metal ion equilibrium concentration in mM. This model is based on a kinetic principle that is the rate of adsorption is equal to the rate of desorption from the surface. The assumptions of the Langmuir model are that each adsorption site can take only one atom or molecule, adsorbed atoms or molecules are adsorbed at definite or localized sites, adsorption energy is constant over all sites or homogeneous surface, and no interactions between adsorbed molecules as they are assumed to be small compared to the adsorbate/adsorbent interactions (Do, 1998). The predicted results from Langmuir model fitting are shown in Figure 5.23 and Figure 5.24 and the parameters are listed in Table 5.13. It is seen that Langmuir equation can describe the isotherms very well for all metal ions with correlation coefficient $R^2 \geq 0.93$. As shown in Table 5.13, the adsorption constant (b) for Pb^{2+} and Zn^{2+} ions increases with increasing oxygen contents. This indicates that the more oxygen functional groups are incorporated on the activated carbon surfaces, the higher affinities would be for Pb^{2+} and Zn^{2+} ions. This trend is in contrast to Cu^{2+} and Ca^{2+} ions where b shows the opposite tendency.

Table 5.13 Langmuir parameters obtained from metal ion adsorption isotherms.

Sample	q_m **(mmol/g)**	b **(L/mmol)**	R^2
Pb^{2+}			
AC (original activated carbon)	0.31	5.88	0.984
H_2O_2 24h	0.39	13.95	0.986
HNO_3 re 1M 24h	0.93	34.81	0.979
Zn^{2+}			
AC (original activated carbon)	0.28	0.47	0.933
H_2O_2 24h	0.29	2.73	0.941
HNO_3 re 1M 24h	0.75	3.42	0.950
Cu^{2+}			
AC (original activated carbon)	0.06	40.12	0.986
H_2O_2 24h	0.13	27.32	0.991
HNO_3 re 1M 24h	0.43	17.37	0.971
Ca^{2+}			
AC (original activated carbon)	0.04	2.60	0.948
H_2O_2 24h	0.05	2.14	0.987
HNO_3 re 1M 24h	0.19	1.51	0.992

The maximum amount of metal ions adsorbed (q_m) derived from Langmuir model was also plotted versus surface acidic functional groups as shown in Figure 5.25. It shows the linear relationship between the maximum amount of metal ion adsorbed and the amount of acidic functional groups for all metal ions which can be represented by

$$y = mx + c \tag{5.8}$$

where y is the maximum amount of metal ions adsorbed in mmol/g, x is the concentration of acidic functional groups in mmol/g, m is the slope of the linear line, and c is the intercept of the line taken as zero. The parameters of these linear relationships are listed in Table 5.14 with the correlation coefficient $R^2 \geq 0.83$. According to Figure 5.25, for all four metal ions, the amount adsorbed increases with increasing of acidic functional groups. This indicates that the adsorption uptake of metal cation species in solution is favored by the presence of acidic functional groups on carbon surface with adsorption achievable by electrostatic attraction (Coulombic) of the metal with these surface active sites.

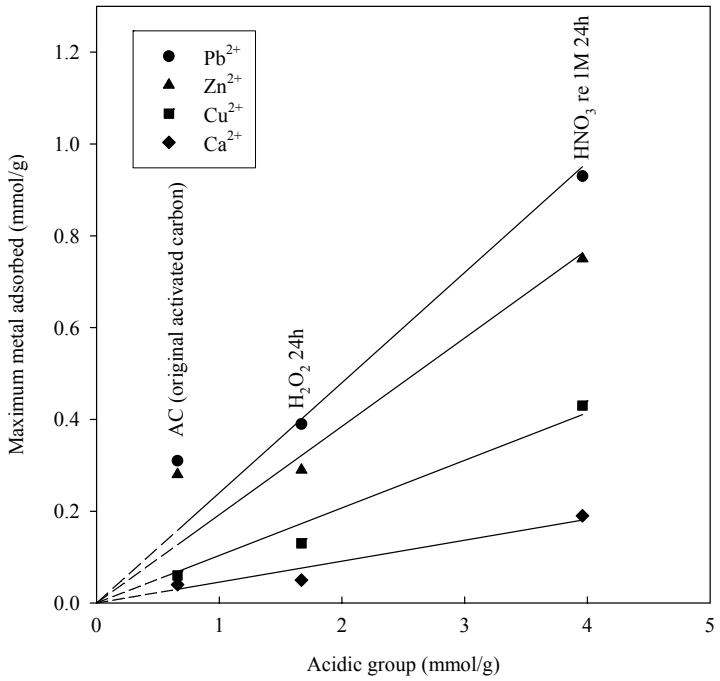

Figure 5.25 Relationship between maximum amount of metal ions adsorbed derived from Langmuir model and content of acidic functional groups of the original and oxidized carbons.

Table 5.14 Parameters obtained from linear relationship between maximum amount of metal ions adsorbed and content of acidic functional groups.

	m	***R²***
Pb^{2+}	0.240	0.897
Zn^{2+}	0.192	0.830
Cu^{2+}	0.104	0.970
Ca^{2+}	0.046	0.938

To investigate the relationship between the protons displaced from the functional groups on the activated carbon surfaces by the adsorption of metal ions, the solution pH was measured before and after adsorptions of Pb^{2+}, Zn^{2+}, Cu^{2+}, and Ca^{2+}. A decrease in solution pH was observed after adsorption for each metal ions, indicating that these metal ions adsorbed displace protons from acidic oxygen functional groups on activated carbon by an ion exchange mechanism. The amount of proton displaced was calculated from the relationship between pH and H^+ as

$$\mathrm{pH} = \log \frac{1}{[\mathrm{H}^+]} \tag{5.9}$$

and the Langmuir equation for proton displacement is

$$H_e = \frac{H_m b_H C_e}{1 + b_H C_e} \tag{5.10}$$

The experimental data of amounts of proton displaced and the fitting of these data with Langmuir model for sample HNO_3 re 1M 24h are shown in Figure 5.26 and the corresponding isotherm parameters are given in Table 5.15. The results show that the values of maximum amount of proton displacement (H_m) obtained from this sample have similar trend to the corresponding parameters determined from metal ions adsorptions equilibrium (q_m) i.e. $Pb^{2+} > Zn^{2+} > Cu^{2+} > Ca^{2+}$.

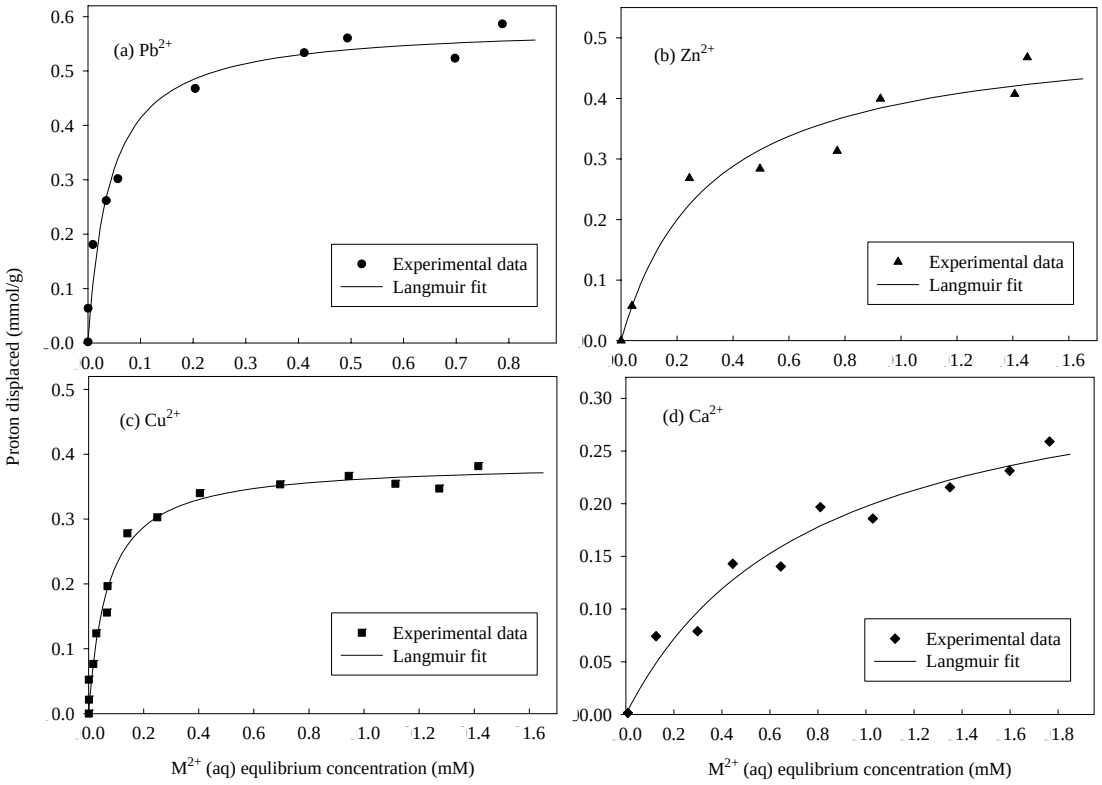

Figure 5.26 Proton displacement of (a) Pb^{2+}, (b) Zn^{2+}, (c) Cu^{2+}, and (d) Ca^{2+} of sample HNO_3 re 1M 24h.

Table 5.15 Langmuir parameters obtained from proton displacement isotherms of sample HNO_3 re 1M 24h.

	H_m (mmol/g)	b_H (L/mmol)	R^2
Pb^{2+}	0.58	24.29	0.970
Zn^{2+}	0.52	3.18	0.926
Cu^{2+}	0.39	14.52	0.981
Ca^{2+}	0.35	1.28	0.960

Figure 5.27 shows the linear graphs of the amount of H^+ displaced versus Pb^{2+}, Zn^{2+}, Cu^{2+}, and Ca^{2+} adsorbed. The number of protons displaced from the surface sites by metal ions can be expressed as,

$$H = gq_e + c \tag{5.11}$$

where H is the amount of protons displaced from the activated carbon surface in mmol/g, q_e is the amount of metal ions adsorbed in mmol/g, g is the gradient, and c is the intercept of the graph taken as zero. These equation neglects the effect of the activity of (H^+) and this is reasonable, considering the condition of dilute solution used in the experiment (Xiao and Thomas, 2004). The linear graphs indicate that the adsorption mechanism of metal ions associated with acidic oxygen functional groups does not vary with metal ion concentrations in the dilute solutions used. The

parameters obtained from equation 5.11 are given in Table 5.16. The displacement ratios of H^+ to metal ions adsorbed obtained from the gradients of the straight lines (*g*) follow the order $Ca^{2+} > Cu^{2+} > Zn^{2+} > Pb^{2+}$. This can be explained that the adsorption of Pb^{2+}, Zn^{2+}, and Cu^{2+} on activated carbons is more complicated than the adsorption of Ca^{2+} because of the complex hydrolysis products in solution which give rise to lower proton displacement ratios (Xiao and Thomas, 2005). Xiao (2004) reported that Ca^{2+} ions do not hydrolyze in dilute solution at pH < 8.0. In the present study, the initial pH was 6.06 – 6.64 for Ca^{2+} adsorption, therefore the calcium ions exist in solution mainly in the form of Ca^{2+} cations. Xiao (2004) and Álvarez-Merino, López-Ramón, and Moreno-Castilla (2005) reported that the amount of the hydrolysis products were initially present in solution with pH ~ 5.5 for $Pb(OH)^+$ and $Cu(OH)^+$ and pH ~ 6.8 for $Zn(OH)^+$. In the present study, the solution pH values were in the range 5.26 – 5.97 for Pb^{2+}, 5.17 – 5.95 for Cu^{2+}, 6.79 – 7.05 for Zn^{2+} and therefore the major species present in the solution were Pb^{2+} cations, Cu^{2+} cations, and Zn^{2+} cations with small amounts of $Pb(OH)^+$, $Cu(OH)^+$, and $Zn(OH)^+$.

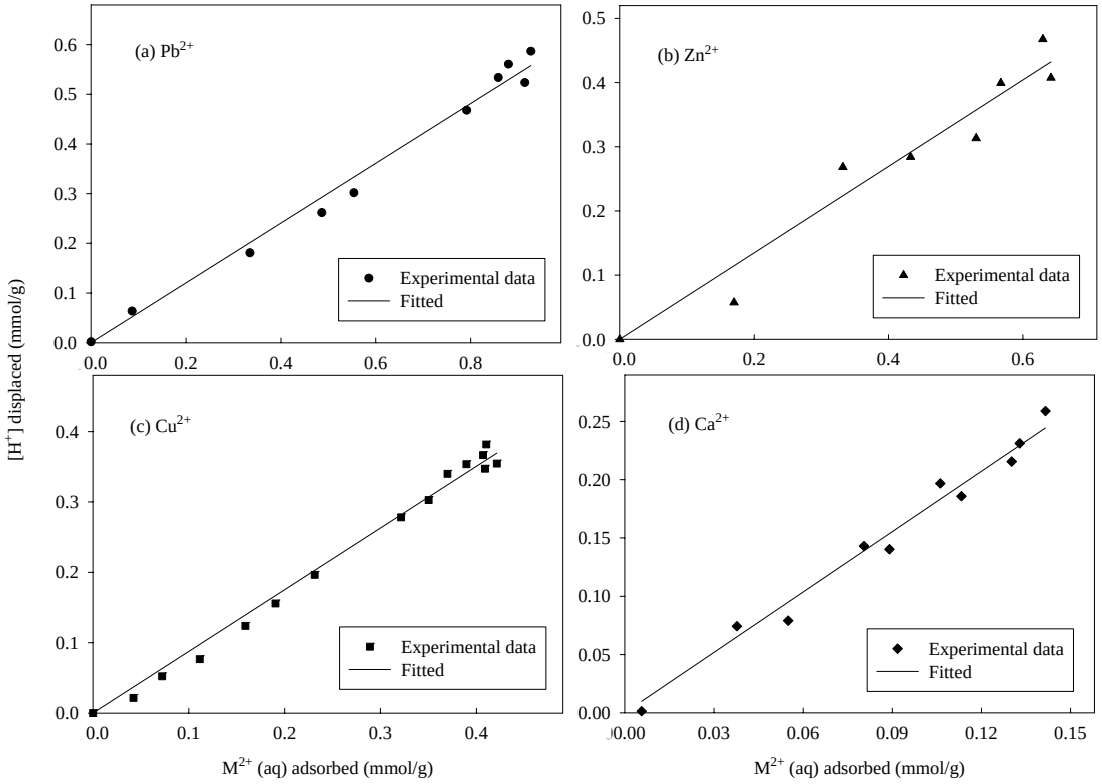

Figure 5.27 Variation of H^+ displaced with (a) Pb^{2+}, (b) Zn^{2+}, (c) Cu^{2+}, and (d) Ca^{2+} ions adsorbed on sample HNO_3 re 1M 24h.

Table 5.16 Relationship between proton displaced and metal ion adsorbed of sample HNO_3 re 1M 24h.

	g	R^2
Pb^{2+}	0.60	0.987
Zn^{2+}	0.67	0.948
Cu^{2+}	0.88	0.991
Ca^{2+}	1.73	0.980

Figure 5.28 compares the amount of metal ion adsorbed and proton displaced. It is suggested that if the mechanism of adsorption involve the ion-exchange between carboxylic acid group and metal ion, the ratio of proton displaced and metal ion adsorbed should equal to two (dash line). However, in the present study, this ratio is less than two for all cases. This indicates that not only carboxylic acid group which has proton exchange capacity is responsible for metal ion adsorption but also by the roles of lactonic and phenolic groups.

(Xiao, 2004) described the adsorption of M^{2+} on activated carbon surfaces by the following equations:

$$S{-}(COOH)_2 + M^{2+} \leftrightarrow S{-}(COO^{-})_2\,M^{2+} + 2H^{+}$$

$$S{-}(COH)_2 + M^{2+} \leftrightarrow S{-}(CO^{-})_2\,M^{2+} + 2H^{+}$$

$$S{-}(CO)_2 + M^{2+} \leftrightarrow S{-}(CO)_2\,M^{2+}$$

or

$$S\text{–}COOH + M(OH)^+ \leftrightarrow S\text{–}COO^-M(OH)^+ + H^+$$

$$S\text{–}COH + M(OH)^+ \leftrightarrow S\text{–}CO^-M(OH)^+ + H^+$$

$$S\text{–}CO + M(OH)^+ \leftrightarrow S\text{–}COM(OH)^+$$

where S is the activated carbon surface and –COOH, –COH, and –CO are surface oxygen functional groups.

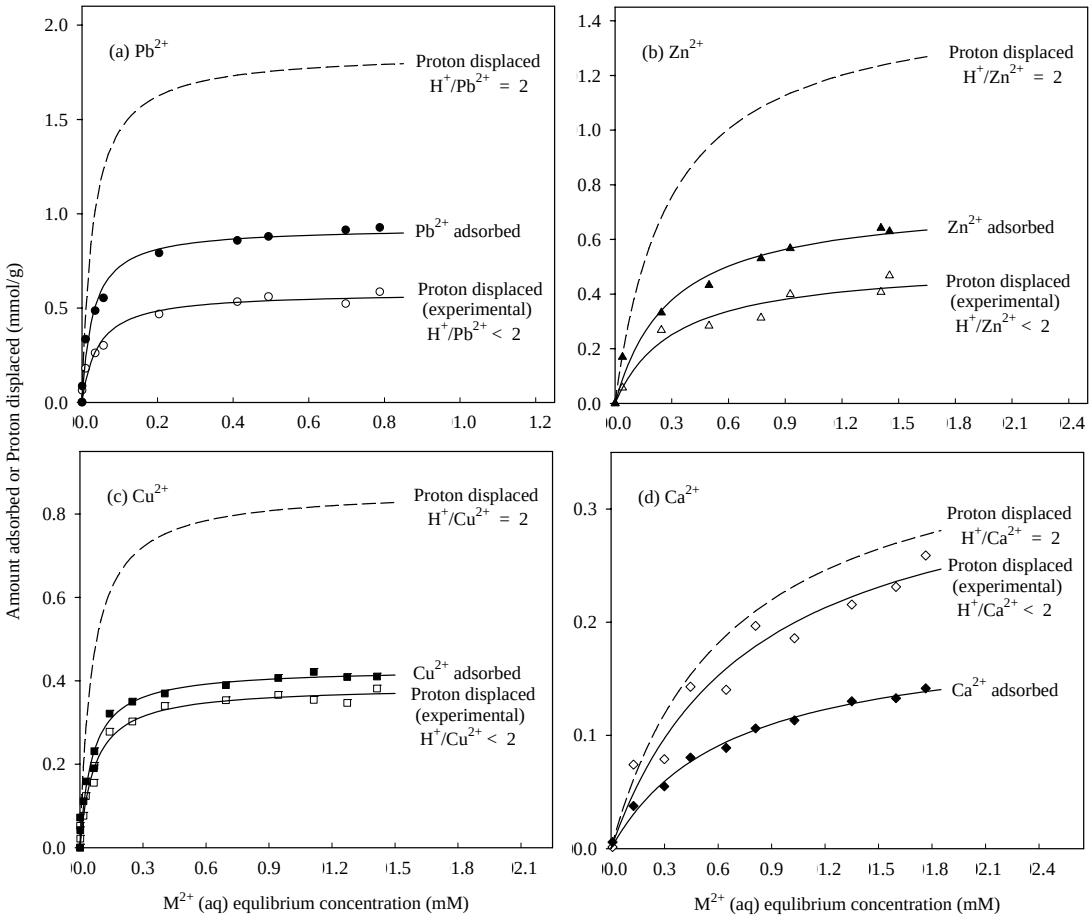

Figure 5.28 Comparison of amount of metal adsorbed and proton displacement of (a) Pb^{2+}, (b) Zn^{2+}, (c) Cu^{2+}, and (d) Ca^{2+} of sample HNO_3 re 1M 24h.

Xiao (2004) also suggested that the adsorption of Cu^{2+} on activated carbon with high concentration of oxygen functional groups underwent an ion-exchange mechanism and may also be involved in coordinated with oxygen functional groups acting as ligands to form surface complexes (Figure 5.29). In this thesis, it is suggested that this complexation reaction can be applied to zinc (II) and lead (II) adsorptions because these two cations in solutions are also in the form of hexaquo ions complex i.e. $[Zn(H_2O)_6]^{2+}$ and $[Pb(H_2O)_6]^{2+}$ (Álvarez-Merino et al., 2005; Gomez-Serrano, Macias-Garcia, Espinosa-Mansilla, and Valenzuela-Calahorro, 1998).

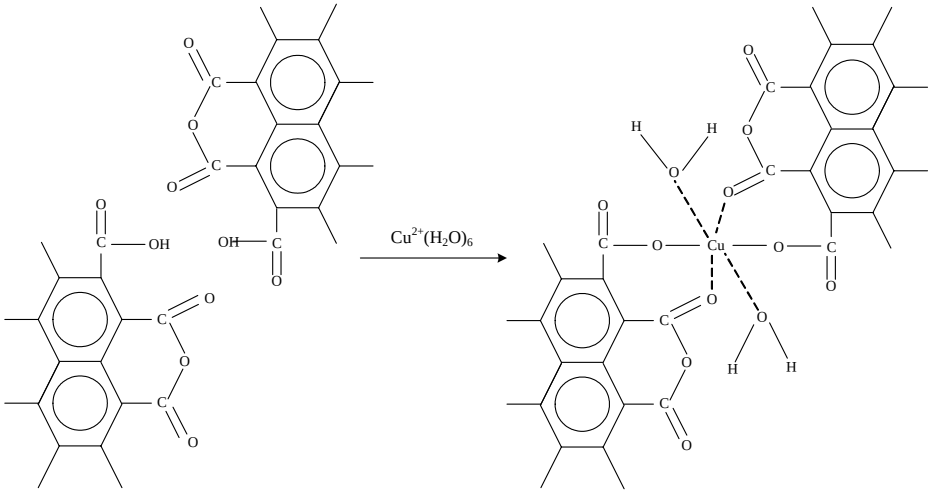

Figure 5.29 Postulated complexation reaction between copper (II) and surface functional groups on activated carbon (Strelko and Malik, 2002).

5.3.2.2 Binary mixture adsorption

Binary adsorptions in mixtures of Pb^{2+}/Cu^{2+}, Pb^{2+}/Zn^{2+}, Zn^{2+}/Cu^{2+}, Pb^{2+}/Ca^{2+}, and Cu^{2+}/Ca^{2+} were investigated using sample HNO_3 re 1M 24h. Figure 5.30, Figure 5.31, and Figure 5.32 show the adsorption isotherms of single ion in comparison with adsorption obtained in binary mixture of Pb^{2+}/Cu^{2+}, Pb^{2+}/Zn^{2+}, and Zn^{2+}/Cu^{2+} on sample HNO_3 re 1M 24h, respectively. The results show that the adsorption of all metal ions are suppressed in the binary system.

As can be seen from Figure 5.30, Pb^{2+} ion could be favorably adsorbed as compared to Cu^{2+} ion and its maximum adsorptive capacity is estimated to be around 0.6 mmol/g, while for Cu^{2+} ion adsorption it is around 0.3 mmol/g. In binary system, the total adsorption capacity of Pb^{2+} ion and Cu^{2+} ion (0.9 mmol/g) exceeds the capacity of Cu^{2+} (0.4 mmol/g) but equal to that of Pb^{2+} in the single system.

As shown in Figure 5.31, Pb^{2+} ion adsorbed more on sample HNO_3 re 1M 24h compared to Zn^{2+} ion and its maximum adsorptive capacity is estimated to be 0.5 mmol/g, while maximum capacity of Zn^{2+} ion is 0.25 mmol/g. The total adsorption capacity in binary system (0.75 mmol/g) exceeds the capacity of Zn^{2+} (0.6 mmol/g) but lowers than that of Pb^{2+} (0.9 mmol/g) in the single system.

In binary system of Zn^{2+}/Cu^{2+} (Figure 5.32), Cu^{2+} ion seems to favorably adsorbed on this sample (0.32 mmol/g) over Zn^{2+} ion (0.3 mmol/g), although Zn^{2+} is favorably adsorbed on this carbon (0.6 mmol/g) compare to Cu^{2+} adsorption in the single system (0.4 mmol/g).

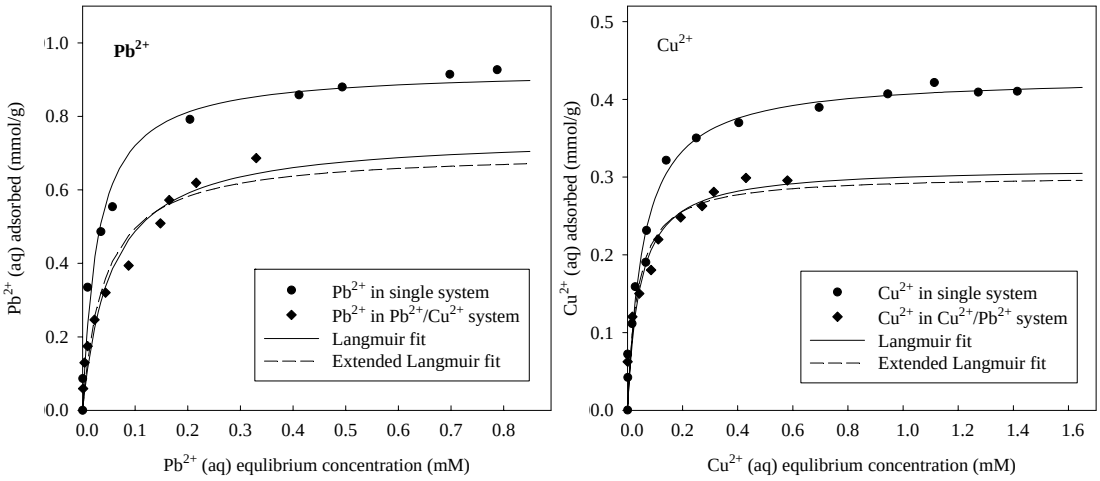

Figure 5.30 Binary system of Pb^{2+} and Cu^{2+} adsorption on sample HNO_3 re 1M 24h at 30°C.

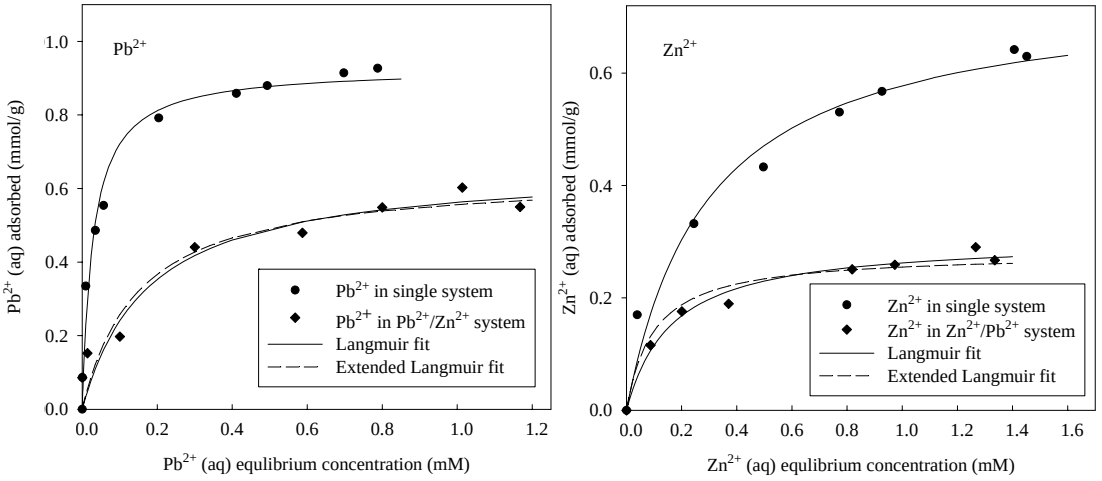

Figure 5.31 Binary system of Pb^{2+} and Zn^{2+} adsorption on sample HNO_3 re 1M 24h at 30°C.

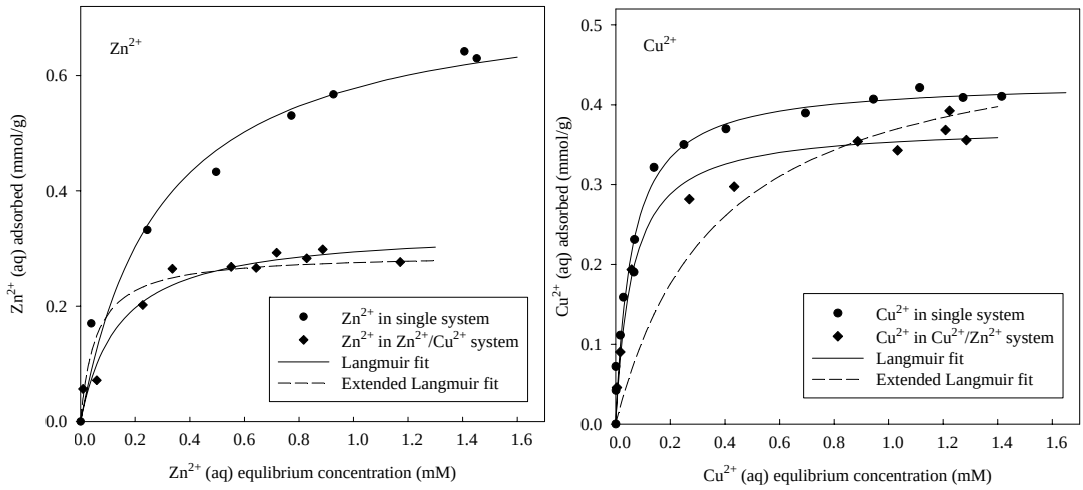

Figure 5.32 Binary system of Zn^{2+} and Cu^{2+} adsorption on sample HNO_3 re 1M 24h at 30°C.

The experimental isotherms of all case were modeled by employed the Langmuir model (equation 5.7) and the extended Langmuir model. The extended Langmuir model used in binary system is in the form,

$$q_{e,i} = \frac{q_{m,i} b_i C_{e,i}}{1 + \sum_{j=1}^{n} b_j C_{e,j}} \tag{5.12}$$

where $q_{e,i}$ is the adsorbed amount of metal ion at equilibrium, $q_{m,i}$ is the maximum amount adsorbed in mmol/g, b_i is the Langmuir constant in L/mmol, $C_{e,i}$ is the equilibrium concentration in mM, and i refers to the metal ion species in the binary adsorption system. The extended Langmuir models for two components are:

$$q_{e,1} = \frac{q_{m,1} b_1 C_{e,1}}{1 + b_1 C_{e,1} + b_2 C_{e,2}} \qquad \text{and} \qquad q_{e,2} = \frac{q_{m,2} b_2 C_{e,2}}{1 + b_1 C_{e,1} + b_2 C_{e,2}} \tag{5.13}$$

The extended Langmuir model was fitted by optimizing the model parameters i.e. $q_{m,1}$, $q_{m,2}$, b_1, and b_2 using a non-linear regression by minimizing the sum square of error (SSE) being defined as

$$\mathrm{SSE} = \sum_{j=1}^{N}\left[(q_{e,1exp} - q_{e,1model})_j^2 + (q_{e,2exp} - q_{e,2model})_j^2\right] \quad (5.14)$$

where N is the number of data points of the isotherm and subscript exp and model are the data from experiment and extended Langmuir model, respectively. The results of this fitted are also shown in Figure 5.30, Figure 5.31, and Figure 5.32 and the parameters and correlation coefficient (R^2) are tabulated in Table 5.17. It is noted that the SSE for Pb^{2+}/Cu^{2+}, Pb^{2+}/Zn^{2+}, and Zn^{2+}/Cu^{2+} systems are 0.028, 0.027, and 0.043, respectively.

It can be found that, for all cases, the extended Langmuir model could describe the experimental data very well except in the case of Cu^{2+} in Cu^{2+}/Zn^{2+}system (see Figure 5.32). However, this model predicts much higher maximum amount adsorbed (q_m) in the case of Pb^{2+} in Pb^{2+}/Cu^{2+}, Pb^{2+} in Pb^{2+}/Zn^{2+}, and Cu^{2+} in Cu^{2+}/Zn^{2+}systems as compared to the experimental data.

Table 5.17 Parameters for metal ions in the binary systems of Pb^{2+}/Cu^{2+}, Pb^{2+}/Zn^{2+}, and Zn^{2+}/Cu^{2+} on sample HNO_3 re 1M 24h.

System	q_m (mmol/g)	b (L/mmol)	R^2
Pb^{2+}/Cu^{2+}			
Pb^{2+} in Pb^{2+}/Cu^{2+} with Langmuir model	0.75	18.66	0.949
Pb^{2+} in Pb^{2+}/Cu^{2+} with extended Langmuir model	3.01	9.42	0.957
Cu^{2+} in Cu^{2+}/Pb^{2+} with Langmuir model	0.31	22.62	0.907
Cu^{2+} in Cu^{2+}/Pb^{2+} with extended Langmuir model	0.39	18.25	0.926
Pb^{2+}/Zn^{2+}			
Pb^{2+} in Pb^{2+}/Zn^{2+} with Langmuir model	0.66	5.72	0.914
Pb^{2+} in Pb^{2+}/Zn^{2+} with extended Langmuir model	2.89	2.21	0.951
Zn^{2+} in Zn^{2+}/Pb^{2+} with Langmuir model	0.30	6.14	0.953
Zn^{2+} in Zn^{2+}/Pb^{2+} with extended Langmuir model	0.36	6.84	0.970
Zn^{2+}/Cu^{2+}			
Zn^{2+} in Zn^{2+}/Cu^{2+} with Langmuir model	0.34	7.15	0.948
Zn^{2+} in Zn^{2+}/Cu^{2+} with extended Langmuir model	0.38	10.10	0.849
Cu^{2+} in Cu^{2+}/Zn^{2+} with Langmuir model	0.37	16.79	0.972
Cu^{2+} in Cu^{2+}/Zn^{2+} with extended Langmuir model	1.72	2.40	0.912

Figure 5.33 (a) and (b) show the adsorption isotherms of single ion in comparison with competitive adsorption in the binary mixtures of Pb^{2+}/Ca^{2+} and Cu^{2+}/Ca^{2+} on original activated carbon (AC) and sample HNO_3 re 1M 24h, respectively. As shown in both figures, the adsorption of Ca^{2+} reaches a maximum at equilibrium solution concentration of about 0.1 mM and then decreases with increasing equilibrium solution concentration. Finally, there are no Ca^{2+} adsorbed at equilibrium solution concentrations higher than 0.2 mM for Cu^{2+}/Ca^{2+} system and 0.4 mM for Pb^{2+}/Ca^{2+} system. The reason that Ca^{2+} did not adsorbed in the binary systems of Pb^{2+} /Ca^{2+} and Cu^{2+}/Ca^{2+} because Ca^{2+} was adsorbed in small amount in single system viz., 0.14 mmol/g for sample HNO_3 re 1M 24h and 0.02 mmol/g for original activated carbon and with much lower electronegativity of this ion compared to Pb^{2+} and Cu^{2+} ions. On the contrary, the adsorption of Pb^{2+} and Cu^{2+} increases with increasing equilibrium solution concentration and the amount adsorbed in the binary mixture system is not much different from that in the single system. This indicates that Ca^{2+} ion is the more weakly adsorbed species than Pb^{2+} and Cu^{2+} ions with the affinity order $Pb^{2+} > Cu^{2+} > Ca^{2+}$. It can be concluded that the presence of Ca^{2+} in the binary system gives virtually no effect on the adsorption of the other ion.

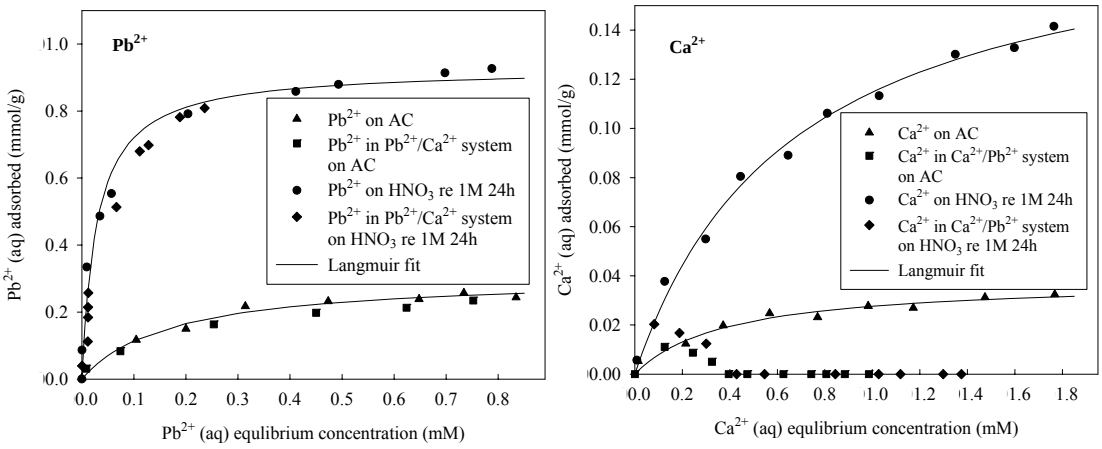

(a) Pb^{2+}/Ca^{2+} system

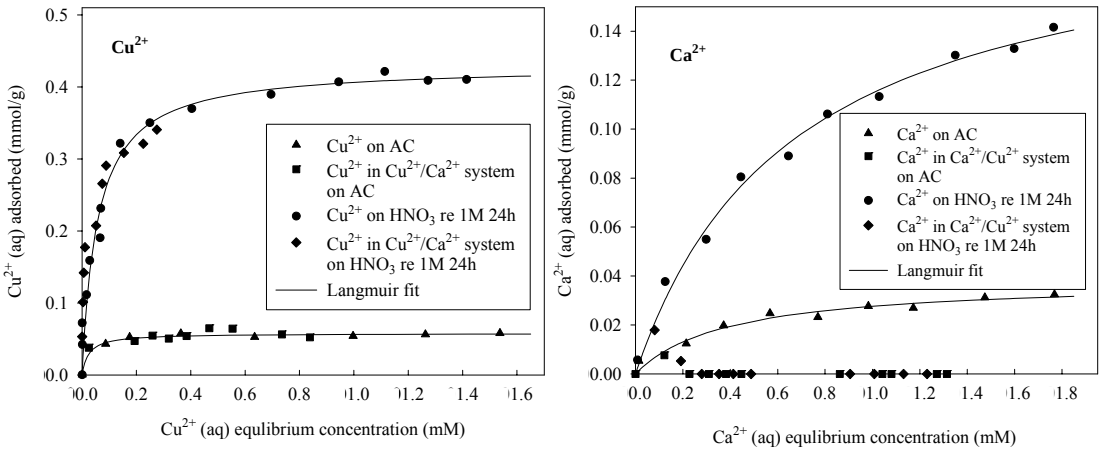

(b) Cu^{2+}/Ca^{2+} system

Figure 5.33 Binary systems of (a) Pb^{2+} and Ca^{2+} and (b) Cu^{2+} and Ca^{2+} adsorptions on original activated carbon (AC) and sample HNO_3 re 1M 24h at 30°C.

Figure 5.34 summarizes the adsorption of all four metal ions on sample HNO_3 re 1M 24h in both single and binary systems. Overall, it may be concluded that the adsorption capacities of activated carbon for Pb^{2+}, Zn^{2+}, Cu^{2+}, and Ca^{2+} decrease in binary systems as compared to the single systems. The adsorption capacities decrease in the following order:

$$Pb^{2+} \sim Pb\text{–}Ca < Pb\text{–}Cu < Pb\text{–}Zn \quad \text{for } Pb^{2+},$$

$$Zn^{2+} < Zn\text{–}Cu < Zn\text{–}Pb \quad \text{for } Zn^{2+},$$

$$Cu^{2+} \sim Cu\text{–}Ca < Cu\text{–}Zn < Cu\text{–}Pb \quad \text{for } Cu^{2+},$$

$$Ca^{2+} << Ca\text{–}Pb \sim Ca\text{–}Cu \quad \text{for } Ca^{2+}.$$

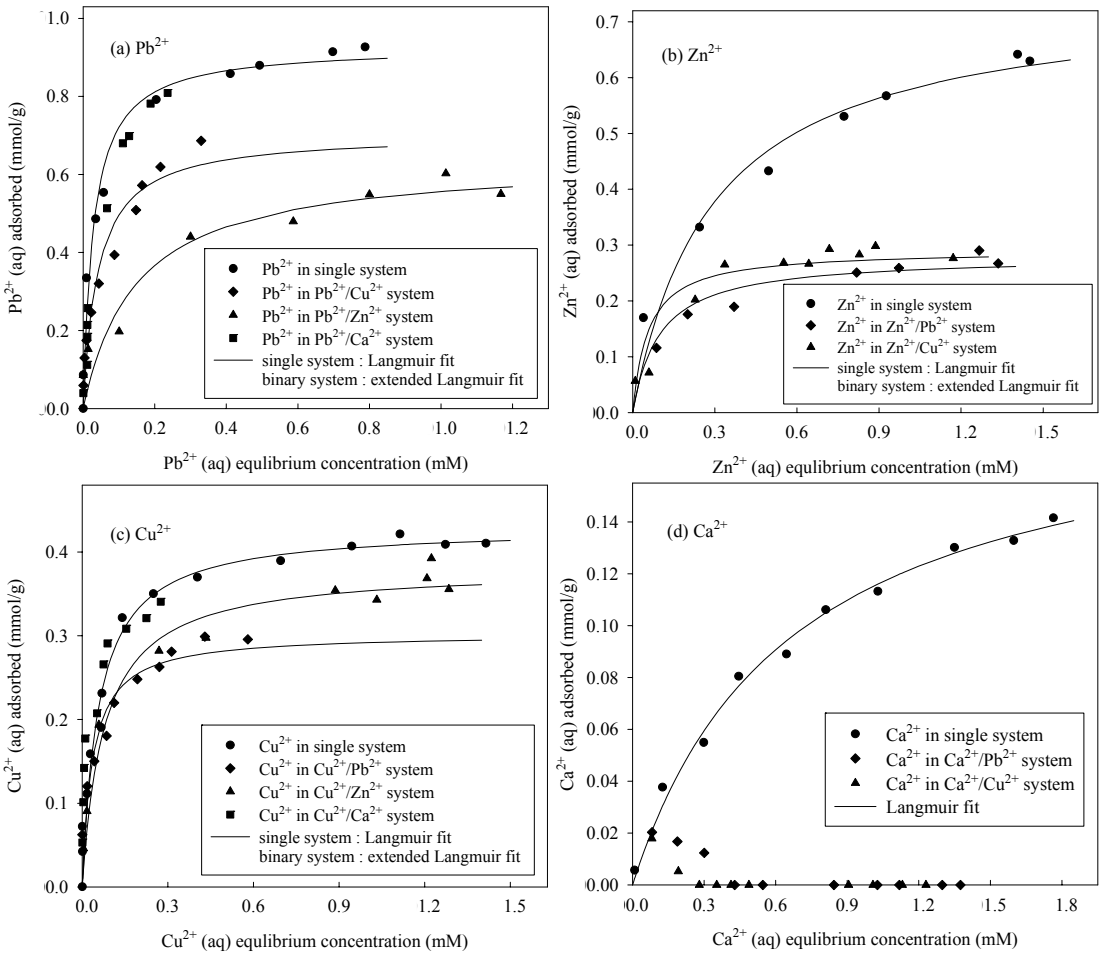

Figure 5.34 Adsorption isotherms of (a) Pb^{2+}, (b) Zn^{2+}, (c) Cu^{2+}, and (d) Ca^{2+} on sample HNO_3 re 1M 24h at 30^{o}C in both single and binary systems.

5.4 Conclusions

The following conclusions can be drawn from the present study:

- It was found that the oxygen functional groups on the activated carbon surface played the role in the adsorption of water vapor and the adsorption depended on the concentration and distribution of these functional groups, with carboxylic acid group showing an important role. The adsorption capacity of water vapor was increased in the presence of oxygen functional groups on the activated carbon

surfaces while the adsorption capacities of *n*-alcohol vapors (methanol and ethanol) decreased. These observations could be explained by the difference in adsorption mechanisms for water and alcohol vapors on activated carbon. It should be emphasized that the main mechanism of water adsorption is by the adsorption of the first water molecule on the hydrophilic functional groups followed by cluster formation of additional molecules via hydrogen bonding. In contrast, alcohol molecule will adsorb more on hydrophobic part of the surface which constitutes the micropores but self-adsorption in larger pores is much less because of the lower polarity.

- Heat treatment process which decreased the amount of carboxylic acid group decreased the amount of water adsorbed at relative pressure < 0.4 for heat-treated sample at 600^{o}C and at relative pressure < 0.6 for heat-treated sample at 800^{o}C. At higher relative pressure range the adsorption is believed to be the consequence of physical adsorption on hydrophobic surfaces and pore filling effect in the larger pore sizes, giving higher amount water adsorbed of the heat-treated sample at the high temperature.

- The isotherms of water adsorption were described using DS and Do and Do equations and applicability of these models showed that DS equation failed to describe the isotherm of activated carbon with a large number of surface functional groups (oxidized with 5 M HNO_3), whereas Do and Do model was able to describe isotherm of activated carbon with highly oxidized carbon surfaces.

- The adsorption capacities of aqueous metal ions on oxidized activated carbons were increased with the order $Pb^{2+} > Zn^{2+} > Cu^{2+} > Ca^{2+}$ and the adsorption mainly involved and ion-exchange mechanism. The presence of acidic oxygen

functional groups rendered the activated carbon surface negatively charged and these substantially improved its ion-exchange properties. Oxidized activated carbon behaved as a cation-exchanger in solution due to the presence of a number of acidic surface functional groups.

- Competitive adsorptions in binary systems decreased the amount of individual metal ions adsorbed with the maximum amount adsorbed follow the order $Pb^{2+} > Zn^{2+} \sim Cu^{2+} >> Ca^{2+}$. The presence of Ca^{2+} in the binary system had no effect on the adsorption of the other co-ion.

- All adsorption isotherms of single metal ions followed the Langmuir model, whereas the extended Langmuir model can describe the isotherms of binary systems fairly well.

- Carboxylic acid group plays an important role in adsorption of polar molecule because it is the strongest acid functional group.

5.5 References

Álvarez-Merino, M. A., López-Ramón, V., and Moreno-Castilla, C. M. (2005). A study of the static and dynamic adsorption of Zn(II) ions on carbon materials from aqueous solutions. **J. Colloid Interface Sci.** 288: 335-341.

Bandosz, T. J., Jagiello, J., Schwarz, J. A., and Krzyzanowski A., (1996). Effect of surface chemistry on sorption of water and methanol on activated carbons. **Langmuir** 12: 6480-6486.

Brennan, J. K., Bandosz, T. J., Thomson, K. T., Gubbins, K. E. (2001). Water in porous carbons. **Colloids Surf. A** 187-188: 539-568.

Chen, J. P., Wu, S., and Chong, K.-H. (2003). Surface modification of a granular activated carbon by citric acid for enhancement of copper adsorption. **Carbon** 41: 1979-1986.

Chubar, N., Carvalho, J. R., and Correia, M. J. N. (2004). Cork biomass as biosorbent for Cu(II), Zn(II) and Ni(II). **Colloids Surf. A** 230: 57-65.

Choma, J., Burakiewicz-Mortka, W., Jaroniec, M., Li, Z., and Klinik J. (1999). Monitoring changes in surface and structural properties of porous carbon modified by different oxidizing agents. **J. Colloid Interface Sci.** 214: 438-446.

Dastgheib, S. A. and Rockstraw, D. A. (2002). A model for the adsorption of single metal ion solutes in aqueous solution onto activated carbon produced from pecan shells. **Carbon** 40: 1843-1851.

Do, D. D. (1998). **Adsorption analysis: Equilibria and Kinetics.** Singapore: Imperial College Press.

Do, D. D. and Do, H.D. (2000). A model for water adsorption in activated carbon. **Carbon** 38: 767-773.

Dubinin, M. M. and Serpinsky, V. V. (1981). Isotherm equation for water vapor adsorption by microporous carbonaceous adsorbents. **Carbon** 19: 402-403.

Fletcher, A. J., Yüzak, Y., Thomas, K. M. (2006). Adsorption and desorption kinetics for hydrophilic and hydrophobic vapors on activated carbon. **Carbon** 44: 989-1004.

Foley, N. J., Thomas, K. M., Forshaw, P. L., Stanton, D., and Norman, P. R. (1997). Kinetics of water vapor adsorption on activated carbon. **Langmuir** 13: 2083-2089.

Gales, L., Mendes, A., and Costa, C. (2000). Hysteresis in the cyclic adsorption of acetone, ethanol and ethyl acetate on activated carbon. **Carbon** 38: 1083-1088.

Gerçel, Ö. and Gerçel, H. F. (2007). Adsorption of lead(II) ions from aqueous solutions by activated carbon prepared from biomass plant material of *Euphorbia rigida*. **Chem. Eng. J.** 132: 289-297.

Gomez-Serrano, V., Macias-Garcia, A., Espinosa-Mansilla, A., and Valenzuela-Calahorro, C. (1998). Adsorption of mercury, cadmium and lead from aqueous solution on heat-treated and sulphurized activated carbon. **Wat. Res.** 32: 1-4.

Goworek, J., Świątkowski, A., and Biniak, S. (1997). Characterization of modified active carbons by adsorption of pure water and benzene vapors and ternary liquid mixture benzene + diethyl ketone + *n*-heptane. **Langmuir** 13: 1225-1228.

Han, R., Lu, Z., Zou, W., Daotong, W., Shi, J., and Jiujun, Y., (2006). Removal of copper(II) and lead(II) from aqueous solution by manganese oxide coated sand II. Equilibrium study and competitive adsorption. **J. Hazard. Mater.** 137: 480-488.

Junpirom, S. (2006). **Activated carbon from longan seed: its activation model and adsorption of water vapor and benzene.** Ph.D. thesis, Suranaree University of Technology, Thailand.

Kimura, T., Kanoh, H., Kanda, T., Ohkubo, T., Hattori, Y., Higaonna, Y., Denoyel, R., Kaaneko, K. (2004). Cluster-associated filling of water in hydrophobic carbon micropores. **J. Phys. Chem. B** 108: 14043-14048.

Neitsch, M., Heschel, W., and Suckow, M. (2001). Water vapor adsorption by activated carbon: a modification to the isotherm model of Do and Do. **Carbon** 39: 1437-1438.

Patrick, J. W. (1995). **Porosity in Carbons: Characterization and Applications.** London: Edward Arnold.

Rao, M. M., Rao, G. P. C., Seshaiah, K., Choudary, N. V., and Wang, M. C. (2007). Activated carbon from *Ceiba pentandra* hulls, an agricultural waste, as an adsorbent in the removal of lead and zinc from aqueous solutions. **Waste Manage.** In Press, Corrected Proof.

Ricordel, S., Taha, S., Cisse, I., and Dorange, G. (2001). Heavy metals removal by adsorption onto peanut husks carbon: characterization, kinetic study and modeling. **Sep. Purif. Technol.** 24: 389-401.

Rouquerol, F., Rouquerol, J., and Sing, K. (1999). **Adsorption by Powders and Porous Solids.** London: Academic Press.

Srivastava, S. K., Gupta, V. K., and Mohan, D. (1996). Kinetic parameters for the removal of lead and chromium from wastewater using activated carbon developed from fertilizer waste material. **Environmental Modeling and Assessment** 1: 281-290.

Strelko, V. Jr. and Malik, D. J. (2002). Characterization and metal sorptive properties of oxidized active carbon. **J. Colloid Interface Sci.** 250: 213-220.

Sun, J. and Satyapal S. (1999). **In Extended Abstracts and Program of the 24th Biennal Conference on Carbon**. Charleston, SC; American Carbon Society. Quoted in Salame, I. I. and Bandosz, T. J. (2000). Adsorption of water and methanol on micro- and mesoporous wood-based activated carbons. **Langmuir** 16: 5435-5440.

Xiao, B. (2004). **Characterisation of functionalized nanoporous carbon materials & adsorption of aqueous metal ions**. Ph.D. thesis, University of Newcastle upon Tyne, United Kingdom.

Xiao, B. and Thomas, K. M. (2004). Competitive adsorption of aqueous metal ions on an oxidized nanoporous activated carbon. **Langmuir** 20: 4566-4578.

Xiao, B. and Thomas, K.M. (2005). Adsorption of aqueous metal ions on oxygen and nitrogen functionalized nanoporous activated carbons. **Langmuir** 21: 3892-3902.

CHAPTER VI

CONCLUSIONS AND RECOMMENDATIONS

6.1 Conclusions

This work involved a systematic study of activated carbons from eucalyptus wood and a new precursor, wattle wood. The research started with the preparation of activated carbons from both woods using H_3PO_4 and CO_2 as activating agents. The next task was concerned with the surface modification of eucalyptus-wood based carbon by oxidation methods. The goal of the surface modification was not only to modify activated carbon to obtain high total acidic oxygen functional groups but also to achieve high content of carboxylic acid group which is the strongest acid functional group. The two hypotheses that, the oxidized carbons derived from activated carbons prepared by using different activation methods (i.e. chemical and physical activation) and activated carbons with varying porous structure should affect the amount and distribution of functional groups on the carbon surface was proposed and tested. The final task was to examine the role of incorporated surface functionality by studying the adsorption equilibrium of water vapor, alcohol vapors (methanol and ethanol), and heavy metal ions by the surface-modified carbons. The conclusions from this work are as follows:

- On the preparation of activated carbons with H_3PO_4, the preparation conditions including carbonization temperature (300^oC – 700^oC), chemical weight ratio of H_3PO_4 solution and wood (0.5:1 – 3:1), carbonization time (0.5 – 2 hour), and

impregnation time (0.5 – 3 hour) were found to affect the porous properties of the obtained carbons. Activated carbons prepared at chemical weight ratio of H_3PO_4 solution and wood 1.5:1, impregnation time 1.5 hour, carbonization temperature 400^oC, and carbonization time 1 hour gave the highest BET surface area of 1857 m^2/g and 1550 m^2/g for eucalyptus and wattle woods, respectively.

- For physical activation with CO_2, the effect of preparation conditions investigated were carbonization temperature (300^oC – 700^oC), carbonization time (1 – 4 hour), activation temperature (600^oC – 900^oC), activation time (1 – 5 hour), and CO_2 concentration (25 – 100 vol%). The best activation conditions that produced the highest porous properties of activated carbons were 900^oC and 1 hour with the maximum surface area of 1491 m^2/g and total pore volume of 0.80 cm^3/g for eucalyptus wood and 800^oC for 5 hours with the maximum surface area of 1032 m^2/g and total pore volume of 0.56 cm^3/g for wattle wood with the carbonization conditions used being 400^oC and 1 hour for both woods.

- For both activation methods, eucalyptus wood gave better pore development than wattle wood under the same preparation conditions.

- For both woods, chemical activation with H_3PO_4 gave activated carbons with higher surface area and total pore volume than that obtained by physical activation with CO_2. Activated carbons derived from both eucalyptus and wattle woods by CO_2 activation produced mainly micropore (constituting about 80% of total pore volume) whereas H_3PO_4 activation produced activated carbons with higher proportions of mesopore and macropore volume.

- On the surface modification of chemically eucalyptus-wood based activated carbon, oxidation treatments with H_2O_2, $(NH_4)_2S_2O_8$, HNO_3, and air resulted in an increase in the number of total acidic oxygen functional groups. The percent increase of acidic types in the oxidized activated carbon as compared to the original carbon was highest for carboxylic acid group followed by phenolic and lactonic for all the oxidation treatment.

- The increasing of oxidation time, oxidation temperature, and acid concentration increases the total acid group and the amount of each acidic functional group, whereas the distribution of each functional group remained unchange after oxidation.

- Air oxidation gave the highest total acidic groups and highest amount of carboxylic acid as compared with the oxidation in liquid phase. However, the drawback of air oxidation is the relatively low yield of final oxidized carbon. For liquid phase oxidation, HNO_3 by reflux method is the strongest oxidation followed by H_2O_2, $(NH_4)_2S_2O_8$, and HNO_3 by soaking method respectively.

- All porous properties of the original carbon decreased after oxidation due to the inaccessibility of N_2 molecules into the internal adsorption sites caused by the presence of functional groups at the pore entrance and possibly by the collapse of some thin pore walls caused by oxidizing agent during the oxidation treatment.

- The results from FTIR, XPS, elemental analysis, and pH_{pzc} confirmed the existence of oxygen functional groups.

- Preparation method of activated carbon had a direct effect on the amount and distribution of functional groups. Oxidation with HNO_3 by reflux method, the original carbon prepared by chemical method with H_3PO_4 gave higher total acidic

groups but created less carboxylic acid group as compared to the original carbon prepared by physical method with CO_2.

- Porous structure of the original carbon had an effect on the incorporation of oxygen functional groups. The highest amounts of acidic functional groups were obtained in the activated carbon having highest surface area and there existed a minimum concentration of HNO_3 corresponding to the available surface area that can produce maximum amount of surface groups.

- The results from heat treatment process revealed that thermal treatment reduced the amount and changed the distribution of acidic functional groups on activated carbon. The order of thermal stability of acidic oxygen functional groups is the following: carboxylic < lactonic < phenolic. Heat treatment process increased all porous properties of heat treated carbons due to the removal of surface functional groups being formed at the pore entrance during heat treatment, so that N_2 molecules can now get access into the internal adsorption sites during isotherm measurement.

- On the adsorption equilibrium study, water vapor adsorption was increased in the presence of oxygen functional groups on the activated carbon surfaces while the adsorption capacities of methanol and ethanol vapors decreased. This difference was attributed to the difference in adsorption mechanisms of water and alcohol vapors on activated carbon. The main mechanism of water adsorption is by the adsorption of the first water molecule on the hydrophilic functional groups followed by the cluster formation of additional molecules via hydrogen bonding. In contrast, alcohol molecule will adsorb more on hydrophobic part of the surface which constitutes the micropores but self-adsorption in larger pores is much less because of the lower polarity.

- Heat treatment process which decreased the amount of oxygen functional groups decreased the amount of water adsorbed at relative pressure < 0.4 for heat-treated sample at 600^{o}C and at relative pressure < 0.6 for heat-treated sample at 800^{o}C. At higher relative pressure range, the heat-treated sample showed higher amount of water adsorbed. This is believed to be the consequence of physical adsorption on hydrophobic surfaces and pore filling effect in the larger pore sizes at higher relative pressures.

- It was found that carboxylic acid group plays a significant role in the adsorption of water vapor compared to other surface acidic groups.

- The Dubinin and Serpinsky (DS) and Do and Do equations were used to describe water adsorption isotherms. It was found that DS equation failed to describe the isotherm of activated carbon with a large number of surface functional groups, whereas Do and Do model was able to describe isotherm of activated carbon with highly oxidized carbon surfaces.

- Adsorption capacities of aqueous metal ions on oxidized activated carbons were increased with the order $Pb^{2+} > Zn^{2+} > Cu^{2+} > Ca^{2+}$ and the adsorption mainly involved an ion-exchange mechanism. The presence of acidic oxygen functional groups rendered the activated carbon surface negatively charged and these substantially improved its ion-exchange properties.

- In the binary system, the amount of each ions adsorbed decreased as compared to the single system with the maximum amount adsorbed following the order $Pb^{2+} > Zn^{2+} \sim Cu^{2+} >> Ca^{2+}$. Therefore, it can be concluded that the presence of Ca^{2+} in the binary system gave almost no effect on the adsorption of the other ions.

- All adsorption isotherms of single metal ions followed the Langmuir model, while extended Langmuir model can describe the adsorption isotherm in binary systems reasonably well.

6.2 Recommendations

The following research topics are worth further investigation:

- In this thesis, the activated carbons were prepared by using H_3PO_4 and CO_2. It is suggested that activated carbons be prepared using other activating agents such as H_2SO_4, $ZnCl_2$, or steam in order to compare the effect of different activating agents on porous properties of the obtained activated carbons. The preparation of activated carbon by a combined chemical and physical activation i.e. impregnation of raw material with a chemical agent and followed by activation with CO_2 or steam should be tried.

- The scanning electron micrographs of wood materials, char (for physical activation), and activated carbon prepared by H_3PO_4 activation with different chemical weight ratio should be performed to clearly show the development of porous structure.

- For this research, the oxygen functional groups were incorporated on eucalyptus wood-based activated carbon surfaces using HNO_3, H_2O_2, $(NH_4)_2S_2O_8$ and air oxidation. The use of other oxidizing agents such as H_2SO_4, $HClO_4$, NaOCl and O_3 should be explored to better understand the underlying mechanism of functional group creation.

- The characterization of surface functional groups by FTIR should be directed toward using oxidized activated carbons with high amount of total acidic functional groups such as samples HNO_3 re 5M 24h, HNO_3 re 10M 24h, air 250^oC 24h, and air 350^oC 24h. The technique of Temperature Program Desorption (TPD) is suggested to characterize the surface functional groups.
- A further study on the incorporation of nitrogen functional groups such as by ammonia treatment on activated carbon should be carried out.
- Study on the metal ion adsorption by surface-modified carbon should be extended to cover the effects of pH, temperature, etc.

APPENDIX

LIST OF PUBLICATIONS

LIST OF PUBLICATIONS

1. Referred Journals

Ngernyen, Y., Tangsathitkulchai, C., and Tangsathitkulchai, M. (2006). Porous properties of activated carbon produced from eucalyptus and wattle wood by carbon dioxide activation. **Korean Journal of Chemical Engineering** 23: 1046-1054.

Ngernyen, Y., Tangsathitkulchai, C., Khaoya, S., Intasa-ard, W., and Tangsathitkulchai, M. (2007). Effect of surface functional groups on water vapor adsorption of eucalyptus wood-based activated carbon. **Suranaree Journal of Science and Technology** 14: 9-23.

2. Conference Abstracts

Ngernyen, Y., Tangsathitkulchai, C., and Tangsathitkulchai, M. (2005). The modification of acidic surface functionality of wood-based activated carbon. **The International Carbon Conference 2005.**

Ngernyen, Y., Tangsathitkulchai, C., and Tangsathitkulchai, M. (2006). Water vapor adsorption on wood-based activated carbon. **13th Regional Symposium on Chemical Engineering.** pp: 263-264.

Luangkiattikhun, P., Ngernyen, Y., Junpirom, S., Tangsathitkulchai, C., and Tangsathitkulchai, M. (2006). A char gasification model for predicting the porous properties of activated carbons. **13th Regional Symposium on Chemical Engineering.** pp: 228-229.

BIOGRAPHY

Miss Yuvarat Ngernyen was born on January, 23, 1980. She graduated in primary school from Santivithaya School and secondary school from Samakkhiwitthayakhom School, Chiang Rai Province. In 2001, she graduated a bachelor degree in Chemical Engineering from Suranaree University of Technology (SUT). In 2002, she continued her doctoral degree study in Chemical Engineering at SUT under the supervision of Assoc. Prof. Dr. Chaiyot Tangsathitkulchai. She received a support in form of scholarship from The Royal Golden Jubilee (RGJ) Ph.D. Program under The Thailand Research Fund (TRF).